Synthesis of Rigid Spin Labels for the Investigation of Transmembrane Peptides by EPR Spectroscopy

DISSERTATION

zur Erlangung des mathematisch-naturwissenschaftlichen Doktorgrades

"Doctor rerum naturalium"

der Georg-August-Universität Göttingen

im Promotionsprogramm Chemie

der Georg-August University School of Science (GAUSS)

vorgelegt von

Janine Wegner

aus Göttingen

Göttingen, 2018

Betreuungsaussschuss

Prof. Dr. Ulf Diederichsen	Institut für Organische und Biomolekulare Chemie, Georg-August-Universität Göttingen
Prof. Dr. Marina Bennati	MPI für Biophysikalische Chemie, Göttingen

Mitglieder der Prüfungskommisson

Referent:	Prof. Dr. Ulf Diederichsen
Korreferentin:	Prof. Dr. Marina Bennati

Weitere Mitglieder der Prüfungskommisson

Prof. Dr. Manuel Alcarazo	Institut für Organische und Biomolekulare Chemie, Georg-August-Universität Göttingen
Prof. Dr. Konrad Koszinowski	Institut für Organische und Biomolekulare Chemie, Georg-August-Universität Göttingen
Dr. Michael John	Institut für Organische und Biomolekulare Chemie, Georg-August-Universität Göttingen
Dr. Franziska Thomas	Institut für Organische und Biomolekulare Chemie, Georg-August-Universität Göttingen

Tag der mündlichen Prüfung: 28.02.2018

Die vorliegende Arbeit wurde im Zeitraum November 2013 bis Februar 2018 am Institut für Organische und Biomolekulare Chemie der Georg-August-Universität Göttingen unter der Leitung von Prof. Dr. ULF DIEDERICHSEN angefertigt.

Diese Arbeit wurde gefördert durch die DEUTSCHE FORSCHUNGSGEMEINSCHAFT über den Sonderforschungsbereich 803 (SFB 803).

Für meine Familie

I have decided to catch a Heffalump.

– A. A. Milne

Parts of chapters 3.3 to 3.5 of this thesis have been published as:

K. Halbmair, J. Wegner, U. Diederichsen, M. Bennati, "*Pulse EPR Measurements of Intramolecular Distances in a TOPP-Labeled Transmembrane Peptide in Lipids*" *Biophys. J.* **2016**, *111*, 2345.

Table of Content

Abbreviations

A	alanine
Ac	acetyl
ACHC	*trans*-2-aminocyclohexanecarboxylic acid
AcOH	acetic acid
Ac_2O	acetic anhydride
AgOCOPh	silver(I)-benzoate
aq	aqueous
Bn	benzyl
Boc	*tert*-butyloxycarbonyl
B_2pin_2	bis(pinacolato)diborone
br	broadened
Bu	butyl
Cbz	benzyl chloroformate
CD	circular dichroism
$CDCl_3$	deuterated chloroform
CW	continuous wave
Cys	cysteine
δ	chemical shift
d	doublet
DBU	1,8-diazabicyclo[5.4.0]undec-7-ene
DCM	dichloromethane
DEER	double electron-electron resonance
DEPBT	3-(diethoxyphosphoryloxy)-1,2,3-benzotriazin-4(3*H*)-one
DIC	*N,N*'-diisopropylcarbodiimide
DIEA	*N,N*-diisopropylethylamine
DMF	dimethylformamide
DMPC	1,2-dimyristoyl-*sn*-glycero-3-phosphocholine

DMSO	dimethyl sulfoxide
DOPC	1,2-dioleoyl-*sn*-glycero-3-phosphocholine
dppf	1,1'-bis(phenylphosphino)ferrocene
ee	enantiomeric excess
EDT	1,2-ethanedithiol
EI	electron ionisation
EPR	electron paramagnetic resonance
eq	equivalents
ESI	electrospray ionisation
Et	ethyl
Et_3N	triethylamine
EtOAc	ethyl acetate
EtOH	ethanol
Et_2O	diethyl ether
Fmoc	fluorenylmethyloxycarbonyl
FRET	FÖRSTER resonance energy transfer
FTIR	Fourier-transform infrared spectroscopy
h	prefix: homologated
HATU	1-[Bis(dimethylamino)methylene]-1*H*-1,2,3-triazolo[4,5-*b*] pyridinium 3-oxid hexafluorophosphate
HBTU	*N,N,N',N'*-tetramethyl-*O*-(1*H*-benzotriazol-1-yl)uronium hexafluorophosphate
HOAt	1-hydroxy-7-azabenzotriazole
HOBt	1-hydroxybenzotriazole
Hpg	hydroxyphenylglycine
HPLC	high performance liquid chromatography
HR	high resolution
HWHM	half width at half maximum

i-BuOCOCl	*iso*-butyl chloroformate
J	coupling constant
K	lysine
L	leucine
Leu	leucine
Lys	lysine
m/z	mass-to-charge ratio
m	multiplet
m-CPBA	*meta*-chloroperoxybenzoic acid
Me	methyl
MeCN	acetonitrile
MeOH	methanol
MLV	multilamellar vesicle
MS	mass spectrometry
MTSSL	methanethiosulfonate spin label
NCL	native chemical ligation
NMP	*N*-methyl-2-pyrrolidone
NMR	nuclear magnetic resonance
OAc	acetate
OSu	*O*-succinimide
PEG	polyethylene glycol
PELDOR	pulsed electron double resonance
Ph	phenyl
Phg	phenylglycine
P/L	peptide-to-lipid
POAC	3-amino-1-oxyl-2,2,5,5-tetramethyl pyrrolidine-4-carboxylic acid
POPC	1-palmitoyl-2-oleoyl-*sn*-glycero-3-phosphocholine
ppm	parts per million

PROXYL	2,2,5,5-tetramethylpyrrolidine-1-oxyl
q	quartet
rt	room temperature
s	singlet
SDSL	site-directed spin labelling
SPPS	solid-phase peptide synthesis
SUV	small unilamellar vesicle
t	triplet
TBDMS	*tert*-butyldimethylsilyl
Tf	triflyl
TFA	trifluoroacetic acid
TFE	trifluoroethanol
Tf_2O	trifluoromethanesulfonic anhydride
THF	tetrahydrofuran
TIS	triisopropylsilane
TLC	thin-layer chromatography
TMS	tetramethylsilane
TOPP	4-(3,3,5,5-tetramethyl-2,6-dioxo-4-oxylpiperazine-1-yl)-L-phenylglycine
TOAC	2,2,6,6-tetramethyl-*N*-oxyl-4-amino-4-carboxylic acid
t_R	retention time
Trp	tryptophan
Trt	trityl
TsCl	*p*-toluenesulfonyl chlorid
UV	ultraviolet
V	valine
Val	valine
Vis	visible

W	tryptophan

1 Introduction and Theoretical Background

Proteins are involved in all biological processes within living cells and their specific function is intrinsically related to their structure. Hence, to gain a better understanding about their function, it is essential to investigate their structural and dynamic features. By far the most dominant techniques regarding detailed structural investigation of biomolecules, are X-ray crystallography and nuclear magnetic resonance (NMR) spectroscopy. However, limitations of their application become especially visible in the case of integral membrane proteins, which are responsible for many processes at the surface of and within the cell membrane. In particular, the associated lipid-protein complex is highly difficult to crystallise and the crystalline state as determined by X-ray diffraction might not reflect the biologically active one.[1,2] On the contrary, NMR offers the opportunity to investigate proteins in more physiologically relevant conditions, but this method is so far system-size limited (solution NMR ~60 kDa).[3,4]

To overcome these restrictions, complementary and sensitive analytical electron paramagnetic resonance (EPR) techniques such as pulsed electron double resonance (PELDOR; also known as double electron-electron resonance, DEER) have been developed. The PELDOR technique is based on the dipole-dipole interaction between two paramagnetic centres. This magnetic interaction bears structural, dynamical and conformational information about biomolecules.

Until the late 1980s, EPR techniques were mostly limited to biomolecules with intrinsic paramagnetic centres like amino acid radicals, metal ions and iron sulfur centres. Then HUBBELL and co-workers successfully introduced paramagnetic centres by site-directed spin labelling (SDSL) onto the diamagnetic bacteriorhodopsin at specific positions *via* cysteine mutation.[5] This pioneering work showed the possibility to synthetically attach suitable paramagnetic spin systems (‘spin label’) to formerly inaccessible diamagnetic biomolecules. Over the years a range of different spin labels was postulated with different properties regarding application, labelling approach and rigidity of the labels,

and sensitivity within the EPR experiment. Besides transition metal-based spin labels with copper(II)[6], gadolinium(III)[7], manganese(II)[8] or nickel (II)[9], and carbon-centred radicals[10], nitroxides are dominantly used in EPR based studies, since they are small, relatively stable and due to the concentrated location of the unpaired electron, they improve the accuracy of EPR experiments. Furthermore, as highlighted recently in reviews from LOVETT and ANDERSON, the heterocyclic scaffold that constitutes these labels is highly 'tuneable' and allows a variety of orthogonal labelling strategies.[11,12]

This thesis focuses on the synthesis of new rigid nitroxide-labelled amino acids and their twofold incorporation into transmembrane peptide models. Furthermore, these double labelled transmembrane peptides are thoroughly characterised and their usability in PELDOR experiments is comprehensively investigated.

In the following, common nitroxide spin labels and labelling methods are described in more detail.

1.1 Nitroxide Spin Labels

The nitroxyl (N–O•) radical is characterised by a π_{N-O} three electron bond which results from the overlap of the $2p_z$ orbitals of the nitrogen and oxygen atom. The spin density is distributed between the nitrogen and oxygen atom, whereby it is slightly higher on the latter, and not delocalised over the adjacent framework.[13]

The nitroxide radical is commonly generated through oxidation of the corresponding secondary amine (**Scheme 1**).[11]

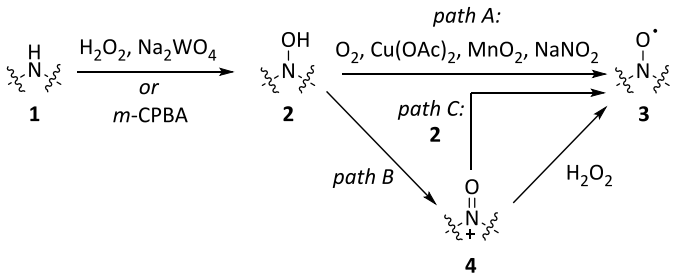

Scheme 1: General procedures to generate nitroxide radicals.

The oxidation of the secondary amine **1** to the corresponding hydroxyl amine **2** can be achieved by using an excess of H_2O_2 with a catalytic amount of Na_2WO_4, or *meta*-chloroperoxybenzoic acid (*m*-CPBA). The hydroxyl amine can be further oxidised to the nitroxide radical **3** in the presence of atmospheric oxygen or using mild oxidants such as MnO_2, $NaNO_2$ or Cu(II) salt in the presence of oxygen (*path A*).

The relatively strong tungsten(VI) oxidant can oxidise the hydroxylamine to the oxoammonium salt **4** (*path B*), which in turn is able to oxidise H_2O_2 to O_2 and reduces itself to the nitroxide radical **3**. It is also possible that the salt **4** reacts with residual hydroxyl amine **2** to form two nitroxide radical molecules (*path C*).

1.1.1 Basic Structures

The structures of nitroxides are mainly based on three cyclic families: six-membered rings (piperidines), five-membered rings (pyrrolines, pyrrolidines, imidazolines, imidazolidines and oxazolidines) or fused ring systems (isoindolines), whereby the nitroxide radical is often flanked by two *gem*-dimethyl substituted quaternary carbon atoms (**Figure 1**).

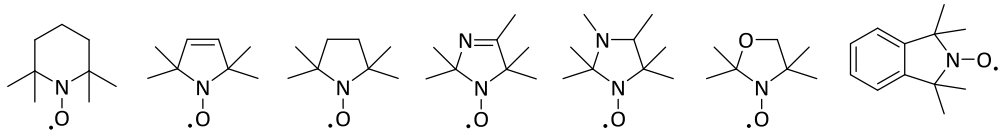

Figure 1: The parent nitroxide structures are six-membered, five-membered, or fused ring systems.

Substitutions on the C_α atoms contribute to the stability of the radical, since they sterically shield the radical to prevent reduction, which especially has to be considered in biological media (redox reaction see **Scheme 2**).[14] Furthermore, due to the absence of α-protons the nitroxide radical does not decompose to the corresponding nitrone (**Scheme 2**).[13]

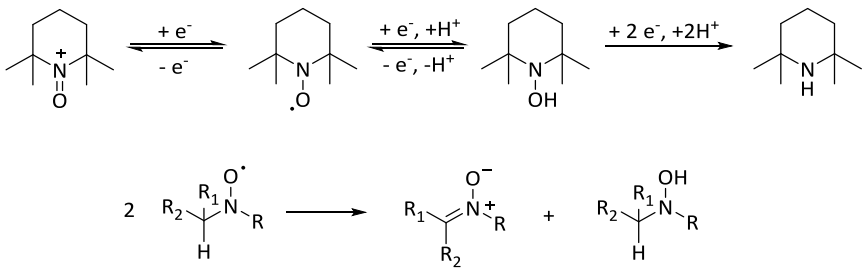

Scheme 2: Top: The redox process of a nitroxide radical. Bottom: Hydrogen atom on C_α can lead to decomposition.

The ring size of nitroxides also influences reduction processes, since it was shown that five-membered rings are more stable towards reduction than six-membered rings.[15] It is conceivable that due to the hybridisation effects of the nitrogen atom the reduction of six membered rings is favoured compared to five-membered rings.[11]
Furthermore, the stability of the radical can be increased by the replacement of the two *gem*-dimethyl groups through two *gem*-diethyl groups or bis(spirocyclohexyl) groups (**Figure 2**).[16]

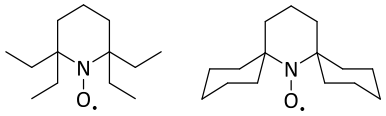

Figure 2: The nitroxide radical can be stabilised by sterically demanding groups such as ethyl- or spirocyclohexyl groups.

The higher flexibility of the ethyl groups increases the shielding effect compared to the more restricted spirocyclohexyl groups.[16,17] Besides the increased stability of the radical, it is proposed that bulky and rigid (i.e. spirocyclic) residues have a positive influence on the spin relaxation time (T_m).[11,18] Normally, spin labels with *gem*-methyl groups have an optimal T_m for a PELDOR experiment at 50 K.[11] Above 70 K the rotation of the methyl groups leads to a significant decrease of T_m.[11] Thus, increasing T_m will enable PELDOR experiments at higher temperatures that allow measurements using liquid nitrogen instead of expensive liquid helium as cooling medium, or even allow

experiments at physiological temperatures. Indeed, a comparative study made by BAGRYANSKAYA and co-workers in 2016 demonstrated that spirocyclohexyl substituents show an advantage in the temperature range of 100–180 K over standard *gem*-dimethyl groups.[19] At ambient temperature this benefit became incremental though. Yet, a year before, EATON and co-workers were able to measure a 3.2 nm distance at 295 K by PELDOR on a double labelled T4 lysozyme using nitroxide labels with spirocyclohexyl substituents.[20] Therefore, it is suggested that for room temperature PELDOR measurements T_m is not only determined by the substituents adjacent to the radical but also by the extended environment within a biomolecule.[19]

1.1.2 Selected Spin Labels and Labelling Methods

Since the development of the SDSL technique the methanethiosulfonate spin label (MTSSL, **5**) is the most frequently used label in literature, especially in EPR distance measurements.

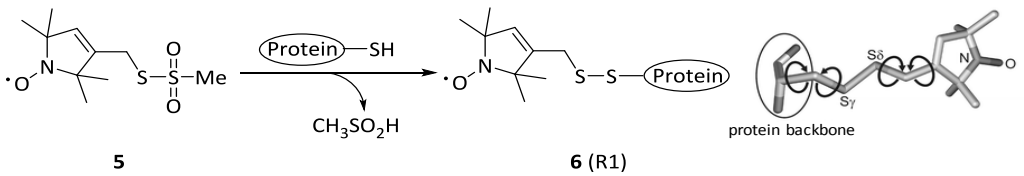

5 **6** (R1)

Scheme 3: Left: The MTSSL **5** can be attached to the protein of interest *via* a disulfide formation (linked side chain known as R1, **6**). Right: Rotating single bonds which increase the conformational space for the spin density. *Reprinted with permission from* [21]*. Copyright 2009 by Springer Science.*

MTSSL reacts selectively with thiol groups and therefore, it can be easily attached to cysteine residues in proteins *via* disulfide formation (**6**, disulfide-linked side-chain commonly known as R1).[5] Due to the small size and the flexible linker between the pyrroline-oxyl moiety and the protein backbone, the influence on the native fold of proteins is minimal. However, this flexibility allows rotational dynamics which opens a large conformational space and leads to a 'blurring' of the spin density (**Scheme 3**, right).

The internal dynamics and rotamers have been intensively studied and rotamer libraries have been developed for α-helices and β-sheets, which allow plausible distance prediction.[22,23] Yet, e.g. in 2013, MATALON *et al.* published a PELDOR study on a labelled WALP23 peptide in a lipid environment that illustrates the limitations of **6**.[24] The distance distributions were broadened and did not match the calculated distribution due to the variety of possible rotamers of the label, which are furthermore influenced by the lipid environment.[24]

In order to decrease the internal motion, MTSSL analogues have been created (**Figure 3**).

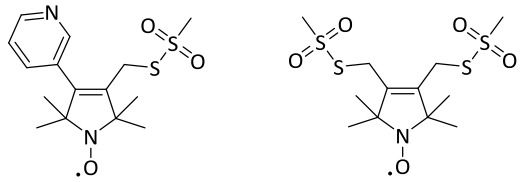

7 (R1p) **8** (RX)

Figure 3: Derivatives of MTSSL. The motion of the label is restricted through substitution on the pyrroline-oxyl moiety (**7**) or by two-point binding (**8**).

It was demonstrated that the motion of the label can be restricted either by substitution, like in the case of the 4-pyridyl substituted label **7** (R1p)[25], or by two-point binding strategies which effectively reduce the conformational freedom like in the case of label **8** (RX)[26]. The latter was successfully applied in a membrane protein study and delivered narrow distances.[27] However, its usage is obviously limited, since it requires two suitable proximal binding sides for each label.

The methanethiosulfonate linkage (**9**) is most commonly used owing to its straightforward handling but over the years different linker and labelling methods were developed. These allow orthogonal labelling strategies. Also, the aspects of increased rigidity with minimal impact on the protein's structure and the use in cells were addressed. Several linkers are illustrated in **Figure 4**.

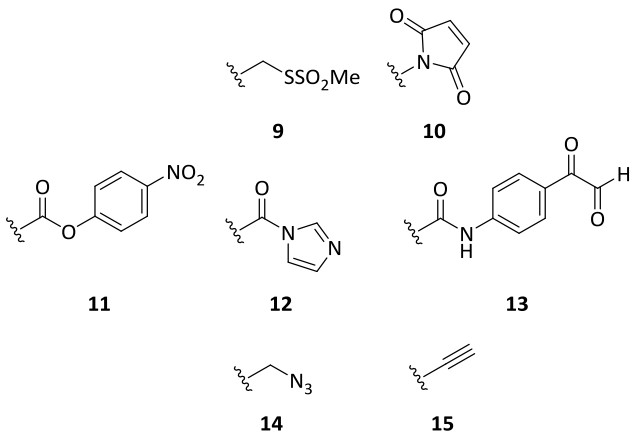

Figure 4: Selected structures of common nitroxide linkers. Top: **9** and **10** linkers react with thiol groups. Centre: Linkers address serine (**11**), tyrosine (**12**) and arginine (**13**). Bottom: **14** and **15** linkers which give the opportunity for click reactions to introduce the spin label.

Besides the MTSSL also maleimide linked nitroxides (**10**) address cysteine residues within a peptide and due to the different coupling chemistry, it can be used under mild reducing conditions.[28] However, side reactions have to be considered, like hydrolysis to the maleamic acid which in turn may react with other maleimides.[29] Besides cysteine also amino acids like serine (**11**)[30], tyrosine (**12**)[31] and arginine (**13**)[32] can be specifically addressed, which enables orthogonal linker chemistry.

Furthermore, KÁLAI *et al.* showed that nitroxide modified azides (**14**) and alkynes (**15**) can be linked to biomolecules *via* Cu(I) catalysed 'click-chemistry' and thus showed that site-selective labelling is also possible by forming triazoles.[33] Another linking strategy exploits the specific binding to polyhistidine motifs (known as His_6-tags), which are often attached to the *N*- or *C*-terminus to enable the purification of recombinant proteins. One example is the label 2,2,5,5-tetramethylpyrrolidine-1-oxyl (PROXYL) tris-nitrilotriacetic acid (P-trisNTA, **16**).

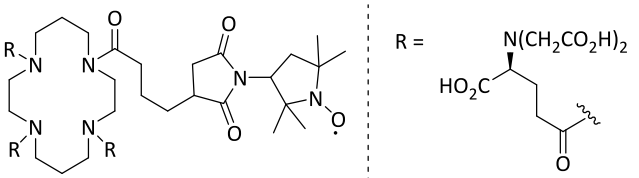

16 (P-trisNTA)

Figure 5: Structure of the P-trisNTA label (**16**). The label binds to a His_6-tag.

It was shown by BALDAUCH *et al*. in 2013 that this label binds successfully to an His_6-tagged MalE in cell lysate.[34] This may open up a new route towards the use of spin labels in living cells.

Nitroxide labels can also be introduced by unnatural amino acids *via* endogenous expression of specifically coded DNA.[35] This *in vivo* method enables the selective labelling of cysteine rich proteins. It is possible to introduce amino acids which already bear a paramagnetic centre like **17**[36] as well as amino acids which can be modified after the insertion like the popular *p*-acetylphenylalanine (modified to **18**, K1)[37] or *p*-azidophenylalanine (modified to **19**, T1)[38,39].

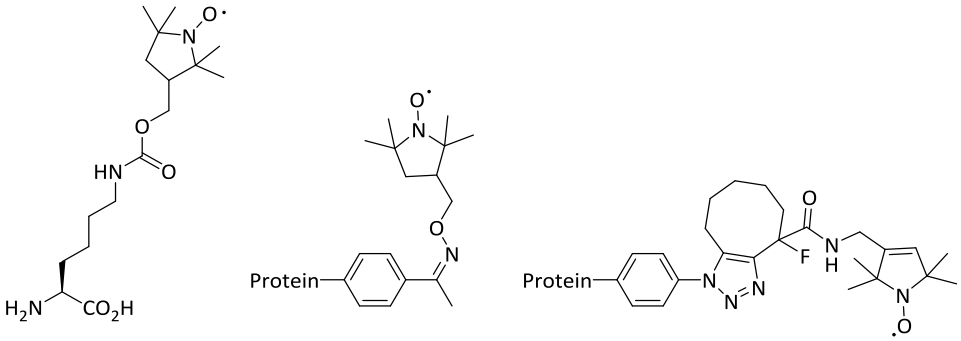

17 **18** (K1) **19** (T1)

Figure 6: The unnatural amino acids are introduced into the peptide *via* endogenous expression. In the cases of **18** and **19** the nitroxide label is attached after the expression.

The motif **19** was successfully incorporated into T4-lysozym *via* a copper-free click

cycloaddition.[38] However, these labels contain flexible linkers and the post-modification method usually requires harsh labelling conditions.[37]

Finally, non-native amino acids can also be introduced in peptide sequences during solid-phase peptide synthesis (SPPS). This has the advantage that no connection to a flexible linker is needed which then allows the investigation of peptide backbone conformations. So far, the most frequently used nitroxide peptide building block in this field is 2,2,6,6-tetramethyl-*N*-oxyl-4-amino-4-carboxylic acid (TOAC, **20**)[40] (**Figure 7**).

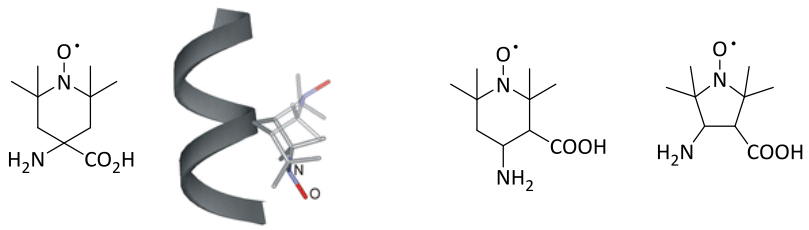

20 (TOAC) **21** (β-TOAC) **22** (POAC)

Figure 7: Structures of TOAC, β-TOAC and POAC which are used as peptide building blocks in SPPS. The motion of the TOAC is restricted due to the cyclic property of the label. *Reprinted with permission from* [21]*. Copyright 2009 by Springer Science.*

TOAC belongs to the family of $C_{\alpha,\alpha}$-disubstituted glycines and due to the cyclic structure, its flexibility is effectively restricted (the cyclic ring has one degree of freedom (**Figure 7**)). It has been applied in several studies to deliver details about dynamics[41,42], backbone conformation[40,41,43] and orientation[44] of peptides. Yet, its restricted conformational space can disrupt the functional structures of peptides.[40,45] Other labels derived from this cyclic nitroxide are β-TOAC (**21**)[46] and 3-amino-1-oxyl-2,2,5,5-tetramethyl pyrrolidine-4-carboxylic acid (POAC, **22**)[47].

To circumvent the impact of the restricted backbone conformation, STOLLER *et al.* developed the non-natural amino acid 4-(3,3,5,5-tetramethyl-2,6-dioxo-4-oxylpiperazine-1-yl)-L-phenylglycine (TOPP, **Figure 8**, **23**).[48]

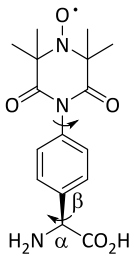

23 (TOPP)

Figure 8: Structure of the TOPP label. The label has two rotatable single bonds on the same axis as the nitroxide radical.

The label is designed based on the amino acid phenylglycine (Phg). As hinted in **Figure 8** the C_α–C_β bond and the nitroxyl group are aligned on the same axis, since the piperazine-2,6-dione moiety is nearly planar, which was confirmed by density functional theory (DFT) calculations.[48] A first study on a double TOPP-labelled alanine-rich peptide showed that the TOPP label **23** does not influence the secondary structure formation in solution and delivers a narrow distance distribution that confirms the calculated distance from the computationally modelled peptide (**Figure 9**).[48]

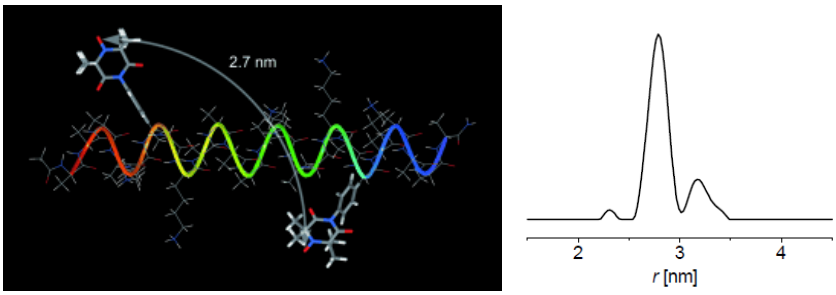

Figure 9: Left: The computationally modelled alanine-rich peptide labelled with two TOPPs. The inter-spin vector was calculated as 2.7 nm. Right: The distance distribution measured by PELDOR. The predominantly measured distance was 2.8 nm. *Reprinted with permission from* [48]. *Copyright 2011 by Wiley-VCH.*

In order to utilise its rigidity, the label was also employed in an orientation-selective PELDOR study performed by TKACH and co-workers.[49] The experimental data suggests that the label has a certain rotational freedom around the two single bonds, since a fit

to a libration of ±20° around the two bonds was required.[49] Note that through one-axis librational averaging this did not alter the position of the nitroxide moiety in space, thus this has no impact on the distance and the width of distribution. Hence, the TOPP is a promising candidate for further applications in the field of structural investigations of e.g. transmembrane peptides and it is a suitable spin label motif that allows a variety of modifications to further enhance its abilities.

2 Outline

The TOPP label **23** was developed for universal application in the field of the structural investigation of peptides without influence on the secondary structure formation. First PELDOR distance measurements on a TOPP-labelled peptide in solution demonstrated its potential as tool for conformational studies of peptides due to its remarkable rigidity compared to established labels such as the MTSSL (**5**).[48]

Thus, it is assumed that the TOPP is a suitable spin label for further applications in the field of transmembrane peptides. Furthermore, the TOPP motif can serve as basic framework for the development of new spin labels. This thesis addresses both issues and proves its usability to deliver sharp distance distributions that contain reliable information about the peptide structure, especially in lipid bilayers.

Synthesis and investigation of a TOPP double labelled transmembrane α-peptide

The first part of the thesis is about the synthesis of the rigid TOPP amino acid L-TOPP-OH **23** (**Figure 10**) and a comprehensive set of twofold labelled transmembrane α-peptides. The latter are thoroughly characterised and their straightforward and revealing application is shown in PELDOR distance measurements.

Synthesis and investigation of TOPP double labelled transmembrane β-peptides

In the second part of the thesis the development and synthesis of a new TOPP based β-amino acid D-β^3-hTOPP-OH **24** is presented (**Figure 10**). Again, a comprehensive set of twofold labelled transmembrane β-peptides is synthesised and thoroughly characterised. Additionally, computationally generated models will be discussed. This complements the final structural investigation of the transmembrane β-peptides by PELDOR.

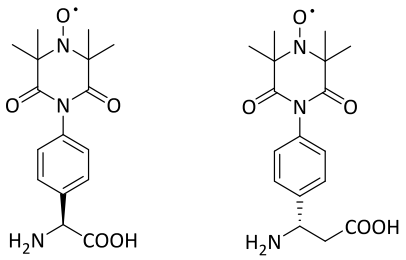

Figure 10: Structures of L-TOPP-OH (**23**) and the newly developed D-β^3-hTOPP-OH (**24**).

3 Synthesis and Structural Investigation of Labelled Transmembrane α-Peptides

There is a strong interest to investigate the structure of integral membrane proteins (transmembrane proteins), since these are responsible for a large number of processes within the membrane and on the membrane surface. It is assumed that the protein's specific function, activity and organisation is strongly depended on the interaction between protein and lipid environment. Integral membrane proteins are often deeply anchored within the lipid bilayer, which makes it challenging to investigate these by X-ray and NMR.[1–4] Alternatively, EPR techniques offer a good opportunity to examine spin labelled membrane proteins in their natural environment and can deliver details about protein-membrane interactions.[50,51]

E.g. the pulsed EPR technique PELDOR allows the determination of distances in a nanometre range (1.5–8.0 nm) between two paramagnetic centres.[52] The TOPP label (**23**, **Figure 8**) is conformationally restricted, since it has only two rotating single bonds on the same axis as the nitroxide radical.[48] The most frequently used spin label is MTSSL (**5**). In comparison to the TOPP label, MTSSL is highly flexible due to various possible rotations.

In order to get information which is directly related to the natural peptide structure, it is necessary to use spin labels which do not influence the peptide structure formation or bias the distance results by their own conformational states. Both factors can make the interpretation of the PELDOR results more complicated. Indeed, a study on a double TOPP-labelled α-peptide showed that the rigid TOPP label does not influence secondary structure formation in solution and delivers a sharp and reliable distance distribution (**Figure 9**, section 1.1.2).[48] Thus, it was shown that the TOPP label acts well in solution and allows straightforward interpretation of EPR data.

In this thesis the capability of the rigid TOPP label to deliver sharp and reliable distances

of a transmembrane peptide within a lipid environment is investigated using the PELDOR technique. Therefore, the TOPP label was re-synthesised under the aspects of simplifying the reaction/purification steps and increasing the yield. Then, a double TOPP-labelled WALP peptide, which should serve as a transmembrane model α-peptide, was synthesised. Additionally, a corresponding MTSSL-labelled WALP peptide was prepared for comparison. Both peptides were investigated in solution and lipid bilayer by circular dichroism (CD) spectroscopy to elucidate their influence on the α-helical structure formation. Finally, the performance of the TOPP within a lipid bilayer was investigated by PELDOR.

The synthesis of the peptides, and the CD and PELDOR results described in this part were published in the *Biophysical Journal*.[53]

3.1 Peptide-Lipid Interactions

As of today, membrane proteins are too complex to examine specific organisation and dynamics in the lipids environment. Hence, simple peptide models which mimic transmembrane regions of proteins as well as membrane models are used to gradually explore protein-lipid interactions. In literature, a series of different transmembrane model peptides have been studied (a detailed review see [54]). KILLIAN and co-workers introduced so-called WALP peptides (for detailed reviews see [54–56]) which were also chosen as a suitable model in this thesis.

3.1.1 WALP Transmembrane Model Peptides

WALP peptides consist of a hydrophobic stretch with alternating Ala and Leu residues, flanked by two Trp residues on both termini of the peptide sequence (**Figure 11**).[57]

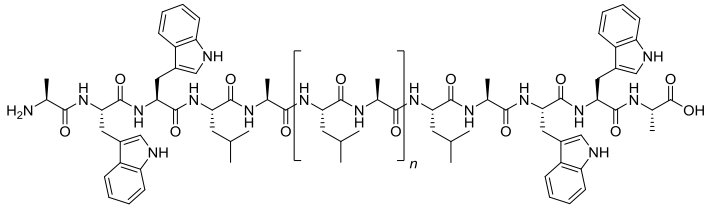

Figure 11: General peptide sequence of WALP peptides. The length of the hydrophobic core can be varied by the number (*n*) of the alternating Ala/Leu residues. The hydrophobic stretch is flanked on both sides by two Trp residues.

Ala and Leu residues are known to form an α-helical peptide structure and indeed, CD spectroscopy demonstrated α-helical structure formation of WALP peptides within a lipid bilayer.[55,57] Thus, these peptides were used to mimic the α-helical regions of transmembrane proteins, since this is one of the common motifs of natural membrane spanning proteins such as the potassium KscA channel (**Figure 12**).[57]

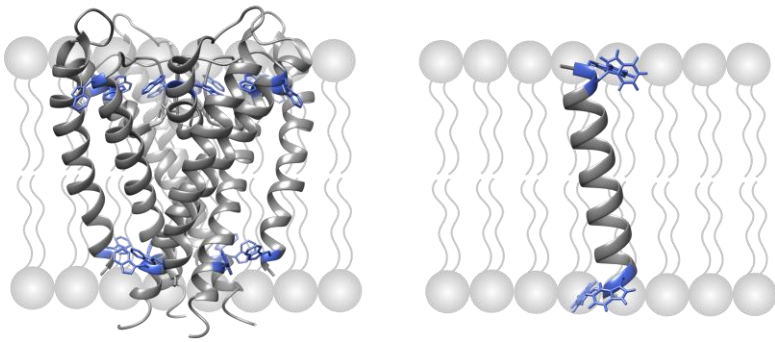

Figure 12: Basic structure of the membrane spanning protein KcsA and in comparison, the α-helical WALP peptide. Left: The structure of the potassium channel KcsA (Protein Data Base entry 1J95). The transmembrane regions are α-helices. The Trp residues are concentrated at the polar-apolar interface. Right: The structure of a WALP peptide. WALP peptides form an α-helical structure within a lipid bilayer. They were designed to mimic the α-helical transmembrane moieties of membrane proteins such as the KcsA protein.

Due to their polarity the tryptophans have a positional preference at the polar-apolar interface and are located in close proximity to the carbonyl groups of the lipids (**Figure 12**).[58,59] It is assumed that, as a result of this property, Trp residues serve as membrane anchors and orient the proteins in the lipid bilayer. E.g. this residue was found cumulative at the membrane-water interface of membrane proteins such as the potassium channel KcsA and maltoporin.[54,59,60]

The length of the hydrophobic core can be modified to fit in any kind of synthetic lipid bilayer (in turn the membrane thickness can be varied to fit a specific kind of peptide as well). Using this flexibility, peptide-lipid interactions were investigated systematically, and new insights were obtained regarding hydrophobic (mis)match situations between peptide and lipid environment.

3.1.2 Hydrophobic Matching

A hydrophobic match situation between a peptide and a lipid environment is achieved when the hydrophobic stretch of the peptide and the hydrophobic thickness of the lipid

bilayer are similar (**Figure 13**). For the description of match situations between peptide and lipid, one quantifies the thickness of a lipid bilayer by the hydrophobic thickness $2D_C$. It is defined by the length of the two opposing lipid acyl chains of the lipid bilayer starting from carbon C2 (**Figure 13**, left).[55,61]

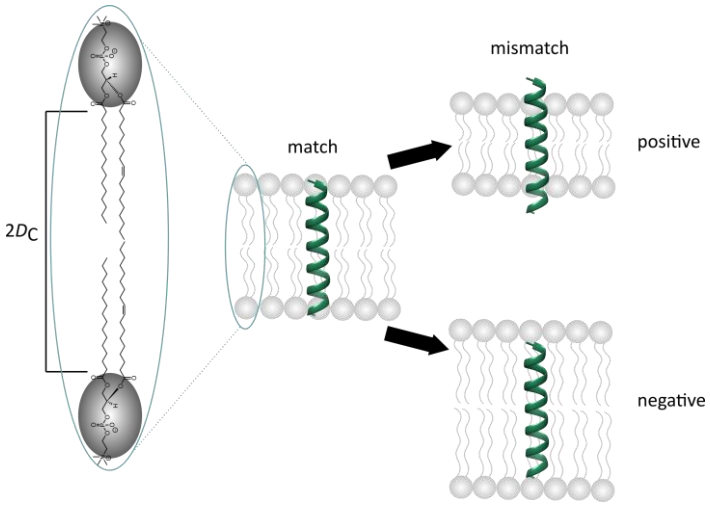

Figure 13: (Mis)match situations between peptides and lipids, and definition of the hydrophobic thickness $2D_C$. Left: Schematic illustration of the hydrophobic thickness value $2D_C$ at a phospholipid. Peptide and lipid bilayer match when the hydrophobic stretch of the peptide and the hydrophobic thickness of the lipid bilayer are similar. Right: Two different mismatch situations are possible. A positive mismatch: The peptide is longer than the thickness of the bilayer. Or a negative mismatch: the peptide is shorter than the thickness of the lipid bilayer.

Several studies were performed using WALP peptides to investigate possible organisation and dynamic processes of protein-lipid interactions. Experiments showed that WALP peptides interact strongly with the lipid environment and are sensitive to so-called mismatching situations (**Figure 13**, right).[54,55]

The idea of positive and negative hydrophobic matching was intensively studied, since it might explain phenomena which were observed in natural membranes. Many possible processes, in which the peptides or the lipids adopt the mismatch, were

postulated and examined by diverse techniques such as X-ray, CD spectroscopy, fluorescence spectroscopy, solid-state NMR and EPR.[57,62,63–66]

In case of a positive hydrophobic mismatch the peptide is relatively long compared to the hydrophobic thickness of the lipid bilayer. To avoid that hydrophobic parts of the peptides get in contact with the aqueous phase, different adaptation processes of peptides and lipids were postulated (**Figure 14**).[54,55]

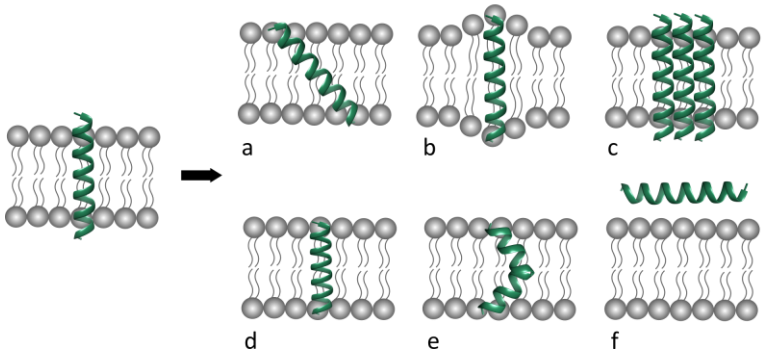

Figure 14: Possible adaptation mechanisms of peptide and lipid in a positive mismatch situation. **a**) Tilting of the peptide. **b**) Stretching of the lipid acyl chains. **c**) Aggregation. **d**) Changes in the effective hydrophobic length of the peptide. **e**) Kinking or flexing of the peptide helix. **f**) No integration.

The adaptation mechanisms depend on the considered peptide/lipid system but in general there are six motifs. The peptide can tilt to fit in the membrane (**a**), the lipid acyl chains in the vicinity of the peptide can stretch to surround the peptide (**b**), aggregation and oligomerisation can occur to minimise unfavourable peptide-lipid contacts (**c**), the peptide backbone is strained to reduce the total length of the peptide (**d**), the peptide kinks or flexes (**e**) or if the mismatch is too high, there can be exclusion of the peptide from the lipid bilayer (**f**).[54–56]

Similar mechanisms occur for a negative hydrophobic mismatch in which the peptide is shorter than the hydrophobic thickness of the lipid bilayer. In this case the unfavourable interaction arises between hydrophobic acyl chains and polar moieties and can be avoided by several adaptation mechanisms (**Figure 15**).[55]

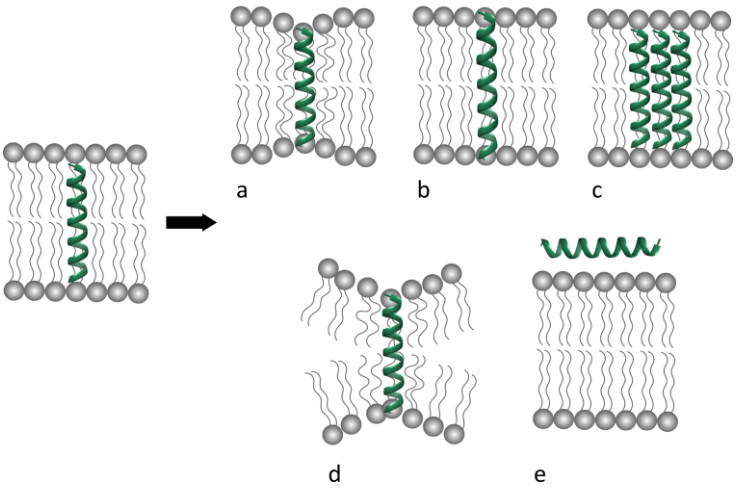

Figure 15: Selective adaptation of a negative hydrophobic mismatch. **a**) Acyl chain disordering. **b**) Peptide backbone stretching. **c**) Aggregation. **d**) Disruption of the lamellar phase formation. **e**) Exclusion.

Possible adaptations are: The length of the lipid acyl chains can change to accommodate the peptide (**a**), the peptide backbone can be stretched (**b**), peptide self-association can occur (**c**), a non-lamellar phase is formed (**d**) or no peptide is incorporated (**e**).[55]

3.2 Project Details

3.2.1 Peptide Design

A WALP peptide was chosen as model peptide, since WALP peptides show a well-defined and stable α-helical structure and a high incorporation extent into a lipid environment.[54] Furthermore, due to the Trp residues WALP peptides are highly anchored within the lipid bilayer and show a lower tendency to aggregate compared to other transmembrane model peptides.[63,64] Thus, the WALP peptide seems to be a good test peptide to estimate the TOPP performance in a lipid environment using the PELDOR technique.

In this thesis, the WALP24 peptide was chosen for further experiments. This peptide consists of overall 24 amino acids and its sequence is presented in **Figure 16**.

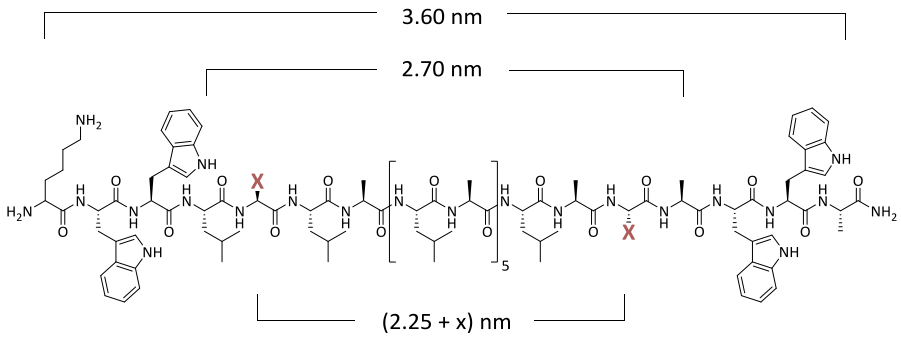

Figure 16: Sequence of the WALP24 model peptide and the estimated length/distance values: whole peptide has a length of 3.60 nm, hydrophobic stretch is 2.70 nm long. The X symbolises the labelling positions of the two labels. The inter-spin vector is estimated as (2.25 + x) nm. The variable x symbolises an additional distance value due to the lengths and orientations of the spin labels.

Compared to the commonly used WALP peptides described in literature, a lysine residue was attached to the *N*-terminus instead of a glycine and the *N*- and *C*-termini were not protected in order to increase the solubility of the mainly hydrophobic peptide. Each amino acid contributes an estimated length of 0.15 nm in an ideal α-helical

structure.[55] Thus, the length of the whole peptide is estimated as 3.60 nm. The hydrophobic stretch, which is the crucial value for selecting the right lipid system, consists of 18 amino acids and the length is estimated as 2.70 nm.

The positions of the labels (marked by X, **Figure 16**) were chosen according to two criteria: first, the intramolecular distance between the two spin labels has to be over 2.0 nm which is a requirement for a PELDOR experiment and second, the TOPP and the Trp residues should not be on the same side or at least not in direct proximity to avoid interactions between these. To take both aspects into account, position 5 and 20 seem to be a good compromise. The distance between the labelling positions was estimated as (2.25 + x) nm due to the assumed length of 0.15 nm for one amino acid.[55] The variable x should illustrate that orientation of the label, thus an additional length, must be additionally taken into account.

Consequently, two labelled WALP24 peptides were synthesised to investigate the behaviour of the TOPP label in a lipid bilayer. In one case the peptide was labelled with the rigid TOPP and in the other with MTSSL for comparison.

3.2.2 Membrane Systems

Due to the design of the WALP24 peptide its length is fixed. Thus, a matching lipid environment must be chosen to investigate the performance of the TOPP label within a membrane. To get a match situation, the length of the hydrophobic stretch of the peptide and $2D_C$ of the lipid bilayer should be similar. The hydrophobic part of WALP24 has a length of 2.70 nm. Thus, the lipid bilayer should also have a hydrophobic thickness of approximately 2.70 nm.

The literature values of $2D_C$ for particular lipids vary, since the hydrophobic thickness is influenced by the experimental conditions such as the temperature and the hydration level. Nonetheless, in consideration of the studies made by KILLIAN and co-workers $2D_C$ of 1-palmitoyl-2-oleoyl-*sn*-glycero-3-phosphocholine (POPC, $2D_C \approx 2.6$ nm) seems to be in the right range to expect a matching situation between peptide and membrane.[55]

Some selected values for POPC taken from different sources are listed in **Table 1**.

Table 1: Selected values of $2D_C$ [nm] for POPC taken from different sources.

$2D_C$ (POPC)	2.58[67]	2.71[68]	2.88[61]

The structure investigation of the WALP24 peptides within the lipid bilayer by CD spectroscopy was performed in small unilamellar vesicles (SUV). The vesicles were formed in a natrium phosphate buffer with a slightly basic pH (pH = 7.5) to prevent the acid labile nitroxide radicals from decomposition.

To potentially determine a tilt angle of the peptide within a membrane, the TOPP-labelled WALP24 was introduced into a non-matching lipid as well. Therefore, the peptides were investigated in a lipid bilayer consisting of 1,2-dimyristoyl-*sn*-glycero-3-phosphocholine (DMPC) with a hydrophobic thickness which is (on average) 0.25 nm thinner than POPC. Selected thickness values of DMPC are listed in **Table 2**.

Table 2: Selected values of $2D_C$ [nm] for DMPC taken from different sources.

$2D_C$ (DMPC)	2.30[69]	2.54[68]	2.57[61]

Hence, the peptide might tilt in DMPC to avoid a mismatch situation in the lipid bilayer. This adaptation mechanism was observed and examined with a WALP23 peptide in bilayers of varying thickness by solid-state NMR.[64,70]

3.3 Synthesis

3.3.1 Synthesis of the α-TOPP Label

The synthetic route of the TOPP label **23** was established by SVEN STOLLER and consists of 11 steps in a linear synthesis.[48] The chosen reaction conditions generate the final L-configurated label **23** with a high enantiomeric excess (*ee*) of 86%. Enantiopure peptide building blocks are desirable, since already small impurities lead to a decreased yield of the final peptide due to the formation of unwanted diastereomers. Furthermore, a separation of a large number of diastereomers by high performance liquid chromatography (HPLC) can be challenging. Finally, remaining stereochemical impurities could lead to incorrect distances measured by EPR because of the inaccurate peptide structure.

The TOPP label **23** was synthesised according to literature.[48] Due to the long and linear synthesis of **23**, there was a strong demand for a revised procedure aiming at the simplification of synthesis steps and the enhancement of yields.

The synthesis started with the protection of the amine and carboxylic function of the commercially available L-4-hydroxyphenylglycine (Hpg) (**25**), to inhibit side reactions of the amino acid backbone, followed by a conversion of the hydroxyl group into a more suitable leaving group (**Scheme 4**).

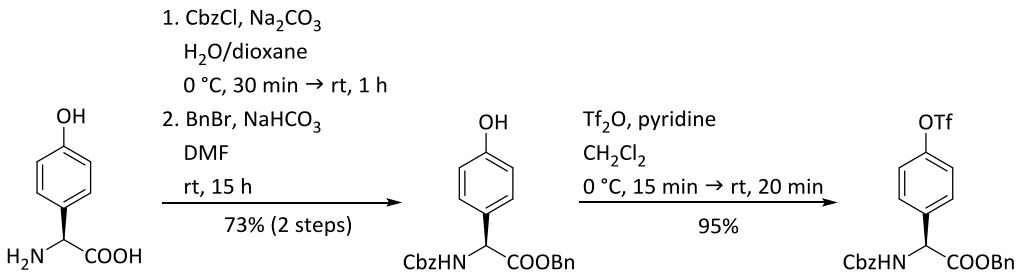

25 **26** **27**

Scheme 4: Protection of the L-4-hydroxylphenylglycine (**25**) using CbzCl and BnBr and functionalisation of the hydroxyl group to a triflate group using Tf_2O.

The protection of the amine group was performed using the standard SCHOTTEN-BAUMANN conditions. Therefore, the free amino acid **25**, dissolved in aq Na_2CO_3 and 1,4-dioxane, was treated first at 0 °C with benzyl chloroformate (CbzCl) and then warmed to room temperature (rt). The NMR of the crude product showed the pure Cbz-L-Hpg-OH. Hence, the carboxylic function was directly protected in an overnight reaction in dimethylformamide (DMF) with a benzyl group using benzyl bromide (BnBr) as electrophile and $NaHCO_3$ as base. In contrast to literature, the crude Cbz-L-Hpg-OBn (**26**) was just purified by washing the precipitate with pentane to remove excesses of BnBr.[48] The pure product **26** was verified by NMR spectroscopy. This simplification increased the yield from 57% to 73%.[48] In order to use the MIYAURA cross-coupling reaction between the aromatic system and a boronic ester, the hydroxyl group of **26** was changed to a triflate group. Therefore, the hydroxyl group was deprotonated with pyridine in DCM. Subsequently, the phenolate ion attacked the trifluoromethane-sulfonic anhydride (Tf_2O) in a nucleophilic substitution reaction with nearly quantitative conversion in overall 35 min. The resulting Cbz-L-Hpg(Tf)-OBn (**27**) was used directly without further purification in the next reaction step, since the NMR spectra again showed the pure product **27**. In literature, the direct cross-coupling between amino acid **27** and bis(pinacolato)diborone (B_2pin_2) afforded the racemic product.[48] To avoid this, the carbamate group of **27** was changed in a 2-step reaction to a benzyl-protected amine followed by the MIYAURA cross coupling (**Scheme 5**).

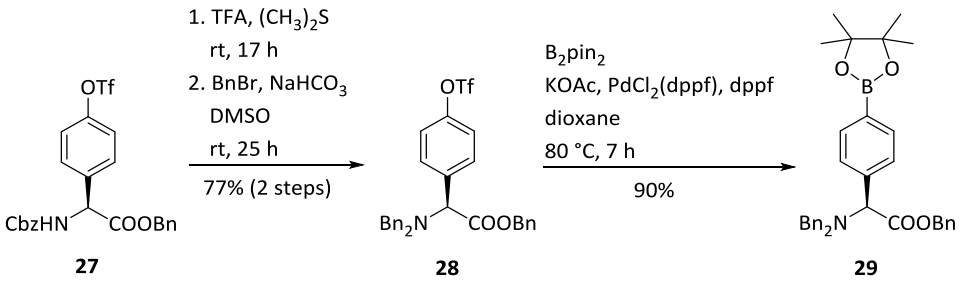

27 **28** **29**

Scheme 5: Change of the amine protecting group and MIYAURA borylation.

Therefore, compound **27** was treated overnight with a high excess of dimethyl sulfide

dissolved in trifluoroacetic acid (TFA). After removal of TFA *via* co-evaporation with toluene, the unprotected amino acid was dissolved in dimethyl sulfoxide (DMSO) and for the benzyl re-protection $NaHCO_3$ was subjoined and BnBr was added drop-wise. Bn_2-L-Hpg(Tf)-OBn (**28**) was formed in 25 h. Finally, the fully protected product **28** was obtained in a yield of 77% over two steps. It should be noticed that the elution system of the flash-column chromatography was changed, compared to literature, to pure pentane for removing excesses of BnBr.[48] The column was then flushed with pure DCM to get product **28** with an increase of yield from 69% to 77%.[48] Afterwards, product **28** was converted into Bn_2-4-pinacolboryl-L-Phg-OBn (**29**) *via* a Pd-catalysed MIYAURA borylation. This reaction was carried out under dry and inert conditions in degassed dioxane at 80 °C using B_2pin_2, $PdCl_2$(dppf) (dppf = 1,1'-bis(phenylphosphino)ferrocene) as catalyst and KOAc as base. The reaction time was decreased from 10 h to 7 h as the thin-layer chromatography (TLC) already showed full conversion after this time. Since the TLC showed only one moving spot, flash-column chromatography was used to separate the catalyst from product **29**. The product **29** was obtained in a good yield of 90%.

The basic structure of the TOPP label **23** is formed in a CHAN-LAM cross-coupling reaction (see below). However, the synthesised arylboronic ester **29** is less reactive than the corresponding boronic acid in this cross coupling.[71–73] Hence, pinacol boronate **29** was dissolved in a mixture of H_2O and acetone, and hydrolysed at rt over 2 d using $NaIO_4$ as oxidant to oxidise the released pinacol to aceton and NH_4OAc to afford Bn_2-4-dihydroxyboron-L-Phg-OBn (**30**) with a yield of 87% (**Scheme 6**).

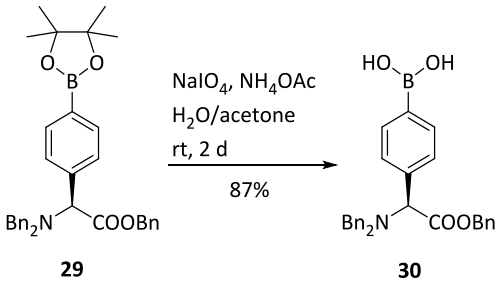

Scheme 6: Hydrolysis of the boronic ester **29** to the boronic acid **30**.

Note that the iodate selectively oxidises the released pincol to aceton whereas oxidants like H_2O_2, $NaBO_3$ or NH_2OH would further oxidise the boronic acid to phenols.[74]

Next, 3,3,5,5-tetramethylpiperazine-2,6-dione (**33**) was generated in three steps (**Scheme 7**).

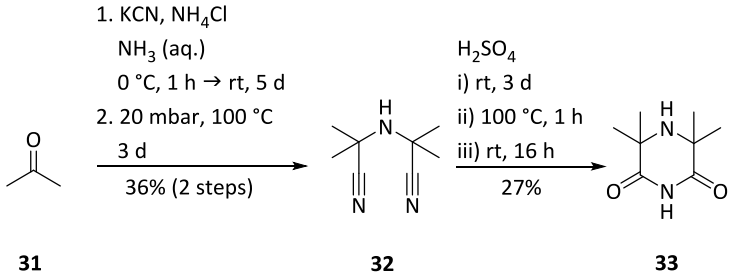

Scheme 7: Synthetic route for the preparation of 3,3,5,5-tetramethylpiperazine-2,6-dione (**33**).

In the first reaction step acetone (**31**) reacted with aqueous NH_3, NH_4Cl and KCN over 5 d at rt to 2-amino-2-methylpropionitrile and then under reduced pressure and heat over 3 d to 2,2'-imino-bis(2-methylpropionitrile) (**32**). The crude nitrile **32** was purified by distillation and was obtained in 36% over two steps. Afterwards, **32** was converted to the desired cyclic dione **33** under acidic conditions and increased temperature over 4 d. The yield was only 27%, since the work-up of dione **33** included the neutralisation with 1 M aq NaOH. Compound **33** is not stable under basic conditions, since hydroxyl

ions can attack the carbonyl function of the heterocycle and lead to the ring opening. Yet, all reagents are cheap, readily available and the reactions can therefore be performed in a relatively large scale.

The active boronic acid **30** was coupled with piperazine-2,6-dione **33** using a copper-mediated CHAN-LAM amination (**Scheme 8**).

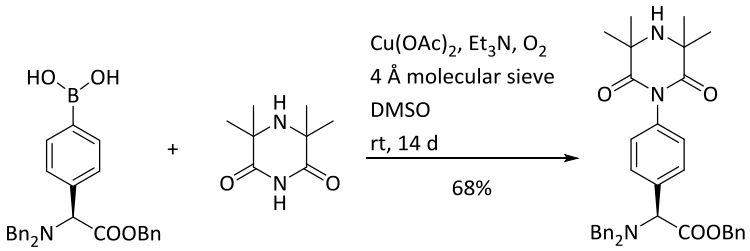

30 **33** **34**

Scheme 8: CHAN-LAM cross coupling reaction.

In contrast to other popular C–N cross coupling reactions, the CHAN-LAM reaction works under mild conditions, which are rt, the use of weak bases and 'open flask' chemistry (oxygen atmosphere).[71–73,75] Additionally, a variety of functional groups are tolerated. In this reaction C–N bond formation is favoured between the amidic nitrogen and the aromatic system. The other amine is unfavourable because it is sterically hindered due to the four methyl groups. Bn_2-4-(3,3,5,5-tetramethyl-2,6-dioxopiperazine-1-yl)-L-Phg-OBn (**34**) was formed in 14 d using triethylamine (Et_3N) as base, anhydrous $Cu(OAc)_2$, powdered molecular sieves (4 Å) and DMSO as solvent. After the reaction, instead of filtration through Celite® as mentioned in literature, a glass fiber filter was used to remove the molecular sieve and other precipitations.[48] To improve phase separation during the work-up, the aqueous phase was acidified with 1 M aq HCl. Compared to the published purification conditions, the isocratic column purification was changed to a gradient elution from 2:1 to 1:1 (pentane/ethyl acetate (EtOAc)) to decrease the retention time (t_R) of product **34**. Amino acid **34** was isolated in a yield of 68%.

In summary, the CHAN-LAM reaction can be considered as one of the crucial steps of the TOPP synthesis due to the extremely long reaction time of 14 d and the formation of the basic structural motif of the TOPP label.

The last steps of the synthetic route involved the conversion of the protecting groups into fluorenylmethyloxycarbonyl (Fmoc)-SPPS suitable groups, followed by the generation of the nitroxide radical. (**Scheme 9**).

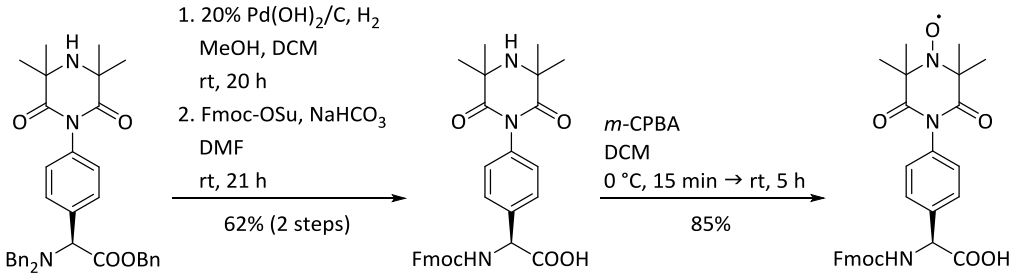

34 **35** **36**

Scheme 9: Generation of the Fmoc-protected amino acid **35**, and oxidation of **35** to obtain the desired Fmoc-L-TOPP-OH (**36**).

First, the benzyl groups of compound **34** were removed through hydrogenation on a Pd/C surface using the PEARLMAN's catalyst. Therefore, compound **34** was dissolved in methanol (MeOH) and a small amount of DCM. Then, a hydrogen flow was passed through the solution to saturate the solvent and the atmosphere in the flask with hydrogen. The reaction was stirred at rt overnight under a hydrogen atmosphere. Previous attempts to perform this reaction showed that best results were obtained in a 0.85 mmol scale. With larger amounts, a precipitation occurred which was not soluble in any kind of polar/nonpolar solvent. During work-up, instead of filtration over Celite®, as used in literature, the suspension was pre-purified through a normal pleated filter and then the filtrate was passed through a micron syringe filter to remove any traces of catalyst.[48] The Fmoc protection of the amine group was performed overnight at rt in DMF using $NaHCO_3$ and *N*-(9-fluorenylmethoxycarbonyloxy)succinimide (Fmoc-OSu),

which was preferred over the more reactive Fmoc-Cl, since it was shown in literature that this reagent supported racemisation of the amino acid.[76] During flash-column chromatography, the gradient and the amount of acetic acid (AcOH) was increased compared to literature which decreased t_R of Fmoc-4-(3,3,5,5-tetramethyl-2,6-dioxopiperazine-1-yl)-L-Phg-OH (**35**) and enabled a better separation.[48] Finally, the amino acid **35** was obtained in a yield of 62%. The final step of the synthesis was the oxidation of the secondary amine to a nitroxide radical. This oxidation was performed in DCM over 5 h using *m*-CPBA. Compared to literature the gradient was decreased in the purification step to prevent mixed fractions of the desired product Fmoc-L-TOPP-OH (**36**) and by-product *m*-chlorobenzoic acid.[48] The nitroxide radical was generated in a good yield of 85%.

Scheme 10 summarises the synthetic route. The final Fmoc-protected product **36** was obtained in an overall yield of 15%. The TOPP-labelled amino acid was further integrated in a transmembrane WALP24 peptide (see section 3.3.2) and investigated by EPR spectroscopy (see chapter 3.5).

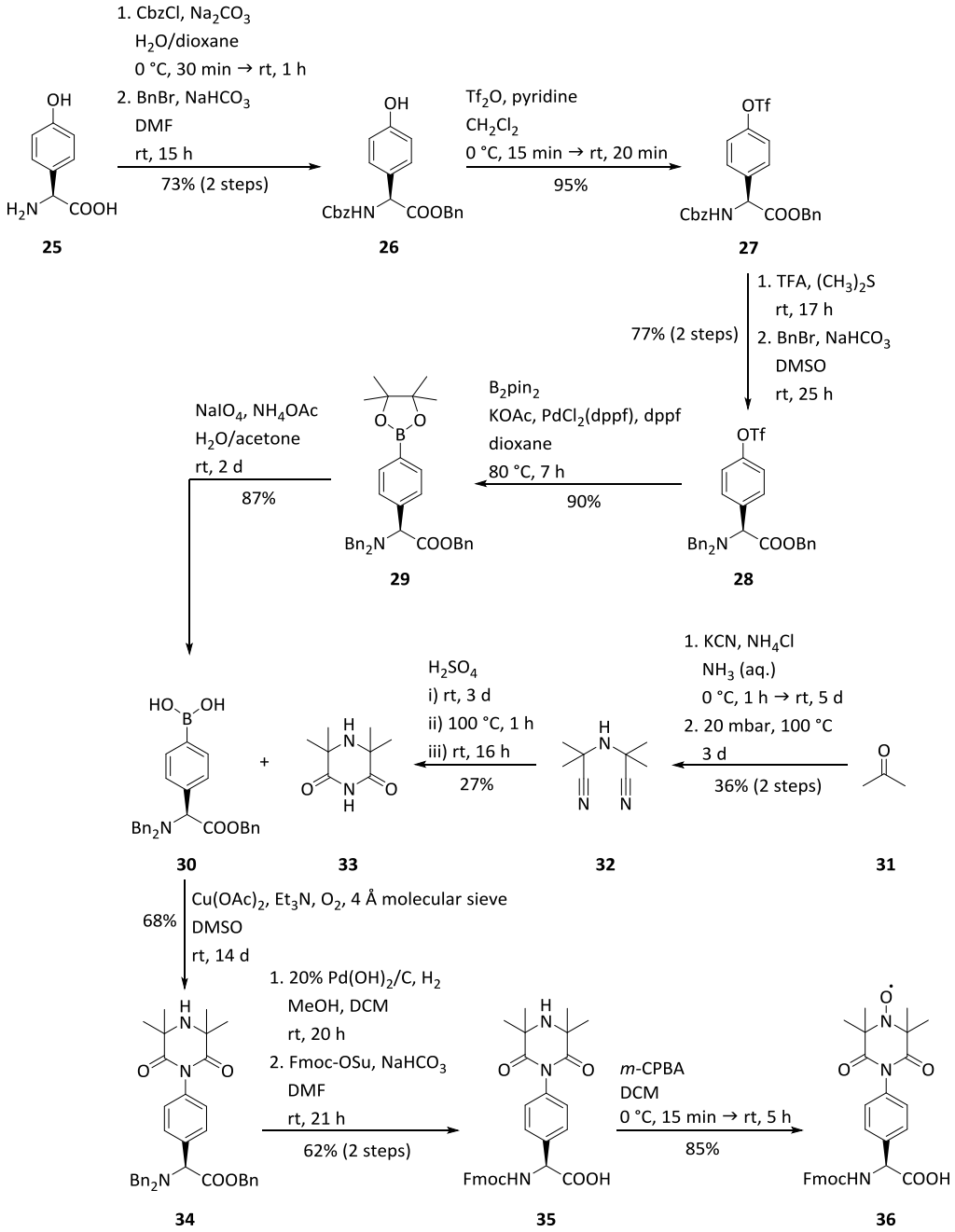

Scheme 10: Overview of the complete synthetic route. The whole synthesis of Fmoc-L-TOPP-OH **36** involving 13 isolated intermediate products. The overall yield of this route is 15%.

3.3.2 Synthesis of the TOPP-Labelled WALP24 Peptide

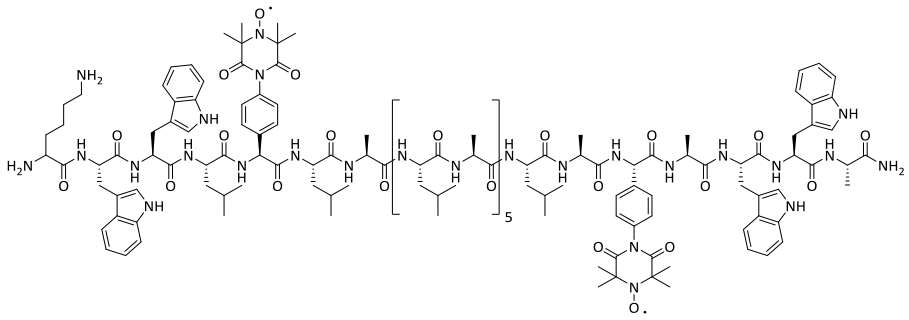

P1

Figure 17: Peptide sequence of the TOPP-labelled WALP24 peptide **P1**.

The synthesis of the WALP24 peptide labelled with TOPP (**P1**) (**Figure 17**) was performed using the efficient Fmoc-based solid-phase peptide synthesis (SPPS) by means of microwave irradiation. The cyclic SPPS strategy is based on the repetition of deprotection and coupling steps on a solid support (polymeric resin) and was developed by R.B. MERRIFIELD in 1963.[77] In 1978, Fmoc-based SPPS was published by MEIERHOFER and SHEPPARD.[78]

The main advantage of SPPS is that the peptide chain will elongate while bound to a solid support and the excess of reagents can be very easily removed by washing the solid support. Additionally, the final cleavage of the peptide from the solid support can include the simultaneous removal of the side-chain protecting groups. E.g. if the peptide is synthesised based on the Fmoc SPPS, all acid-labile protecting groups such as the *tert*-butyloxycarbonyl (Boc) group will be removed during the acidic cleavage process using e.g. TFA.

Due to the challenging and long synthesis of the TOPP label **23,** it is necessary to increase the efficiency of the peptide synthesis by choosing most suitable conditions. The synthetic route of **P1** is illustrated in the following **Scheme 11** (for experimental details see subsection 5.3.2.1).

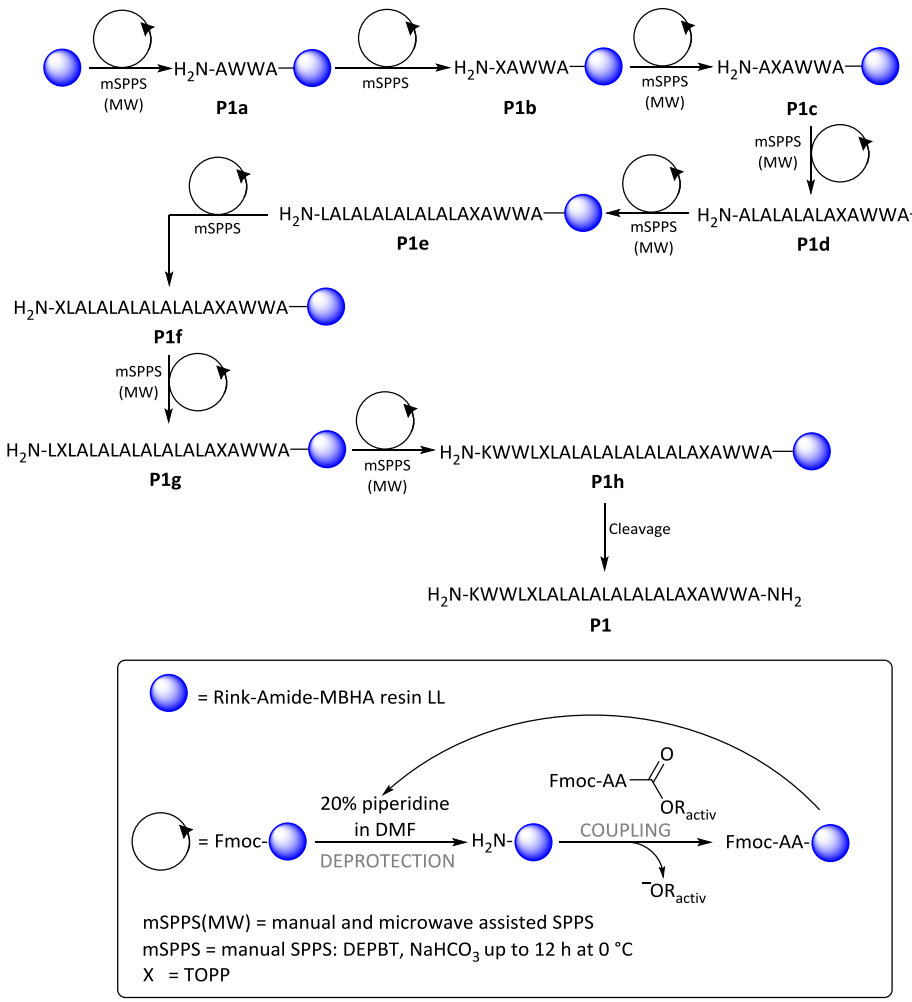

Scheme 11: Reaction scheme for the synthesis of peptide **P1**. After selected steps of the synthesis test cleavages were performed to monitor chain elongation (marked with peptide **P1a**, **P1b**, etc.). The natural amino acids were coupled as mentioned in the lower panel. The Fmoc SPPS is based on the repetition of deprotection and coupling steps on a solid support. First, the Fmoc protecting group is removed by piperidine (20% in DMF). In the coupling step the amine group of the amino acid bound to the resin attacks the carbonyl group of the active ester. A new amino acid is incorporated. The TOPP label (X) is coupled under special conditions (DEPBT, $NaHCO_3$, at 0 °C up to 12 h).

Test cleavages were performed after selected steps of the peptide synthesis to monitor the elongation process *via* mass spectrometry. Therefore, a small amount of peptide was cleaved from the resin under acidic conditions (TFA/H_2O/TIS (95:2.5:2.5, *v*/*v*/*v*)).

WALP peptides and their synthesis are well-studied, however they have never been labelled with TOPP **23**. Problems which lead to unsuccessful coupling, might occur with 'difficult sequences' such as hydrophobic peptides (intermolecular hydrophobic aggregation, e.g. lower solubility) or peptides including unnatural amino acids with relatively high steric demand such as the TOPP label **23**.[79] These difficult sequences require repeated test-cleavages to get a better control of the peptide chain elongation. Thus, manual synthesis was performed which, in contrast to automatic procedures, allows straightforward observation and adjustments in case of unsuccessful couplings.

As solid support a low loaded Rink Amide MBHA resin was utilised. Low loaded resins can minimise steric effects during the peptide synthesis due to the low level of substitutions.[80] Additionally, low loaded resins can minimise aggregation of the peptide chains during the synthesis. Aggregation is unwanted, since interchain interactions could decrease the swelling ability of the resin. Nevertheless, a good solvation of the peptide-resin complex is essential for a successful chain elongation.[79–81] Especially in the case of hydrophobic peptides, such as transmembrane peptides, aggregations could occur during synthesis.[82,83]

The solvent system also influences the efficiency of the synthesis. A mixture of *N*-methyl-2-pyrrolidone (NMP) and DMF (1:1) was chosen, since both of these solvents present good solvation properties for the peptide-resin as well as the reactants.[83,84]

The standard coupling reagent system *N*,*N*,*N'*,*N'*-tetramethyl-*O*-(1*H*-benzotriazol-1-yl)uronium hexafluorophosphate (HBTU)/ 1-hydroxybenzotriazole (HOBt), which is known to be an efficient coupling mixture with low tendency towards racemisation of the amino acid, was used to form the active ester with the natural amino acids.[85] As base *N*,*N*-diisopropylethylamine (DIEA) was utilised, which is one of the most frequently used bases in peptide synthesis. In summary, the final coupling mixture contained an excess of 5.00 equivalents (eq) amino acid, 5.00 eq HOBt, 4.90 eq HBTU and 10.0 eq DIEA dissolved in NMP/DMF. The chain elongation was performed by repeating Fmoc deprotection steps with 20% piperidine in DMF and double coupling steps of the amino

acids supported by microwave irradiation (50 °C, 25 W, 10 min). The resin was thoroughly washed between steps with different solvents (NMP, DCM and DMF) to remove residual reagents. Before insertion of the first TOPP label the **P1a** peptide sequence was examined by mass spectrometry. Since the mass spectrum included the peak of the desired product **P1a**, the synthesis could further progress by incorporating the TOPP amino acid **36** using special coupling conditions. Previous studies showed that the use of the standard peptide coupling conditions led to racemisation of the TOPP amino acid.[76] Therefore, the dry resin was transferred to a SCHLENK flask and the coupling was performed under an argon atmosphere in dry tetrahydrofuran (THF), at low temperature (0 °C) and a coupling time of 5 h using $NaHCO_3$ as base and 3-(diethoxyphosphoryloxy)-1,2,3-benzotriazin-4(3*H*)-one (DEPBT) as coupling reagent, which is known to reduce racemisation.[48,86] Additionally, to save material only 2.00 eq of amino acid **36** was used for coupling. After this step, the resin was suspended in DCM and transferred back to a syringe. Mass spectrometry verified successful coupling and the desired peptide sequence **P1b**. However, small amounts of **P1a** were observed as well, hence in a further attempt double coupling was performed with a longer reaction time of 12 h. The mass spectrum still included a peak corresponding to peptide **P1a**. Attempts to further increase the yield by additional coupling steps were dismissed to save valuable TOPP label. Therefore, after coupling the TOPP label, the free amine groups that remained uncoupled were acetylated using acetic anhydride (Ac_2O)/2,6-lutidine/NMP (1:2:7, *v*/*v*/*v*). This effectively eliminated peptide fragments with wrong sequences in the further synthesis.

Coupling of the next amino acid (Ala) (**P1c**) was again evaluated by mass spectrometry, since the coupling of the TOPP was incomplete and its steric demand might also influence the coupling of the next amino acid. Yet, the mass spectrum revealed formation of peptide **P1c** without the miscoupled sequence **P1b**.

Further chain elongation was executed under the standard microwave-assisted conditions described above for the natural amino acids and under likewise described

specific conditions for the second TOPP. It is worth to note that before coupling of the second TOPP in the peptide sequence, two additional test cleavages were performed, one after achieving peptide sequence **P1d** and the other before the integration of the second TOPP. Mass spectrometry confirmed the desired peptide sequences **P1d** and **P1e**.

The incorporation of the second TOPP label was also not efficient, hence, a third coupling was performed to increase the amount of peptide **P1f**. Free amine groups were capped as mentioned above. The coupling of the following Leucin was successful, since mass spectrometry showed the peak corresponding to the expected mass of **P1g**. After peptide sequence **P1h** was obtained, the whole peptide was cleaved from the resin under acidic condition (TFA/H_2O/TIS (95:2.5:2.5, *v*/*v*/*v*)). Triisopropylsilane (TIS) and H_2O served as scavenger to avoid side reaction during the cleavage process. Pre-purification can be achieved by precipitation of the peptide in cooled diethyl ether (Et_2O) in which the cleavage reagents are soluble.

It should be noted that nitroxide radicals are not stabile under the utilised cleavage conditions. The low pH and the reductive properties of TIS lead to the formation of hydroxyl amine (**Scheme 12**).[48,87]

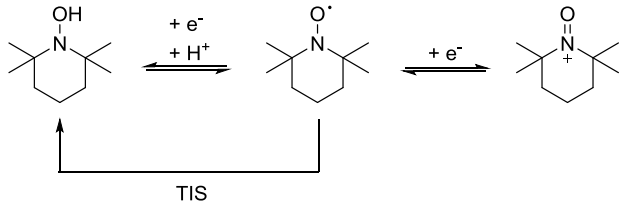

Scheme 12: Redox reaction of TEMPO. Treatment with TIS and acid leads to the reduced species.

A hydroxyl amine can be oxidised to a nitroxide radical by using copper(II) as oxidant.[48] Initially, the oxidation was performed on the purified peptide **P1** but due to the removal of impurities, the solubility of the peptide in the solvent (MeOH) decreased. Therefore, the crude peptide was treated for 2 h with $Cu(OAc)_2$ in MeOH and only then purified by

analytical HPLC (**Figure 18**) and investigated by mass spectrometry (mass spectrum see Appendix).

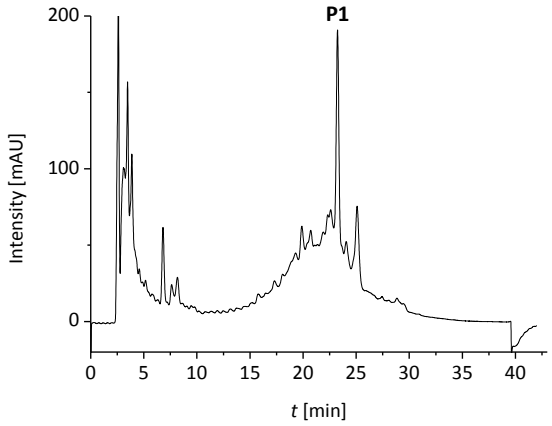

Figure 18: HPLC chromatogram of the crude peptide **P1**. Absorption was recorded at 280 nm. Analytical HPLC was performed using a gradient 80 → 100% B (A: H_2O + 0.1% TFA and B: MeOH + 0.1% TFA) in 30 min, flow 1.0 mL/min.

Because the radical might not be stable over a sufficiently long period of time, **P1** was oxidised and purified only in small amounts to provide fresh samples for each PELDOR experiment. Additional information about the stability of the radical will be given in section 3.5.1 and subsection 4.3.1.2.

3.3.3 Synthesis of the MTSSL-Labelled WALP24 Peptide

Compared to spin labels like the TOPP (**23**) or TOAC (**20**) that must be elaborately introduced into the peptide sequence, MTSSL (**5**) benefits from a much easier incorporation. In general, it is only attached to a cysteine mutated peptide after the peptides synthesis *via* disulfide bond formation.

The sequence of the cysteine mutated WALP24 peptide **P2** is illustrated in **Figure 19**.

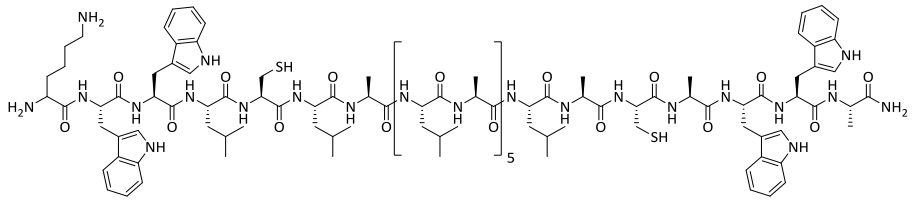

P2

Figure 19: Sequence of peptide **P2**.

Peptide **P2** was synthesised using a microwave-assisted automatic peptide synthesiser, since the peptide sequence only consists of natural amino acids. Like in the case of the manual SPPS, the synthesiser elongates the chain by repeating Fmoc deprotection steps with 20% piperidine in NMP, double coupling steps of the amino acids supported by microwave irradiation (75 °C, 25 W, 5 min) and washing steps.

For routine peptide synthesis the automation will outperform manual SPPS in terms of time and obtained yields.

As solid support Rink amide MBHA resin was used and the coupling mixture contained HOBt/HBTU (5.00 eq/4.90 eq) and DIEA (10.0 eq) in NMP. Note that the cysteine was coupled at reduced temperature (50 °C) to avoid racemisation.

After the synthesis, the whole peptide was cleaved under acidic conditions (TFA/H_2O/TIS (95:2.5:2.5, *v*/*v*/*v*)). The scavengers TIS, 1,2-ethanedithiol (EDT) and H_2O should prevent side reactions on the peptide chain. Especially EDT should suppress alkylations of the thiol groups. Then, the peptide **P2** was pre-purified by Et_2O precipitation.

Initially, peptide **P2** was purified by HPLC before attaching the MTSSL. However, due to the exposure of oxygen inter- and intramolecular disulfide bond formation occurred and was observed in the mass spectrum. Therefore, the functionalisation of the peptide with MTSSL was performed using the crude peptide dissolved in MeOH and the reaction with MTSSL could proceed overnight under an argon atmosphere. Afterwards, the labelled peptide **P3** was purified by analytical HPLC (**Figure 20**).

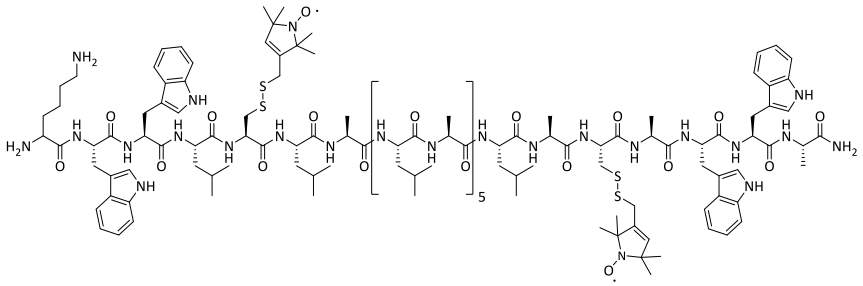

P3

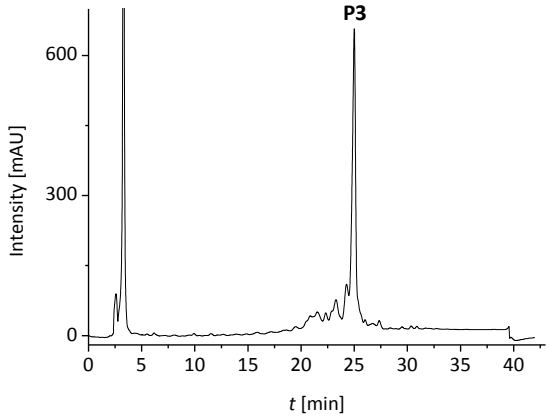

Figure 20: Top: Peptide sequence of **P3**. Bottom: HPLC chromatogram of the crude peptide **P3.** Absorption was recorded at 254 nm. HPLC was performed using a gradient 80 → 100% B (A: H_2O + 0.1% TFA and B: MeOH + 0.1% TFA) in 30 min, flow 1.0 mL/min.

To provide fresh samples for each PELDOR experiment, the labelling procedure and purification were executed only in small amounts right before those measurements.

3.4 Secondary Structure Determination by CD Spectroscopy

CD spectroscopy is a straightforward tool to investigate secondary structure formation of peptides and proteins in different environments, e.g. in solution or in lipid bilayers. It is based on the differential absorption of left- and right-handed circularly polarised light by optically active molecules such as peptides and proteins.[88]

WALP peptides were designed to mimic α-helical transmembrane regions of membrane proteins.[57] A typical α-helical peptide shows highly characteristic negative bands at around 208 and 222 nm and a strong positive band at 190 nm in its CD spectrum. This is attributed to electron transitions in the amide chromophores of the peptide bond.[89]

3.4.1 Labelled WALP24 Peptides in Solution and in Lipid Bilayer

The CD spectra of **P1** in solution (MeOH) as well as in matching (POPC) and mismatching (DMPC) lipid bilayer are illustrated in **Figure 21**.

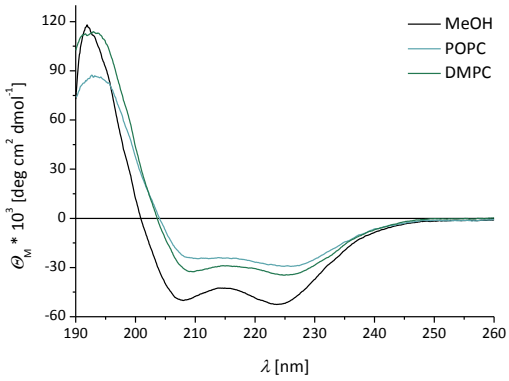

Figure 21: CD spectra of **P1** in MeOH, POPC and DMPC SUVs. Conditions in MeOH *c*(**P1**) = 9.8 μM at 10 °C. Conditions in the lipid bilayers P/L = 1/30, *c*(**P1**) = 9.8 μM, phosphate buffer (50 mM, pH 7.5) at 25 °C.

The CD spectra recorded for peptide **P1** in MeOH, POPC and DMPC show the typical pattern of an α-helical structure. In MeOH, two minima can be observed at 208 and 224 nm and a maximum at 192 nm. Compared to the solution measurement, the bands

observed in the lipid bilayers are slightly shifted to higher wavelengths. In POPC the two minima are registered at 209 and 225 nm, and the maximum at 193 nm. In DMPC the bands occur at 210, 225 and 193 nm. Changes in the environment can lead to shifts in the CD spectra, since different dielectric media can influence the electron transitions of the amide bonds in different ways.[90,91]

In summary, the obtained CD measurement suggest that the labelling with TOPP did not inhibit secondary structure formation, confirming results presented in literature.[48] Also, the situation of a mismatch between peptides and membrane thickness such as in the case of the DMPC bilayer did not influence the formation of the α-helix.

Obviously, differences in the intensity of the ellipticity Θ_M can be explained with a variance of peptide concentration within vesicles, since the peptide incorporation within the lipid bilayer was not quantitative and can vary between experiments with the same conditions.

Similar to **P1,** peptide **P3** showed an α-helical structure in all the tested environments (**Figure 22**).

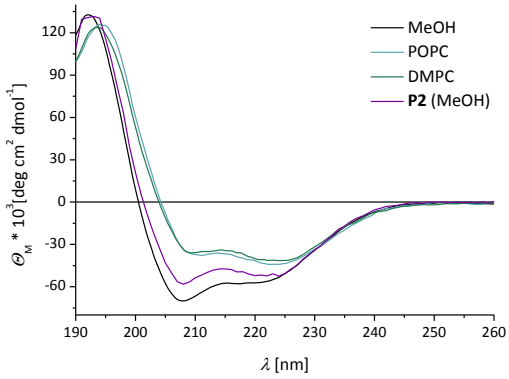

Figure 22: CD spectra of **P3** in MeOH, POPC and DMPC SUVs. Comparison with **P2** in MeOH. Conditions in MeOH *c*(**P2**/**P3**) = 33.2 μM at 10 °C. Conditions in the lipid bilayers P/L = 1/30, *c*(**P3**) = 16.6 μM, phosphate buffer (50 mM, pH 7.5) at 25 °C.

In MeOH, the CD spectrum of **P3** shows two minima at 208 and 217 nm and a maximum at 192 nm. In the case of the non-labelled peptide **P2** in MeOH the bands are like **P3**,

only the second minimum is shifted to 224 nm. Due to the different physical properties of the cysteine's thiol group compared to those of the MTSSL, small changes like this one can occur in a CD spectrum. The bands observed for **P3** in the lipid bilayers are again slightly shifted to higher wavelengths compared to those measured in MeOH. In POPC the CD spectrum reveals two minima at 210 and 223 nm and a maximum at 194 nm. In DMPC the bands occur at 210, 224 and 193 nm. These slight shifts and the variance in the intensity of the ellipticity Θ_M can also be explained through the change in environment and the peptide uptake into the vesicles.

It is worth to note that the distance measurements of peptide **P1** and **P3** by the PELDOR technique had to be performed at strongly decreased peptide-to-lipid ratio (P/L) (around 1/6000) to avoid aggregation effects which were observed at a P/L ratio of around 1/250.[53] Aggregation leads to an increased number of measurable distances between spin labels, since not only the intramolecular distance will be measured but also intermolecular distances.

Aggregation effects may also lead to changes in the secondary structure which are detectable by CD spectroscopy.[92] Thus, **P3** was investigated at P/L ratios of 1/50 and 1/100. CD spectra with different P/L ratios are illustrated in **Figure 23**.

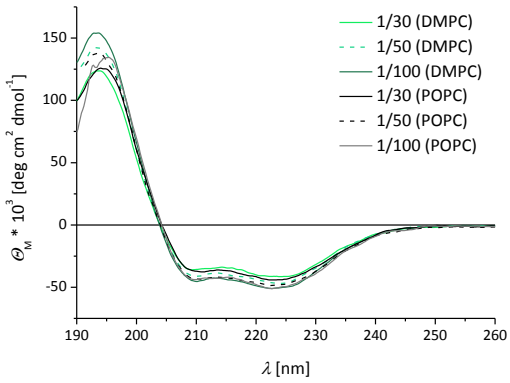

Figure 23: CD spectra of **P3** in POPC and DMPC SUVs with different P/L ratios. Conditions in the lipid bilayers P/L = 1/30, 1/50, 1/100 *c*(**P3**) = 16.6 μM, phosphate buffer (50 mM, pH 7.5) at 25 °C.

Assays with higher P/L ratios were not reported, since the transparency of the peptide-lipid suspension decreased drastically. Consequently, the CD signal intensity is sophisticated because the transmitted light was reduced due to light scattering and absorption by the sample.

All CD spectra in **Figure 23** reveal the typical pattern of an α-helix with two minima around 210 and 223 nm, and a maximum around 195 nm. No changes in the secondary structure formation can be observed, since the spectra do not show any differences within the different P/L ratios besides a slight increase of the intensity of Θ_M from 1/30 to 1/100. This observation might be explained by a more quantitative uptake of the peptide into the lipid bilayer, i.e. a higher final concentration of peptide within the ubiquitous vesicles (1/100).

In summary, for the studied range of P/L ratios, no changes of the crucial α-helical structure formation were observed by CD spectroscopy. This hints that either no aggregation occurs within this range or aggregation occurs and the α-helical structure is preserved. An EPR study about aggregation of a WALP23 by HUBER and co-workers demonstrated that WALP23 peptides were not associated in the liquid-crystalline phase of the lipid but in the gel phase.[51] Compared to the liquid-crystalline phase, the gel phase is solid-like and the acyl chains are highly ordered.[93] The PELDOR experiments were carried out at 50 K which means that the membrane is in the gel phase. All CD experiments were performed at 25 °C, thus in the liquid-crystalline phase.

3.5 Inter-Spin Distance Determination by PELDOR

The pulsed EPR technique PELDOR is frequently employed to determine distances between two paramagnetic centres. The PELDOR experiment is based on a two-frequency four pulse sequence (**Figure 24**).[94]

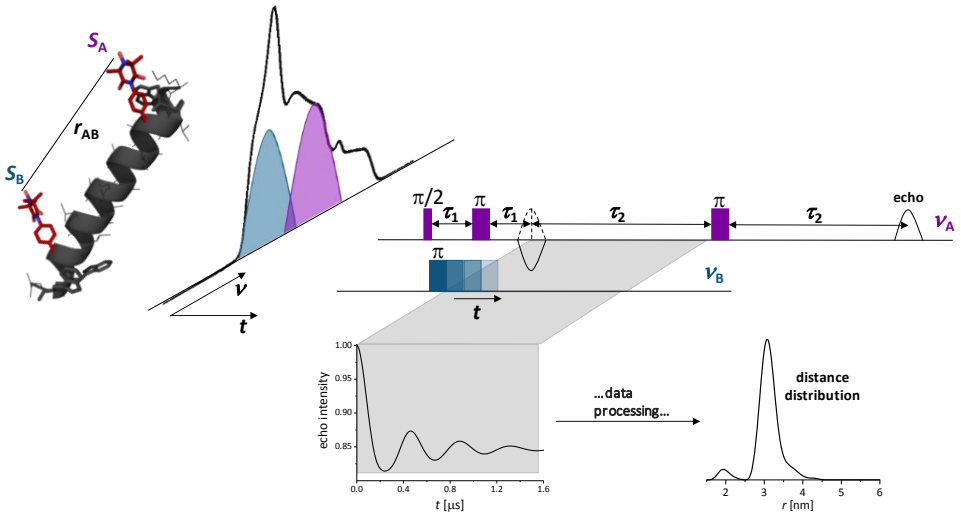

Figure 24: General principle of the two-frequency four pulse PELDOR experiment. Two different spin systems (S_A and S_B) are addressed selectively by two different frequencies (ν_A and ν_B, respectively). The pump pulse ν_B occurs at different times and influences the intensity of the echo signal of S_A. The resulting time trace includes the distance information and data processing leads to the distance distribution.

Twofold labelled biomolecules show inhomogeneous electron spin resonance spectra in which spin systems S_A (violet) and S_B (blue) can be selectively addressed by two adjusted frequencies ν_A and ν_B, respectively. In a series of experiments the detected spin system S_A is excited by a spin echo sequence while S_B experiences a pump pulse excitation. Since both spins are dipolar coupled, the echo intensity of S_A can be modulated by varying the time at which the pump pulse occurs. The resulting time trace of the spin echo is characterised by a dipolar frequency which is proportional to $1/r^3$. Usually, distances up to 10 nm can be observed.[95] Appropriate processing of the time trace data reflects the spatial uncertainty, mainly due to a certain conformational

allocation of the label, and thereby gives a distance distribution. To get sharp distance distributions, it is necessary to use rigid spin labels like the TOPP label **23**, which has only two rotating single bonds on the same axis as the nitroxide radical. A study performed in solution on an α-helical alanine-rich peptide showed that this label gave sharp, reliable distance distributions. Thus, it was demonstrated that the TOPP label **23** performed well in solution.[48]

A previously published PELDOR study of a WALP23 peptide in a lipid environment was carried out using different flexible labels such as the MTSSL (**5**).[24] The distance distributions were broadened and did not match the calculated distribution due to the different possible conformations of the label which were in turn additionally influenced by the lipid environment.[24]

In this study, the capability of the rigid TOPP label within a lipid environment is investigated by PELDOR. Two WALP24 peptides (hydrophobic stretch ~ 2.7 nm) were used for the study, which were labelled in one case with TOPP (**P1**) and the other with MTSSL (**P3**) for comparison. The PELDOR experiments were performed in two different lipid systems, namely in POPC (match situation, $2D_C$ = 2.58–2.71 nm) and DMPC (mismatch situation, $2D_C$ = 2.30–2.54 nm).[55,68] To evaluate these results, theoretical structures of the peptides were prepared.[53,55,68] Molecular modelling and EPR experiments were performed by KARIN HALBMAIR, MPI for Biophysical Chemistry.

3.5.1 Results and Discussion of Measurements in Solution

The PELDOR experiments were carried out at Q-band frequencies and corresponding fields (34 GHz/1.2 T) at 50 K using peptide concentrations of 20–30 μM. The PELDOR results of both peptides **P1** and **P3** in MeOH (20% glycerol) are illustrated in **Figure 25**.

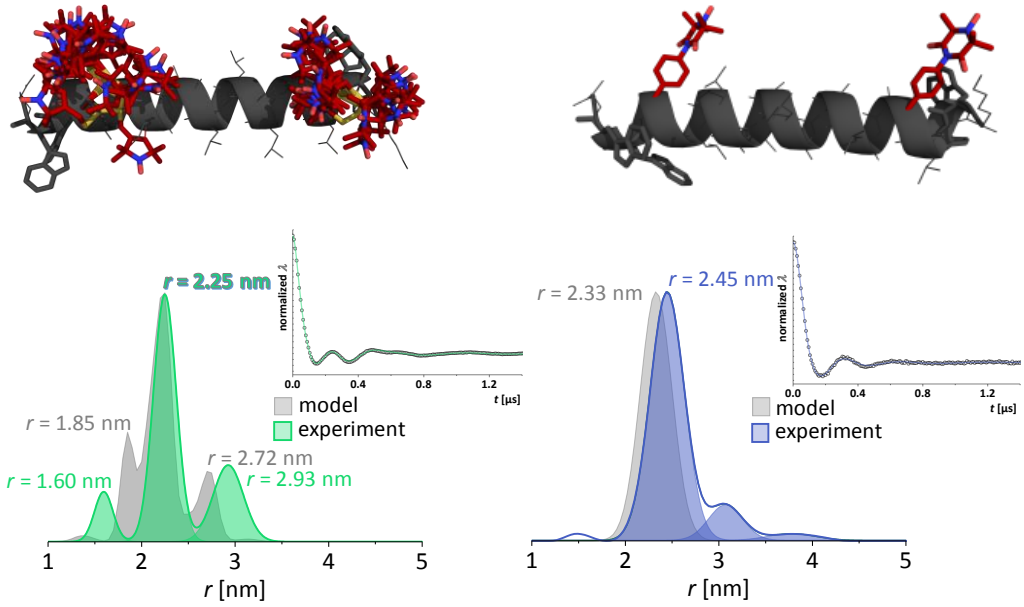

Figure 25: Top: Theoretical structure obtained by molecular modelling for (left) MTSSL-labelled WALP24 peptide **P3** with overlay of possible rotamers of the label and (right) TOPP-labelled WALP24 peptide **P1**. Bottom: Results of the PELDOR experiments in MeOH. Left: Distance distribution of peptide **P3** including the time trace. Right: Distance distribution of peptide **P1** including the time trace. Distance distributions derived from (different) rotamer models are shown for comparison (grey).

The time traces of both labels show visible dipolar oscillations. However, the modulation of the MTSSL-labelled peptide **P3** includes multiple frequencies and leads to a distance distribution with three discernible maxima. The maxima correspond to one main inter-spin distance of r = 2.25 nm and two others at r = 1.60 and r = 2.93 nm. This pattern was expected, since a calculation of the distance distribution using a theoretical model of **P3** and possible rotamers of MTSSL (obtained from rotamer libraries[23,96] using the open-source program: MMM (ETH Zürich)) results in a similar distribution, illustrated in **Figure 25** left.

Thus, already in solution the interpretation of distance measurements using MTSSL is more complex, since the distance information is biased by different energetically favoured conformations of the label.

Notably, the deviations between model and experiments could occur due to differences between a simplified structural model and experimental behaviour of the peptide **P3** in solution.

Compared to the multiple-distance distribution of MTSSL, the time trace of the TOPP-labelled WALP24 **P1** in MeOH shows one dominating dipolar frequency and the analysis gave a single-peak distance distribution with a maximum at r = (2.45 ± 0.05) nm and a narrow half width at half maximum (HWHM) of 0.2 nm (**Figure 25** right). The comparison with the calculated distance distribution, which was estimated from a simplified theoretical model of **P1** and shows a maximum at r = 2.33 nm (for details see literature[53]), demonstrates that both values are in good agreement ($\Delta \approx 0.1$ nm).

A minor peak occurs in the distance distribution of **P1** at approximately r = 3.00 nm, which in previous published studies was assigned to be a not well-defined species of the peptide.[48] The CD measurement did not show any indication of a different structure than α-helical. Moreover, this population is minuscule compared to the main distance distribution.

Since the TOPP is a quasi-rigid label, orientation selection might occur in the PELDOR distance measurement which influences the distance determination. Therefore, to exclude the possible effect of orientation selectivity, more detailed studies were performed and it was proven that there is no orientation selection under the utilised experimental setup.[53]

The labelling efficiency, i.e. the number of spins within the molecule, can be determined by the direct comparison of the spin concentration measured by CW EPR spectroscopy with the total peptide concentration determined by e.g. ultraviolet (UV) absorbance of the tryptophans. For the MTSSL-labelled peptide **P3**, labelling efficiencies reached 80–90% for different batches.

Due to a potential overlap of the TOPP label and the tryptophan residues in the UV

absorption spectrum, the labelling efficiency of **P1** had to be estimated by an alternative approach: In this case the labelling efficiency was approximated through the software DEERanalysis (see reference[53]). Here, PELDOR results (i.e. the modulation depth) from **P3** (for which the spin concentration was known) were correlated with results for **P1**. According to this procedure labelling efficiencies reached about 65–75% for different batches.

The decreased labelling efficiency of **P1** can be further examined: It is known that five-membered ring nitroxides are more stable towards reduction than six-membered rings.[11] However, experiments on the Fmoc-protected TOPP amino acid **36** showed that after purification with HPLC and lyophilisation a small amount of the radical underwent reduction (**37**, **Figure 26**).

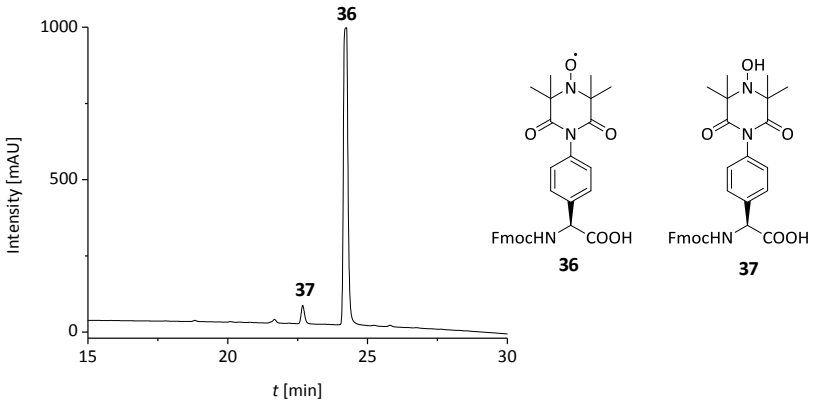

Figure 26: HPLC chromatogram of the Fmoc-protected TOPP label **36**. Absorption was recorded at 215 nm. Analytical HPLC was performed using a gradient 10 → 100% C (A: H_2O + 0.1% TFA and C: MeCN + 0.1% TFA) in 30 min, flow 1.0 mL/min. Investigation of the stability of the nitroxide radical after HPLC purification and lyophilisation. Both species were observed, the EPR active radical species **36** and the inactive hydroxyl amine species **37**.

In the HPLC chromatogram the radical species of the α-TOPP label **36** and a small amount of the hydroxyl amine species **37** are observed. The mass spectrum gave no hint for this observation.

Further stability studies were performed with the β^3-hTOPP label **24**. For more details see subsection 4.3.1.2.

3.5.2 Results and Discussion of Measurements in Lipid Bilayers

The distance measurements in a lipid environment were performed in multilamellar vesicles (MLVs) using deuterated phospholipids POPC and DMPC in a P/L ratio of around 1:6000 and a peptide concentration of approximately 20 μM (which translates into a spin concentration of 40 μM if the labelling efficiency was 100%). An aggregation study within DMPC (mismatch situation) demonstrated that at this ratio clustering of peptides did not occur and thus, intermolecular distances did not influence the experiment.[53] Normally, WALP peptides show no tendency to aggregate in a matching situation and slightly aggregate to a dimer in mismatch situation at very high P/L ratio of ~1:30.[63] It should be mentioned that in literature self-association experiments were carried out at an extremely low final peptide concentration (≤ 1μM) within the lipid bilayer.[63,97] Thus, higher concentrations might force the peptides to form aggregates. Additionally, it is important to note that PELDOR experiments were carried out at 50 K which means that the membrane is in the gel phase. This phase is solid-like and the acyl chains are highly ordered.[93] Experiments in the gel phase showed a preferred formation of oligomerises compared to the liquid-crystalline phase.[97,98] Nonetheless, a simple decrease of the P/L led to the desired monomeric state of the peptide at 50 K. The results of the measurements in DMPC and POPC are illustrated in **Figure 27**. For comparison, the solution measurements are also shown.

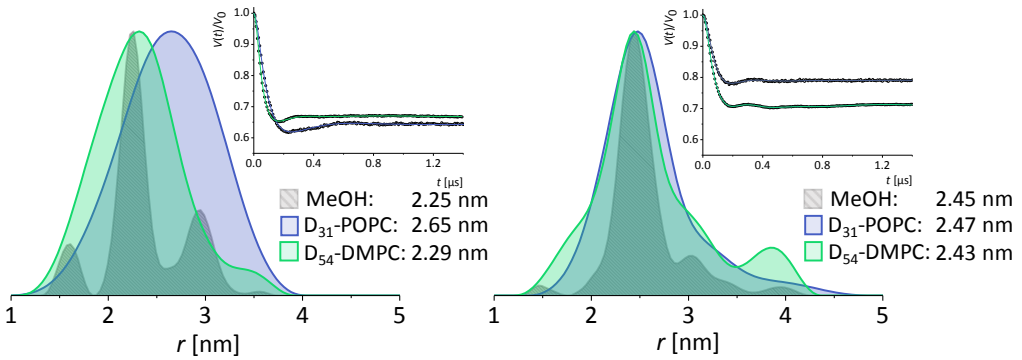

Figure 27: PELDOR traces and distance distributions of **P1** and **P3** in MeOH, POPC and DMPC. Left: MTSSL-labelled peptide **P3**. Right: TOPP-labelled peptide **P1**.

In the case of the MTSSL-labelled peptide **P3**, the PELDOR experiment gives a different distance for each environment and compared to the measurement in MeOH the distributions are massively broadened. This presumably results from an increased number of energetically favourable rotamers. All PELDOR distance distribution maxima (*r*) and the distribution widths (HWHM) of **P3** and **P1** in the different environments and the $2D_C$ values for POPC and DMPC are summarised in **Table 3**.

Table 3: PELDOR distance *r* [nm] and the HWHM values [nm] of **P3** and **P1** in the different environments and the $2D_C$ values [nm] for POPC and DMPC.

		P3 (MTSSL)		**P1 (TOPP)**	
	$2D_C$	***r***	**HWHM**	***r***	**HWHM**
MeOH	-	2.25	a)	2.45	± 0.2
POPC	2.58–2.71	2.65	± 0.6	2.47	± 0.4
DMPC	2.30–2.54	2.29	± 0.5	2.43	± 0.4

a) No specification in the width of the distribution, since it consists of multiple peaks.

In DMPC the distance of *r* = 2.29 nm is slightly larger (Δ = 0.04 nm) than in MeOH. This might be in the range of experimental error (no error was determined for MTSSL, for TOPP the error was 0.05 nm). The difference of Δ = 0.4 nm in POPC (measured distance *r* = 2.65 nm) is more conspicuous. Compared to solutions the environment of a

phospholipid bilayer is inhomogeneous due to its amphiphilic nature – hydrophobic core and hydrophilic headgroup region. Because of its dominant hydrophobic character, it was expected that the MTSSL is preferentially oriented towards the hydrophobic lipid chains.[24,99] But the results of the PELDOR measurement might indicate that the nitroxide moiety is favourably located in the interface of the head group region and acyl chains, since the measured distances between the nitroxides reflected $2D_C$ of the lipid bilayers. This is supported by a previous EPR study performed by FREED and co-workers about the behaviour of spin-labelled lipids in the gel phase.[100] The authors suggest that the spin label is excluded from the highly organised core region (due to the gel phase) of the lipids and located at the interface of the head and chain region. As mentioned above, the presented PELDOR experiments were carried out at 50 K. Thus, the lipids are also in the gel phase and a very similar effect can be expected in which the two MTSSL bend towards the 'inner and outer' interface, respectively. This corresponds to a small separation in case of DMPC and a larger for POPC.

As mentioned in section 3.1.2, different adaptation mechanisms to avoid a mismatch situation between peptide and lipid are possible. A conceivable adaptation to a mismatch can be a distortion of the α-helical structure. However, this was not expected for the peptides because of the results for the TOPP-labelled WALP peptide (see below).

In conclusion, by using MTSSL the information about the internal peptide structure and possible responsive actions of the peptide to a mismatch situation, like tilting, compression, or kinking (a, d and e, **Figure 14**), within a lipid bilayer are massively influenced by the label's conformational bias. Hence, their interpretation becomes increasingly challenging.

On the contrary, the PELDOR distance measurement using the rigid TOPP label did not show any dependence on the lipid environment. The reported distances are all close to r = 2.45 nm (**Figure 27**, **Table 3**). Additionally, the distance distributions are only slightly

broader than those in solution ($\Delta \approx 0.2$ nm). Taking these distance results into account, two assumptions can be made, either the peptide tilted to fit in the membrane or the lipid chains in vicinity to the peptide stretched to accommodate the peptide. All the other possible adaptations can be excluded because these lead to a change of the inter-spin distance (compare **Figure 14**). Both adaptations have been observed for WALP peptides before.[64,101] In the present study, the MTSSL-labelled peptide **P3** delivered a shorter distance of about $r = 2.3$ nm in DMPC, which indicates that the lipid acyl chains do not stretch. Therefore, the study points towards the tilting mechanism, which remains to be further elucidated. In turn, the rigid TOPP-labelled peptide seems to be a promising test peptide for ongoing projects which aim at the development of an EPR-based method to observe the tilt angle within the lipid bilayer.

3.6 Summary: Labelled WALP24 Peptides

In this part the synthetic route towards the α-TOPP label **23** was thoroughly described and the importance of mild reaction steps that preserve the stereochemistry of the amino acid was highlighted. The α-TOPP label **23** was successfully re-synthesised with substantial simplifications during the purification steps that shortens this otherwise time- and material-consuming linear synthesis.

Solution distance measurement by PELDOR demonstrated that the rigid TOPP label is a suitable label for distance measurements.[48] In this study the TOPP label performance in a lipid environment was investigated. Therefore, a TOPP-labelled WALP24 (**P1**) and a MTSSL-labelled WALP24 (**P3**) were effectively synthesised and it was demonstrated by CD spectroscopy that the α-helical structure formation was not hindered due to the labels.

Already in solution, the distance measurements by PELDOR showed impressive differences between the two label types: The TOPP label delivered one distinct distance while the MTSSL label delivered a multiple-distance distribution. Thus, MTSSL clearly gave information on the peptide that is biased by the conformation of the label and makes the interpretation of the results more challenging.

The measurements in a lipid environment proved even more that the TOPP label is a suitable label for the structure investigation of transmembrane peptides, since it again delivered a constant distance of approximately $r = 2.4$ nm and a sharp distance distribution in POPC and DMPC. Thus, the inter-spin distance was not influenced by the environment. Compared to that, the flexible MTSSL delivered a different distance in each environment and the distributions were extensively broadened.

In summary, it was demonstrated that the TOPP label is a useful label to investigate peptides in different environments as it delivers reliable distances directly related to the peptide structure, whereas the MTSSL gives information that is biased by the conformation of the label.

3.7 Extended Results and Outlook for the α-TOPP Label

3.7.1 Enhancement of the TOPP Rigidity

So far, it was suggested that the rotation around the C_α–C_β and C–N bond is restricted and that the two ring systems preferably adopt a perpendicular orientation (**Figure 28**).

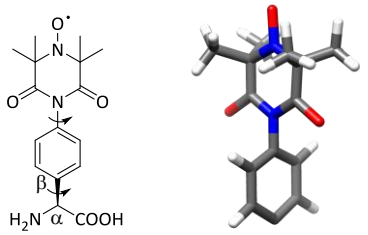

23

Figure 28: The TOPP label **23** allows rotation about two single bonds which are on the same axis as the nitroxide moiety. Quantum mechanical calculations suggested that the two ring systems are oriented in perpendicular planes.

However, high-field/frequency (3.5 T/94 GHz) orientation-selective PELDOR measurements showed that the TOPP label **23** undergoes subtle orientational modifications that can only be detected with difficulties in the experiment and further require more complex theoretical treatment/modelling.[49] The experimental data suggests that the label has a certain rotational freedom around the two single bonds, since the data fit to a libration of ±20° around the two bonds. The synthesis of a more rigid TOPP label derivative has become a main goal of a new research project. Several possible synthesis concepts and preliminary results will be described in the following part in which one of the still existing 'rotating single bonds' (C–N bond) will be restricted by substitution at the aromatic moiety (**Scheme 13**). Thus, compared to the TOPP label **23** only one degree of freedom will remain, which might allow simplified theoretical treatment/modelling in orientation-selective experiments.

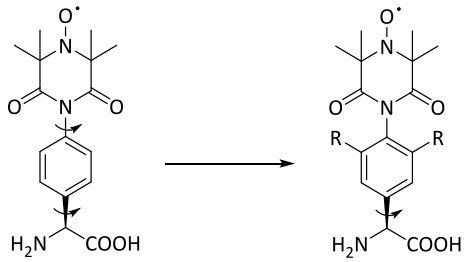

Scheme 13: Enhanced restricted structure of the TOPP label. Substitution of the aromatic moiety should stop libration of the C–N bond.

The insertion of alkyl groups in *ortho*-positions to the piperazine-2,6-dione moiety at the aromatic ring should increase the rotation energy. In a first approach the suitability of *iso*-propyl groups was tested. Preliminary but extended studies on an *iso*-propyl derivative of the TOPP label are included in the Appendix and should be consulted in future attempts.

A conceivable retrosynthetic route which is mainly based on the α-TOPP synthesis is illustrated in **Scheme 14**.

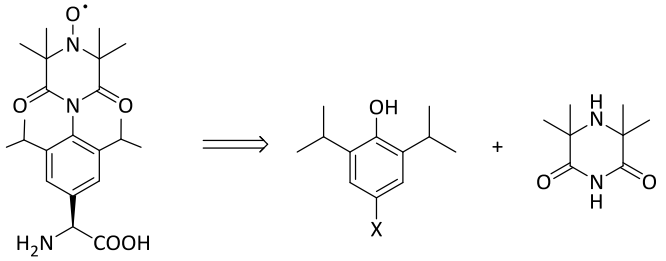

38 **39** **33**

Scheme 14: Retrosynthesis of 4-(3,3,5,5-tetramethyl-2,6-dioxo-4-oxylpiperazine-1-yl)-L-2,6-diisopropyl-Phg (**38**). Compound **38** might be generated using phenol derivative **39** and piperazine-2,6-dione **33**. X should illustrate the functionalisation which is needed to introduce the amino acid backbone.

Preliminary attempts showed that the commercially available 2,6-diisopropylphenol (**40**) can be converted into the functionalised 2,5-diisopropylphenyl trifluoromethane-sulfonate (**41**), but not to the boronic ester **42** under the used conditions (MIYAURA

borylation) (**Scheme 15**).

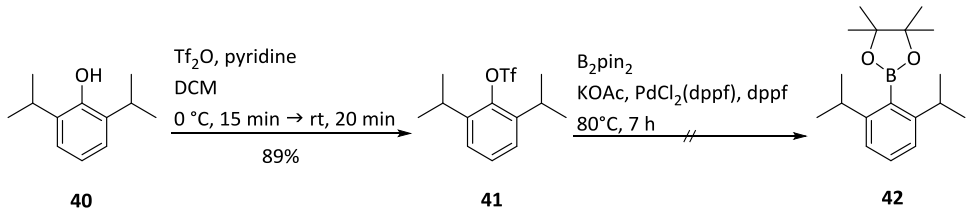

Scheme 15: Functionalisation of phenol derivative **40** using Tf_2O and MIYAURA borylation.

Most probably, the steric demand of the *iso*-propyl groups limits the possible synthesis strategies, hence, a substitution with methyl groups might be more suitable (**Scheme 16**).

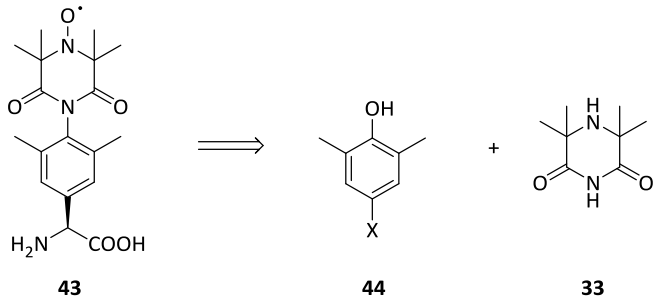

Scheme 16: Retrosynthesis of 4-(3,3,5,5-tetramethyl-2,6-dioxo-4-oxylpiperazine-1-yl)-L-2,6-dimethyl-Phg (**43**). Compound **43** might be generated using phenol derivative **44** and piperazine-2,6-dione **33**. X should illustrate the functionalisation which is needed to introduce the amino acid backbone.

Due to the spatial proximity to the carbonyl groups of the piperazine-2,6-dione, the rotation of the C–N bond should also be restricted through two methyl groups in *ortho*-position.

A possible synthetic route for amino acid **46** using 2,6-dimethylphenol (**44**) as starting material is illustrated in **Scheme 17**.

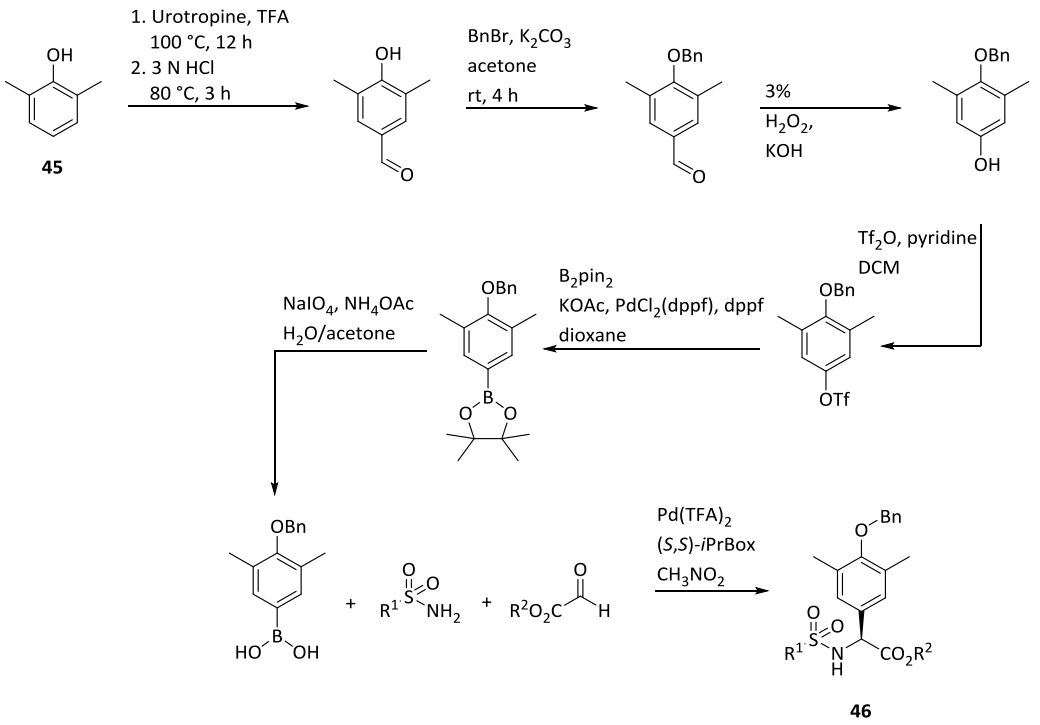

Scheme 17: A conceivable synthetic route for generating amino acid **46**. The phenol derivative **45** is functionalised in para position to make it suitable for a Pd-catalysed cross coupling[102] to generate the amino acid backbone.

Preliminary attempts were performed using the commercially available 2,6-diisopropylphenol (**47**) of compound **45**. Phenol **47** was formylated according to SMITH[103] using urotropine and TFA (2,5-diisopropyl-4-hydroxy benzylaldehyde (**48**)) and then directly protected with benzyl to avoid side reactions during functionalisation (2,5-diisopropyl-4-benzyloxy benzylaldehyde (**49**), **Scheme 18**).

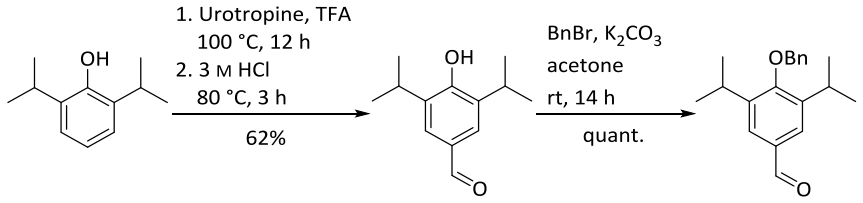

Scheme 18: Test reaction with the phenol derivative **47**. Formylation of the aromatic ring (compound **48**) and benzyl protection of the hydroxyl group (compound **49**).

It was proven that there is a possibility to obtain two first products from the designed synthetic route. Thus, due to similar properties the used reaction conditions should be applicable for the dimethyl analogue **45**. The proposed subsequent reaction steps are literature known and can be performed in large scale.
Coupling of the amino acid **46** and the piperazine-2,6-dione **33** might be achieved using the same procedure described for the α-TOPP label **23**.

3.7.2 Future Application of the α-TOPP Label

The α-TOPP label **23** gives important information about peptide structures due to sharp and reliable distance distributions. To extend the application of the TOPP label **23**, it could be incorporated into small proteins (transmembrane proteins) to determine their structures in their natural environment by PELDOR. To reach this goal, however, preliminary studies on a less complicated model system need to be done. Therefore, first the possibility to connect two peptide sequences containing the TOPP label *via* native chemical ligation (NCL) has to be determined (**Scheme 19**).

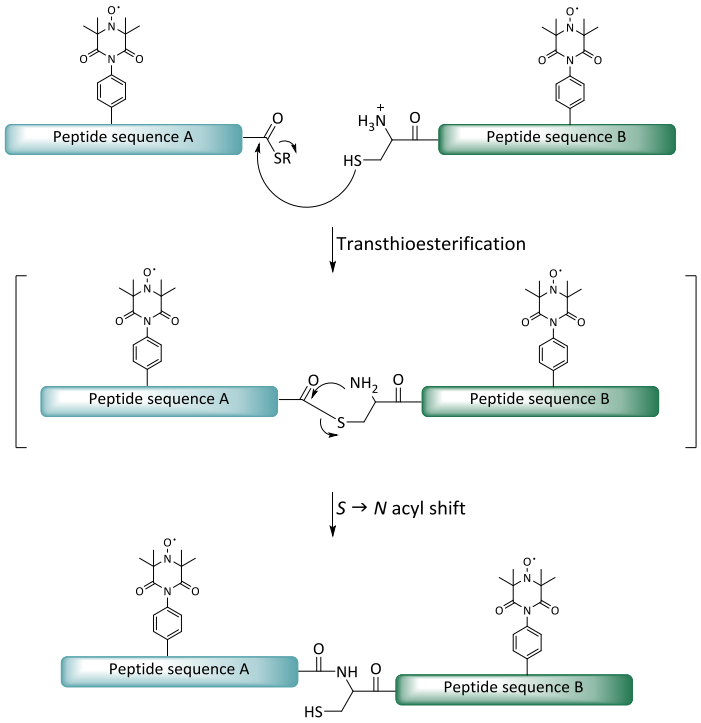

Scheme 19: General principle of NCL. Both peptide sequence fragments are connected through a newly formed amide bond.

Problems during the NCL process like side reactions with or due to the nitroxide radical might be solved using a suitable protecting group. E.g. in 2014, GÖBEL and co-workers developed a promising photolabile protecting group strategy for nitroxides.[104]

4 Synthesis and Structural Investigation of Labelled Transmembrane β-Peptides

Since the discovery that β-peptides can form stable and well-defined secondary structures, this versatile class of unnatural oligomers has been extensively studied. It turned out that β-peptides have unique chemical characteristics and can adopt various structural motifs (for reviews see [105–107]). Compared to natural peptides and proteins, β-peptides are enzymatically[108] and metabolically[109] stable *in vitro* and *in vivo*, which makes them a feasible starting point for new peptide-based biomedical applications such as antibiotics[110] and antifungals[111]. Furthermore, the variety of secondary structures makes them a promising framework for the design of specific foldamers and therefore allows an extended examination of protein structures. Especially, as a new class of transmembrane model systems they can give further insights into protein-lipid interactions which supposedly influence function, activity and organisation of proteins to a large extent.

Of all β-peptide structures, the 3_{14}-helical structure (also less precisely referred to as 14-helix) is the most comprehensively investigated foldamer. So far, it was mainly studied in solution by NMR[112–114] and in solid-state by X-ray diffraction[114–116].
In part 3 it is demonstrated that the TOPP label is an additional powerful and straightforward tool to investigate peptides, which gives information that was directly related to the peptide structure. To enable PELDOR examinations of β-peptides by this tool, a synthetic route for the so called β^3-hTOPP label **24** was developed and the label was synthesised. Several reaction steps were investigated regarding their enantioselectivity. Furthermore, the stability of the label was investigated. Then, four double TOPP-labelled transmembrane β^3-peptides were synthesised which allow the examination of one turn of the 3_{14}-helix. All β^3-peptides were investigated in solution and in a lipid bilayer by CD spectroscopy to test any influence of the label on the

secondary structure formation. Finally, the 3_{14}-helical structure was investigated in solution and preliminary examined within a lipid bilayer by PELDOR.

4.1 β-Peptides

This part is focussed on the preparation and structural details of β^3-amino acids and their corresponding β-peptide structure, in particular the 3_{14}-helix.

β-Peptides are oligomers consisting of a sequence of β-amino acids. Compared to α-amino acids they have an additional methylene group in the amino acid backbone (**Figure 29**).

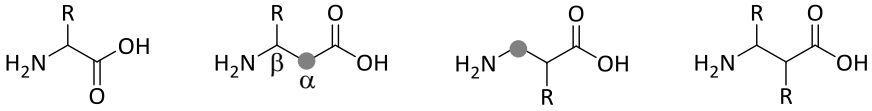

Figure 29: General structure of α- and β-amino acids. Compared to α-amino acids β-amino acids have an additional methylene group (marked grey). In β^3-amino acids the side-chain is located at the C_β. β^2-amino acids have the residue at the C_α. $\beta^{2,3}$-amino acids have substitutions on both, C_α and C_β.

Due to the additional methylene group two different regioisomers are possible, denoted as β^3- and β^2-amino acids.[106,117] In the case of β^3- amino acids the residue is located at the C_β and in the case of β^2 at the C_α. Substitution on both positions, C_α and C_β, leads to a $\beta^{2,3}$-amino acid.[106]

β-amino acids can be prepared using various methods.[118,119] In the mid-1990s, SEEBACH and co-workers described a way to synthesise enantiomerically pure β^3-amino acids with proteinogenic side-chains *via* the ARNDT-EISTERT reaction (**Scheme 20**), variants of this approach are still frequently used.[120–122]

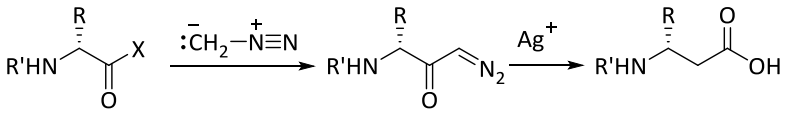

Scheme 20: ARNDT-EISTERT homologation of α-amino acids. First, the activated α-amino acid is converted into the corresponding diazo ketone using diazomethane and afterwards the β^3-amino acid is obtained in a silver(I)-catalysed WOLFF rearrangement.

In this homologation α-amino acids are used as starting material (homologated α-amino acids have prefix h). This is a substantial benefit, since α-amino acids are cheap, commercially available and enantiopure.[121] In general, the first step of the ARNDT-EISTERT reaction transforms the activated *N*-protected α-amino acid into the corresponding diazo ketone using diazomethane.[123,124] Then, the diazo ketone is converted into the β^3-amino acid *via* a WOLFF rearrangement which is catalysed by silver(I) ions.[123–125]

4.1.1 Secondary Structures

Initially, it was expected that because of the increased flexibility due to the additional rotating single bond between C_α and C_β (**Figure 29**), β-peptides may not form stable foldamers that are analogous to α-peptides. Yet, intensive structural investigations demonstrated that β-peptides form various types of stable 'protein-like' helices[105,107], parallel[121,126,127] and antiparallel[114,126,128] sheets and hairpin turns[129] (detailed information about several β-peptide structures can be found in excellent review articles [105–107]). Stable helical structures can be formed with as little as six residues whereas comparable α-peptides require more than ten residues under the same conditions.[114,119,126–128,130] These observations have led to the general perception that the stability of helices formed by β-peptides is superior to those formed by α-peptides. It is further known that β-peptides can form different types of helical structures: namely the 14-, 12-, 10/12- and 8-helix, where the numbers are defined by the atoms within a 'helix-specific' hydrogen-bond ring (**Figure 30**).[107,131] E.g. the 14-helix includes 14 members in the hydrogen bond ring between N–H (*i*) and C═O (*i*+2).

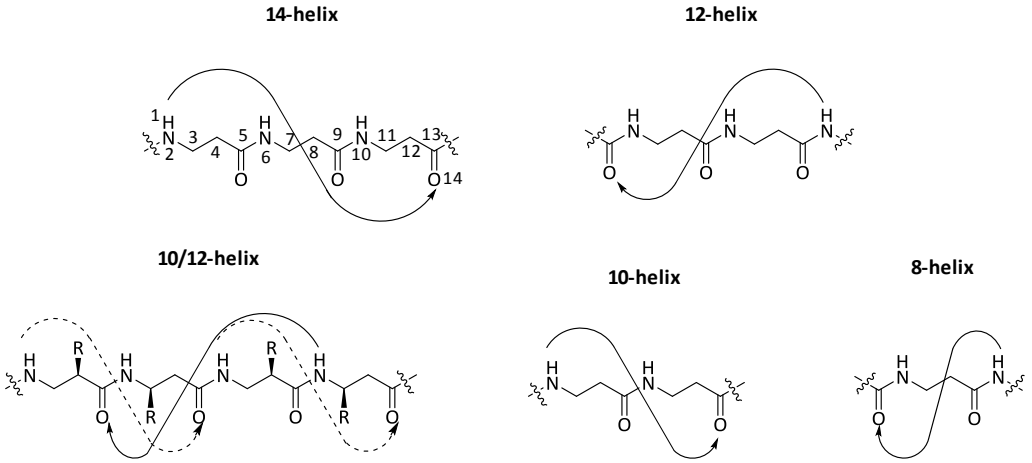

Figure 30: Helical structures of β-peptides. The helix type is defined by the number of atoms of a hydrogen-bond ring. The arrows illustrate the hydrogen bond.

The conformation of the α-peptide backbone is defined by the three torsion angles ϕ, ψ and ω.[132] β-peptides are characterised by an additional angle θ (**Figure 31**).

Figure 31: Torsion angles of α- and β-peptides. For α-amino acids the torsion angle ψ is defined by the planes containing atoms $NC_{C=O}C_\alpha$ and $C_{C=O}C_\alpha N'$ (short: $NC_{C=O}C_\alpha N'$), ϕ by $C_{C=O}C_\alpha NC'_{C=O}$ and ω by $C_\alpha NC_{C=O}C'_\alpha$.[132] For β-amino acids this scheme is extended by the torsion angle θ which is defined through $C_{C=O}C_\alpha C_\beta N$ according to BALARAM.[133]

The torsion angle ψ is defined by the planes containing atoms $NC_{C=O}C_\alpha$ and $C_{C=O}C_\alpha N'$ (short: $NC_{C=O}C_\alpha N'$), ϕ by $C_{C=O}C_\alpha NC'_{C=O}$ and ω by $C_\alpha NC_{C=O}C'_\alpha$[132] Due to the additional single bond between C_α and C_β a torsion angle θ which is described through $C_{C=O}C_\alpha C_\beta N$ must be defined for β-amino acids (**Figure 31**).

The torsion angle θ plays an important role in the formation of secondary structures of β-peptides, since β-peptides prefer a gauche (60°) conformation about this torsion angle.[131] As θ is additionally affected by the location of the residues in the β-amino acid the substitution pattern also influences the secondary structure formation.[131] E.g.

a β-peptide consisting of alternating β^2- and β^3-amino acids prefers to fold in a 10/12-helix, whereas the 14-helix is preferably formed by acyclic, monosubstituted β-amino acids (β^2 or β^3).[107,134]

The 14-helix is particularly well documented and several of its characteristics such as pitch (vertical distance between consecutive turns of the helix) and net dipole, which can be readily compared to the typical α-helix, are illustrated in **Figure 32**.

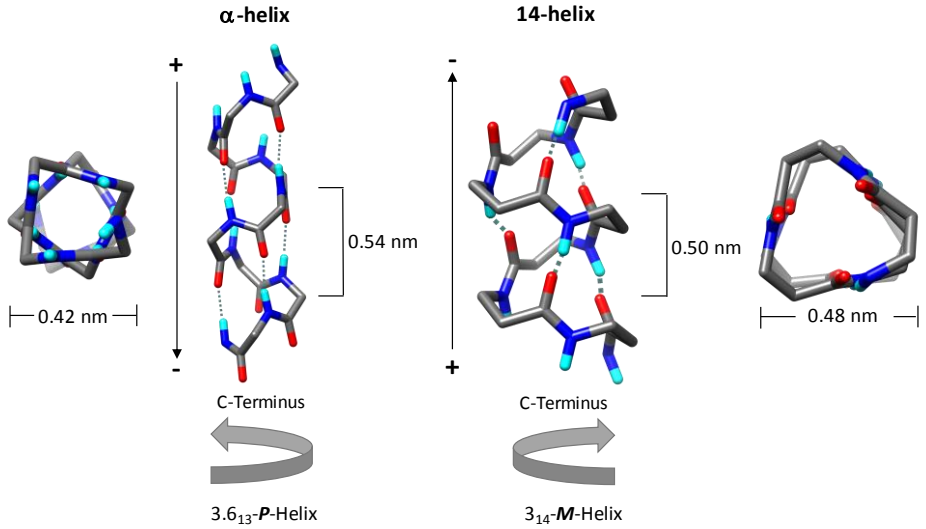

Figure 32: Comparison of α-helix and 14-helix. The diameter of a 14-helix is slightly larger (0.48 nm *vs* 0.42 nm) and the pitch is shorter (0.50 nm *vs* 0.54 nm).[106] In addition, the net dipole is converse oriented, and the 14-helix is left-handed whereas the α-helix is right-handed (in both cases consisting of L-amino acids).

An α-peptide consisting of L-amino acids folds into a right-handed helix, whereas the β^3-amino acids lead to a left-handed helical β-peptide. Compared to the α-helix, the diameter of a 14-helix is slightly larger (0.42 nm *vs* 0.48 nm).[131] The α-helix repeats after 3.6 residues with a pitch of 0.54 nm, the 14-helix repeats after about 3 residues with a pitch of 0.50 nm.[106] In an ideal 14-helix the residues *i* and *i*+3 are exactly atop of each other as observable in an oligopeptide consisting of *trans*-2-aminocyclohexane-carboxylic acid (ACHC) (**Figure 33**).[106]

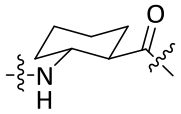

Figure 33: Structure of ACHC.

Since ACHC is conformationally constrained and the C_α–C_β bond is incorporated into the six-membered ring, the torsion angle θ is locked at ± 55°.

By NMR spectroscopic investigations of a β^3-eicosapeptide consisting of the 20 homologated proteinogenic amino acids (L-β^3-amino acids) SEEBACH and co-workers observed an offset from the ideal 3_{14}-helix by approximately 15° in a right-handed direction.[135] This means that the turn of the helix is defined by approximately 3.2 residues.

Recently, DIEDERICHSEN and co-workers showed that transmembrane β-peptides (like **P4**, **Figure 34**) with proteinogenic side-chains form a stable 3_{14}-helix in solution and in a lipid bilayer.[136,137]

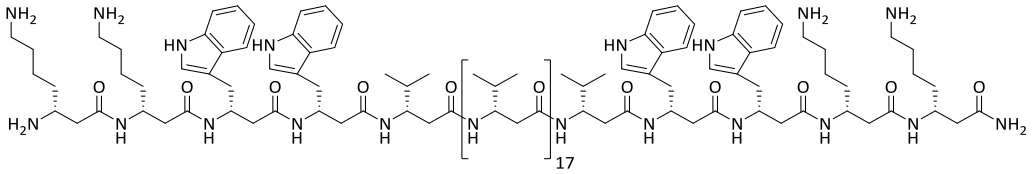

P4

Figure 34: Peptide sequence of the transmembrane β-peptide **P4**.

The β-peptide consists of a hydrophobic stretch with β^3-hVal flanked by two β^3-hTrp and two β^3-hLys at each side of the sequence.

Similar to other transmembrane peptides (such as the WALP peptides, see section 3.1.1) the hydrophobic stretch of the transmembrane β-peptide **P4** consists of hydrophobic residues. Here, β^3-hVal residues were chosen, since it has been demonstrated that β^3-hVal residues stabilise the 3_{14}-helix.[138] It is furthermore assumed that the indole

moieties of tryptophan serve as membrane anchors and orient proteins in the lipid bilayer as they have a positional preference at the polar-apolar interface.[58,59] Indeed, for the transmembrane β-peptide **P4** X-ray diffraction[136] and tryptophan fluorescence spectroscopy[137] showed that the indole residues are located in close proximity to the carbonyl groups of the lipids.

Since the peptide **P4** consists mainly of hydrophobic residues, lysine residues were attached to the *N*- and *C*-termini of the peptide to increase the solubility in aqueous medium.[136] Lysine residues are often used in the design of transmembrane α-peptides such as KALP peptides.[65] Compared to the tryptophan residues the lysine residues are located near the polar region of the head groups and the aqueous phase.[66]

4.2 Project Details

4.2.1 Peptide Design

To get further information about the structure of β^3-peptides (3_{14}-helix) in solution and within a lipid environment, β^3-hTOPP-labelled derivatives of peptide **P4** (**Figure 34**) were chosen as model peptide for PELDOR studies. This peptide is especially promising, since it was successfully incorporated into a lipid environment before and showed a well-defined and stable 3_{14}-helical structure.[136,137] Furthermore, FÖRSTER resonance energy transfer (FRET) studies demonstrated that this type of peptide is monomeric in the lipid bilayer which is desirable, since assembled peptides can make the interpretation of the PELDOR results more ambiguous.[137]

Peptide **P4** consists of overall 27 homologated proteinogenic amino acids. To investigate one turn of the 3_{14}-helix, four β^3-hTOPP double labelled β^3-peptide were designed (**Figure 35**).

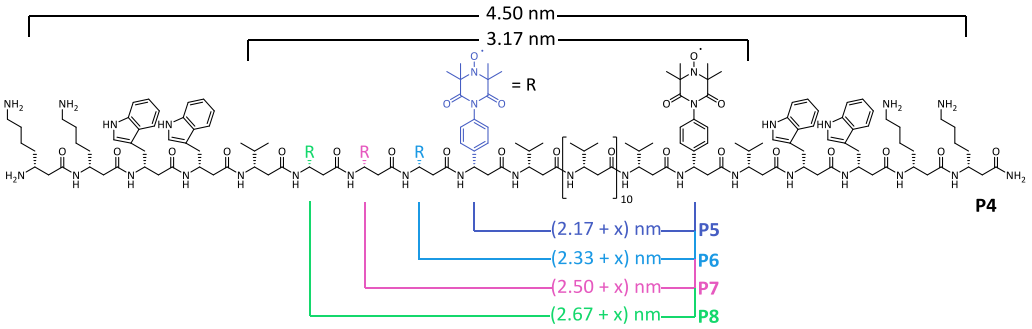

Figure 35: The label positions within the peptide sequence of **P4** and estimated distances. Sequence of the model peptide, label positions (symbolised by the coloured R) and the estimated length/distance values: the whole peptide has a length of 4.50 nm, and a hydrophobic stretch of 3.17 nm. The inter-spin vectors are estimated as (2.17 + x) nm (**P5**), (2.33 + x) nm (**P6**), (2.50 + x) nm (**P7**) and (2.67 + x) nm (**P8**). The variable x should show that there is an additional distance value due to the lengths and orientations of the spin labels.

The ideal 3_{14}-helix is defined by three β-amino acids per turn and a pitch of 0.5 nm.

Taking this basic data into account, the length of the whole peptide is estimated to be 4.50 nm. The hydrophobic stretch consists of 19 β^3-hVal residues and the length is estimated to be 3.17 nm.

As already stated for the α-peptides, the positions of the labels were chosen according to two criteria: The intramolecular distance between the two spin labels has to be over 2.0 nm, which is a requirement for the PELDOR experiment, and the TOPP and the Trp residues should not be on the same side or at least not in direct proximity to avoid interactions between these. Therefore, the peptides were labelled at the position 9, 22 (**P5**), 8, 22 (**P6**), 7, 22 (**P7**) and 6, 22 (**P8**). The distances between the labelling positions were estimated to be (2.17 + x) nm (**P5**), (2.33 + x) nm (**P6**), (2.50 + x) nm (**P7**) and (2.67 + x) nm (**P8**). The variable x should illustrate that the orientation of the labels will certainly add to these approximations to give larger final inter-spin distances (precise distances are listed in chapter 4.5: Inter-Spin Distances from Modelled β^3-Peptides).

Consequently, four β^3-hTOPP-labelled β^3-peptides were designed and synthesised to investigate the 3_{14}-helix in solution and within a lipid bilayer using the PELDOR technique.

4.2.2 Membrane Systems

Previously published studies using the peptide motif **P4** were performed in 1,2-dioleoyl-*sn*-glycero-3-phosphocholine (DOPC).[136,137] In order to keep comparability, CD measurements of the four peptides were performed in DOPC as well.

Analogous to the peptide-lipid interaction investigations using transmembrane α-peptides, a hydrophobic match situation between peptide and lipids environment is expected when the hydrophobic stretch of the peptide and the hydrophobic thickness of the lipid bilayer are similar (**Figure 13**, section 3.1.2). Recall, that an useful reference value for the hydrophobic thickness of a lipid bilayer is $2D_C$ which, however, varies between different sources, since the hydrophobic thickness is influenced by the experimental conditions. Some selected values for DOPC taken from different sources

are listed in **Table 4**.

Table 4: Selected values of $2D_C$ [nm] for DOPC taken from different sources.

$2D_C$ (DOPC)	2.70[69]	2.68[68]	3.00[136]

The hydrophobic stretch of the peptide can be estimated by the basic parameters of the ideal 3_{14}-helix (**3.0_{14}**) (three amino acids per turn and a pitch of 0.5 nm). For completeness **Table 5** already shows additional values that are estimated from structural models as explained in chapter 4.5.

Table 5: Estimated values of the hydrophobic stretch of the β-peptide **P4**. The hydrophobic stretch is given in nm. The terms **3_{14} lit.**, **3_{14} crystal** and **3_{14} ideal** are taken from chapter 4.5 and symbolise the specific helical structures of theoretical models of peptide **P4** (details see chapter 4.5). **3.0_{14}** is based on the basic parameters of the ideal 3.0_{14}-helix (three amino acids per turn and a pitch of 0.5 nm).

	3_{14} lit.	**3_{14} crystal**	**3_{14} ideal**	**3.0_{14}**
hydrophobic stretch	2.86	2.80	2.52	3.17

In consideration of $2D_C$ and the hydrophobic stretch of the peptide a match situation between peptide and membrane can be expected. The hydrophobic stretch of the peptide might be slightly larger than the hydrophobic thickness of the peptide. From a recently published study the positive hydrophobic mismatch situation was adapted by the peptide *via* tilting by 16°.[136]

The PELDOR measurements of α-peptides (part 3) have been performed in deuterated POPC. The deuterated lipid led to longer electron spin relaxation times which enhance the quality of data in the PELDOR experiment.[53] Unfortunately, deuterated DOPC is not commercially available. Therefore, the PELDOR experiments are performed in POPC. Note that DOPC and POPC (*confer* (cf.) **Table 4** and section 3.2.2 **Table 1**) have similar $2D_C$ values and a match is expected as well. To evaluate this estimation, additional CD measurements were performed in POPC.

4.3 Synthesis

4.3.1 Development and Synthesis of the β³-hTOPP Label

The development of the synthetic route for the β^3-amino acid version of the TOPP label is based on the established synthesis of the α-TOPP label **23** which afforded, besides various other desirable factors, a high *ee*-value of the label (see chapter 3.3).

The β-hydrogen atom of β^3-amino acids is not as acidic as the α-hydrogen of α-amino acids due to its distance to the carboxyl group. Thus, the reaction conditions used in the α-TOPP synthesis should indeed influence the stereogenic centre of a β^3-amino acid even less and therefore, products of high enantiomeric purity should be obtained. For details about the determination of the *ee* values see subsection 4.3.1.1.

All preceding studies about β^3-peptides in the group of DIEDERICHSEN were done with D-β^3-amino acids. Therefore, to keep the comparability to previous studies the label was synthesised in D-configuration.

To avoid side reactions at the TOPP residue, first, the homologation of the α-amino acid to the β^3-amino acid was performed. Thus, the synthesis of the β^3-hTOPP label **24** started with the protection of the amine function under SCHOTTEN-BAUMANN conditions and the protection of the hydroxyl group to inhibit side reactions during the functionalisation (**Scheme 21**).

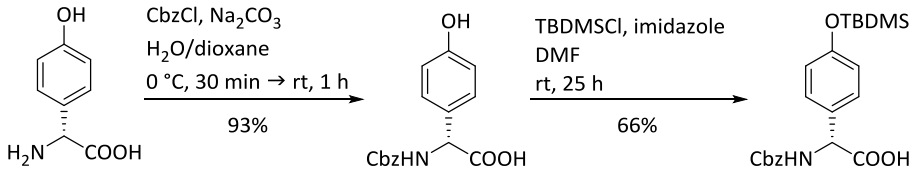

50 **51** **52**

Scheme 21: Protection of the amine group and the hydroxyl group of the phenol moiety.

Therefore, the commercially available D-4-Hpg (**50**) was dissolved in aq Na_2CO_3 solution and 1,4-dioxane, cooled to 0 °C, treated with CbzCl and then allowed to warm up to rt.

The reaction was stirred for 1 h and after work-up the NMR showed the pure Cbz-D-Hpg-OH (**51**). The Cbz-protected amino acid **51** was synthesised in a high yield of 93%. Next, the hydroxyl group of the phenol moiety was protected with a silyl ether, since previous attempts showed that this hydroxyl group also reacted with the activation reagents in a subsequent ARNDT-EISTERT homologation.[139] The silyl ether was chosen due to its orthogonal cleavage conditions to the other protecting groups (Cbz and Bn) and its stability against acidic treatment. Thus, as described by COREY the hydroxyl function was protected with *tert*-butyldimethylsilyl (TBDMS) in an overnight reaction in DMF using TBDMSCl as electrophile with imidazole as catalyst and base.[140] Note that initially the crude Cbz-D-Hpg(TBDMS)-OH (**52**) was then used without further purification. However, loss of product in the first step of the ARNDT-EISTERT reaction occurred after repetition of the synthesis step (see below) and therefore, the crude product **52** was purified by flash-column chromatography and was obtained in a yield of 63%.

The α-amino acid **52** was converted into the corresponding β^3-amino acid by insertion of an additional methylene group *via* the ARNDT-EISTERT homologation (**Scheme 22**).

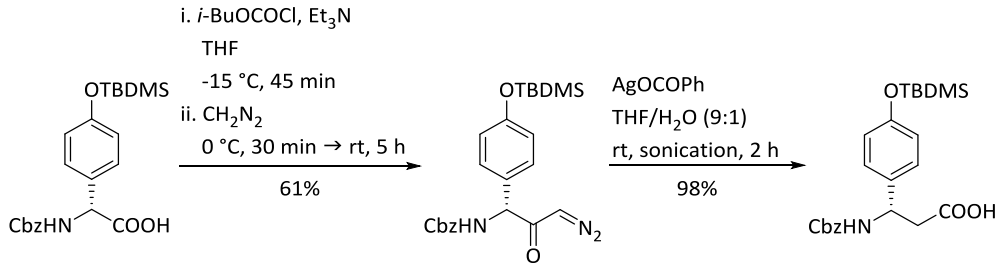

Scheme 22: ARNDT-EISTERT homologation using α-amino acid **52** as starting material.

The first step of the ARNDT-EISTERT homologation consists of the activation of the carboxyl group and the nucleophilic reaction with diazomethane. Therefore, the carboxyl group of amino acid **52** was first deprotonated with Et_3N and then activated with *iso*-butyl chloroformate (*i*-BuOCOCl) at a low temperature (-15 °C). Afterwards, the

carbonyl group was addressed by a nucleophilic attack through diazomethane (CH_2N_2) to give Cbz-D-Hpg(TBDMS)-CHN_2 (**53**) after 5 h. The crude diazo ketone **53** was purified by flash-column chromatography and was obtained in a yield of 61%. It is important to note that in subsequent repetitions of this synthesis yields dropped to values as low as 39%. This was addressed by first evaluating the influence of the temperature. Yet, even at -78 °C, side reactions were not markedly reduced compared to -15 °C.[141] However, with different batches of diazomethane again yields of roughly 60% were achieved. Hence, the reaction should be performed using freshly distilled diazomethane. In the second step of the homologation the diazo ketone **53** was converted to the β^3-amino acid Cbz-D-β^3-hHpg(TBDMS)-OH (**54**) *via* a WOLFF rearrangement catalysed by silver(I) ions with a good yield of 98%. Therefore, the diazo ketone **53** was dissolved in a 9:1 mixture of THF/H_2O and catalytic amounts of silver(I)-benzoate (AgOCOPh) were added. Afterwards, the reaction was sonicated for 2 h, N_2 was released and after the nucleophilic attack of H_2O the carboxylic acid **54** was formed.

Then, the silyl ether of compound **54** was cleaved using hydronium ions to get the free hydroxyl group for further functionalisation steps. As the carboxyl group is also activated under acidic conditions, a simultaneous protection of this functionality is possible using various alcohols. In a previous work, attempts to deprotect the TBDMS were performed in MeOH because of the good solubility of compound **54** and conc. HCl in this solvent (**Scheme 23**).[139]

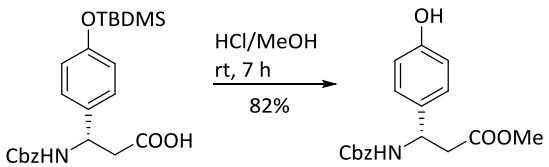

54 **55**

Scheme 23: The deprotection of the TBDMS group using HCl in MeOH led to Cbz-D-β^3-hHpg-OMe (**55**).

Hence, the methyl ester **55** was formed. In the following route towards the β^3-hTOPP

label **24** this proved to be highly problematic. After several subsequent steps deprotection of the methyl ester involved basic LiOH (**Scheme 24**).[139] However, this not only led to the free carboxylic acid (product **56**) but also to the ring opening of the piperazine-2,6-dione moiety (compound **58**, **Scheme 24**).[139]

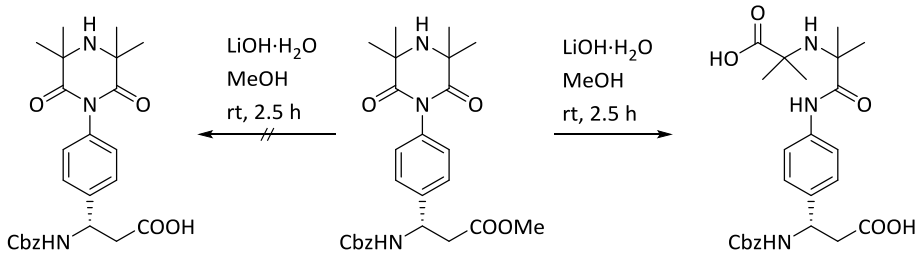

56 **57** **58**

Scheme 24: Basic deprotection of the methyl ester leads to ring opening of the piperazine-2,6-dione moiety (compound **58**).

Hence, to avoid the basic deprotection conditions another protecting group was chosen for the carboxyl group. Due to its stability and the opportunity to deprotect the Cbz group under the same conditions (hydrogenation catalysed by Pd/C), the benzyl group seemed to be a suitable protecting group (cf. chapter 3.3) (**Scheme 25**).

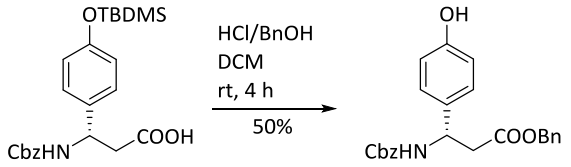

54 **59**

Scheme 25: Deprotection of the silyl ether and simultaneous protection of the carboxyl group with Bn.

Due to its prevalent hydrophobic properties BnOH is not soluble in purely aqueous solution of HCl. Therefore, DCM was added which enhanced the solubility of BnOH in the reaction mixture. Hence, compound **54** was dissolved in DCM and BnOH, and conc. HCl was added. The conversion was controlled by TLC and after 4 h the starting material

was no longer observable. After purification by flash-column chromatography the pure Cbz-D-β^3-hHpg-OBn (**59**) was obtained in a yield of 50%. This yield was not as high as under MeOH-solvent/reactant conditions (82%) (**Scheme 23**) which is probably because of the insufficient solubility of BnOH in aq HCl. Better yields can be observed by protecting the carboxylic group directly during the WOLFF rearrangement, which was shown by MATTHIAS KRULL (**Scheme 26**).[141]

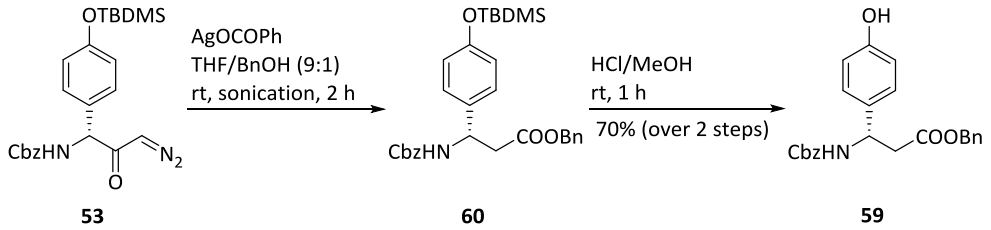

Scheme 26: The WOLFF reaction catalysed by silver(I) ions led to Cbz-D-β^3-hHpg(TBDMS)-OBn (**60**) using BnOH, and the subsequent deprotection reaction in HCl/MeOH led to **59**.

Here, BnOH was used as nucleophile instead of H_2O. After standard work-up the crude Cbz-D-β^3-hHpg(TBDMS)-OBn (**60**) with remaining traces of BnOH was directly utilised in the TBDMS deprotection step. Therefore, MeOH and conc. HCl were added to the crude compound **60**, and the reaction was performed at rt for 1 h. It is worth to note, that longer reaction times led to the replacement of the benzyl ester by the methyl ester. After purification of the crude product **59** *via* flash-column chromatography and compared to the first approach (see **Scheme 22** and **Scheme 25**), the yield was increased from 49% (taking into the account the WOLFF rearrangement and the deprotection) to 70%.

After the successful formation of the protected β^3-amino acid backbone, the next steps included the functionalisation of the β^3-amino acid residue.
First, the hydroxyl group of compound **59** was converted to a triflate group, since this group is a suitable leaving group in a subsequent MIYAURA borylation (**Scheme 27**).

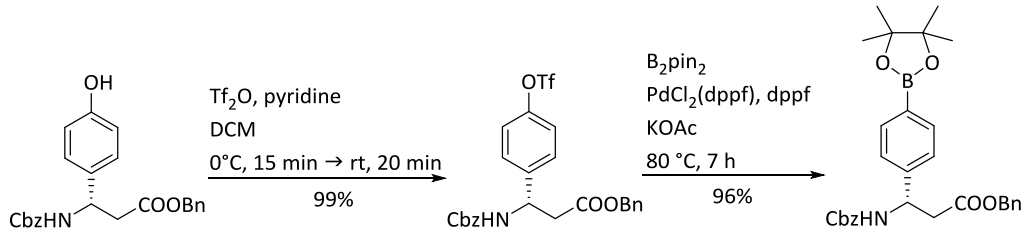

59 **61** **62**

Scheme 27: Triflate functionalisation using amino acid **59** as starting material and MIYAURA cross coupling which led to Cbz-4-pinacolboryl-D-β^3-hPhg-OBn (**62**).

The phenol derivative **59** was dissolved in DCM and cooled to 0 °C. The hydroxyl group was then deprotonated using pyridine and the resulting phenolate ion attacked the Tf_2O in a nucleophilic substitution. Cbz-D-β^3-hHpg(Tf)-OBn (**61**) was formed with nearly quantitative conversion (99%) in overall 35 min. Amino acid **61** was utilised in the following MIYAURA cross coupling without further purification, since the NMR spectra showed the pure β^3-amino acid **61**. Next, the Pd-catalysed MIYAURA borylation transformed β^3-amino acid **61** into the Cbz-4-pinacolboryl-D-β^3-hPhg-OBn (**62**). This cross coupling was performed under dry and inert conditions in degassed dioxane at 80 °C utilising B_2pin_2, $PdCl_2$(dppf) as catalyst and KOAc as base. After 7 h the TLC showed full product formation of the boronic ester **62**. TLC showed only product **62** and flash-column chromatography was then used to separate the catalyst and the desired amino acid **62**. The product **62** was obtained in a good yield of 96%.

Afterwards, the arylboronic ester **62** was hydrolysed to Cbz-4-dihydroxyborane-D-β^3-hPhg-OBn (**63**) (**Scheme 28**).

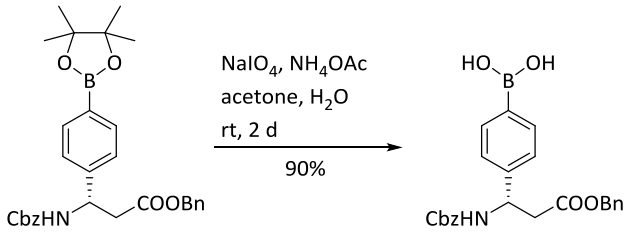

62 **63**

Scheme 28: Compound **62** was hydrolysed to the corresponding boronic acid **63**.

According to literature, boronic esters are less reactive than the corresponding boronic acids in a subsequent CHAN-LAM cross coupling.[71,72,75] Hence, boronate **62** was dissolved in H_2O and acetone, and hydrolysed to the boronic acid **63** in a yield of 90% at rt over 2 d. $NaIO_4$ oxidised the released pincol to aceton selectively.

Then, the basic structure of the β^3-hTOPP label **24** was formed *via* a copper-mediated CHAN-LAM amination (**Scheme 29**).

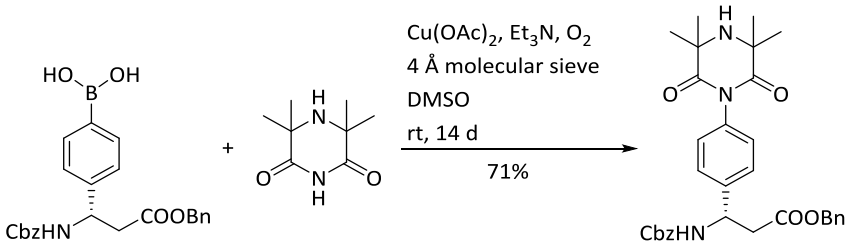

63 **33** **64**

Scheme 29: Copper-mediated CHAN-LAM coupling using β^3-amino acid **63** and piperazine-2,6-dione **33**.

The used piperazine-2,6-dione **33** was synthesised according to the procedure described in chapter 3.3.

As already stated for the α-amino acid, the CHAN-LAM coupling is a mild amination and the optimal choice for the 'stereochemistry-conserving' formation of the basic structure of the β^3-hTOPP motif. Hence, boronic acid **63** and piperazine-2,6-dione **33**

were dissolved in DMSO and Et_3N, anhydrous $Cu(OAc)_2$ and powdered molecular sieves (4 Å) were added, and within 14 d product Cbz-4-(3,3,5,5-tetramethyl-2,6-dioxopiperazine-1-yl)-D-β^3-hPhg-OBn (**64**) was formed. After the reaction the suspension was filtered through a glass fiber filter to remove the molecular sieve and other precipitations. During the normal work-up the phase separation between organic phase and aqueous phase decreased. The aqueous phase was acidified with 1 M HCl and phase separation was increased. After flash-column purification compound **64** was isolated in a yield of 71%. Note that this reaction led only to the C–N bond formation between the amidic nitrogen and the aromatic system. The other *sec*. amine is unfavoured because of the steric demand of the four methyl groups in the vicinity.

In order to use the β^3-hTOPP amino acid **24** in a Fmoc-based SPPS, the next two steps involved the deprotection of the Cbz and the Bn group of compound **64** to get the free amino acid, and the re-protection of the primary amine with Fmoc (**Scheme 30**).

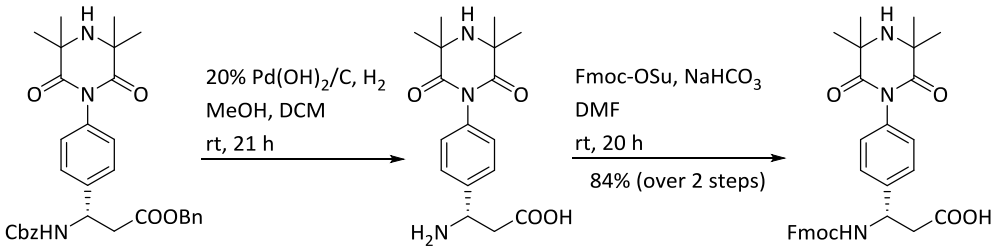

64 **65** **66**

Scheme 30: Deprotection of Cbz and Bn group and subsequent Fmoc protection.

The Cbz and Bn group of amino acid **64** were cleaved through hydrogenation on a Pd/C surface using the PEARLMAN's catalyst. Therefore, the protected compound **64** was dissolved in MeOH and DCM. The DCM increased the solubility of amino acid **64** in MeOH. Afterwards, a hydrogen flow was passed through the solution to saturate the solvents and the atmosphere in the flask with hydrogen. The reaction was stirred at rt under a hydrogen atmosphere overnight. Results for the α-TOPP label demonstrated

that this reaction worked best at a 0.85 mmol scale (see chapter 3.3). After the reaction the catalyst was removed in two filtration steps. First, the suspension was pre-purified through a normal pleated filter and then the filtrate was passed through a micron syringe filter to remove any traces of Pd catalyst. The crude 4-(3,3,5,5-tetramethyl-2,6-dioxopiperazine-1-yl)-D-β^3-hPhg-OH (**65**) was obtained and used in the next step without further purification. In order to introduce a Fmoc group on the amine group, compound **65**, $NaHCO_3$ and Fmoc-OSu were suspended in DMF and the reaction was carried out at rt overnight. Recall that the application of Fmoc-Cl led to the racemisation of the α-TOPP and therefore the less reactive Fmoc-OSu was introduced and substantially improved the *ee*.[76] Thus, Fmoc-OSu was used for the protection of the β^3-hTOPP as well. After flash-column chromatography the Fmoc-protected amino acid Fmoc-4-(3,3,5,5-tetramethyl-2,6-dioxopiperazine-1-yl)-D-β^3-hPhg-OH (**66**) was isolated. The yield over the simultaneous deprotection of the amine and carboxyl group, and the subsequent protection of the NH_2 function was 84%. In the final step of the synthesis the nitroxide radical was generated *via* the oxidation of the *sec.* amine using *m*-CPBA (**Scheme 31**).

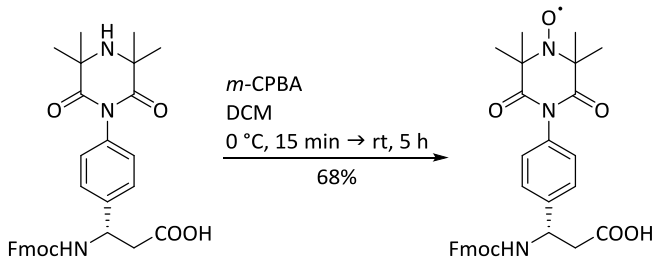

66 **67**

Scheme 31: Oxidation of the *sec*. amine of the β^3-amino acid **66** yielded the desired Fmoc-protected β^3-hTOPP amino acid **67.**

The *m*-CPBA mediated oxidation was carried out in DCM and compound **66** was oxidised to the desired Fmoc-D-β^3-hTOPP-OH (**67**) in 5 h. It is worth to note, that initially, label **67** was purified by flash-column chromatography using the same gradient

(DCM/MeOH/AcOH, 99.5:0.5:0.1 → 96.5:3.5:0.1, *v*/*v*/*v*) as for the Fmoc-protected α-TOPP label **37**, since the only difference between these two labels is the additional methylene group. Interestingly, first attempts of coupling label **67** into a β^3-peptide sequence then did not lead to the desired peptide product. This is hinted by a peak in the mass spectrum which did not belong to the expected mass of the peptide sequence. Due to this unexpected problem, the β^3-hTOPP label fraction from the flash-column chromatography was further purified by HPLC (**Figure 36**).

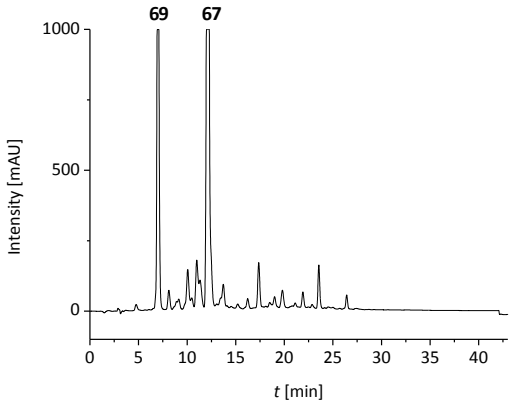

Figure 36: HPLC chromatogram of the Fmoc-protected β^3-hTOPP amino acid **67** purified by flash-column chromatography using DCM/MeOH/AcOH, 99.5:0.5:0.1 → 96.5:3.5:0.1. Absorption was recorded at 254 nm. Analytical HPLC was performed using a gradient 75 → 100% B (A: H_2O + 0.1% TFA and B: MeOH + 0.1% TFA) in 30 min, flow 1.0 mL/min.

Two intensive peaks occurred, one with t_R = 7 min and one with t_R = 12 min. Both compounds were investigated by NMR and mass spectrometry. It turned out that the compound with t_R = 7 min is *m*-chlorobenzoic acid (**69**), which is the reduced product of *m*-CPBA (**68**) (**Scheme 32**).

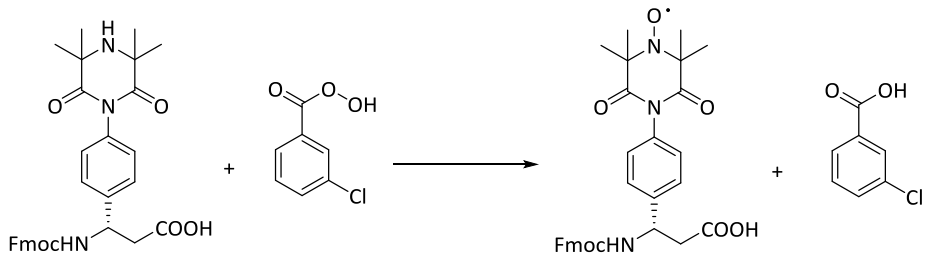

66 **68** **67** **69**

Scheme 32: Redox reaction between amine **66** and *m*-CPBA (**68**).

The compound with t_R = 12 min is the desired β^3-hTOPP label **67**. Due to the additional methylene group of the Fmoc-protected β^3-hTOPP amino acid **67** compared to the Fmoc-protected α-TOPP amino acid **37**, t_R is changed and has the same t_R as *m*-chloro-benzoic acid (**69**) under the above-mentioned conditions used for the flash-column chromatography. Furthermore, benzoic acid **69** can also form an ester in the coupling step of SPPS. Calculation of the peptide mass indeed confirmed that acid **69** was coupled to the peptide sequence, instead of the β^3-hTOPP amino acid **67**. Due to this observation the gradient of the flash-column purification step was optimised to 100:0:0.1 → 98:2:0.1 (DCM/MeOH/AcOH, *v*/*v*/*v*). The pure Fmoc-protected β^3-hTOPP label **67** was then obtained in a yield of 68% (HPLC chromatogram: **Figure 37**).

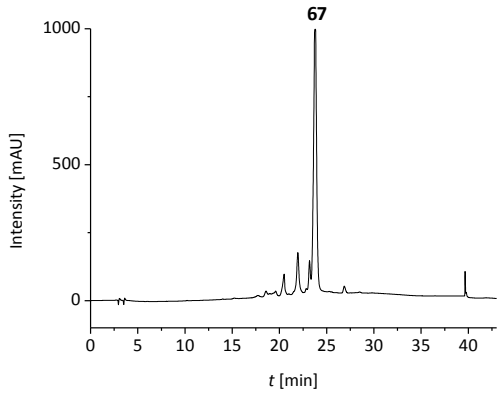

Figure 37: HPLC chromatogram of β^3-hTOPP amino acid **67** purified by flash-column chromatography using the optimised gradient (DCM/MeOH/AcOH 100:0:0.1 → 98:2:0.1). The absorption was recorded at 215 nm. Analytical HPLC was performed using a gradient 10 → 100% C (A: H_2O + 0.1% TFA and C: MeCN + 0.1% TFA) in 30 min, flow 1.0 mL/min. The small peak with t_R = 22 min is the hydroxyl amine of **73** (see subsection 4.3.1.2).

The complete synthetic route for the preparation of the Fmoc-protected β^3-hTOPP label **67** is summarised in **Scheme 33**. The synthesis involved 15 isolated intermediary products and the overall yield of this route was 9%.

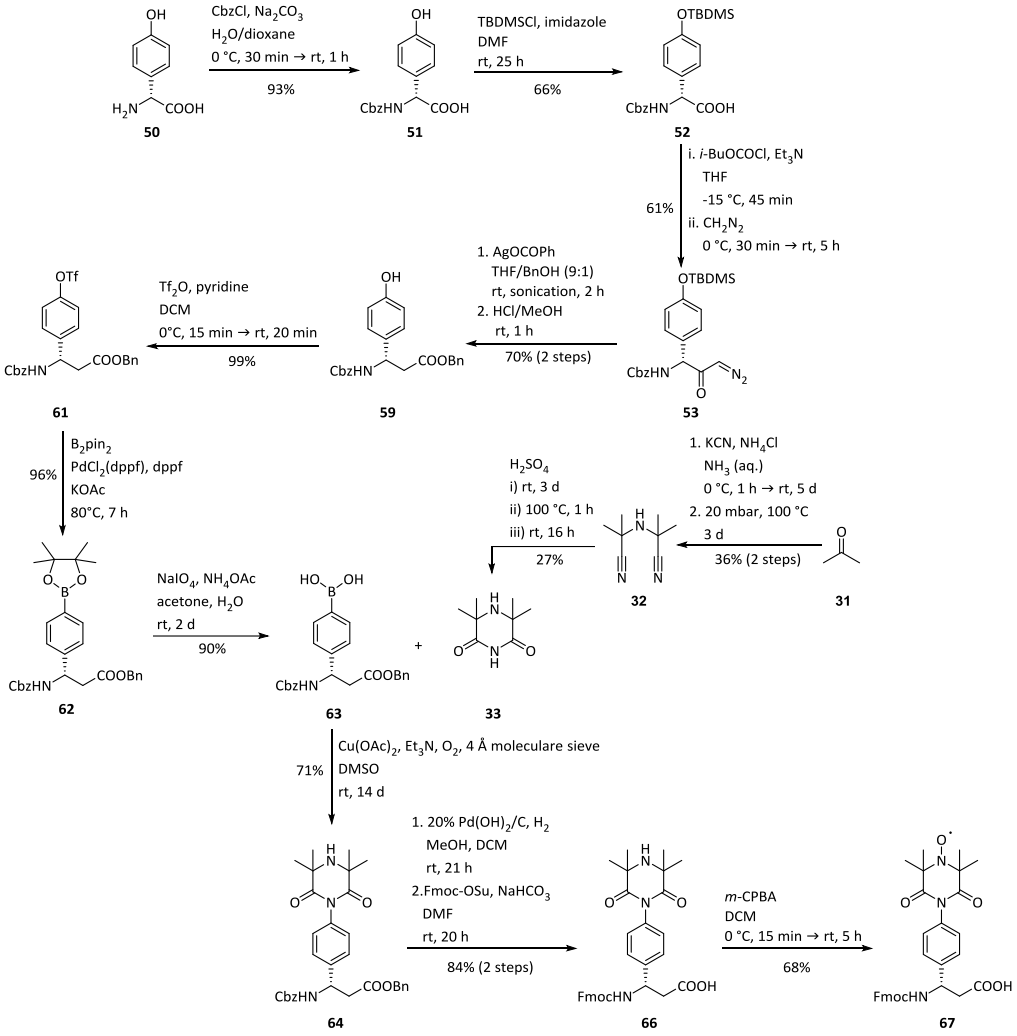

Scheme 33: Overview of the complete synthetic route. The whole synthetic route for Fmoc-D-β^3-hTOPP-OH (**67**) involving 15 isolated intermediate products. The overall yield of this route is 9%.

Pairs of the Fmoc-D-β^3-hTOPP-OH (**67**) were further used for the synthesis of double labelled transmembrane β^3-peptides (see section 4.3.3) which in turn were investigated by CD spectroscopy (see chapter 4.4) and EPR spectroscopy (see chapter 4.6) in order to examine the 3_{14}-helix in solution and lipid bilayer.

4.3.1.1 Investigation of the Enantioselectivity of Selected Reaction Steps

Already small enantiomeric impurities lead to a decreased yield of the final peptide due to the formation of unwanted diastereomers. Furthermore, the separation of a large number of diastereomers by HPLC can be challenging. Finally, remaining stereochemical impurities could lead to biased distances measured by EPR.

Hence, several reaction steps of the β^3-hTOPP label synthesis were investigated regarding their enantioselectivity *via* HPLC using chiral columns. For this approach references are needed. This is usually the racemate of the corresponding product of the synthesis step. The racemate was synthesised using the same condition as for the D-β^3-amino acids (see section 4.3.1 and for more details 5.3.5) starting with a mixture of D-4-Hpg (**50**) and L-4-Hpg (**25**) (1:1).

The *ee* was not examined for the first two compounds **51** and **52** (**Scheme 34**), since the enantioselectivity of the Cbz protection (*ee* ≥ 99%) is already well described in literature.[48]

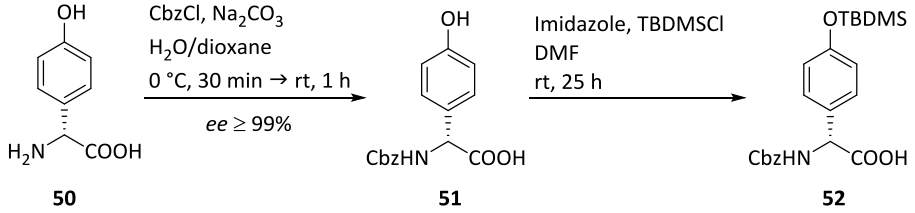

Scheme 34: Introducing of Cbz and TBDMS protecting group. The *ee* value (≥ 99%) of compound **51** was taken from literature.[48] The *ee* value for **52** was not determined, since the TBDMS protection was performed under mild conditions, no epimerisation was expected.

The TBDMS protection is also assumed to be enantioselective, since it was carried out under mild reaction conditions.[140]

Whereas common amino acids, such as Lys, Trp and Val, can convert into the enantiopure β-analogous by the ARNDT-EISTERT reaction, Phg undergoes epimerisation (90:10, i.e. *ee* ≥ 80%) during the activation of the carboxyl group.[120,142]

Since the β^3-hTOPP label is a derivative of Phg, the ARNDT-EISTERT reaction might not be

enantioselective in this case as well. Thus, product **60** was investigated regarding its *ee* by HPLC (**Figure 38**).

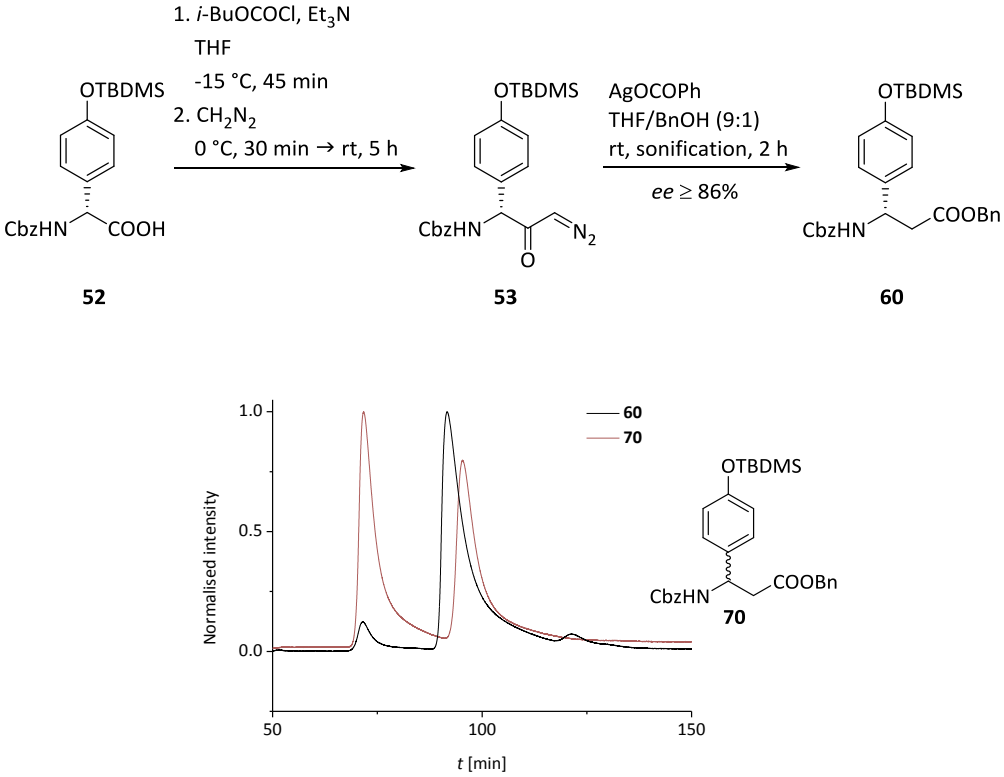

Figure 38: Investigation of compound **60** regarding its *ee* by HPLC. Top: ARNDT-EISTERT reaction using compound **52** as starting material. Bottom: Normalised HPLC chromatograms of **60** and the racemate **70** recorded at 254 nm. HPLC was performed using a Chiralpak® IA column and hexane/isopropanol as eluent (isocratic 92:8 (150 min), flow 0.6 mL/min)**.**

Indeed, in the HPLC chromatogram a small amount of the L-enantiomer occurred. Integration of the peak areas yielded in an *ee* value of 86% (93:7) which was higher than for the common Phg and still sufficient for the successful peptide synthesis. Recall that the final α-TOPP label **23** has an *ee* of 86% which was high enough to get good yields of the peptides.[48]

For the TBDMS deprotection it was not possible to conclusively separate the two enantiomers (**Figure 39**).

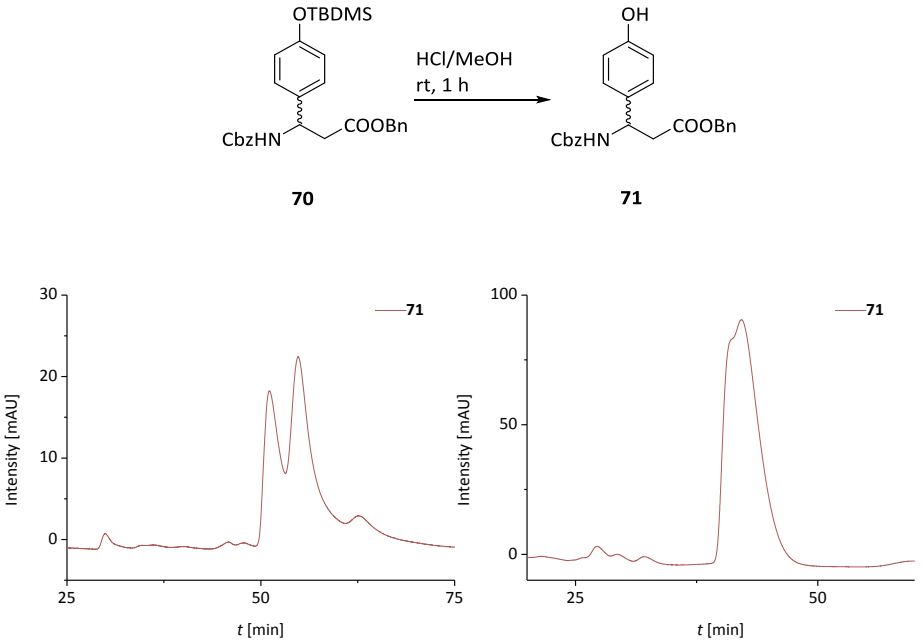

Figure 39: Investigation of compound **71** regarding its *ee* by HPLC. Top: Deprotection reaction which led to compound **71**. Bottom: HPLC chromatograms of **71.** Absorption was recorded at 254 nm. Left: HPLC was performed using a Chiralpak® IA column and hexane/isopropanol as eluent (isocratic 87/13 (100 min), flow 0.6 mL/min). Right: HPLC was performed using a Chiralcel® OD column and hexane/isopropanol as eluent (isocratic 80/20 (90 min), flow 0.6 mL/min)**.**

Different ratios of the eluent (hexane/isopropanol) and two different columns (Chiralpak® IA and Chiralcel® OD) were used but unfortunately, no condition lead to baseline separation of the two enantiomers. This might result from the polarity of the hydroxyl group. At this point, product **59** (section 4.3.1, **Scheme 26**) was not investigated as the racemate of the next reaction step (triflate functionalisation, compound **61**) showed better separation properties using the Chiralpak® IA column (**Figure 40**).

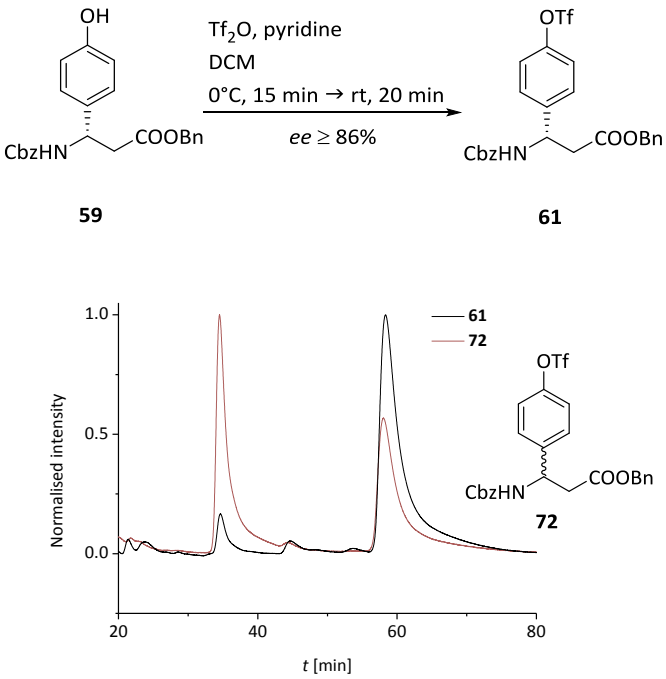

Figure 40: Investigation of compound **61** regarding its *ee* by HPLC. Top: Reaction conditions which were used to convert compound **59** into product **61**. Bottom: Normalised HPLC chromatograms of **61** and the racemate **72** recorded at 254 nm. HPLC was performed using a Chiralpak® IA column and hexane/isopropanol as eluent (isocratic 90:10 (90 min), flow 0.6 mL/min)**.**

The integration of the peak areas in the HPLC chromatogram (**Figure 40**) yielded an *ee* of 86% (93:7). Thus, it was demonstrated that over two reaction steps (TBDMS deprotection and triflate group insertion) the *ee* value did not change.

Due to its distance to the carboxyl group, the β-hydrogen of β^3-amino acids are not as acidic as the α-hydrogen of the α-analogous. It is known that β^3-amino acids 'cannot racemise during activation and coupling'.[143] Thus, the reaction conditions for the β^3-hTOPP synthesis, which are similar to those of the α-TOPP label should not alter the stereogenic centre of the β^3-amino acids in an unwanted manner.

Hence, for the final Fmoc-protected D-β^3-hTOPP label **67** two peaks were expected in a ratio of 93:7. Therefore, the Fmoc-protected D-β^3-hTOPP amino acid **67** was examined

via HPLC using a chiral column. Two different columns Chiralpak® IA and Chiralcel® OD-R were tested. **Figure 41** shows two selected HPLC chromatograms.

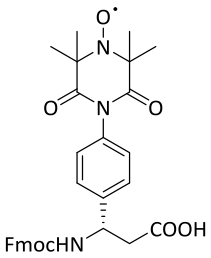

67

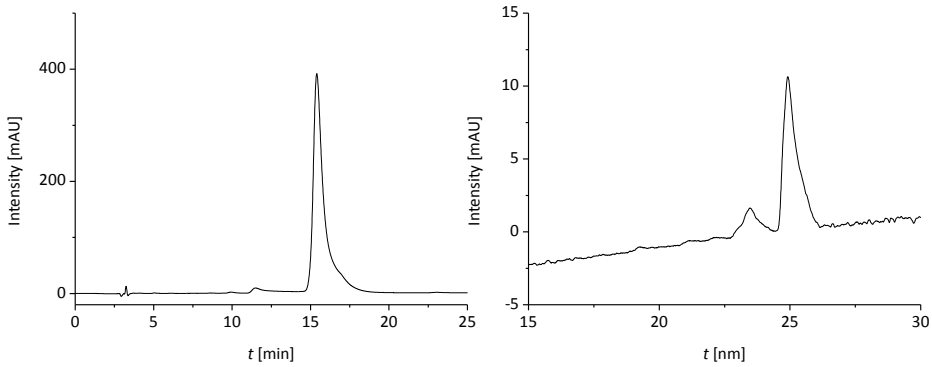

Figure 41: Investigation of compound **67** regarding its *ee* by HPLC. Top: Illustration of the Fmoc-protected β^3-hTOPP label **67**. Bottom: Absorption was recorded at 254 nm. Left: HPLC was performed using a Chiralpak® IA column and gradient 45 → 55% C (A: H_2O + 0.1% TFA and C: MeCN + 0.1% TFA) in 30 min, flow 1.0 mL/min. Right: Excerpt HPLC chromatogram (full chromatogram see Appendix). HPLC was performed using a Chiralcel® OD-R column and a gradient 10 → 100% C (A: H_2O + 0.1% TFA and C: MeCN + 0.1% TFA) in 30 min, flow 1.0 mL/min.

The tested HPLC conditions did not lead to an unambiguous result. In the case of using MeCN/H_2O (0.1% TFA) as eluent and Chiralpak® IA as column (**Figure 41**, left) no hint of the L-enantiomer is observed. In the case of MeCN/H_2O (0.1% TFA) and Chiralcel® OD-R column (**Figure 41**, right) a small peak is observed at t_R = 23.4 min, which might be the L-enantiomer, since the ratio between the two peaks would fit to the *ee* value (86%) observed before. But, nevertheless, it is also conceivable that this is the hydroxyl amine

species **73** of the Fmoc-protected β^3-hTOPP label **67** (cf. HPLC chromatograms illustrated in **Figure 43**, subsection 4.3.1.2). Mass spectrometry of the small peak could not answer this question.

In conclusion, over two steps it was shown that the *ee* value was constant (86%, compound **59** and **61**). For the final Fmoc-protected β^3-hTOPP label **67** an unambiguous result for the *ee* was not possible. Thus, a reference is needed. However, the peptide synthesis (synthesis of diastereomers) and the corresponding HPLC experiments (separation of diastereomers) (section 4.3.3), CD (chapter 4.4) and PELDOR results (chapter 4.6) demonstrated that the β^3-hTOPP label was synthesised with a sufficient *ee* value.[143]

4.3.1.2 Stability of the Radical

To test the stability of the radical species **67** against reduction to the hydroxyl amine species **73** (**Figure 42**), both compounds were examined under conditions which were similar to those used during the cleavage form the resin/purification of the labelled peptides (e.g. see section 5.3.7).

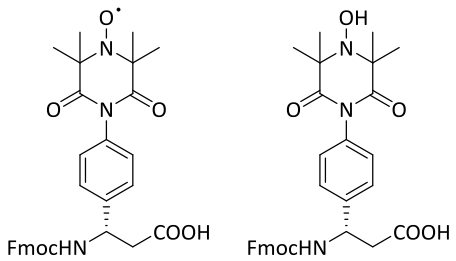

67 **73**

Figure 42: The β^3-hTOPP label **67** and the hydroxylamine species **73**.

HPLC was performed to verify a possible reduction of the radical species. Chromatograms are illustrated in **Figure 43**.

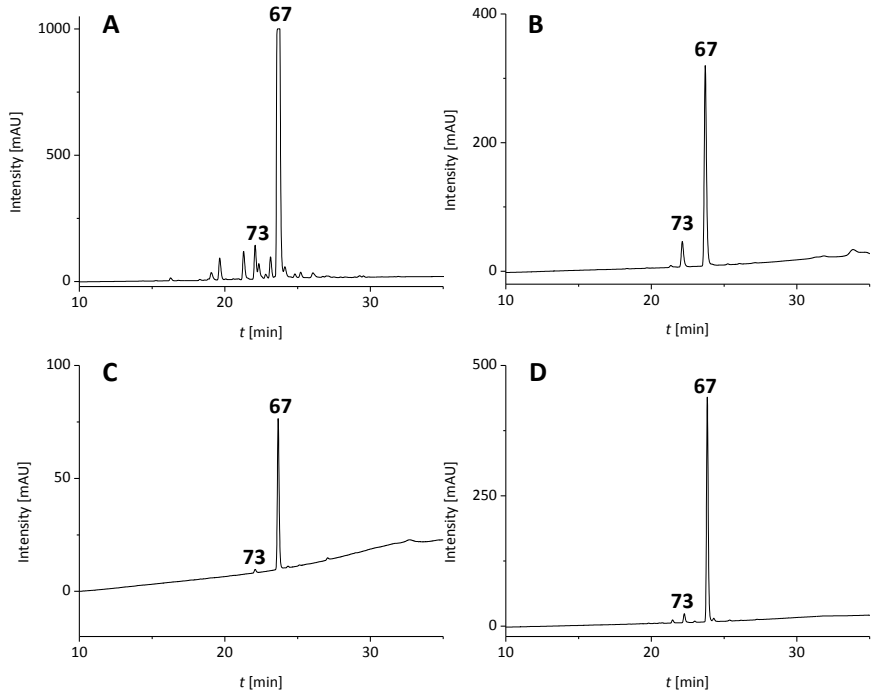

Figure 43: Investigation of the stability of the radical species **67**. Analytical HPLC experiments were performed with a gradient 10 → 100% C (A: H_2O + 0.1% TFA and C: MeCN + 0.1% TFA) in 30 min, flow 1.0 mL/min. Absorption was recorded at 254 nm. **A**: HPLC chromatogram after pre-purification by column chromatography. **B**: HPLC chromatogram after HPLC purification and lyophilisation. **C**: HPLC chromatogram (normalised to 0) after HPLC purification and direct injection of the collected HPLC peak **67**. **D**: HPLC chromatogram of the HPLC purified and lyophilised fraction **67** which was kept at rt and overnight dissolved in MeCN/H_2O.

The radical **67** was first pre-purified by flash-column chromatography and then isolated by HPLC (**Figure 43**, **A**). The HPLC separated compounds were identified as radical species **67** and hydroxyl amine species **73** by mass spectrometry. After lyophilisation the radical was still the main species (**Figure 43**, **B**). Integration of the peak areas yielded a **67/73** ratio of 22:3 (radical species 88%). The isolated radical **67** was directly re-examined by HPLC (**Figure 43**, **C**). The hydroxyl amine species occurred again but its amount was just about 2%. Surprisingly, storage of the HPLC purified and lyophilised radical in MeCN/H_2O at rt for 12 h led to a nearly quantitative conversion into the radical

species (96%) (**Figure 43**, **D**; cf. **B**).

Similar experiments were then performed with the hydroxyl amine species **73**. The HPLC chromatograms are illustrated in **Figure 44**.

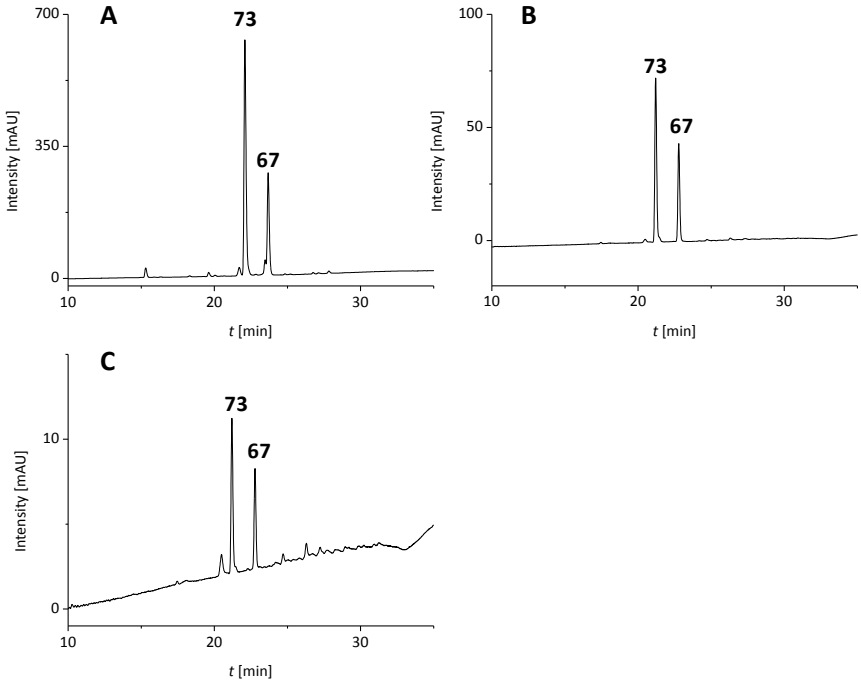

Figure 44: Investigation of the stability of the hydroxyl amine species **73**. Bottom: Analytical HPLC experiments were performed with a gradient 10 → 100% C (A: H_2O + 0.1% TFA and C: MeCN + 0.1% TFA) in 30 min, flow 1.0 mL/min. Absorption was recorded at 254 nm. **A**: HPLC chromatogram of the crude hydroxyl amine **73**. **B**: HPLC chromatogram after HPLC purification and lyophilisation of peak **73**. **C**: HPLC chromatogram (normalised to 0) after HPLC purification and direct injection of the collected HPLC peak of **73**.

To generate the hydroxyl amine species **73**, compound **67** was treated under the same conditions (TFA/TIS/H_2O (95:2.5:2.5, *v*/*v*/*v*)) as used for cleavage of the peptide from the resin, at rt for 2 h (see section 5.2.9). The reagents were removed under a N_2 stream and the crude hydroxyl amine was purified by HPLC (**Figure 44**, **A**).

The HPLC chromatogram showed that the reaction was not quantitative. Besides the

reduced compound **73**, the nitroxide radical species **67** was still present. Integration of the peak areas led to a **73**/**67** ratio of 37/13 (hydroxyl amine species 74%). After purification, amino acid **73** was lyophilised and the purity was checked by HPLC (**Figure 44**, **B**). Again, the radical species **67** is observed. Integration of the peak areas yielded in a **73/67** ratio of 63/37. After collecting the peak of compound **73**, it was directly re-investigated by HPLC (**Figure 44**, **C**). The HPLC chromatogram again showed both compounds. Integration of the peak areas gave a ratio of 29/21 (hydroxyl amine species 58%). In literature a similar observation was made in which exposition with air led to a quantitative yield of a nitroxide radical.[144]

In summary, the results presented above strongly suggest that unwanted hydroxyl amine **73** was oxidised back to the wanted radical species **67**, presumably by atmospheric oxygen. This further increases the applicability of the β^3-hTOPP radical **24**.

4.3.2 Synthesis of β³-Amino Acids for the β-Peptides

The transmembrane β-peptides **P5**, **P6**, **P7** and **P8** consist of three further β³-amino acids: Fmoc-D-β³-hLys(Boc)-OH (**74**), Fmoc-D-β³-hTrp(Boc)-OH (**75**) and Fmoc-D-β³-hVal-OH (**76**) (**Figure 45**).

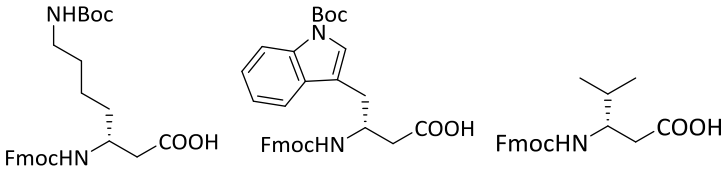

74 **75** **76**

Figure 45: Structures of the β³-amino acids used in the β³-peptide synthesis: Fmoc-D-β³-hLys(Boc)-OH (**74**), Fmoc-D-β³-hTrp(Boc)-OH (**75**) and Fmoc-D-β³-hVal-OH (**76**).

SEEBACH and co-workers published synthetic routes towards enantiomerically pure β³-amino acids based on the ARNDT-EISTERT reaction. [120,122] The three building blocks **74**, **75**, **76** were synthesised according to a variant described by GUICHARD *et al.* (**Scheme 35**).[122]

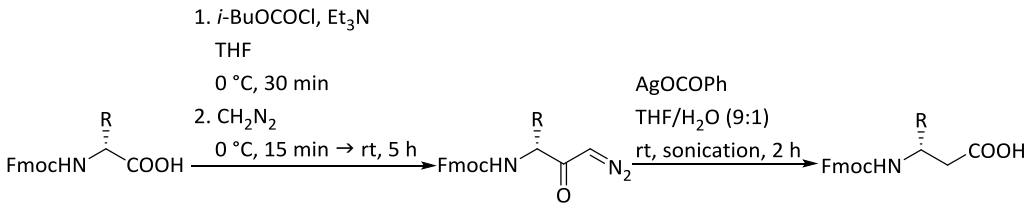

77 **78** **79**

Scheme 35: ARNDT-EISTERT homologation. R correspond to the appropriate amino acid side-chain. First, the α-amino acid **77** was activated, then attacked by CH_2N_2 and afterwards converted into the β³-amino acid **79** *via* the WOLFF rearrangement using silver(I) ions.

First the commercially available protected D-α-amino acid **77** (Fmoc-D-Lys(Boc)-OH, Fmoc-D-Trp(Boc)-OH or Fmoc-D-Val-OH) was dissolved in dry THF. Then the carboxylic group was deprotonated by Et_3N and activated using *i*-BuOCOCl. The resulting reactive anhydride was directly converted into the diazo ketone **78** using diazomethane.

Without purification the diazo ketone **78** was transformed to the corresponding β^3-amino acid **79** *via* a WOLFF rearrangement. Therefore, compound **78** was dissolved in a mixture of THF/H_2O (9:1) and AgOCOPh was added. Sonication at rt for 2 h led to the crude β^3-amino acid **79**. In the cases **74** and **75** the crude amino acid was purified by precipitation within cold pentane (-22 °C). β-amino acid **76** was purified by flash-column chromatography using a DCM/MeOH/AcOH mixture as eluent. This gave pure products as signalled by corresponding NMR spectra. The yields of these reactions are listed in **Table 6**.

Table 6: Overall yields given in % of the β-amino acids Fmoc-D-β^3-hLys(Boc)-OH (**74**), Fmoc-D-β^3-hTrp(Boc)-OH (**75**) and Fmoc-D-β^3-hVal-OH (**76**).

β-amino acid	**Yield**
Fmoc-D-β^3-hLys(Boc)-OH (74)	82
Fmoc-D-β^3-hTrp(Boc)-OH (75)	79
Fmoc-D-β^3-hVal-OH (76)	68

The β^3-amino acids **74**, **75** and **76** were further used for the synthesis of transmembrane β^3-peptides (see section 4.3.3).

4.3.3 Development and Synthesis of the TOPP-Labelled β^3-Peptides

All four TOPP-labelled transmembrane β^3-peptides **P5**, **P6**, **P7** and **P8** were synthesised using manual microwave-assisted Fmoc SPPS. The peptide sequences are shown in **Figure 46.**

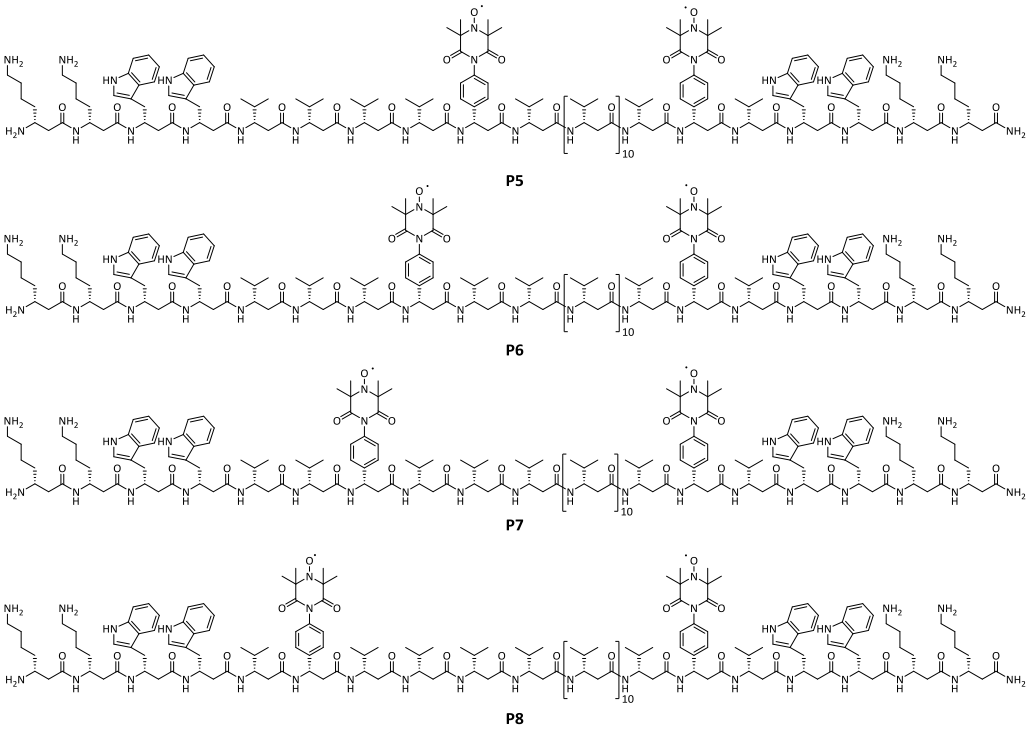

Figure 46: Peptide sequences of the TOPP-labelled β-peptides **P5**, **P6**, **P7** and **P8**.

The synthesis strategy for the TOPP-labelled β-peptides is based on modern Fmoc SPPS protocols especially from the group of DIEDERICHSEN.[137,143,145–147] However, expensive building blocks (especially the β^3-hTOPP label) required further developments to achieve highly efficient, material-saving synthesis strategies as shown in the following discussion.

The synthetic route of **P5** is shown in **Scheme 36**. The scheme in particular illustrates intermediary peptide fragments (**P5B**, **P5C**, **P5D**, …, **P5I**) which were verified by HPLC and mass spectrometry after test cleavages.

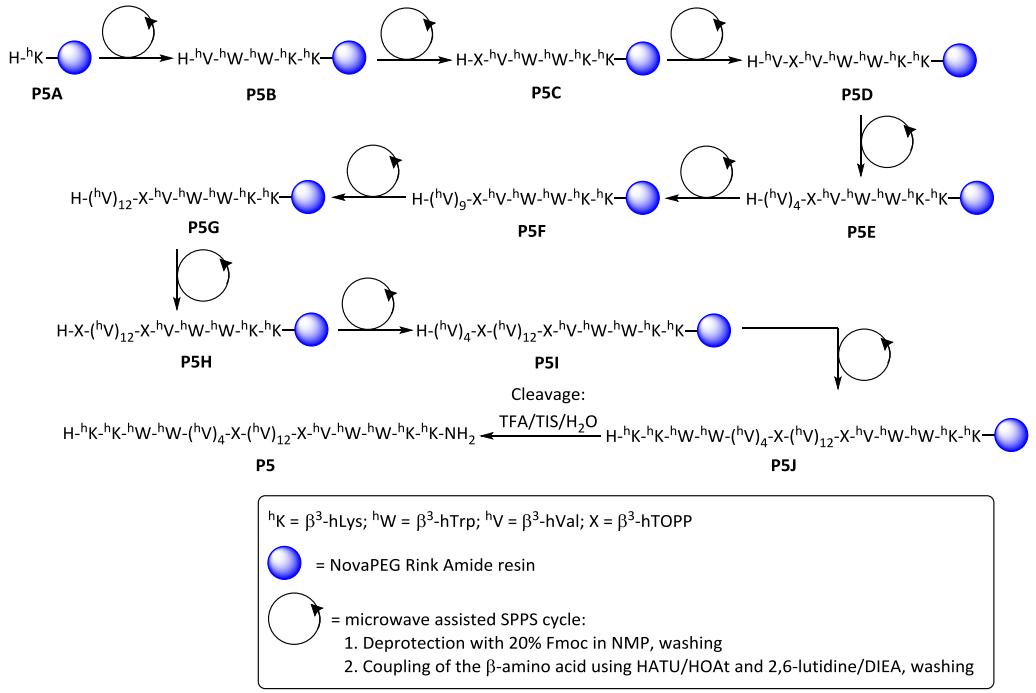

Scheme 36: Synthesis route of **P5**. The proteinogenic β^3-amino acids are designated after the one letter code and the β^3-hTOPP label is symbolised by X. The chain elongation was performed on a NovaPEG Rink Amide resin and the resin was pre-loaded with β^3-hLys (**P5A**)**.** After selected steps of the synthesis test cleavages were performed to monitor chain elongation (marked with peptide **P5B**, **P5C**, **P5D**, …, **P5I**). The Fmoc SPPS is based on the repetition of deprotection and coupling steps on a solid support by means of microwave irradiation.

This extensive test cleavage protocol allows a comprehensive examination of the efficiency of the utilised conditions.

As mentioned in section 3.3.2, low loaded resins can minimise aggregation of the peptide chains and steric hinderance due to the steric demand of the β^3-hTOPP label **24**.[80,148] Furthermore, polyethylene glycol (PEG) based resins have been proven to additionally prevent aggregation of hydrophobic peptides.[149] Hence, the peptides were synthesised on a low loaded NovaPEG Rink Amide resin. Additionally, this type of resin shows good swelling behaviour in the commonly used solvents for SPPS.[149] A good solvation of the peptide-resin complex is also essential for a successful chain

elongation.[79–81,150] Thus, a mixture of NMP/DMF/DMSO (1:0.8:0.2, *v*/*v*/*v*) was used as solvent system, since these solvents are known to fulfil this demand.[83,84] Additionally, this mixture grants the solubility of all subsequently utilised reactants.[83,84] Note that in particular DMSO is known to have the ability to disaggregate unwanted peptide bundles and it has been demonstrated that the addition of DMSO increases the yields of difficult sequences.[151]

The resin was loaded with β^3-hLys (**P5A**) using Fmoc-β^3-hLys(Boc)-OH (**2**) under the standard microwave-assisted (60 °C, 35 W, 15 min) procedure as described for α-peptides using *N,N*'-diisopropylcarbodiimide (DIC) and HOBt as coupling reagents and NMP as solvent. Double coupling was performed. After the first amino acid coupling step, to prevent the formation of wrong peptides sequences, uncoupled positions on the resin were acetylated using Ac_2O/2,6-lutidine/NMP (1:2:7, *v*/*v*/*v*).

The following amino acids were coupled using 1-[Bis(dimethylamino)methylene]-1*H*-1,2,3-triazolo[4,5-*b*]pyridinium 3-oxid hexafluorophosphate (HATU)/1-hydroxy-7-azabenzotriazole (HOAt) as coupling reagent system and a mixture of 2,6-lutidine/DIEA as base. The activation reagents HATU/HOAt form a highly reactive active ester with the amino acid, which is more reactive than the corresponding ester using HBTU/HOBt.[152] In conclusion, the final coupling mixture contained an excess of 4.00 eq amino acid, 4.00 eq HOAt, 3.90 eq HATU and 4.80 eq/3.20 eq 2,6-lutidine/DIEA dissolved in NMP/DMF/DMSO. In the case of double coupling the second mixture consists of 3.00 eq amino acid, 3.00 eq HOAt, 2.90 eq HATU and 3.60 eq/2.40 eq 2,6-lutidine/DIEA in NMP/DMF/DMSO. The chain elongation was performed by repeating microwave-assisted Fmoc deprotection steps with 20% piperidine in NMP and coupling steps of the amino acids. The resin was washed thoroughly between the steps with different solvents (NMP, DCM and DMF) to remove remaining reagents.

Thus, the initial synthesis of β^3-peptide **P5** was performed using Fmoc-β^3-hLys(Boc)-OH (**74**), Fmoc-β^3-hTrp(Boc)-OH (**75**) and Fmoc-β^3-hVal-OH (**76**) and microwave irradiation

(60 °C, 35 W, 15 min). For the second hLys in the peptide sequence single coupling was performed. The hTrp and hVal were added to the sequence by using double coupling. To validate peptide sequence **P5B**, a test cleavage was performed under acidic conditions (TFA/H_2O/TIS (95:2.5:2.5, *v*/*v*/*v*)). The coupling success was verified by HPLC and mass spectrometry (see Appendix). Next, the hTOPP label **23** was inserted. In contrast to the α-analogous of the TOPP, no special coupling conditions were used because β^3-amino acids are not prone to racemise during coupling.[143] To save material, 2.00 eq of Fmoc-β^3-hTOPP-OH (**67**) were used. In summary, the hTOPP was coupled using microwave irradiation (60 °C, 25 W, 15 min) and HATU/HOAt, 2,6-lutidine/DIEA, and double coupling was performed. The HPLC chromatogram of the products obtained after a test cleavage is shown in **Figure 47**.

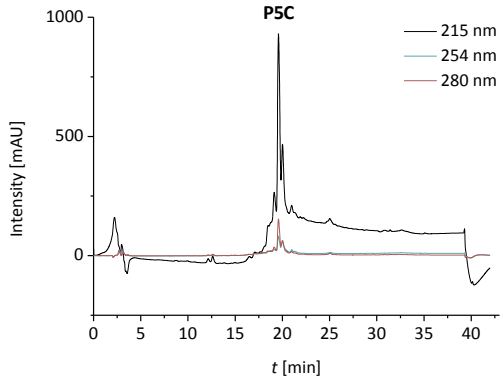

Figure 47: HPLC chromatogram of the crude peptide **P5C**. Absorption was recorded at 215, 254 and 280 nm. Analytical HPLC was performed using a gradient 10 → 100% B (A: H_2O + 0.1% TFA and B: MeOH + 0.1% TFA) in 30 min, flow 1.0 mL/min.

HPLC demonstrated the effective coupling of the hTOPP label (t_R = 19.6 min). Two additional, smaller peaks appeared in the chromatogram. The peak at t_R = 19 min belongs to a diastereomer of **P5C**, since the hTOPP label was not fully enantiopure (see subsection 4.3.1.1). It is assumed that the second small peak at t_R = 20 min belongs to an aggregate of **P5C** because the mass spectrum only showed a species that has the same mass as peptide **P5C** (see Appendix).

The hVal after the TOPP was coupled as mentioned above (60 °C, 35 W, 15 min) and double coupling was performed. **P5D** was obtained in high purity (see Appendix). According to literature, single coupling was then performed to achieve **P5E**.[137] The coupling efficiency was verified by HPLC and mass spectrometry. It turned out that the used conditions were not favourable and the conditions had to be improved. **Figure 48** left shows the HPLC chromatogram of peptide sequence **P5E** under the above-mentioned conditions and **Figure 48** right illustrates the HPLC chromatogram using improved conditions.

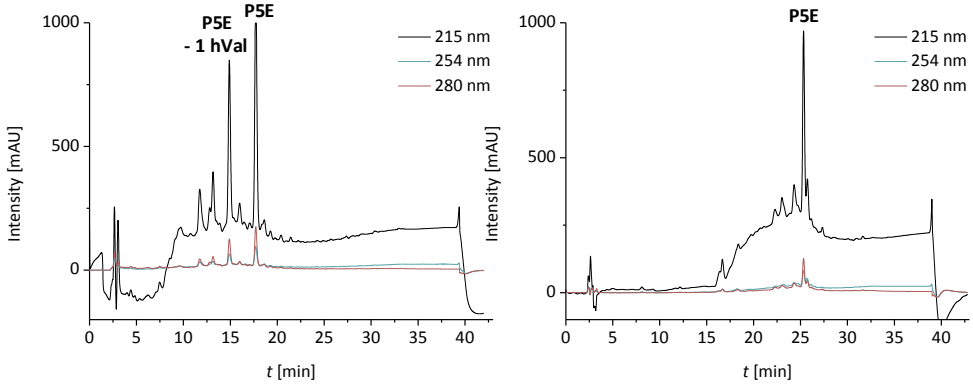

Figure 48: HPLC chromatograms of the crude **P5E** using different coupling conditions. Absorption was recorded at 215, 254 and 280 nm. Left: Analytical HPLC was performed using a gradient 50 → 100% B (A: H_2O + 0.1% TFA and B: MeOH + 0.1% TFA) in 30 min, flow 1.0 mL/min. An unwanted species **P5E – 1 hVal** occurred. Right: HPLC chromatogram using improved coupling conditions (**P5E-6**, **Table 7**) for synthesising **P5E.** Analytical HPLC investigation was performed using a gradient of 10 → 100 B (A: H_2O + 0.1% TFA and B: MeOH + 0.1% TFA) in 30 min, flow 1.0 mL/min.

In the HPLC chromatogram (**Figure 48** left) a significant portion of unwanted peptide species occurred at t_R = 15 min. This species belongs to a peptide sequence without one hVal (**P5E – 1 hVal**, mass spectrum see Appendix). Due to this observation coupling conditions of the steps from peptide sequence **P5D** to **P5E** were optimised. In particular, this involved changes in coupling time, temperature and the addition of LiCl. According to literature, chaotropic salts can improve the coupling efficiency of difficult α- and β-

peptide sequences by disrupting aggregation and secondary structure formation.[145,153] The tested conditions are illustrated in **Table 7**.

Table 7: Tested conditions to improve the coupling conditions of the synthesis from peptide sequence **P5D** to **P5E**. The different conditions are named after **P5E**.

Term	Condition
P5E-1	60 °C, 25 W, 15 min, NMP/DMF/DMSO, double coupling
P5E-2	60 °C, 25 W, 20 min, NMP/DMF/DMSO, double coupling
P5E-3	45 °C, 25 W, 20 min, 0.8 M LiCl in NMP/DMF/DMSO, double coupling
P5E-4	60 °C, 25 W, 20 min, 0.8 M LiCl in NMP/DMF/DMSO, double coupling
P5E-5	60 °C, 25 W, 20 min, 0.8 M LiCl in NMP, double coupling
P5E-6	60 °C, 20 W, 30 min, 0.8 M LiCl in NMP/DMF/DMSO, double coupling

The most suitable condition was determined according to the efficiency of the coupling as estimated by the appearance of the unwanted peaks in the chromatogram (also see Appendix). Since the HPLC chromatogram of **P5E-6** (**Figure 48** right) mainly showed the desired peptide, these conditions were chosen as the most promising conditions. The amino acids were double coupled using HATU/HOAt, 2,6-lutidine/DIEA dissolved in a solvent mixture of 0.8 M LiCl in NMP/DMF/DMSO and microwave irradiation (60 °C, 30 min). Due to the ionic strength of the LiCl the power of the microwave had to be decreased (for specific details see section 5.3.7).

Test cleavages and mass spectrometric measurements were performed after each coupling of hVal, and it turned out that only the fourth hVal after the hTOPP label has a lower tendency to couple. Since β-peptides can form stable secondary structures already with six residues[106] at this point of the synthesis, the β-peptide might have

started to form a secondary structure which prevented successful coupling. A similar phenomenon was observed for natural peptides before.[80] Additionally, aggregates might have occurred which were not fully disrupted by the Li salt and DMSO. HPLC experiments at different temperatures showed that indeed **P5E** has a tendency to aggregate (**Figure 49**).

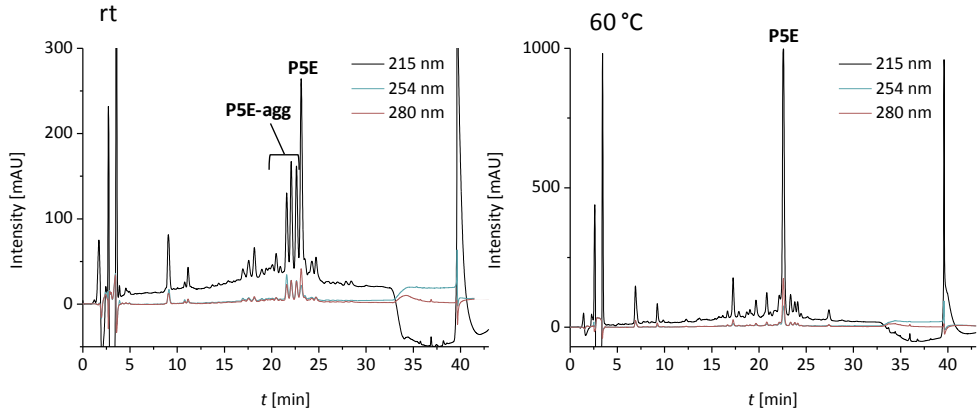

Figure 49: HPLC chromatograms of the crude peptide **P5E** at different temperatures. Absorption was recorded at 215, 254 and 280 nm. Left: Analytical HPLC investigation of **P5E** was performed at rt using a gradient of 20 → 60% C (A: H_2O + 0.1% TFA and C: MeCN + 0.1% TFA) in 30 min, flow 1.0 mL/min. Right: Analytical HPLC was performed as described for the rt experiment but at 60 °C. Mass spectrometry confirmed that the compound at t_R = 23 min is the desired peptide **P5E**.

The HPLC chromatogram illustrated in **Figure 49** left, shows that at rt multiple peaks occurred (**P5E-agg**). In contrast to that at higher temperature (60 °C), **Figure 49** right, only one intensive peak occurred while using the exact same conditions as before (also note the reduced intensity of peaks at rt). Mass spectrometry confirmed that the single peak (**Figure 49** right) belongs to a species which has the same mass as peptide **P5E**. Thus, it is assumed that at rt several distinct aggregates exist which interact differently with the column material and therefore, show different t_R. By increasing the temperature, the monomer is favoured (or there is a fast interconversion between all species) and only one distinct peak is observed.

Nevertheless, the fourth hVal after the hTOPP label was finally coupled with a longer

reaction time of 35 min and the miscoupled peptide species was eliminated by capping. The resin was then washed with 5% DIEA in NMP. Unfortunately, not only an acetylated species missing one hVal was included in the mass spectrum but also an acetylated species of **P5E** (**P5E-cap**, t_R = 26.3 min) was observed (HPLC chromatogram **Figure 50**, mass spectrum see Appendix).

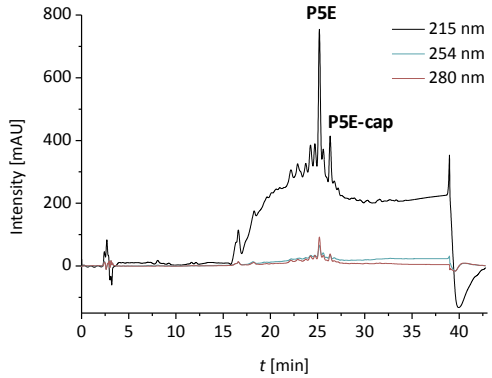

Figure 50: HPLC chromatograms of **P5E** after acetylation. Absorption was recorded at 215, 254 and 280 nm. Analytical HPLC investigation of **P5E** was performed at rt using a gradient of 10 → 100% B (A: H_2O + 0.1% TFA and B: MeOH + 0.1% TFA) in 30min, flow 1.0 ml/min.

Indeed, it is very likely that the nitroxide moiety was acetylated, which then prohibited further capping steps after insertion of the hTOPP label.

The following β^3-amino acids, including the hTOPP label, were all coupled according to the novel and successful coupling protocol, i.e. using HATU/HOAt, 2,6-lutidine/DIEA dissolved in a solvent mixture of 0.8 M LiCl in NMP/DMF/DMSO and microwave irradiation (60 °C, 30 min). Every fourth amino acid after the first TOPP and the second hTOPP label were coupled for 35 min. Test cleavages of **P5F**, **P5G**, **P5H** and **P5I** were investigated by HPLC and mass spectrometry (HPLC chromatograms and mass spectra see Appendix). All peptides were obtained in high purity. The last four β-amino acids (hTrp and hLys) were coupled with an increased reaction time of 40 min. After successful synthesis of the complete peptide sequence (**P5J**), the peptide was cleaved

from the resin under acidic condition (TFA/H_2O/TIS (95:2.5:2.5, *v*/*v*/*v*)). The trialkylsilane TIS and H_2O are used as scavengers to minimise the formation of by-products during the cleavage. Then the β^3-peptide was pre-purified by precipitation in cooled Et_2O.

As mentioned in section 3.3.2, the nitroxide radicals within the peptide are reduced to the hydroxyl amine under the acidic cleavage conditions and due to the reductive properties of TIS.[11,48,87] Hence, the hydroxyl amine was re-oxidised to the nitroxide species by using copper(II) ions as oxidant. Therefore, the crude peptide was treated with $Cu(OAc)_2$ in a solvent mixture of MeCN and MeOH for 2 h and purified by analytical HPLC. First attempts to purify peptide **P5** were performed using MeOH/H_2O as eluent for the HPLC (**Figure 51** left). However, no separation between peptide **P5** and the unwanted peptide sequences was possible. Thus, the solvent system was changed to MeCN/H_2O (**Figure 51** right). The chromatograms obtained for both eluent systems are presented in **Figure 51**.

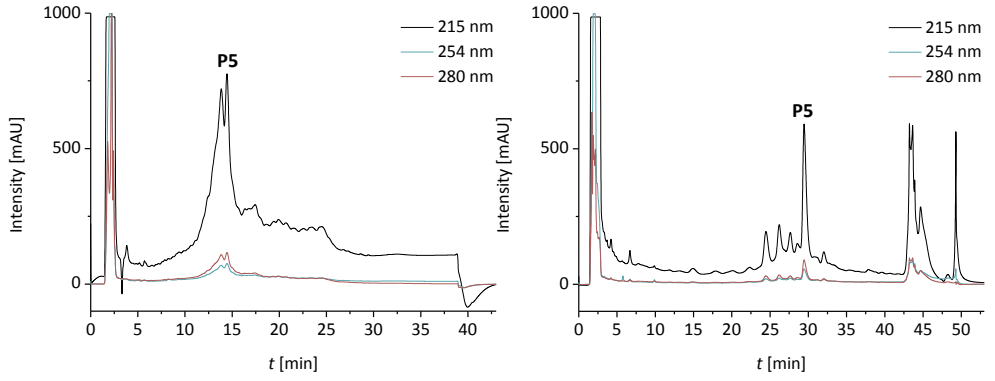

Figure 51: HPLC chromatograms of **P5** using different eluent systems. Absorption was recorded at 215, 254 and 280 nm. Left: HPLC chromatogram of **P5** using a gradient 72.5 → 97.5% B (A: H_2O + 0.1% TFA and B: MeOH + 0.1% TFA) in 30 min at 60 °C, flow 1.0 ml/min. Right: HPLC chromatogram of **P5** using a gradient 68 → 80% C (A: H_2O + 0.1% TFA and C: MeCN + 0.1% TFA) in 40 min at 60 °C, flow 1.0 ml/min.

The HPLC chromatogram showed a sufficient separation of peptide **P5** (t_R = 29.43 min) and unwanted peptides (mass spectrum see Appendix).

The peptides **P6**, **P7** and **P8** were synthesised according to the novel and successful coupling protocol, which is summarised in detail in **Table 8**. Recall that the position of the TOPP is changed according to **Figure 46**.

Table 8: Conditions of the β-peptide synthesis. The conditions are listed from the *C*- to the *N*-terminus of the peptides. The power of the microwave irradiation (MW) differs because of the ionic strength of the Li salt. For details see 5.3.7.

	Conditions
hLys (loading of the first amino acid)	60 °C, 35 W, 15 min, HOBt/DIC in NMP, double coupling
Until the 7th amino acid, including the first hTOPP label	60 °C, 25 W, 15 min, HATU/HOAt, 2,6-lutidine/DIEA in NMP/DMF/DMSO, double coupling
The 7th and the following amino acids	60 °C, MW, 30 min, HATU/HOAt, 2,6-lutidine/DIEA in 0.8 M LiCl NMP/DMF/DMSO, double coupling
Every 4th amino acid after the first hTOPP and the second hTOPP label	60 °C, MW, 35 min, HATU/HOAt, 2,6-lutidine/DIEA in 0.8 M LiCl NMP/DMF/DMSO, double coupling
The last 4 amino acids	60 °C, MW, 40 min, HATU/HOAt, 2,6-lutidine/DIEA in 0.8 M LiCl NMP/DMF/DMSO, double coupling

After acidic cleavage (TFA/H_2O/TIS (95:2.5:2.5, *v*/*v*/*v*)) from the resin the crude reduced species of **P6**, **P7** and **P8** were oxidised using $Cu(OAc)_2$ dissolved in MeCN/MeOH, purified by HPLC and verified by mass spectrometry (HPLC chromatograms and mass spectra see Appendix).

For subsequent investigations by PELDOR all β-peptides were oxidised and purified only in small amounts to provide fresh samples.

4.4 Secondary Structure Determination by CD Spectroscopy

CD spectroscopy has proven valuable in the study of α-peptides, as shown in chapter 3.4, since information about secondary structure formation of peptides can be readily obtained.

3_{14}-Helical β-peptides have been intensively investigated through CD spectroscopy by SEEBACH and co-workers.[113,121,154,155] They characterised the CD pattern of a left-handed 3_{14}-helix in MeOH with specific characteristics: a maximum near 200 nm, a zero-crossing between 205 and 210 nm, and a minimum between 215 and 220 nm.[155]

Recently, DIEDERICHSEN and co-workers published CD data of right-handed 3_{14}-helical transmembrane peptides, which are similar to the peptides **P5**–**P8** that are investigated in this thesis, in trifluoroethanol (TFE) and within lipid bilayers.[136,137,147] In TFE a minimum near 190 nm, a zero-crossing at approximately 201 nm and a maximum around 211 nm were observed. In the lipid bilayers a minimum between 186 and 196 nm, a zero-crossing at 199 nm, and a maximum between 205 and 220 nm were detected. These mirrored results (due to right-handed 3_{14}-helical peptides) are in good agreement with SEEBACH's observations for the left-handed 3_{14}-helix.

It is known from literature that aromatic amino acids such as Trp can show characteristic CD bands in the 220–250 nm region.[156] Since there are indeed four aromatic hTrp in the transmembrane β-peptides, an additional weak maximum (shoulder) was described at approximately 230 nm.[136,137]

The transmembrane peptides **P5**, **P6**, **P7** and **P8** were designed to form a right-handed 3_{14}-helix. Thus, to validate this behaviour, CD measurements were performed in solution as well as in lipid bilayers.

4.4.1 Results and Discussion of Measurements in Solution

The secondary structure formation of the peptides was investigated in solution (TFE, MeOH) with a peptide concentration of 10 μM. The CD spectra of **P5**, **P6**, **P7**, **P8** and the reference peptide **P4** (transmembrane peptide without hTOPP labels (see **Figure 34**,

section 4.1.1); synthesised by BRIGITTE WORBS (GEORG-AUGUST University Göttingen) according to the protocol developed in section 4.3.3) in TFE and MeOH are illustrated in **Figure 52** left in TFE and right in MeOH.

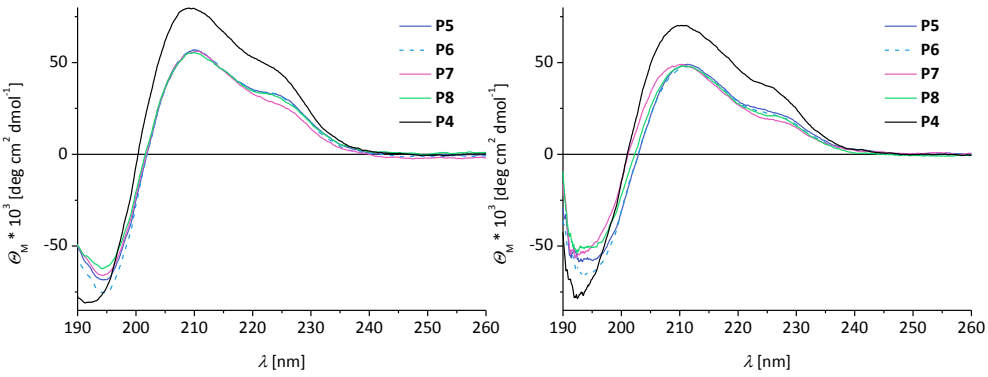

Figure 52: CD investigation of the β-peptides **P5**, **P6**, **P7**, **P8** and the reference peptide **P4** in solution. The peptide concentration was 10 μM and the measurements were performed at 10 °C. The spectra show the typical pattern of a right-handed 3_{14}-helix (minimum at approximately 194 nm, a zero-crossing at 202 nm and a maximum at about 210 nm) and an additional shoulder at approximately 224 nm which is typical for aromatic residues (here hTrp). Left: CD spectra recorded in TFE. Right: CD spectra recorded in MeOH.

First, all peptides were investigated in TFE, since this alcohol is known to stabilise the secondary structure formation.[157,158] It is assumed that TFE disrupts interaction between peptide and solvent molecules, which strengthens intramolecular interactions like the structure-stabilising hydrogen bonds.[157] Thus, the TFE measurement should show a 'reference' helical structure without disrupting effects. Additionally, the structure formation was investigated in MeOH which is also the solvent for subsequent PELDOR experiments. Both CD experiments demonstrated that all β^3-peptides, including the reference peptide **P4**, had the same secondary structure. The characteristic CD peaks are listed in the following **Table 9**.

Table 9: CD bands of the solution measurement in TFE and MeOH. All observed CD signals in nm are listed according to solvent, peptides (**P5**, **P6**, **P7**, **P8** and **P4** as reference) and characteristic key values.

		P5	**P6**	**P7**	**P8**	**P4**
TFE	Minimum	195	195	195	195	192
	Zero crossing	202	202	202	202	200
	Maximum	210	210	210	210	209
	Shoulder	224	224	224	224	224
MeOH	Minimum	194	194	194	194	193
	Zero crossing	203	203	201	202	201
	Maximum	211	211	210	211	210
	Shoulder	226	226	226	226	226

In TFE the CD spectra of all labelled peptides show a minimum at 195 nm, a zero-crossing at 202 nm and a maximum at 210 nm. A small shoulder occurs in the spectra at 224 nm. The non-labelled reference peptide **P4** shows only small changes (192, 200, 209 and 224 nm). Similar results can be observed in MeOH. A minimum occurs at 193 nm, a zero crossing at about 202 nm, a maximum at 211 nm and a small shoulder at 226 nm. For **P4** similar bands occur at 193, 201, 210 and 226 nm. The results fit perfectly to the observations for a 3_{14}-helix in literature as mentioned above.

In conclusion, the CD spectra indicated right-handed 3_{14}-helical structure formation in solution for all peptides. The comparison of the data between labelled peptides and the reference peptide **P4** demonstrated that the β^3-hTOPP label **24** did not influence the structure formation of the β^3-peptides in TFE and MeOH. The higher intensity of the molar ellipticity Θ_M of peptide **P4** might result from approximations that were used for the determination of concentrations: The determination was based on the absorption of the hTrp at 280 nm in the UV/vis spectrum and the literature value of the Trp absorption coefficient. It is likely that the absorption of the aromatic hTOPP label overlaps with the hTrp absorption at 280 nm. Thus, the concentration of solutions of

peptides **P5**, **P6**, **P7** and **P8** may be underestimated and finally result in the decreased intensity.

4.4.2 Results and Discussion of Measurements in Lipid Bilayers

To determine the structure formation within a lipid environment all peptides were investigated in SUVs of DOPC and POPC (P/L = 1/20, *c*(β-peptides) = 20 μM, phosphate buffer (50 mM, pH 7.5) at 20 °C). The CD spectra of **P5**, **P6**, **P7**, **P8** and the reference peptide **P4** in DOPC and POPC are illustrated in **Figure 53** (left in DOPC and right in POPC).

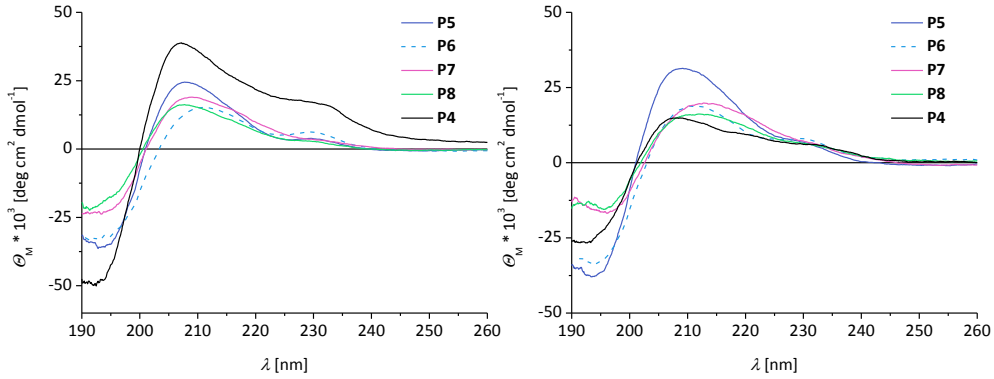

Figure 53: CD investigation of the β-peptides **P5**, **P6**, **P7**, **P8** and the reference peptide **P4** in lipid bilayers. DOPC and POPC SUVs (P/L = 1/20, *c*(β-peptides) = 20 μM, phosphate buffer (50 mM, pH 7.5)). The CD measurements were performed at 20 °C. Left: CD spectra recorded in DOPC. The data illustrate an average of three spectra (**P5**, **P6** and **P7**) and of two spectra (**P8**). Right: CD spectra recorded in POPC.

The illustrated CD spectra of **P5**, **P6** and **P7** in DOPC are an average of three data sets, for **P8** an average of two sets is taken (each spectrum is illustrated in the Appendix). In both lipid systems (DOPC and POPC, **Figure 52**) all peptides, including the reference peptide **P4**, show the same typical CD pattern of a right-handed 3_{14}-helical structure. All characteristic CD bands are listed in detail in **Table 10**.

Table 10: CD bands of the measurement in lipid bilayers of DOPC and POPC. All observed CD signals in nm are listed according to lipid system, peptides (**P5**, **P6**, **P7**, **P8** and reference peptide **P4**) and characteristic key values. All values are in nm and given as an approximate value.

		P4	**P5**	**P6**	**P7**	**P4**
DOPC	Minimum	193	193	192	195	192
	Zero crossing	201	203	200	202	200
	Maximum	208	211	209	210	209
	Maximum[a)]	230	230	-	-	232
POPC	Minimum	194	194	196	196	192
	Zero crossing	201	202	203	203	201
	Maximum	209	211	213	211	208
	Maximum[a)]	229	229	-	-	232

a) due to the aromatic hTrp a second maximum with low intensity was observed. In the case of **P6** and **P7** this maximum was (nearly) vanished.

In DOPC the CD spectra of all labelled peptides show a minimum between 193 and 195 nm (**P4**: 192 nm), a zero-crossing at 202 nm (**P4**: 200 nm) and a maximum between 208 and 211 nm (**P4**: 209 nm). A second maximum occurs at 230 nm in the spectra of **P5** and **P6** (**P4**: 232 nm). Interestingly, this band (nearly) vanishes in the spectra of **P7** and **P8**. This might be due to the closer contact between the aromatic hTOPP amino acid and the hTrp residues in the lipid environment. Both aromatic functionalities might interact with each other and influence conformational states which induces subtle electronic changes also visible in the CD spectra.[159] Similar results are observed in POPC. A minimum occurs between 194 and 196 nm (**P4**: 192 nm), a zero crossing at 202 nm (**P4**: 201 nm), a maximum between 209 and 211 nm (**P4**: 208 nm) and a small shoulder for **P5** and **P6** at 229 nm (**P4**: 232 nm). Slight shifts in the lipid bilayer within the four peptides might be explainable due to the heterogeneous lipid environment and the slightly different peptide sequences. As mentioned in 3.4.1, different dielectric media can influence the electronic transitions of the amide bonds.[90,91]

Differences in the intensity of the molar ellipticity Θ_M might occur due to varying concentrations of peptides within vesicles, since their incorporation within the lipid bilayer was presumably not quantitative and differed between attempts using the same conditions (see Appendix). Analogous results are presented in section 4.4.1, the molar ellipticity Θ_M of the reference peptide **P4** is increased in DOPC which further corroborates the assumption of a systematically overestimated concentration for this particular peptide. In POPC the molar ellipticity Θ_M is lower than in DOPC; most probably due to inconsistencies in the concentration calculation. This assumption must be verified in future experiments.

In summary, the CD results prove that the transmembrane peptides **P5**, **P6**, **P7** and **P8** also form a right-handed 3_{14}-helix in the lipid bilayers.

Further PELDOR experiments within solution and POPC allow a more detailed discussion of the β^3-peptides.

4.5 Inter-Spin Distances from Modelled β^3-Peptides

To obtain more reliable distance estimations between the two labels, theoretical models of the four right-handed 3_{14}-helical peptides were designed. Therefore, coordinates of the backbone atoms were generated from literature known torsion angles (see **Table 11**).

Table 11: Backbone torsion angles of the 3_{14}-helix for generating the theoretical models of the β-peptides. The angles are given in degrees.

helix	ψ	θ	ϕ	ω
3_{14} lit.[a]	139.9	-60	134.3	-180
3_{14} crystal[b]	132.3	-54.2	135.1	-180
3_{14} ideal[c]	139.3	-55	123.4	-180

a) Derived from quantum mechanics optimisation.[160]
b) Derived from a crystal structure.[116]
c) Derived from energy optimisation using the basic parameter of an ideal 3_{14}-helix.[161]

Since there were several definitions of the backbone torsion angles, each peptide was generated according to three backbone angle sets derived from *i*) quantum mechanics optimisation designated as **3_{14} lit.**[160], *ii*) a crystal structure designated as **3_{14} crystal**[116] and *iii*) the computed ideal 3_{14}-helix *via* an energy-optimised backbone designated as **3_{14} ideal**[161]. E.g. the three theoretical models for **P5** are shown in **Figure 54**.

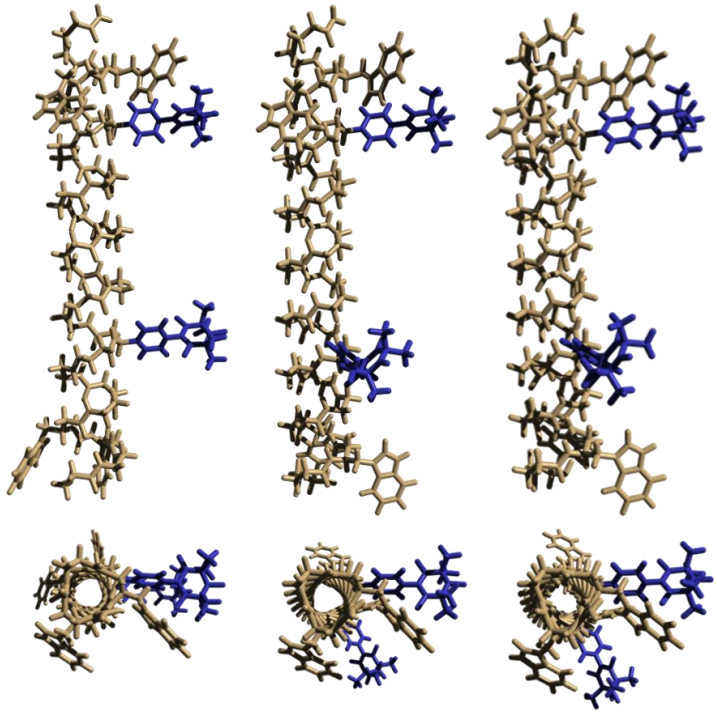

Figure 54: Theoretical models of β-peptide **P5**. Top: Side view. Bottom: Top view in the direction from the *C*- to the *N*-terminus. Left: Model created according to **3_{14} lit**. Centre: Model created according to **3_{14} crystal**. Right: Model created according to **3_{14} ideal**. To introduce the TOPP moiety, its DFT optimised structure[48] as well as the peptide backbone were kept fixed. Then both fragments were forced by molecular mechanics (MMFF94[162] force field as implemented in Avogadro[163]) to rotate about their connecting bond and thereby adopt a reasonable mutual orientation. Note that the models are individually scaled.

The labelled peptide models were built by first generating peptide backbones from the angular data of **3_{14} lit.**, **3_{14} crystal** and **3_{14} ideal**. These fixed angles allow to cut-down the structure, i.e. the valine and lysine side-chains were dismissed. Next, two DFT optimised (planar) TOPP residues[48] had to be introduced into each model. Therefore, the peptide backbone and the TOPP geometry were kept fixed, yet their mutual orientation about the connecting bond was adjustable. A reasonably adjusted orientation was achieved by applying the MERCK molecular force field (MMFF94[162]; algorithm: steepest descents, convergence: 10^{-9}) as implemented in Avogadro[163].

The distances between the two nitroxide radicals were determined as the average of distances $O_{TOPP\ I}$–$O_{TOPP\ II}$, $N_{TOPP\ I}$–$O_{TOPP\ II}$, $O_{TOPP\ I}$–$N_{TOPP\ II}$ and $N_{TOPP\ I}$–$N_{TOPP\ II}$, since the radical is delocalised over the N–O bond. The determined distances are listed in **Table 12** (all values are given in the Appendix).

Table 12: Calculated inter-spin distances of the labelled β-peptides. The distances *r* [nm] were determined as averages of the distances between the atoms $O_{TOPP\ I}$–$O_{TOPP\ II}$, $N_{TOPP\ I}$–$O_{TOPP\ II}$, $O_{TOPP\ I}$–$N_{TOPP\ II}$ and $N_{TOPP\ I}$–$N_{TOPP\ II}$. Numbers in the brackets symbolise the label positions.

	P5 (9, 22)	**P6** (8, 22)	**P7** (7, 22)	**P8** (6, 22)
***r* (3_{14} lit.)**	2.06	2.88	2.94	2.53
***r* (3_{14} crystal)**	2.33	3.09	2.36	2.71
***r* (3_{14} ideal)**	2.17	2.92	2.13	2.43

In comparison to the basic data of an ideal 3_{14}-helix (three amino acids per turn and a pitch of 0.5 nm) the distances do not increase linearly. Due to the label orientation and the helical structure the curve of the distances is ‘wavelike’ (**Figure 55**).

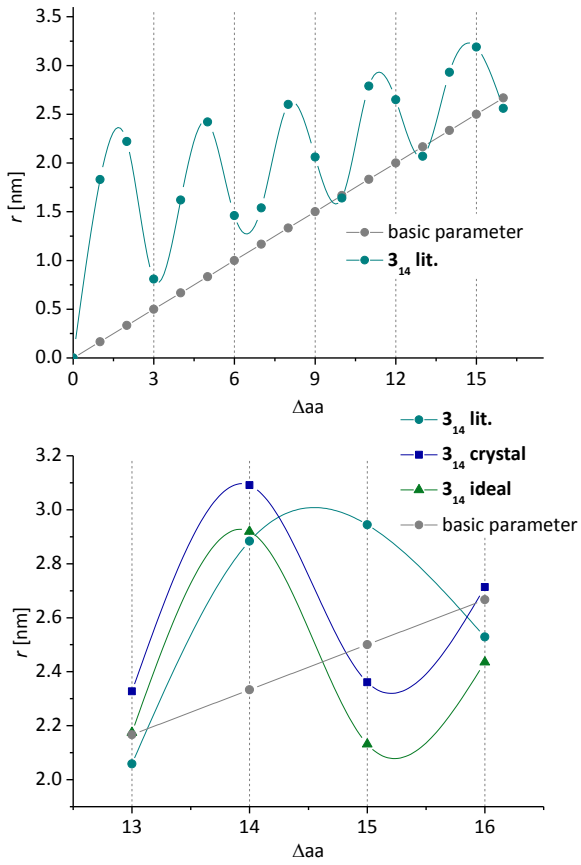

Figure 55: Graphical illustration of the inter-spin distances. Top: The curves are based on the basic parameters of an ideal 3_{14}-helix (grey curve) and on a theoretical model of **P5** (3_{14}-helix which was generated using the torsion angles **3_{14} lit**. (**Table 11**)). The curves illustrate all inter-spin distances between the fixed label position (position 22 of the peptide sequence), a hypothetical second label (positions 21–10) and the 'real' label positions of the second β^3-hTOPP label **24** (position 6, 7, 8 and 9). The x-axis reflects the number of amino acids between label position 22 (set as 0) and the other positions. Bottom: The curves illustrate the inter-spin distances of all theoretical generated peptide models of **P5**, **P6**, **P7** and **P8**. The values are taken from **Table 12** and the basic parameters of the ideal 3_{14}-helix (grey curve).

The curves illustrated in **Figure 55** top are based on the basic parameters of an ideal 3_{14}-helix and a 3_{14}-helix theoretically generated using the torsion angles from **3_{14} lit**. in **Table 11**. The curves show all distances between the fixed label position (position 22

within the peptide sequence), hypothetical second label positions (positions 21–10) and the 'real' second label positions of the β^3-hTOPP label **24**, i.e. the positions that were synthetically achieved (position 6, 7, 8 and 9 within the peptide sequence). The x-axis reflects the number of amino acids between label position 22 (x-axis set as 0) and the other positions.

The graphs illustrated in **Figure 55** bottom show the distances of the 'real' labelled β-peptides. The data are based on the computationally determined distance parameters mentioned in **Table 12** and the basic parameters of the ideal 3_{14}-helix.

4.6 Inter-Spin Distance Determination by PELDOR

To get information which is directly related to the natural peptide structure, it is necessary to use spin labels which do not influence the peptide structure formation or distort the distance results by their own conformational states. In part 3 it was demonstrated that the α-TOPP label **23** is a useful tool to investigate peptides in different environments, since it delivers reliable distances directly related to the peptide structure.

Thus, in this study the capability of the β^3-hTOPP label was exploited to investigate the 3_{14}-helical structure of a β^3-peptide (**P4**).

EPR experiments in solution were performed by KARIN HALBMAIR, MPI for Biophysical Chemistry.

4.6.1 Results and Discussion of Measurements in Solution

The PELDOR experiments were carried out at Q-band frequencies and corresponding fields (34 GHz/1.2 T) at 50 K using peptide concentrations of ~50 μM. The obtained distance results of all four β^3-peptides (**P5**, **P6**, **P7** and **P8)** in MeOH (10–20% glycerol) are illustrated in (**Figure 56**, **B** and **C**).

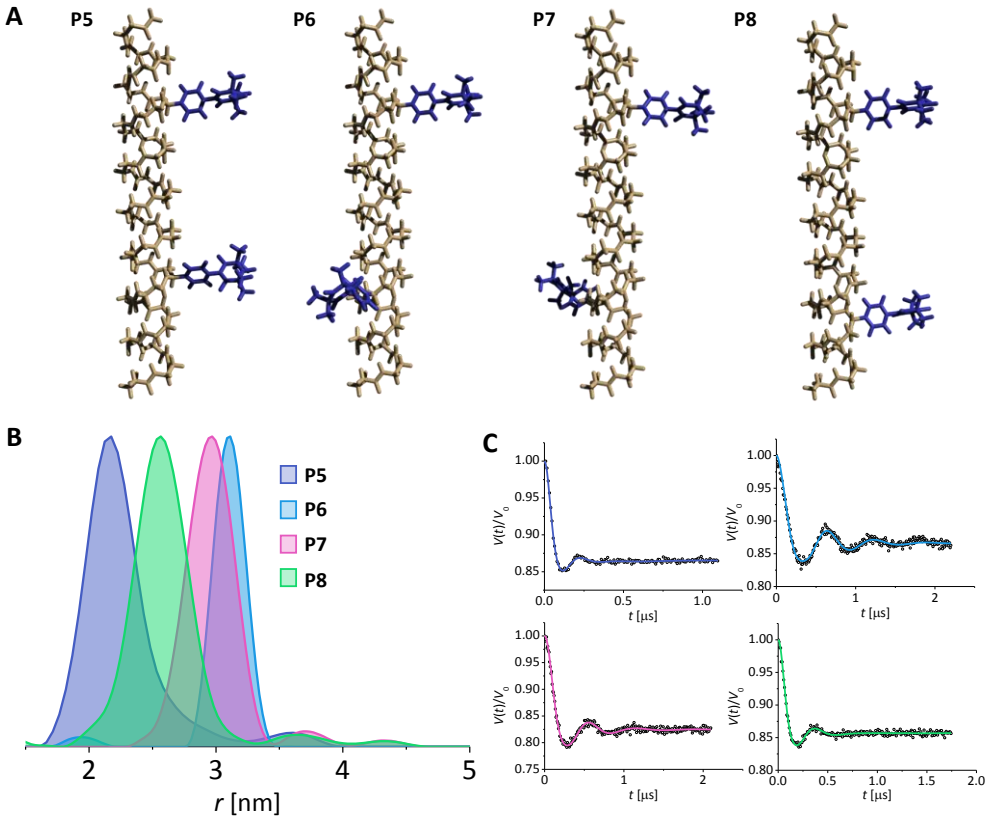

Figure 56: A: Side view of the theoretical peptide models generated from the backbone torsion angles of $\mathbf{3_{14}}$ **lit. B**: PELDOR distance distributions of all peptides (**P5**, **P6**, **P7** and **P8**). **C**: PELDOR experimental time traces and their fits for each peptide (curve colours according to B).

The time traces of all peptides show visible dipolar oscillations with just one dominating dipolar frequency for each peptide (**Figure 56**, **C**). The analysis of each modulation gave a single-peak distance distribution with a narrow HWHM (**Figure 56**, **B**). The detailed values are listed in **Table 13** and are illustrated in comparison to the inter-spin distances of the theoretical models in **Figure 57** (for models see chapter 4.5).

Table 13: PELDOR distribution maxima *r* [nm] and the HWHM values [nm] of **P5**, **P6**, **P7** and **P8** in MeOH.

	P5 (9, 22)	**P6** (8, 22)	**P7** (7, 22)	**P8** (6, 22)
r	2.17	3.09	2.95	2.55
HWHM	0.24	0.15	0.21	0.21

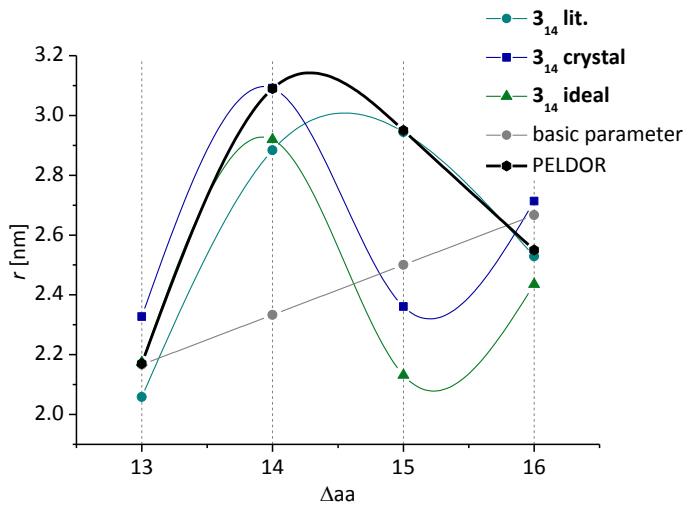

Figure 57: PELDOR distance results in comparison with the calculated distances from theoretical β^3-peptide models. The black curve represents the PELDOR distance results. The other curves are based on the theoretical models which were generated using the torsion angle sets **3_{14} lit.**, **3_{14} crystal**, **3_{14} ideal** (for all three sets see chapter 4.5 **Table 11**) and on the basic parameter of an ideal 3_{14}-helix (three amino acids per turn and a pitch of 0.5 nm; grey curve). The curves illustrate the inter-spin distances between the fixed label position (position 22 of the peptide sequence) and the label positions of the second β^3-hTOPP label **24** (position 6, 7, 8 and 9). The x-axis reflects the number of amino acids between the label position 22 (set as 0) and the other positions.

As shown in **Figure 57** the PELDOR distance results (inter-spin distance and the corresponding shape of the curve) are in close agreement with distances calculated from the model **3_{14} lit.** (see chapter 4.5). Slight deviations (Δaa 13 and Δaa 15 show differences of 0.12 nm and 0.21 nm, respectively) are acceptable, since variances

between models and experiments could occur especially due to the cut-down peptide structure and the disregard of solvent. However, the curve shape of the PELDOR results is characteristic and by far best matched by the structure **3_{14} lit**. This implies that the helical turn is defined by 3.25 amino acid residues[160] (ideal 3_{14}-helix is defined by three amino acid residues per turn). This finding is confirmed by an NMR study in MeOH made by SEEBACH and co-workers.[135] A β^3-eicosapeptide consisting of all 20 homologated proteinogenic amino acids (L-β^3-amino acids, left-handed 3_{14}-helix) showed that there is an offset from the ideal 3_{14}-helix by 10 to 20° in a right-handed direction.[135] This gives 3.1 to 3.4 residues per turn.[135]

In conclusion, it was demonstrated that the newly developed β^3-hTOPP label **24** delivers sharp and reliable distances directly related to the peptide structure and that the four labelled peptides **P5**, **P6**, **P7** and **P8** fold into a "3.2_{14}"-helix (in accordance with SEEBACH[107]) in MeOH. Considering the consistent CD results the "3.2_{14}"-helix can be also expected for the non-labelled peptide **P4**.

The labelling efficiency which gives evidence about the number of spins within the molecule was determined to be approximately 50% for different batches.

However, it was shown that after purification with HPLC and lyophilisation a small amount of the radical underwent reduction (see subsection 4.3.1.2). Yet, it was also demonstrated that the hydroxyl amine species **73** is indeed re-oxidised under exposure to atmospheric oxygen. Thus, the spin concentration might be increased by longer exposure to oxygen.

4.7 Summary: β^3-hTOPP-Labelled β-Peptides

In this part the development and the successful synthesis of the new β^3-hTOPP label **24** was thoroughly described. The Fmoc-protected β^3-hTOPP label **67** was synthesised in a linear synthesis with a yield of 9% over 12 steps. The importance of mild reaction conditions that preserve the stereochemistry of the amino acid was highlighted and it was demonstrated that β^3-amino acids are not prone to racemisation. Furthermore, it was shown that the reduced species of the label **73** can be easily oxidised to the radical species by atmospheric oxygen which allows a very convenient handling.

A novel and successful coupling protocol for β^3-peptides was developed and all four β^3-hTOPP-labelled β-peptides (**P5**, **P6**, **P7** and **P8**) were effectively synthesised. It was demonstrated by CD spectroscopy in solution and in lipid bilayers that the 3_{14}-helical structure formation was not hindered due to the labels. Furthermore, distance measurements in MeOH by PELDOR demonstrated that the newly developed rigid β^3-hTOPP **24** delivers sharp 'single-distance' distributions.

Additionally, the distance measurements by PELDOR were compared to computationally modelled peptides. Of these models, **3_{14} lit.** showed by far the best agreement with the PELDOR measurements (this is additionally confirmed in an NMR study by SEEBACH and co-workers[135]). Hence, the labelled β-peptides **P5**, **P6**, **P7** and **P8** and the non-labelled β-peptide **P4** probably fold into a "3.2_{14}"-helix in MeOH. This showed that EPR measurements of peptides labelled with the β^3-hTOPP label **24** in combination with theoretical means, allow straightforward and reliable structure determination.

4.8 Extended Results and Outlook for Labelled Transmembrane β-Peptides

4.8.1 Preliminary PELDOR Measurements in Lipid Bilayer

Preliminary EPR experiments in lipid bilayer were performed by GABRIELE VALORA, MPI for Biophysical Chemistry. PELDOR experiments for **P5** and **P8** in a lipid environment were performed in MLVs using deuterated phospholipids POPC in a P/L ratio of 1:6000 and a peptide concentration of 20 μM (related to a spin concentration of 40 μM if labelling efficiency was 100%). The peptide/lipid vesicles for the PELDOR experiment were prepared as described in literature for the labelled WALP peptides **P1** and **P3**. This includes hydration at rt for 1 min, three freezing-thawing cycles using liquid N_2 and intermittent vortexing.[53] The results of the PELDOR experiments for **P5** and **P8** are illustrated in **Figure 58**.

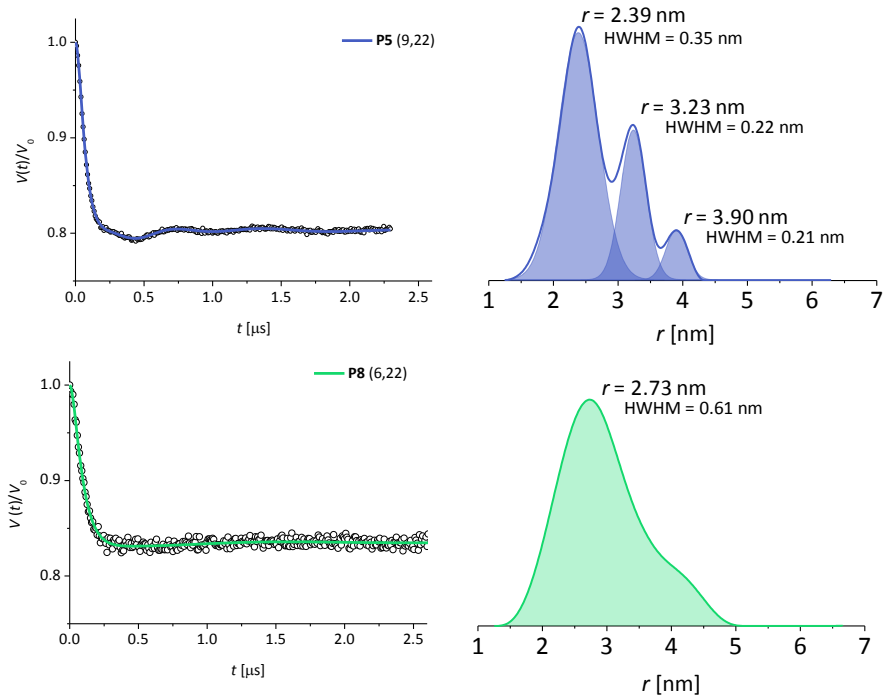

Figure 58: PELDOR distance results of **P5** and **P8** in POPC. Left: Time traces of β-peptides **P5** (top) and **P8** (bottom). Right: Corresponding distance results.

In both cases the time traces of the peptides show visible dipolar oscillations. The modulation for **P5** includes multiple frequencies and gives a distance distribution with three discernible maxima at 2.39, 3.23 and 3.90 nm (**Figure 58**, top). β-Peptide **P8** shows one hardly visible, long dipolar oscillation which gives a single, broadened distribution centred around 2.73 nm (**Figure 58**, bottom). However, these results should not be discussed further, since supplementary electron spin-echo envelope modulation (ESEEM) experiments indicate that the β-peptide was not incorporated in the lipid bilayer (**Figure 59**, left).

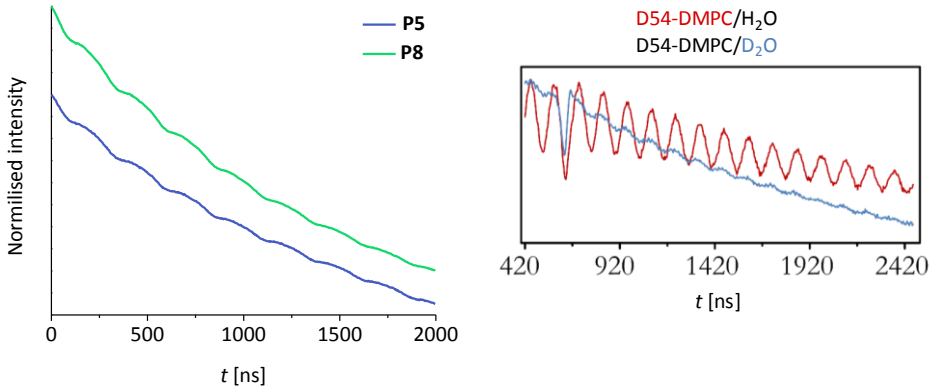

Figure 59: ESEEM results using **P5** and **P8**, and the TOPP-labelled WALP24 peptide **P1** in lipids. Left: Just a weak ESEEM is observed for **P5** and **P8** in deuterated POPC. Right: TOPP-labelled WALP24 **P1** showed a discernible modulation of the ESEEM signal in deuterated DMPC whereas in D_2O just a weak modulation is visible. Hence, the peptide **P1** is incorporated in DMPC.

ESEEM is based on the interaction between the electron spin of the nitroxide radical and a nearby nuclear spin (here ^2H). The amplitude of the ESEEM signal is influenced by the number of these nearby nuclei and their distances towards the electron spin.[164] Only a very weak ESEEM is observed for the β^3-hTOPP-labelled peptides **P5** and **P8** in the deuterated POPC. Usually, a control experiment in D_2O is necessary to qualitatively distinguish between strong and weak intensity (**Figure 59** right) and thereby determine the close and distant environment, respectively. However, in the case of **P5** and **P8** the

pronouncedly weak ESEEM in deuterated POPC directly indicate that the peptides were not taken up into the lipid bilayer. This is additionally supported by a preliminary CD experiment of reference peptide **P4** in MLVs of POPC (**Figure 60**).

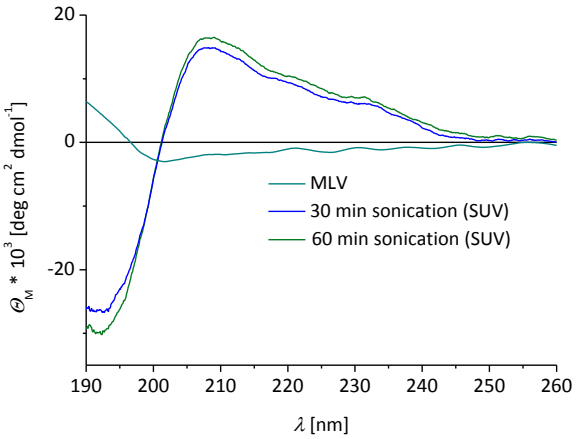

Figure 60: CD investigation of the β-peptide **P4** in MLVs and SUVs of POPC. POPC MLVs/SUVs (P/L = 1/20, *c*(β-peptides) = 20 μM, phosphate buffer (50 mM, pH 7.5)). The CD measurements were performed at 20 °C. In MLV no secondary structure formation is visible whereas after formation of SUVs the CD spectrum show the typical pattern of a 3_{14}-helix.

The MLVs were prepared in a slightly different manner by hydrating the peptide/lipid film at rt for 1 h, followed by vortexing the mixture for 1 min in 5 min intervals (3 x). In this case the typical features of a 3_{14}-helical peptide structure are missing in the CD spectrum. Indeed, the spectrum is almost featureless and exhibits only low intensities. Preparing SUVs from the exact same solution, i.e. sonication of the MLV sample for 30 and 60 min according to section 5.2.11 dramatically alters the CD pattern. Intensities increase and the typical signs for 3_{14}-helical peptide structure formation are visible at 192, 201, 208 and 232 nm.

In summary, the β^3-hTOPP label **24** again reliably delivered distance distributions for the β-peptides **P5** and **P8** by PELDOR measurements. However, the distributions themselves do not give reliable information about transmembrane peptides, since it

must be assumed that the peptides were not incorporated into the lipid bilayer during EPR measurements. This was supported by CD spectroscopy. These findings illustrate the importance of vesicle preparation which has not been addressed in detail so far and must clearly be in the focus of future investigations.

The mild MLV preparation was initially applied in order not to alter the spin concentration within the peptide. Yet, it has been demonstrated in this thesis that the nitroxide radical species is highly stable. Thus, the sample preparation for the PELDOR measurements in POPC can be promptly adjusted. Besides sonication to obtain SUVs, an increased MLV preparation temperature (from rt to 40 °C) allows to test the dependence of peptide incorporation into lipid bilayer on the provided (thermal) energy. Eventually, the transmembrane peptides will certainly be incorporated into the lipid bilayer. Then PELDOR experiments might show changes in the 3_{14}-helical structure of **P4** in POPC. A recently published study by DIEDERICHSEN and co-workers showed that the β-peptide motif **P4** tilted by 16° in DOPC.[136] This tilting might indeed result from a mismatch situation between lipid and peptide.[136] If the tilting process is the only mechanism within the membrane, the distances and corresponding curve shape in a diagram (see graph in **Figure 57**, section 4.6.1) should be similar. It is also conceivable that the 3_{14}-helix structure of the β-peptide varies within the lipid environment compared to the solution measurement, since other stabilisation/destabilisation effects may influence the structure formation.

5 Experimental Part

5.1 Materials and Methods

Solvents

Solvents for the syntheses were used in the highest quality available (p.a., absolute). Extra-dry solvents were purchased from SIGMA-ALDRICH (Taufkirchen, Germany) and ACROS ORGANICS (Geel, Belgium) covered with a rubber septum and stored over molecular sieves. All technical grade solvents were distilled before use. Analytic and HPLC grade solvents were provided by FLUKA (Taufkirchen, Germany), VWR INTERNATIONAL (Fontenay-sous-Bois, France), ACROS ORGANICS (Geel, Belgium) and SIGMA-ALDRICH (Taufkirchen, Germany). Solvents for the NMR experiments were supplied by DEUTERIO (Kastellaun, Germany). The ultra-pure water (electrical conductivity 18 MΩ·cm) was obtained by purification of demineralised water using the purification systems SYMPLICITY from MERCK MILLIPORE (Bedford, UK) and arium® mini from SATORIUS (Göttingen, Germany). Degassing of solvents were obtained by passing argon through them.

Reagents

All utilised, commercial available materials and chemicals were purchased in the highest quality available by ABCR (Karlsruhe, Germany), ACROS ORGANICS (Geel, Belgium), ALFA AESAR (Karlsruhe, Germany), BACHEM (Bubendorf, Switzerland), CARL ROTH (Karlsruhe, Germany), FISCHER SCIENTIFIC (Nidderau, Germany), FLUKA (Taufkirchen, Germany), MERCK (Darmstadt, Germany), RIEDEL-DE HAËN (Seelze, Germany), TCI (Eschborn, Germany) and VWR (Darmstadt, Germany) and were used as supplied.

The Fmoc-protected α-amino acids, coupling reagents and the resins were obtained from GL BIOCHEM (Shanghai, China), IRIS (Marktredwitz, Germany), ACROS ORGANICS (Geel, Belgium) and MERCK (Darmstadt, Germany). MTSSL was purchased by SANTA CRUZ BIOTECHNOLOGY (Texas, USA). All used lipids were supplied by AVANTI POLAR LIPIDS (Alabama, USA).

Reactions

Air and moisture sensitive reactions were performed in dried laboratory glassware under an argon atmosphere (> 99.996%). Therefore, the glass apparatus was heated under reduced pressure. After cooling down to rt the glassware was purged with dried argon. This procedure was repeated three times overall. Solids were added in a counter stream of argon and solutions through a septum *via* a syringe equipped with a cannula.

Freeze-drying

Building blocks and peptides were dissolved/suspended in water with minimal amounts of MeCN or MeOH were frozen in liquid nitrogen and freeze-dried using a CHRIST ALPHA-2-4 lyophiliser (Osterode am Harz, Germany) equipped with a high vacuum pump. Samples with a volume bigger than 2 mL were lyophilised in round bottom flasks, whereas samples with volumes smaller than 2 mL in an EPPENDORF safe-lock microcentrifuge tube in speedvac devices RVC 2-18 or RVC 2-18 CD plus of CHRIST (Osterode am Harz, Germany) connected to the lyophiliser.

Thin layer chromatography (TLC)

The stationary phase consisted of aluminium-backed plates coated with a 0.20 nm thin silica gel 60 F_{254} layer provided by MERCK (Darmstadt, Germany). Substances on the TLC plates were visualised by fluorescence quenching at 254 nm or by dipping in a ninhydrin solution (3% ninhydrin in ethanol (EtOH)) followed by heat-drying to detect amine groups.

Flash column chromatography

Flash column chromatography was performed using silica gel of the type 60 with a particle size of 40–63 μm supplied by MERCK (Darmstadt, Germany) and a pressure of 0.1–1.0 bar. The silica gel was suspended in the elution system and filled in an appropriated glass column equipped with a glass frit. The samples were loaded either

by pre-loading on silica gel or as concentrated solution.

High performance liquid chromatography (HPLC)

High performance liquid chromatography was performed on JASCO (Gross-Umstadt, Germany) instruments equipped with an analytical column (Nucleodur® RP C-18 analytical HPLC column (250 nm x 4.6 mm, 5 μm) from MACHEREY-NAGEL (Düren, Germany) with a flow of 1.0 mL/min. The compounds were detected by UV absorptions at 215, 254 and 280 nm. Applied elution systems were either A: bi-demineralised H_2O + 0.1% TFA and B: MeOH + 0.1% TFA or A: bi-demineralised H_2O + 0.1% TFA and C: MeCN + 0.1% TFA (see relevant chapters for more information). Compounds and elongation of peptide sequences were investigated on a JASCO system equipped with a MD-2010plus multiwavelength detector, LC-Net II/ADC, CO-2060plus intelligent column thermostat, AS-2055plus intelligent sampler and two PU-2085plus semi-micro HPLC pumps. Peptides were purified with a JASCO system equipped with a MD-2010plus multiwavelength detector, LC-Net II/ADC, a DG-2080-53 3-line degasser and two PU-2086plus intelligent HPLC pumps. For the purification of the β-peptides the column was heated in a PHARMACIA LKB HPLC column oven 2155. The samples were dissolved in mixtures of bi-demineralised water and either MeOH or MeCN followed by filtering through CHROMAFIL® RC-45/15 MS (MACHERY-NAGEL) filter.

Nuclear Magnetic Resonance (NMR)

NMR experiments for the characterisation of synthesised compounds were performed on VARIAN (California, USA) instruments (Mercury (VX) 300, Unity 300, Inova-500). The sample temperature was set for $CDCl_3$ to 298 K and for CD_3OD, D_2O and DMSO-d_6 to either 298 K or 308 K. The effective measuring frequencies are mentioned in the analytic data of the substances. All ^{13}C-NMR experiments were proton-decoupled. The chemical shift δ is indicated in ppm (TMS = 0 ppm). The chemical shift of the solvents served as internal standard [$CDCl_3$: 7.26 ppm (^{1}H) and 77.16 ppm (^{13}C), CD_3OD:

3.31 ppm (^{1}H) and 49.00 ppm (^{13}C), D_2O: 4.79 ppm (^{1}H), DMSO-d_6: 2.50 ppm (^{1}H) and 39.52 ppm (^{13}C)]. Signal multiplicities are abbreviated as followed s = singlet, d = doublet, t = triplet, q = quartet, hept = heptet, m = multiplet and s_{br} = broadened singlet. The coupling constant $^{n}J_{X,Y}$ is indicated in Hertz (Hz) (n = number of the bonds between the coupling nuclei, X,Y = coupling nuclei).

Mass spectrometry

The characterisation by mass spectrometry was performed using the ionisation techniques electrospray ionisation (ESI) or electron ionisation (EI). The data is presented in mass-to-charge ratio (*m/z*). The ESI and high resolution ESI (HR-ESI) experiments were carried out using either a BRUKER (Massachusetts, USA) micrOTOF-Q II or a BRUKER maXis ESI-QTOF-MS instrument. EI-experiments were performed using a JEOL (Tokyo, Japan) AccuTOF GCv device.

UV/vis spectroscopy

UV/vis spectroscopy was utilised for the concentration determination of peptide solutions by means of the absorption of Trp at 280 nm (ε = 5600 cm^{-1} M^{-1})[165] and for the analysis of the resin loading efficiency (see 5.2.3). Concentration determination was performed in the case of α-peptides (dissolved in MeOH) on a V-650 JASCO spectrophotometer equipped with a JASCO temperature controller ETCS-761 and a thermostat from JULABO F250 (Seelbach, Germany) and in the case of β-peptides (dissolved in EtOH) on a THERMO SCIENTIFIC device (NanoDrop 2000c, cuvette function [*d* = 1 cm]). The quartz glass cuvettes Suprasil® (QS) were provided by HELLMA (Müllheim, Germany). The concentration was calculated using the LAMBERT-BEER law

$$c = \frac{A}{\varepsilon \cdot d} \tag{1}$$

and the variables are defined as *A* = measured absorption at 280 nm, ε = molar

extinction coefficient in $cm^{-1} \cdot M^{-1}$ and d = path length in cm (1 cm). The pure solvent served as reference.

Circular Dichroism (CD) spectroscopy

CD spectroscopy for the investigation of secondary structure formation of peptides was performed on a J-1500 spectropolarimeter provided by JASCO equipped with a JASCO PTC-510 peltier thermostatted rectangular cell holder and a JULABO F250 thermostat. The device was purged with nitrogen before and during the operations. All experiments were carried out in a 1.0 mm quartz glass cuvette of HELLMA (Suprasil® QS) and the temperature was controlled by the sensor in the holder. The following specific parameters were used for the experiments:

Parameter	WALP24-TOPP	
	MeOH	lipid
Measurement range [nm]	260–190	
Data pitch [nm]	0.1	
CD scale [mdeg/dOD]	200/0.1	
FL scale [mdeg/dOD]	200/0.1	
D.I.T. [sec]	4	
Bandwidth [nm]	1.0	
Scanning speed [nm/min]	50	
Accumulation	30	

Parameter	WALP24-MTSSL	
	MeOH	lipid
Measurement range [nm]	260–190	
Data pitch [nm]	0.2	
CD scale [mdeg/dOD]	200/0.1	
FL scale [mdeg/dOD]	200/0.1	
D.I.T. [sec]	1	
Bandwidth [nm]	1.0	
Scanning speed [nm/min]	50	
Accumulation	3	5

Parameter	β-peptide		
	TFE	MeOH	lipid
Measurement range [nm]	260–180	260–190	
Data pitch [nm]	0.1		
CD scale [mdeg/dOD]	200/1.0		
FL scale [mdeg/dOD]	200/1.0		
D.I.T. [sec]	4		
Bandwidth [nm]	1.0		
Scanning speed [nm/min]	50		
Accumulation	20		25

All illustrated data are background-corrected. Control samples without peptides served as background.

Note that the background-corrected data of the WALP24-MTSSL were smoothed using a SAVITZKY-GOLAY filter (convolution width = 13). The ellipticity unit Θ [mdeg], which is given by the instrument's program, was converted into the molar ellipticity Θ_M [deg·cm^2·dmol^{-1}] by the means of the JASCO software SpectraManager™, which uses following equation (2):

$$\Theta_M = \frac{\Theta}{100 \cdot c \cdot d} \quad (2)$$

The variables are defined as Θ = ellipticity in mdeg, c = concentration in mol/L and d = path length in cm.

Enantiomeric excess (*ee*) value

The experiments for the determination of the *ee* value were performed on a SHIMADZU (Kyōto, Japan) or JASCO HPLC system. The SHIMADZU HPLC system was equipped with a DGU-20A3/prominence degasser, two pumps LC-20AD/prominence liquid chromatography, a CBM-20A/prominence communication BUS module, a SPD-M20A/ prominence diode array detector and a SIL-20AC/prominence auto sampler. The JASCO system was equipped with a MD-2010plus multiwavelength detector, LC-Net II/ADC, CO-2060plus intelligent column thermostat, AS-2055plus intelligent sampler and two

PU-2085plus semi-micro HPLC pumps. Chiral columns from DAICEL (Mainz, Germany) (Chiralpak® IA, Chiralcel® OD and OD-R) were used.

Melting point

The melting point was measured using a STUART melting point SMP10 device in a capillary tube (75 x 2.0 mm) from MARIENFELD (Lauda-Königshofen, Germany).

Programs

NMR data were processed using the software MestReNova (version: 10.0.2-15465). All graphs were created with the program OriginPro 8.5G. Calculation of molecular masses and the design of molecular structures were performed by ChemBioDraw (PERKIN ELMER (Waltham, USA), version: 14.0.0.117). The theoretical peptide models were created using the molecular editor Avogadro[163] (Version 1.1.1).

5.2 General Synthetic Procedures

5.2.1 Synthesis of D-β³-Amino Acids (ARNDT-EISTERT Homologation)

The Fmoc-protected β-amino acids were synthesised according to the procedure described by GUICHARD *et al.*:[120,122]

Under an Ar atmosphere, the Fmoc-protected D-α-amino acid (15.5 mmol, 1.00 eq) was dissolved in dry THF (73.0 mL) and cooled to 0 °C. Then, Et_3N (1.10 eq) and *i*-BuOCOCl (1.10 eq) were added and the reaction mixture was stirred at 0 °C for 30 min. Afterwards, diazomethane (0.6 M in Et_2O, 2.00 eq) was added under light exclusion. The mixture was allowed to warm up to rt and was stirred 5 h at this temperature. The reaction was quenched with AcOH (4.00 eq). Then, 6% aq $NaHCO_3$ (100 mL) and EtOAc (100 mL) were added and the phases were separated. The aqueous phase was extracted with EtOAc (2 x 100 mL). The combined organic phases were washed with a saturated aq NH_4Cl solution (2 x 100 mL) and a saturated aq NaCl solution (2 x 100 mL), dried over $MgSO_4$ and removal of the solvent in vacuum led to the desired diazo ketone. The crude diazo ketone was used without further purification steps.

The diazo ketone was dissolved in THF/H_2O (9:1, 94.0 mL) and AgOCOPh (0.10 eq) was added under light exclusion. The reaction mixture was sonicated in an ultrasound bath at rt for 2 h. Afterwards, H_2O and EtOAc were added and the aqueous phase was acidified with 2 M HCl solution to a pH of 2. The aqueous phase was extracted with EtOAc (3 x 100 mL) and the combined organic phases were washed with saturated aq NaCl solution (3 x 50.0 mL), dried over $MgSO_4$ and the solvent was removed under reduced pressure to give the desired crude D-β³-amino acid.

5.2.2 Loading of the First Amino Acid

In a BD Discardit II syringe (BECTON DICKINSON, Fraga, Spain) equipped with a PE frit, the resin (1.00 eq) was swollen in solvent (α-peptides: DMF or β-peptides: DCM) for a specific time (α-peptides: 2 h or β-peptides: 30 min) at rt. Afterwards, it was washed

with NMP (5 x) followed by microwave-assisted Fmoc deprotection with 20% piperidine in solvent (α-peptides: DMF or β-peptides: NMP) (1: 50 °C, 25 W, 30 s; 2: 50 °C, 25 W, 3 min) using a DISCOVER microwave (CEM, North Carolina, USA). Between the two deprotection steps the resin was washed with NMP (3 x) and afterwards with NMP, DCM, DMF (10 x each) and NMP (3 x). Then, a solution of the specific amino acid (5.00 eq), HOBt (5.00 eq) and DIC (5.00 eq) in solvent (α-peptides: DMF or β-peptides: NMP) was added and the coupling was carried out by microwave irradiation (α-peptides: 40 °C, 20 W, 10 min; β-peptides: 60 °C, 35 W, 15 min) using a DISCOVER microwave (CEM). Double coupling was performed for each peptide. Between the coupling steps the resin was washed with NMP (3 x) and after final coupling thoroughly with NMP, DCM, DMF (10 x each), then with MeOH, Et_2O and DCM (5 x each) and dried *in vacuo*. After synthesis, the loading density was estimated *via* UV analysis (5.2.3), followed by capping (5.2.4) and washing with NMP, DCM, DMF and NMP (10 x each).

5.2.3 UV/vis Analysis of the Resin Loading Efficiency

The experimental procedure was performed according to literature.[166] Dry resin was placed in a 10 mL graduated flask, 2 mL of a 2% DBU solution in DMF was added and the mixture was slowly shaken at rt for 2 h. Then the flask was filled up with MeCN to 10 mL. Afterwards, 2 mL of this solution were taken, and it was fill up with MeCN to 25 mL. A reference solution was prepared using the same procedure, but without resin. The absorption of the solution was measured at 304 nm and 20 °C. The following equation (3) was used for calculating the resin loading:

$$\text{resin loading}\left[\frac{\text{mmol}}{\text{g}}\right] = (Abs_{\text{sample}} - Abs_{\text{ref}}) \cdot \frac{16.4}{(\text{mg of resin})} \qquad (3)$$

5.2.4 Capping

For the acetylation of free amine groups, a solution of Ac_2O/2,6-lutidine/NMP (1:2:7, *v*/*v*/*v*) was added to the swelled resin and the mixture was shaken at rt for 5 min. Then,

the capping solution was removed, and the procedure was repeated. After removing of the reaction mixture, the resin was washed thoroughly with NMP, DCM (10 x each) and DMF (5 x).

5.2.5 Manual SPPS: α-Peptide

The Fmoc-Ala-preloaded resin (0.05 mmol, 1.00 eq) was swollen in DMF in a 2 mL BD Discardit II syringe equipped with a PE frit at rt for 2 h, followed by washing with NMP (5 x). Each coupling cycle was started with microwave-assisted double Fmoc deprotection by adding 20% piperidine in DMF (1: 50 °C, 25 W, 30 s; 2: 50 °C, 25 W, 3 min) using a DISCOVER microwave (CEM). Washing between the deprotection steps with NMP (3 x) was performed and afterwards thoroughly with NMP, DCM, DMF and NMP (10 x each). The coupling mixture consisted of the respective amino acid (5.00 eq) in NMP (0.25 mL), a solution of HOBt/HBTU (5.00 eq/4.90 eq) in DMF (500 μL) and a 2 M solution of DIEA (10.0 eq) in NMP (250 μL). The mixture was added, and the coupling was carried out by microwave irradiation (50 °C, 25 W, 10 min) using a DISCOVER microwave (CEM). Double coupling was performed, and the resin was washed between the coupling steps with NMP (3 x) and afterwards thoroughly with NMP, DCM, DMF and NMP (10 x each). The following amino acids were coupled using standard conditions as mentioned above. Upon completion of the sequence, the resin was dried *in vacuo*.

5.2.6 Manual SPPS: β-Peptide

The Fmoc-β-amino acid loaded resin (1.00 eq) was swollen in DCM in a BD Discardit II syringe equipped with a PE frit at rt for 30 min, followed by washing with NMP (5 x). Each coupling cycle was started with microwave-assisted double Fmoc deprotection by adding 20% piperidine in NMP (1: 50 °C, 25 W, 30 s; 2: 50 °C, 25 W, 3 min) using a DISCOVER microwave (CEM) and washing between the deprotection steps with NMP (3 x) and afterwards thoroughly with NMP and DCM (10 x each), DMF (5 x) and NMP (3 x). The β-amino acid (4.00 eq) and the activation reagents HOAt/HATU (4.00 eq/3.90 eq)

were placed in a small sample vessel. Then a solvent mixture of NMP/DMF/DMSO (1:0.8:0.2, *v*/*v*/*v*) was added and the solution was sonicated. Afterwards, the activation bases (2,6-lutidine/DIEA, 4.80 eq/3.20 eq) were added and the mixture was subjoined with the resin. The coupling was carried out by microwave irradiation (60 °C, 25 W, 15 min) using a DISCOVER microwave (CEM). Double coupling was performed (3.00 eq amino acid; 2,6-lutidine/DIEA, 3.60 eq/2.40 eq) and the resin was washed between the coupling steps with NMP (3 x) and afterwards thoroughly with NMP and DCM (10 x each), DMF (5 x) and NMP (3 x). The coupling conditions described above were changed after the 7th coupled amino acid. Then, the solvent mixture contained 0.8 M LiCl in NMP/DMF/DMSO (1:0.8:0.2, *v*/*v*/*v*), the power was changed (for more details see section 5.3.7) and the reaction time was increased to 30 min (for every 4th amino acid after the β^3-hTOPP it was increased to 35 min and for the last 5 amino acids to 40 min coupling time). Upon completion of the sequence, the resin was dried *in vacuo*.

5.2.7 Automatic SPPS

The Fmoc-amino acid preloaded resin (1.00 eq) was swollen in NMP at rt for 2 h. The chain elongation was performed using a microwave-assisted automatic peptide synthesiser LibertyTM (CEM) equipped with a DISCOVER microwave (CEM). Each coupling cycle started with a microwave-assisted double Fmoc deprotection by a 20% piperidine solution in NMP (1: 50 °C, 25 W, 30 s; 2: 50 °C, 25 W, 3 min) followed by the coupling step. Each amino acid was activated by HOBt/HBTU (5.00 eq/4.90 eq) and DIEA (10.0 eq). Double coupling was performed with microwave irradiation (75 °C, 25 W, 5 min). Cysteine was coupled at a lower temperature (50 °C, 25 W, 5 min). After synthesis, the resin was dried *in vacuo*.

5.2.8 Coupling of the β-TOPP Label

All β-peptides contained two hTOPP labels within the sequence. Both hTOPP labels were coupled with 2.00 eq using the activation reagents HOAt/HATU (2.00 eq/1.90 eq)

and the activation bases 2,6-lutidine/DIEA (2.40 eq/1.60 eq). The first label was coupled in a solvent mixture of NMP/DMF/DMSO (1:0.8:0.2, *v*/*v*/*v*) and microwave irradiation (60 °C, 25 W, 15 min). The coupling of the second label was carried out in a solvent mixture of 0.8 M LiCl in NMP/DMF/DMSO (1:0.8:0.2, *v*/*v*/*v*) and by microwave irradiation (60 °C, power see Chapter, 35 min). Afterwards, the resin was successively washed with NMP and DCM (10 x each), DMF (5 x) and NMP (3 x).

5.2.9 Cleavage and Post-Cleavage Work-Up

The peptide cleavage from the resin and simultaneous deprotection of the protecting groups were performed at rt for 2 h in a mixture of

- TFA/H_2O/TIS (95:2.5:2.5, *v*/*v*/*v*) for all peptides without cysteine
- TFA/H_2O/EDT/TIS (94:2.5:2.5:1, *v*/*v*/*v*/*v*) for the cysteine mutated peptide.

After cleavage of the peptide from the resin, the resulting solution was concentrated in a nitrogen stream and the addition of ice-cold Et_2O led to precipitation of the peptide. The resulting suspension was centrifugated at -5 °C followed by decanting of the supernatant and washing of the peptide pellet with ice-cold Et_2O (3 x). The crude peptide was dried *in vacuo*.

5.2.10 Re-oxidation of the TOPP Label

The crude peptide (1.00 eq) was dissolved in MeOH (α-peptide) or in MeCN/MeOH (β-peptide; ratio see section 5.3.7) (100 µL for 2 mg), $Cu(OAc)_2$ (3.00 eq for each TOPP label) was added and the resulting mixture was stirred at rt for 2 h followed by purification *via* HPLC.[48]

5.2.11 Preparation of Peptide-Lipid Vesicles: SUV

The CD experiments in lipids (α-peptides: POPC and DMPC, β-peptides: DOPC and POPC) were performed using a P/L ratio of 1/30 for the α-peptides and 1/20 for the β-peptides in a 50 mM sodium phosphate buffer (pH 7.5, 150 µL) and peptide concentrations of α-peptides: 9.80 µM (0.03 mg/mL) for **P1** and 16.6 µM (0.05 mg/mL) of **P2** and **P3** and β-

peptides: 20 μM for all peptides. For the preparation of the SUVs, solutions of the peptide in MeOH (150 μL) and the lipids in $CHCl_3$ were mixed, followed by removal of the solvents in a nitrogen stream. The resulting lipid film was dried over night *in vacuo* at 50 °C. The buffer was added, and the film swollen for a specific time (α-peptides: at rt for 30 min, β-peptides: 40 °C for 2 h) followed by vortexing the mixture for 1 min in 5 min intervals (3 x). To form SUVs, the mixture was treated with the ultrasound sonifier sonoplus HD2076 (BANDELIN, Berlin, Germany; 30 min, Cycle 4, 60% power).

5.3 Synthesis

5.3.1 Synthesis of Fmoc-L-TOPP-OH

The α-TOPP building block **36** was synthesised according to the procedures described by SVEN STOLLER.[48] Changes in the synthesis are mentioned in chapter 3.3.

5.3.1.1 Cbz-L-Hpg-OBn (26)

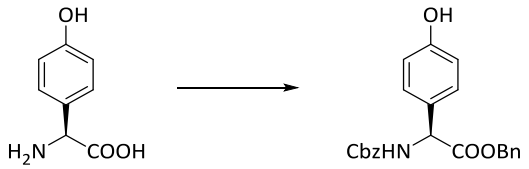

$C_{16}H_{15}NO_5$
[301.30]
25

$C_{23}H_{21}NO_5$
[391.42]
26

4-Hydroxyphenylglycine (**25**) (5.59 g, 33.5 mmol, 1.00 eq) was dissolved in an aqueous solution of Na_2CO_3 (10%, 75.0 mL) and was cooled to 0 °C. Then, CbzCl (5.21 mL, 6.05 g, 35.5 mmol, 1.10 eq) in toluene (5.21 mL) and dioxane (56.0 mL) was added drop-wise to the stirred solution. The final reaction mixture was stirred at 0 °C for 30 min and then at rt for 1 h. The organic solvent was evaporated. Ice-water (185 mL) was added to the residual aqueous phase and the aqueous phase was washed with EtOAc (3 x 50.0 mL). Afterwards, the aqueous phase was acidified with 2 M aq HCl to pH 2 and extracted with EtOAc (3 x 75.0 mL). The combined extracts were washed with water (50.0 mL), saturated aq NaCl solution (50.0 mL), and then dried over $MgSO_4$. The solvent was evaporated under reduced pressure and the Cbz-protected amino acid (9.62 g, 31.9 mmol, 95%) was obtained as a colourless solid.

A suspension of the Cbz-protected amino acid (8.50 g, 28.2 mmol, 1.00 eq) and $NaHCO_3$ (2.47 g, 29.3 mmol, 1.04 eq) in dry DMF (142 mL) was cooled to 0 °C and BnBr (5.85 g, 34.2 mmol, 1.21 eq) was added drop-wise. Then, the reaction mixture was stirred at rt

for 15 h. Afterwards, H_2O (213 mL) was added to the mixture. The aqueous phase was extracted with EtOAc (3 x 100 mL). The combined organic phases were washed with H_2O (160 mL), saturated aq NaCl solution (3 x 100 mL) and dried over $MgSO_4$. The solvent was removed under reduced pressure. The crude residue was washed with pentane to give the pure product **26** (8.53 g, 21.8 mmol, 77%) as a colourless solid.

^{1}H-NMR (300 MHz, $CDCl_3$): δ (ppm) = 7.47–6.98 (m, 12 H, aromatic C*H*), 6.79–6.61 (m, 2 H, aromatic C*H*), 5.80 (d, $^3J_{HH}$ = 7.0 Hz, 1 H, N*H*), 5.32 (d, $^3J_{HH}$ = 7.0 Hz, 1 H, α-C*H*), 5.27-4.92 (m, 4 H, CH_2).

^{13}C-NMR (126 MHz, $CDCl_3$): δ (ppm) = 170.89 (*C*OOBn), 156.18, (aromatic *C*-OH), 155.54 (Cbz *C*ONH), 136.13, 135.19, 128.62, 128.60, 128.50, 128.43, 128.29, 128.20, 128.02, 121.58, 116.00, 115.93 (aromatic *C*), 67.60, 67.43 (*C*H_2), 57.76 (α-*C*).

ESI-MS: *m/z* = 392.2 $[M+H]^+$, 414.1 $[M+Na]^+$, 805.3 $[2M+Na]^+$, 390.1 $[M-H]^-$, 781.3 $[2M-H]^-$.

ESI-HRMS: *m/z* calculated for $C_{23}H_{21}NO_5Na$ $[M+Na]^+$: 414.1312, found: 414.1311.

5.3.1.2 Cbz-L-Hpg(Tf)-OBn (27)

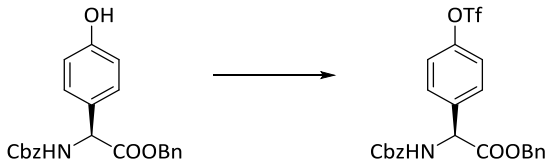

$C_{23}H_{21}NO_5$
[391.42]
26

$C_{24}H_{20}F_3NO_7S$
[523.48]
27

A solution of Cbz-L-Hpg-OBn (**26**) (4.79 g, 11.8 mmol, 1.00 eq) and pyridine (2.75 mL, 2.69 g, 35.4 mmol, 3.00 eq) in dry DCM (36.0 mL) was cooled to 0 °C. Then, Tf_2O (2.89 mL, 5.00 g, 17.7 mmol, 1.50 eq) was added slowly and the reaction mixture was stirred at 0 °C for 15 min. The solution was allowed to warm up to rt and then stirred for 20 min. The reaction was quenched with saturated $NaHCO_3$ solution (62.0 mL) and the resulting aqueous phase was extracted with DCM (3 x 50.0 mL). The combined organic phases were washed with saturated aq NaCl solution (3 x 50.0 mL), dried over $MgSO_4$ and the solvent was removed under reduced pressure. Pyridine was removed as an azeotropic mixture with toluene to give the product **27** (6.26 g, 11.6 mmol, 99%) as an orange solid.

^{1}H-NMR (300 MHz, $CDCl_3$): δ(ppm) = 7.49–7.03 (m, 14 H, aromatic C*H*), 6.04 (d, $^3J_{HH}$ = 7.0 Hz, 1 H, N*H*), 5.46 (d, $^3J_{HH}$ = 7.0 Hz, 1 H, α-C*H*), 5.22–4.97 (m, 4 H, CH_2).
^{13}C-NMR (126 MHz, $CDCl_3$): δ(ppm) = 169.86 (*C*OOBn), 155.35 (aromatic *C*-OTf), 149.49 (Cbz *C*ONH), 137.41, 136.01, 134.77, 129.22, 128.70, 128.67, 128.44, 128.33, 128.13, 121.88 (aromatic *C*), 118.84 (q, $^1J_{CF}$ = 321.3 Hz, *C*F_3), 67.96, 67.45 (*C*H_2), 57.35 (α-*C*).
^{19}F-NMR (282 MHz, $CDCl_3$): δ(ppm) = -72.81 (s, 3 F, C*F*$_3$).
ESI-MS: *m/z* = 524.1 $[M+H]^+$, 546.1 $[M+Na]^+$, 1069.2 $[2M+Na]^+$.
ESI-HRMS: *m/z* calculated for $C_{24}H_{20}F_3NO_7SNa$ $[M+Na]^+$: 546.0805, found: 546.0787.

5.3.1.3 Bn_2-L-Hpg(Tf)-OBn (28)

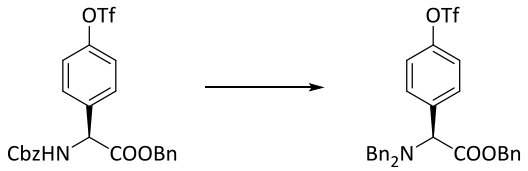

$C_{24}H_{20}F_3NO_7S$
[523.48]
27

$C_{30}H_{26}F_3NO_5S$
[569.60]
28

A solution of Cbz-L-Hpg(Tf)-OBn (**27**) (9.84 g, 18.8 mmol, 1.00 eq) and $(CH_3)_2S$ (41.3 mL, 35.0 g, 564 mmol, 30.0 eq) in TFA (168 mL) was stirred at rt for 17 h. Then, TFA was evaporated as an azeotropic mixture with toluene to give the crude deprotected amino acid. DMSO (99.0 mL) and $NaHCO_3$ (9.47 g, 113 mmol, 6.00 eq) were added to the crude intermediate. Afterwards, BnBr (28.0 mL, 57.8 g, 338 mmol, 18.0 eq) was added drop-wise. The reaction mixture was stirred at rt for 25 h. Then, H_2O (600 mL) and EtOAc (200 mL) were added and the aqueous phase was extracted with EtOAc (2 x 200 mL). The combined organic phases were washed with H_2O (200 mL), saturated aq NaCl solution (3 x 200 mL) and dried over $MgSO_4$. The solvent was removed under reduced pressure. The crude product was purified by flash-column chromatography (100% pentane, then 100% DCM) to give the product **28** (4.12 g, 7.23 mmol, 77%) as a colourless oil.

^{1}H-NMR (300 MHz, $CDCl_3$): δ(ppm) = 7.59–7.05 (m, 19 H, aromatic C*H*), 5.35 (d, $^2J_{HH}$ = 12.0 Hz, 1 H, CH_2), 5.23 (d, $^2J_{HH}$ = 12.0 Hz, 1 H, CH_2), 4.66 (s, 1 H, α-C*H*), 3.79 (d, $^2J_{HH}$ = 15.0 Hz, 2 H, CH_2), 3.79 (d, $^2J_{HH}$ = 15.0 Hz, 2 H, CH_2), 3.71 (d, $^2J_{HH}$ = 12.0 Hz, 2 H, CH_2).

^{13}C-NMR (126 MHz, $CDCl_3$): δ(ppm) = 171.18 (*C*OOBn), 149.07 (aromatic *C*-OTf), 139.01, 137.49, 135.66, 130.71, 128.85, 128.75, 128.73, 128.68, 128.51, 121.29 (aromatic *C*),

118.86 (q, $^{1}J_{CF}$ = 318.8 Hz, *C*F_3), 66.67 (*C*H_2), 65.07 (α-*C*), 54.43 (*C*H_2).

^{19}F-NMR (282 MHz, $CDCl_3$): δ(ppm) = -72.80 (s, 3 F, C*F*$_3$).

ESI-MS: *m/z* = 570.2 $[M+H]^+$, 592.1 $[M+Na]^+$.

ESI-HRMS: *m/z* calculated for $C_{30}H_{27}F_3NO_5S$ $[M+H]^+$: 570.1557, found: 570.1549.

5.3.1.4 Bn_2-4-pinacolboryl-L-Phg-OBn (29)

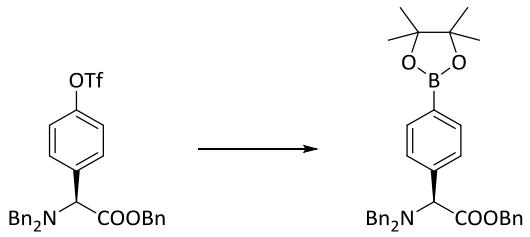

$C_{30}H_{26}F_3NO_5S$
[569.60]
28

$C_{35}H_{38}BNO_4$
[547.50]
29

Under an Ar-atmosphere, a suspension of hydroxyphenylglycine derivative **28** (3.17 g, 5.57 mmol, 1.00 eq), B_2pin_2 (1.69 g, 6.69 mmol, 1.20 eq), KOAc (1.65 g, 16.8 mmol, 3.02 eq), $PdCl_2$(dppf) (410 mg, 560 μmol, 0.10 eq) and dppf (310 mg, 560 μmol, 0.10 eq) in degassed dioxane (57.0 mL) was stirred at 80 °C for 7 h. Afterwards, the suspension was mixed with EtOAc (254 mL). Then, the organic phase was washed with saturated aq NaCl solution (3 x 100 mL), dried over $MgSO_4$ and the solvent was removed under reduced pressure. Purification by flash-column chromatography (pentane/EtOAc, 97:3 → 3:2) led to the desired product **29** (2.75 g, 5.03 mmol, 90%) as a light yellowish oil.

^{1}H-NMR (300 MHz, $CDCl_3$): δ (ppm) = 7.78 (d, $^3J_{HH}$ = 8.1 Hz, 2 H, aromatic C*H*), 7.41–7.17 (m, 17 H, aromatic C*H*), 5.31 (d, $^2J_{HH}$ = 12.0 Hz, 1 H, CH_2), 5.19 (d, $^2J_{HH}$ = 12.0 Hz, 1 H, CH_2), 4.67 (s, 1 H, α-C*H*), 3.75 (s, 4 H, CH_2), 1.34 (s, 12 H, CH_3).

^{13}C-NMR (126 MHz, $CDCl_3$): δ (ppm) = 171.92 (*C*OOBn), 139.82, 139.50, 135.92, 134.87, 128.90, 128.65, 128.58, 128.43, 128.36, 128.30, 127.12 (aromatic *C*), 83.94 (*C*$(CH_3)_2$), 66.34 (*C*H_2), 66.01 (α-*C*), 54.32 (*C*H_2), 25.15, 25.02, 24.96 (*C*H_3).

ESI-MS: *m/z* = 548.3 $[M+H]^+$.

ESI-HRMS: *m/z* calculated for $C_{35}H_{39}BNO_4$ $[M+H]^+$: 548.2973, found: 548.2967.

5.3.1.5 Bn_2-4-dihydroxyboron-L-Phg-OBn (30)

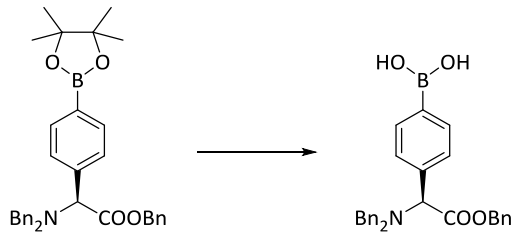

$C_{35}H_{38}BNO_4$
[547.50]
29

$C_{29}H_{28}BNO_4$
[465.36]
30

Boronic ester **29** (3.46 g, 6.32 mmol, 1.00 eq) was dissolved in acetone (287 mL) and H_2O (253 mL). Then, $NaIO_4$ (4.19 g, 19.6 mmol, 3.10 eq) and NH_4OAc (1.46 g, 19.0 mmol, 3.00 eq) were added. The resulting reaction mixture was stirred at rt for 2 d. Afterwards, the organic solvent was evaporated under reduced pressure and the residual aqueous phase was extracted with Et_2O (3 x 100 mL). The combined organic phases were washed with saturated aq NaCl solution (3 x 50 mL) and dried over $MgSO_4$. Removal of the organic solvent under reduced pressure gave the final product **30** (2.55 g, 5.48 mmol, 87%) as a colourless solid.

^{1}H-NMR (300 MHz, $CDCl_3$): δ(ppm) = 8.22 (d, $^3J_{HH}$ = 7.9 Hz, 2 H, aromatic C*H*), 7.51 (d, $^3J_{HH}$ = 7.9 Hz, 2 H, aromatic C*H*), 7.48–7.18 (m, 15 H, aromatic C*H*), 5.39 (d, $^2J_{HH}$ = 12.2 Hz, 1 H, CH_2), 5.26 (d, $^2J_{HH}$ = 12.2 Hz, 1 H, CH_2), 4.78 (s, 1 H, α-C*H*), 3.83 (s, 4 H, CH_2).
^{13}C-NMR (126 MHz, $CDCl_3$): δ(ppm) = 171.82 (*C*OOBn), 141.51, 139.44, 135.89, 135.77, 128.94, 128.70, 128.59, 128.50, 128.44, 127.22 (aromatic *C*), 66.47 (*C*H_2), 66.04 (α-*C*), 54.44 (*C*H_2).
ESI-MS: *m/z* = 480.2 $[M+CH_3+H]^+$, 502.2 $[M+Na]^+$.
ESI-HRMS: *m/z* calculated for $C_{30}H_{32}BNO_4$ $[M+CH_3+H]^+$: 480.2346, found: 480.2360.

5.3.1.6 Bn_2-4-(3,3,5,5-tetramethyl-2,6-dioxopiperazine-1-yl)-L-Phg-OBn (34)

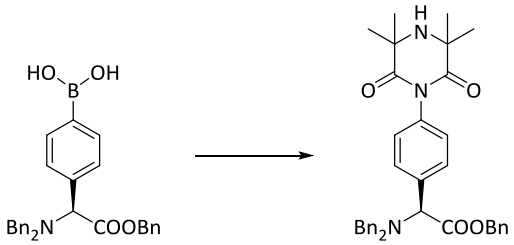

$C_{29}H_{28}BNO_4$
[465.36]
30

$C_{37}H_{39}N_3O_4$
[589.74]
34

A suspension of the boronic acid **30** (3.56 g, 7.65 mmol, 1.00 eq), piperazine-2,6-dion **33** (1.30 g, 7.65 mmol, 1.00 eq), $Cu(OAc)_2$ (1.39 g, 7.65 mmol, 1.00 eq), Et_3N (1.48 mL, 1.08 g, 10.70 mmol, 1.40 eq) and 4 Å molecular sieve powder (4.00 g) in DMSO (160 mL) was stirred at rt under an oxygen atmosphere for 14 d. Afterwards, the reaction mixture was filtered using a glass fiber filter. EtOAc (220 mL), H_2O (200 mL) and 1 M aq HCl (100 mL) were added to the filtrate and the phases were separated. The aqueous phase was extracted with EtOAc (3 x 100 mL). Then, the organic phases were combined and washed with saturated aq NaCl solution (3 x 100 mL) and dried over $MgSO_4$. The solvent was removed under reduced pressure. Purification *via* flash-column chromatography (pentane/EtOAc, 2:1 → 1:1) gave the product **34** (3.07 g, 5.21 mmol, 68%) as a light yellowish solid.

^{1}H-NMR (300 MHz, $CDCl_3$): δ (ppm) = 7.47 (d, $^3J_{HH}$ = 8.4 Hz, 2 H, aromatic C*H*), 7.41–7.22 (m, 15 H, aromatic C*H*), 7.07 (d, $^3J_{HH}$ = 8.4 Hz, 2 H, aromatic C*H*), 5.36 (d, $^2J_{HH}$ = 12.2 Hz, 1 H, CH_2), 5.19 (d, $^2J_{HH}$ = 12.2 Hz, 1 H, CH_2), 4.69 (s, 1 H, α-C*H*), 3.83 (d, $^2J_{HH}$ = 14.0 Hz, 2 H, CH_2), 3.73 (d, $^2J_{HH}$ = 14.0 Hz, 2 H, CH_2), 1.52 (s, 12 H, CH_3).

^{13}C-NMR (126 MHz, $CDCl_3$): δ (ppm) = 176.61 (*C*$CONR_2$), 171.49 (*C*OOBn), 139.18, 136.90, 135.81, 135.01, 129.47, 128.84, 128.64, 128.58, 128.42, 128.36, 128.25, 127.13

(aromatic *C*), 66.38 (α-*C*), 65.47 (*C*H_2), 56.05 (*C*(CH_3)$_2$), 54.29 (*C*H_2), 28.54, 28.51 (*C*H_3).

ESI-MS: *m/z* = 590.3 $[M+H]^+$.

ESI-HRMS: *m/z* calculated for $C_{37}H_{40}N_3O_4$ $[M+H]^+$: 590.3013, found: 590.3015.

5.3.1.7 Fmoc-4-(3,3,5,5-tetramethyl-2,6-dioxopiperazine-1-yl)-L-Phg-OH (35)

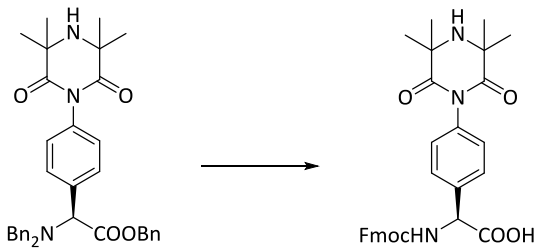

$C_{37}H_{39}N_3O_4$
[589.74]
34

$C_{31}H_{31}N_3O_6$
[541.60]
35

Amino acid **34** (500 mg, 850 μmol, 1.00 eq) was dissolved in MeOH (20.0 mL) and DCM (3.00 mL). Then, $Pd(OH)_2/C$ (50% H_2O, 100 mg, 71.2 μmol, 0.08 eq) was added and the solvent was degassed with H_2. Afterwards, the reaction mixture was stirred at rt under a H_2 atmosphere for 20 h. The suspension was filtered through a pleated filter and then the filtrate was passed through a micron syringe filter. The filtrate was concentrated in *vacuo* and the residue was dissolved in DMF (5.10 mL) and $NaHCO_3$ (143 mg, 1.70 mmol, 2.00 eq). After, Fmoc-OSu (287 mg, 850 μmol, 1.00 eq) was added. The mixture was stirred at rt for 21 h. Then, to the suspension was added H_2O (25.0 mL). The aqueous phase was acidified with 2 M aq HCl to pH 2 and extracted with EtOAc (3 x 50.0 mL). The combined organic phases were washed with saturated aq NaCl solution (50.0 mL), dried over $MgSO_4$ and the solvent was removed under reduced pressure. Purification by flash-column chromatography (DCM/MeOH/AcOH, 98:2:0.1 → 96:4:0.5) led to the product **35** (285 mg, 560 μmol, 62%) as a colourless solid.

^{1}H-NMR (300 MHz, DMSO-d_6): δ(ppm) = 8.27 (d, $^3J_{HH}$ = 8.1 Hz, 1 H, N*H*), 7.89 (d, $^3J_{HH}$ = 7.5 Hz, 2 H, aromatic C*H*), 7.83–7.70 (m, 2 H, aromatic C*H*), 7.53 (d, $^3J_{HH}$ = 8.0 Hz, 2 H, aromatic C*H*), 7.45–7.07 (m, 6 H, aromatic C*H*), 5.27 (d, $^2J_{HH}$ = 8.1 Hz, 1 H, α-C*H*), 4.36–4.20 (m, 3 H, Fmoc C*H*, Fmoc CH_2), 1.41 (s, 12 H, CH_3).

^{13}C-NMR (126 MHz, DMSO-d_6): δ(ppm) = 176.55 (*C*ONR$_2$), 171.72 (*C*OOH), 155.82 (*C*ONH), 143.75, 143.74, 140.65, 136.93, 135.72, 128.82, 128.59, 128.23, 128.11, 127.57, 127.02 119.99 (aromatic *C*), 65.99 (Fmoc *C*H$_2$), 57.69 (α-*C*), 55.36 (*C*(CH$_3$)$_2$), 46.60 (*C*H$_2$), 27.99 (*C*H$_3$).

ESI-MS: *m/z* = 542.2 $[M+H]^+$, 559.3 $[M+NH_4]^+$, 564.2 $[M+Na]^+$, 1083.5 $[2M+H]^+$, 540.2 $[M-H]^-$, 1081 $[2M-H]^-$.

ESI-HRMS: *m/z* calculated for $C_{31}H_{32}N_3O_6$ $[M+H]^+$: 542.2286, found: 542.2279.

5.3.1.8 Fmoc-4-(3,3,5,5-tetramethyl-2,6-dioxo-4-oxylpiperazine-1-yl)-L-Phg-OH (36)

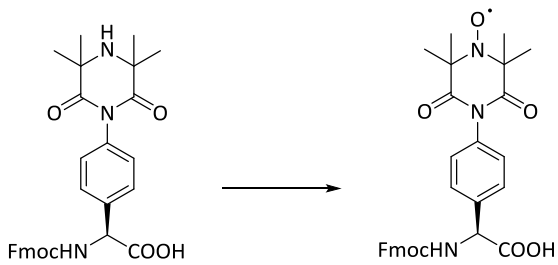

$C_{31}H_{31}N_3O_6$
[541.60]
35

$C_{31}H_{30}N_3O_7$
[556.60]
36

Fmoc-protected amino acid **35** (400 mg, 740 µmol, 1.00 eq) was dissolved in DCM (98.0 mL) and cooled to 0 °C. Then, a solution of *m*-CPBA (70%, 364 mg, 1.48 mmol, 2.00 eq) in DCM (2.00 mL) was added. The reaction mixture was stirred at 0 °C for 15 min and then at rt for 5 h. The solvent was removed under reduced pressure and the crude product was purified by flash-column chromatography (DCM/MeOH/AcOH, 99.5:0.5:0.1 → 96.5:3.5:0.1) to get the final product **36** (350 mg, 630 µmol, 85%) as an orange solid.

ESI-MS: *m/z* = 574.3 $[M+NH_4]^+$, 579.2 $[M+Na]^+$, 1135.4 $[2M+Na]^+$, 555.2 $[M-H]^-$.
ESI-HRMS: *m/z* calculated for $C_{31}H_{29}N_3O_7$ $[M-H]^-$: 555.2011, found: 555.2006.

5.3.1.9 2,2'-Imino-bis(2-methylpropionitrile) (32)[167]

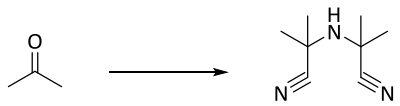

C_3H_6O
[58.08]
31

$C_8H_{13}N_3$
[151.21]
32

KCN (78.1 g, 1.20 mol, 1.24 eq), NH_4Cl (77.0 g, 1.44 mol, 1.48 eq) and aq NH_3 (33%, 500 mL) were mixed and cooled to 0 °C. At this temperature acetone (**31**) (71.2 mL, 56.3 g, 970 mmol, 1.00 eq) was added drop-wise over 1 h. The resulting reaction mixture was stirred at rt for 5 h. Afterwards, the aqueous phase was extracted with DCM (3 x 250 mL). The combined organic phases were dried over $MgSO_4$ and the solvent was removed *in vacuo*. Purification *via* distillation (20 mbar, 52 °C) of the residue gave the pure intermediate product 2-amino-2-methylpropionitrile (62.2 g, 0.74 mmol, 74%). Afterwards, this was stirred at 20 mbar and 100 °C for 3 d to form product **31**. The crude compound **32** was purified *via* distillation (20 mbar, 40 °C) to get the pure product **32** (27.7 g, 180 μmol, 36%) as a yellowish solid.

^{1}H-NMR (400 MHz, $CDCl_3$): δ (ppm) = 1.65 (s, 12 H, CH_3).

^{13}C-NMR (101 MHz, $CDCl_3$): δ (ppm) = 123.46 (*C*N), 49.20 (*C*$(CH_3)_2$), 29.14 (*C*H_3).

ESI-HRMS: *m/z* calculated for $C_8H_{14}NO_2$ $[M+H]^+$: 152.1182, found: 152.1176; *m/z* calculated for $C_8H_{13}NO_2Na$ $[M+Na]^+$: 174.1002, found: 174.1005.

5.3.1.10 3,3,5,5-Tetramethylpiperazine-2,6-dione (33)[167]

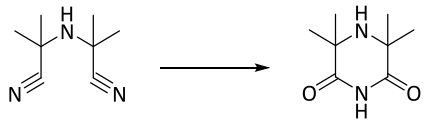

$C_8H_{13}N_3$
[151.21]
32

$C_8H_{14}N_2O_2$
[170.21]
33

H_2SO_4 (68%, 62.0 mL) was cooled to 5 °C and compound **32** (8.85 g, 58.5 mmol, 1.00 eq) was added portion-wise over 2 h. The resulting solution was stirred at rt for 3 d. Then, the mixture was stirred at 100 °C for 1 h and finally at rt for 16 h. Afterwards, the reaction mixture was added to ice (750 g) and 10 M aq NaOH solution was added slowly until the aqueous phase was neutralised. The solvent was removed under reduced pressure. The residue was suspended in MeOH. The white precipitation (Na_2SO_4) was filtered off and the filtrate was concentrated *in vacuo*. The crude product was washed with H_2O and pentane to give the pure product **33** (2.62 g, 15.4 mmol, 26%) as a colourless solid.

^{1}H-NMR (300 MHz, DMSO-d_6): δ (ppm) = 10.60 (s, 1 H, N*H*), 2.72 (s, 1 H, N*H*), 1.27 (s, 12 H, CH_3).
^{13}C-NMR (126 MHz, DMSO-d_6): δ (ppm) = 177.67 (*C*ONHR), 54.67 (*C*$(CH_3)_2$), 27.73 (*C*H_3).
ESI-MS: *m/z* = 171.1 $[M+H]^+$, 193.1 $[M+Na]^+$, 169.1 $[M-H]^-$.
ESI-HRMS: *m/z* calculated for $C_8H_{15}N_2O_2$ $[M+H]^+$: 171.1128, found: 171.1131.

5.3.2 α-Peptide Synthesis

5.3.2.1 Synthesis of P1

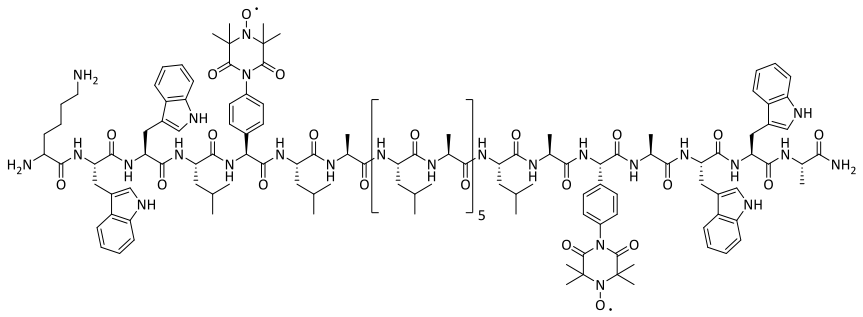

$C_{157}H_{224}N_{34}O_{30}$
[3067.73]
P1

The peptide synthesis of **P1** was performed on a Rink Amide MBHA resin LL (50.0 μmol, 0.36 mmol/g, 1.00 eq). Loading of the resin with Fmoc-Ala-OH was carried out according to procedure described in section 5.2.2. Chain elongation was performed according to the procedure shown in section 5.2.5 using the amino acids Fmoc-Trp(Boc)-OH, Fmoc-Leu-OH, Fmoc-Ala-OH and Fmoc-Lys(Boc)-OH. The amino acid Fmoc-TOPP-OH (2.00 eq) was coupled under inert atmosphere in a flask with the coupling reagent DEPBT (2.00 eq) and the base $NaHCO_3$ (2.00 eq) in dry THF (1.00 mL) at 0 °C for 4.5 h and then at rt for 30 min. After coupling, the resin was washed with NMP, DCM, MeOH, Et_2O and DCM (10 x each). Double coupling was executed with a longer reaction time of the second coupling (at 0 °C for 11.5 h and at rt for 30 min). Afterwards, capping was performed using the protocol described in section 5.2.4. The native amino acids were coupled using standard conditions as mentioned in section 5.2.5. The second TOPP label was coupled as mentioned above. A third coupling was performed with the same reaction time as for the second coupling. The peptide was cleaved from the resin using procedure described in section 5.2.9. The re-oxidation of

the two radicals were carried out using the protocol given in section 5.2.10.

HPLC: (gradient 80 → 100% B in 30 min): t_R = 23.05 min.

ESI-MS: *m/z* = 1023.5 $[M+3H]^{3+}$, 1534.8 $[M+2H]^{2+}$.

ESI-HRMS: *m/z* calculated for $C_{157}H_{227}N_{34}O_{30}$ $[M+3H]^{3+}$: 1534.8629, found: 1534.8638.

5.3.2.2 Synthesis of P3

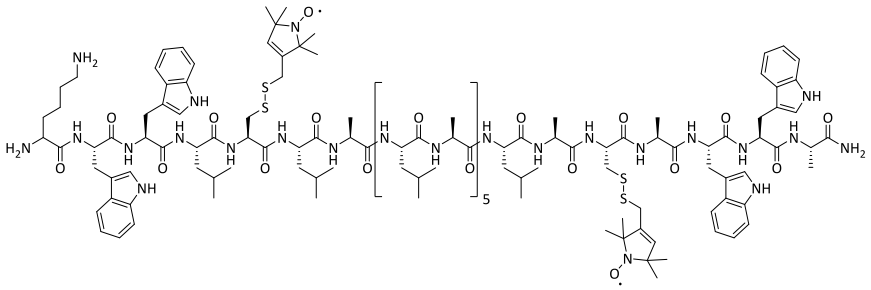

$C_{149}H_{226}N_{32}O_{26}S_4$
[3009.89]
P3

The synthesis of the cysteine mutated peptide **P2** was performed on a Rink Amide MBHA resin (1.00 mmol, 0.57 mmol/g, 1.00 eq). Loading of the resin with Fmoc-Ala-OH was carried out using procedure described in section 5.2.2. Chain elongation was performed *via* automatic SPPS according to the protocol described in section 5.2.7 using the amino acids Fmoc-Trp(Boc)-OH, Fmoc-Leu-OH, Fmoc-Ala-OH and Fmoc-Cys(Trt)-OH. The peptide was cleaved from the resin using the procedure shown in section 5.2.9.

To attach the MTSSL, the raw cysteine mutated peptide **P2** (1.00 eq) was dissolved in MeOH (100 µL for 2.00 mg) and MTSSL (3.00 eq for each cysteine) was added. The resulting mixture was shaken at rt over night, and then purified by HPLC to get the pure **P3**.

HPLC (gradient 80 → 100% B in 30 min): t_R = 24.20 min.

ESI-MS: *m/z* = 753.7 $[M+4H]^{4+}$, 1004.2 $[M+3H]^{3+}$, 1505.8 $[M+2H]^{2+}$.

ESI-HRMS: *m/z* calculated for $C_{149}H_{229}N_{32}O_{26}S_4$ $[M+3H]^{3+}$: 1004.2170, found: 1004.2181.

5.3.3 Synthesis of a Spin label with Enhanced Rigidity

5.3.3.1 2,5-Diisopropylphenyl trifluoromethanesulfonate (41)[168]

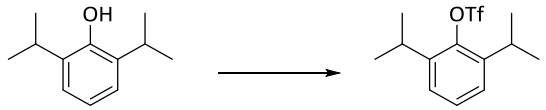

$C_{12}H_{18}O$
[178.28]
40

$C_{13}H_{17}F_3O_3S$
[310.33]
41

The reaction was performed using procedure described in subsection 5.3.1.2 and compound **40** (2.19 mL, 2.11 g, 11.8 mmol, 1.00 eq) was used as starting material. Product **41** (3.25 g, 10.5 mmol, 89%) was isolated as a pale yellow liquid.

^{1}H-NMR (400 MHz, $CDCl_3$): δ (ppm) = 7.37–7.30 (m, 1 H, aromatic C*H*), 7.28–7.23 (m, 2 H, aromatic C*H*), 3,37 (hept, $^3J_{HH}$ = 6.8 Hz, 2 H, C*H*), 1.27 (d, $^3J_{HH}$ = 6.8 Hz, 12 H, CH_3).

^{13}C-NMR (101 MHz, $CDCl_3$): δ (ppm) = 143.73, 142.20 (aromatic C), 118.87 (q, $^1J_{CF}$ = 324.2 Hz, *C*F_3), 27.49 (*C*H), 23.74 (*C*H_3).

^{19}F-NMR (376 MHz, $CDCl_3$): δ (ppm) = -73.45 (s, 3 F, C*F*$_3$).

EI: *m/z* = 135.1 $[M+H-CF_3SO_3-(Me)_2]^+$, 310.1 $[M]^+$.

5.3.3.2 2,5-Diisopropyl-4-hydroxy benzylaldehyde (48)[169]

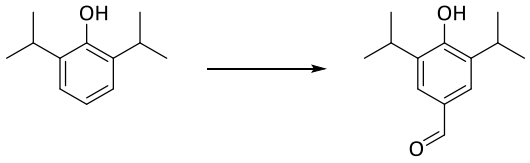

$C_{12}H_{18}O$
[178.28]
47

$C_{13}H_{18}O_2$
[206.29]
48

Compound **47** (2.08 mL, 2.00 g, 11.2 mmol, 1.00 eq), urotropine (3.15 g, 22.4 mmol, 2.00 eq) and TFA (11.0 mL) were mixed and the resulting reaction mixture was stirred at 90 °C for 12 h. Afterwards, the reaction mixture was cooled to rt and the aqueous phase was neutralised with saturated aq $NaHCO_3$ solution and extracted with EtOAc (3 x 50.0 mL). The solvent was removed under reduced pressure. Then, the residue was suspended in 3 M aq HCl and the mixture was stirred at 80 °C for 3 h. The precipitate was filtered off and washed with H_2O. Recrystallisation from EtOH gave product **48** (1.43 g, 6.94 mmol, 62%) as a pale yellow solid.

^{1}H-NMR (300 MHz, $CDCl_3$): δ (ppm) = 9.86 (s, 1 H, CO*H*), 7.62 (s, 2 H, aromatic C*H*), 3.19 (hept, $^3J_{HH}$ = 6.6 Hz, 2 H, C*H*), 1.31 (d, $^3J_{HH}$ = 6.9 Hz, 12 H, CH_3).
^{13}C-NMR (101 MHz, $CDCl_3$): δ (ppm) = 191.95 (*C*OH), 156.17 (aromatic *C*-OH), 134.59 (aromatic *C*H), 129.83 (aromatic *C*), 126.37 (aromatic *C*H), 27.23 (*C*H$(CH_3)_2$), 22.66 (*C*H_3).
ESI-MS: *m/z* = 207.2 $[M+H]^+$, 229.1 $[M+Na]^+$, 205.1 $[M-H]^-$.
ESI-HRMS: *m/z* calculated for $C_{13}H_{19}O_2$ $[M+H]^+$: 207.1380, found: 207.1836.

5.3.3.3 2,5-Diisopropyl-4-benzyloxy benzylaldehyde (49)[170]

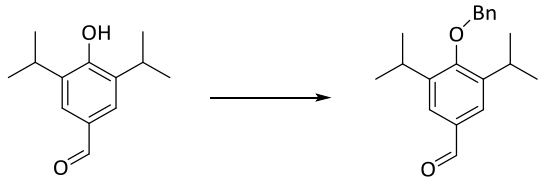

$C_{13}H_{18}O_2$
[206.29]
48

$C_{20}H_{24}O_2$
[296.41]
49

Aldehyde **48** (500 mg, 2.42 mmol, 1.00 eq) was dissolved in acetone and BnBr (291 µL, 419 mg, 2.45 mmol, 1.01 eq) and K_2CO_3 (670 mg, 4.85 mmol, 2.00 eq) were added to the solution. The suspension was stirred at rt for 14 h. Then, the solvent was removed under reduced pressure. The residue was dissolved in EtOAc (20.0 mL) and washed with H_2O (20.0 mL) and saturated aq NaCl solution (20.0 mL). The organic phase was dried over $MgSO_4$ and the solvent was removed under reduced pressure to give the final product **49** (717 mg, 2.42 mmol, quant.) as a pale yellow oil.

^{1}H-NMR (300 MHz, $CDCl_3$): δ(ppm) = 9.96 (s, 1 H, RCO*H*), 7.70 (s, 2 H, aromatic C*H*), 7.53–7.30 (m, 5 H, aromatic C*H*), 4.86 (s, 2 H, CH_2), 3.41 (hept, $^3J_{HH}$ = 6.9 Hz, 2 H, C*H*), 1.28 (d, $^3J_{HH}$ = 6.9 Hz, 12 H, CH_3).

^{13}C-NMR (101 MHz, $CDCl_3$): δ(ppm) = 192.08 (R*C*OH), 158.84 (aromatic *C*-OBn) 143.44, 137.05, 133.38, 128.79, 128.37, 127.54, 126.44 (aromatic *C*), 76.70 (*C*H_2), 26.95 (*C*H(CH_3)$_2$), 24.02 (*C*H_3).

ESI-MS: *m/z* = 297.2 $[M+H]^+$, 319.2 $[M+Na]^+$.

ESI-HRMS: *m/z* calculated for $C_{20}H_{24}O_2Na$ $[M+Na]^+$: 319.1669, found: 319.1662.

The following subsections describe synthetic routes of compounds which are mentioned in the Appendix.

5.3.3.4 2-Aminoisobutyric ethylester hydrochlorid (A-7)[171]

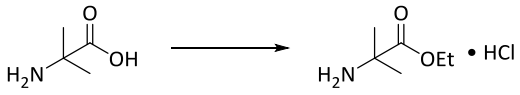

$C_4H_9NO_2$
[103.12]
A-6

$C_6H_{14}ClNO_2$
[167.63]
A-7

EtOH (9.8 mL) was cooled to -78 °C and $SOCl_2$ (900 µL, 1.46 g, 12.2 mmol, 1.25 eq) was added drop-wise. After addition of 2-aminoisobutyric acid (**A-6**) (1.00 g, 9.79 mmol, 1.00 eq), the reaction mixture was warmed up to rt and then stirred under reflux for 2 h. The reaction was cooled to rt and the solvent was removed under reduced pressure. The crude product was dissolved in MeOH (10.0 mL) and the solvent was removed under reduced pressure to give the final product **A-7** (1.64 g, 9.79 mmol, quant) as a colourless solid.

^{1}H-NMR (301 MHz, CD_3OD): δ (ppm) = 4.29 (q, $^3J_{HH}$ = 7.1 Hz, 2 H, CH_2), 1.58 (s, 6 H, CH_3), 1.32 (t, $^3J_{HH}$ = 7.1 Hz, 3 H, CH_3).

^{13}C-NMR (126 MHz, CD_3OD): δ (ppm) = 172.71 (*C*OOEt), 63.88 (*C*$(CH_3)_2$), 57.79 (*C*H_2), 24.00 (C(*C*$H_3)_2$), 14.30 (*C*H_3).

ESI-MS: *m/z* = 132.1 $[M+H-HCl]^+$.

ESI-HRMS: *m/z* calculated for $C_6H_{14}NO_2$ $[M+H-HCl]^+$: 132.1019, found: 132.1018.

M_p = 158 °C [Lit. 156–157 °C].

5.3.3.5 2-Tosyl-isobutyric ethylester (A-9)

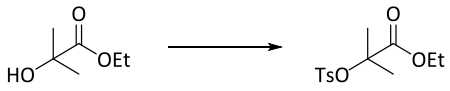

$C_6H_{12}O_3$
[132.16]
A-8

$C_{13}H_{18}O_5S$
[286.34]
A-9

Ethyl 2-hydroxyisobutyrate (**A-8**) (510 µL, 500 mg, 3.78 mmol, 1.00 eq) and TsCl (2.20 g, 11.4 mmol, 3.00 eq) were dissolved in dry $CHCl_3$ (4.00 mL), cooled to 0 °C and pyridine (1.47 mL, 1.44 g, 18.9 mmol, 5.00 eq) was added. The reaction mixture was warmed up to rt and stirred at rt for 40 h. Afterwards, the reaction was quenched with 2 M aq HCl (20.0 mL) and the phases were separated. The aqueous phase was extracted with $CHCl_3$ (3 x 50.0 mL). The combined organic phases were washed with saturated aq NaCl solution (50.0 mL) and dried over $MgSO_4$. The solvent was removed under reduced pressure. Purification of the crude product *via* flash-column chromatography (pentane/DCM, 7:3 → DCM) led to the desired product **A-9** (660 mg, 2.32 mmol, 61%) as a colourless solid.

^{1}H-NMR (400 MHz, $CDCl_3$): δ (ppm) = 7.81–7.52 (m, 2 H, aromatic C*H*), 7.34–7.29 (m, 2 H, aromatic C*H*), 4.27 (q, $^3J_{HH}$ = 7.1 Hz, 2 H, CH_2), 2.47–2.40 (m, 3 H, Tosyl CH_3), 1.69 (s, 6 H, CH_3), 1.32 (t, $^3J_{HH}$ = 7.1 Hz, 3 H, CH_3).

^{13}C-NMR (101 MHz, $CDCl_3$): δ (ppm) = 171.56 (*C*OOEt), 144.49, 136.01, 129.67, 127.65 (aromatic *C*), 86.08 (*C*$(CH_3)_2$), 62.13 (*C*H_2), 25.95 (C(*C*$H_3)_2$), 21.75 (Tosyl *C*H_3), 14.12 (*C*H_3).

ESI-MS: *m/z* = 309.1 $[M+Na]^+$, 595.2 $[2M+Na]^+$.

ESI-HRMS: *m/z* calculated for $C_{13}H_{18}O_5SNa$ $[M+Na]^+$: 309.0767, found: 309.0773.

5.3.3.6 3,3,5,5-Tetramethylmorpholine-2-one (A-12)[172]

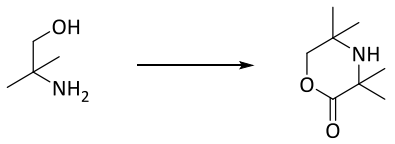

$C_4H_{11}NO$
[89.14]
A-11

$C_8H_{15}NO_2$
[157.21]
A-12

Under argon atmosphere, **A-11** (10.0 g, 112 mmol, 1.00 eq), acetone (82.0 mL, 65.0 g, 1.12 mol, 10.0 eq) and $CHCl_3$ (13.5 mL, 20.0 g, 168 mmol, 1.50 eq) were placed in a 250 mL three neck flask and cooled to 0 °C with an acetone/ice bath. The mixture was stirred vigorously with a KPG stirrer. Then, powdered NaOH (22.4 g, 560 mmol, 5.00 eq) was added keeping the internal temperature below 5 °C. The resulting suspension was stirred vigorously at 10 °C and afterwards at rt for 16 h. The reaction mixture was filtrated over Celite® and washed with acetone and MeOH. The filtrate was concentrated *in vacuo* to give the crude sodium carboxylate as a white solid. To this solid conc. HCl (150 mL) was added and the mixture was stirred under reflux for 6 h. The mixture was cooled to rt and HCl was removed under vacuum. Then, the flask was placed in an ice bath and a saturated aq $NaHCO_3$ solution was added slowly until the solution became basic. The mixture was extracted with EtOAc (3 x 100 mL). The combined organic phases were washed with saturated aq NaCl solution (100 mL), dried over $MgSO_4$ and the solvent was removed under reduced pressure to give product **A-12** (9.01 g, 57.0 mmol, 51%) as a brownish liquid.

^{1}H-NMR (300 MHz, $CDCl_3$): δ(ppm) = 4.08 (s, 2 H, C*H*$_2$), 1.33 (s, 6 H, C*H*$_3$), 1.10 (s, 6 H, C*H*$_3$).

^{13}C-NMR (76 MHz, $CDCl_3$): δ(ppm) = 175.16 (*C*OOR), 78.05 (*C*H$_2$), 54.60, 49.14 (*C*(CH$_3$)$_2$), 30.65, 26.45 (*C*H$_3$).

ESI-MS: *m/z* = 158.1 $[M+H]^+$, 180.1 $[M+Na]^+$.

ESI-HRMS: *m/z* calculated for $C_8H_{16}NO_2$ $[M+H]^+$: 158.1176, found: 158.1177.

5.3.3.7 *N*-(1-Carboxy-1-methylethyl)-2-methylalanine (A-3)[76]

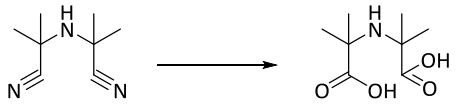

$C_8H_{13}N_3$
[151.21]
32

$C_8H_{15}NO_4$
[189.21]
A-3

Conc. HCl (37%, 4.10 mL) was added to compound **32** (1.05 g, 6.96 mmol, 1.00 eq) and the mixture was stirred first at rt for 30 min, then under reflux for 2 h. Afterwards, the reaction mixture was neutralised with conc. aq NH_3 and the solvent was removed *in vacuo*. The residue was recrystallised from H_2O to give the final product **A-3** (400 mg, 2.08 mmol, 30%) as a colourless solid.

^{1}H-NMR (300 MHz, D_2O): δ(ppm) = 1.65 (s, 12 H, C*H*$_3$).

^{13}C-NMR (126 MHz, D_2O): δ(ppm) = 175.05 (*C*OOH), 55.66 (*C*$(CH_3)_2$), 21.07 (*C*H_3).

ESI-HRMS: *m/z* calculated for $C_8H_{14}NO_4$ $[M-H]^-$: 188.0928, found: 188.0925.

5.3.3.8 4-Bromo-2,6-diisopropyl aniline (A-5)[173]

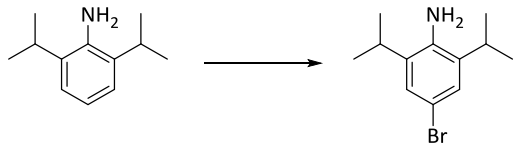

$C_{12}H_{19}N$
[177.29]
A-4

$C_{12}H_{18}BrN$
[256.19]
A-5

Compound **A-4** (1.06 mL, 1.00 g, 5.46 mmol, 1.00 eq) was dissolved in DMF (12.4 mL) and cooled to 0–5 °C under an argon atmosphere. Then, over a period of 20 min NBS (1.00 g, 5.64 mmol, 1.00 eq) dissolved in DMF (6.60 mL) was added drop-wise to the solution. The reaction mixture was stirred at 0–5 °C for 2 h. Afterwards, H_2O (20 mL) was added and the mixture was stirred at rt for 2 h. EtOAc (50.0 mL) was added and the phases were separated. The aqueous phase was extracted with EtOAc (2 x 50.0 mL). Then, the combined organic phases were washed with saturated aq NaS_2O_3 solution (25.0 mL), H_2O (25.0 mL), saturated aq NaCl solution (25.0 mL) and dried over $MgSO_4$. The solvent was removed under reduced pressure to give product **A-5** (1.40 g, 5.46 mmol, 97%) as a red, brown liquid.

^{1}H-NMR (300 MHz, $CDCl_3$): δ (ppm) = 7.14 (s, 2 H, aromatic C*H*), 2.97–2.82 (m, 2 H, C*H*), 1.27 (d, $^3J_{HH}$ = 6.8 Hz, 12 H, CH_3).

^{13}C-NMR (76 MHz, $CDCl_3$): δ (ppm) = 139.33, 134.64 (aromatic *C*), 125.80 (aromatic *C*H), 111.20 (aromatic *C*), 28.22 (*C*H), 22.45(*C*H_3).

ESI-MS: *m/z* = 256.1 (41) $[M+H]^+$, 254.1 (17) $[M-H]^-$.

ESI-HRMS: *m/z* calculated for $C_{12}H_{19}BrN$ $[M+H]^+$: 256.0695, found: 256.0696.

5.3.4 Synthesis of Fmoc-D-β³-hTOPP-OH

5.3.4.1 Cbz-D-Hpg-OH (51)[48]

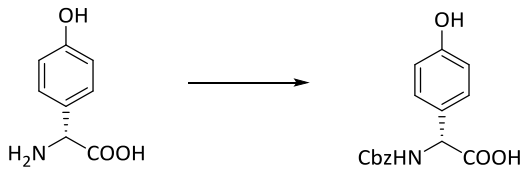

$C_8H_9NO_3$
[167.16]
50

$C_{16}H_{15}NO_5$
[301.30]
51

4-Hydroxy-D-phenylglycine (**50**) (5.00 g, 29.9 mmol, 1.00 eq) was dissolved in an aqueous solution of Na_2CO_3 (10%, 67 mL) and cooled to 0 °C. CbzCl (4.48 mL, 5.42 g, 31.7 mmol, 1.06 eq) in toluene (4.48 mL) and dioxane (50.0 mL) was added drop-wise to the solution. The final reaction mixture was stirred at 0 °C for 30 min and then at rt for 1 h. The organic solvent was evaporated. Ice-water (166 mL) was added to the aqueous phase and it was washed with EtOAc (3 x 50.0 mL). Afterwards, the aqueous phase was acidified with 2 M aq HCl to pH 2 and extracted with EtOAc (3 x 75.0 mL). The combined organic phases were washed with water (50.0 mL), saturated aq NaCl solution (50.0 mL) and then dried over $MgSO_4$. Finally, evaporation of the solvent under reduced pressure gave compound **51** (8.35 g, 27.7 mmol, 93%) as a colourless solid.

^{1}H-NMR (300 MHz, DMSO-d_6): δ(ppm) = 12.51 (s, 1 H, COO*H*), 9.52 (s, 1 H, aromatic O*H*), 7.89 (d, $^3J_{HH}$ = 8.0 Hz, 1 H, N*H*), 7.55–7.26 (m, 5 H, aromatic C*H*), 7.23 (d, $^3J_{HH}$ = 8.5 Hz, 2 H, aromatic C*H*), 6.76 (d, $^3J_{HH}$ = 8.5 Hz, 2 H, aromatic C*H*), 5.17–4.98 (m, 3 H, CH_2, α-C*H*).

^{13}C-NMR (75 MHz, DMSO-d_6): δ(ppm) = 172.50 (*C*OOH), 157.19 (aromatic *C*-OH), 155.82 (*C*ONH), 137.00, 128.97, 128.33, 127.80, 127.71, 127.28, 127.18, 115.18 (aromatic *C*), 65.56 (*C*H_2), 57.61 (α-*C*).

ESI-MS: *m/z* = 302.1 $[M+H]^+$, 324.1 $[M+Na]^+$, 625.2 $[2M+Na]^+$, 300.1 $[M-H]^-$, 601.2 $[2M-H]^-$.

ESI-HRMS: *m/z* calculated for $C_{16}H_{15}NO_5Na$ $[M+Na]^+$: 324.0842, found: 324.0843.

5.3.4.2 Cbz-D-Hpg(TBDMS)-OH (52)

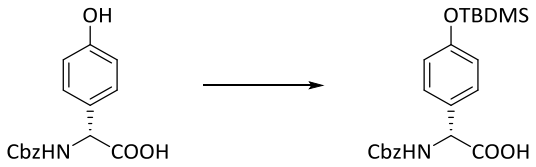

$C_{16}H_{15}NO_5$
[301.30]
51

$C_{22}H_{29}NO_5Si$
[415.56]
52

Under an argon atmosphere, amino acid **51** (3.00 g, 9.97 mmol, 1.00 eq) and imidazole (1.70 g, 24.9 mmol, 2.50 eq) were dissolved in dry DMF (6.00 mL). Then, TBDMSCl (1.80 g, 11.9 mmol, 1.20 eq) was added and the final reaction mixture was stirred at rt for 25 h. Afterwards, the mixture was diluted with EtOAc (50.0 mL) and H_2O (50.0 mL) and the two phases were separated. The aqueous phase was extracted with EtOAc (3 x 50.0 mL). The combined organic phases were washed with saturated aq NaCl solution (50.0 mL) and then dried over $MgSO_4$. Afterwards, the solvent was evaporated under reduced pressure. Purification by flash-column chromatography (DCM/MeOH/AcOH, 9:1:0.1 → 7:1:0.1) gave the pure product **52** (2.70 g, 6.58 mmol, 66%) as a white solid.

^{1}H-NMR (300 MHz, DMSO-d_6): δ (ppm) = 7.90 (d, $^3J_{HH}$ = 7.9 Hz, 1 H, N*H*), 7.41–7.24 (m, 7 H, aromatic C*H*), 6.81 (d, $^3J_{HH}$ = 8.5 Hz, 2 H, aromatic C*H*), 5.11–5.00 (m, 3 H, CH_2, α-C*H*), 0.95 (s, 9 H, 3 x CH_3), 0.19 (s, 6 H, 2 x CH_3).

^{13}C-NMR (126 MHz, DMSO-d_6): δ (ppm) = 172.11 (*C*OOH), 155.65 (Cbz *C*ONH), 154.66 (aromatic *C*-O(TBDMS)), 136.88, 130.14, 128.90, 128.21, 127.67, 127.59, 119.48 (aromatic *C*), 65.45 (*C*H$_2$), 57.49 (α-*C*), 25.46 (C(*C*H$_3$)$_3$), 17.69 (*C*(CH$_3$)$_3$), -4.63 (*C*H$_3$).

ESI-MS: *m/z* = 416.2 $[M+H]^+$, 438.2 $[M+Na]^+$, 853.3 $[2M+Na]^+$, 300.1 $[M-H]^-$, 601.2 $[2M-H]^-$.

ESI-HRMS: *m/z* calculated for $C_{22}H_{29}NO_5SiNa$ $[M+Na]^+$: 438.1707, found: 438.1696.

5.3.4.3 Cbz-D-Hpg(TBDMS)-CHN_2 (53)

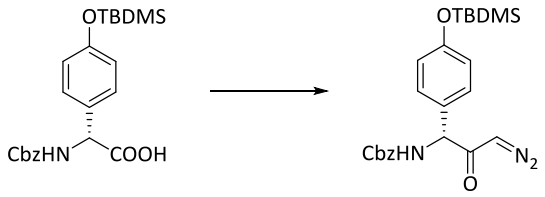

$C_{22}H_{29}NO_5Si$
[415.56]
52

$C_{23}H_{29}N_3O_4Si$
[439.59]
53

Amino acid **52** (3.99 g, 9.60 mmol, 1.00 eq) was dissolved in dry THF (48.0 mL) under an argon atmosphere and cooled down to -15 °C. Subsequently, Et_3N (1.07 mL, 1.46 g, 10.6 mmol, 1.10 eq) and isobutyl chloroformate (1.44 mL, 1.37 g, 10.6 mmol, 1.10 eq) were added to the mixture and stirred at -15 °C for 45 min. The reaction was warmed up to 0 °C and then treated with diazomethane solution (0.60 M in Et_2O, 32.0 mL, 2.00 eq) under light exclusion. The reaction mixture was stirred at 0 °C for 30 min. Afterwards, the mixture was warmed up to rt and stirred at rt for 5 h. The reaction was quenched with AcOH (2.20 mL, 2.30 g, 53.2 mmol, 4.00 eq). Then 6% aq $NaHCO_3$ solution (100 mL) and EtOAc (50.0 mL) were added. The phases were separated, and the aqueous phase was extracted with EtOAc (2 x 50.0 mL). The combined organic phases were washed with saturated aq NH_4Cl solution (3 x 50.0 mL), saturated aq NaCl solution (3 x 50.0 mL), dried over $MgSO_4$ and the solvent was removed under reduced pressure. Purification by flash-column chromatography (pentane/EtOAc, 7:1 → 3:1) gave the desired compound **53** (2.98 g, 6.78 mmol, 61%) as a yellow oil.

^{1}H-NMR (300 MHz, DMSO-d_6): δ (ppm) = 8.04 (d, $^3J_{HH}$ = 8.2 Hz, 1 H, N*H*), 7.43–7.23 (m, 7 H, aromatic C*H*), 6.82 (d, $^3J_{HH}$ = 8.5 Hz, 2 H, aromatic C*H*), 6.11 (s, 1 H, C*H*), 5.22 (d, $^3J_{HH}$ = 8.2 Hz, 1 H, β-C*H*), 5.06 (s, 2 H, CH_2), 0.95 (s, 9 H, 3 x CH_3), 0.19 (s, 6 H, 2 x CH_3).
^{13}C-NMR (75 MHz, DMSO-d_6): δ (ppm) = 192.38 (*C*OCHN_2), 155.65 (Cbz *C*ONH), 154.85

(aromatic *C*-O(TBDMS)), 136.77, 129.64, 129.13, 128.21, 127.70, 127.63, 119.66 (aromatic *C*), 65.62 (*C*H_2), 61.42 (β-*C*), 53.52 (CO*C*HN_2), 25.43 (C(*C*H_3)$_3$), 17.79 (*C*(CH_3)$_3$), -4.65 (*C*H_3).

ESI-MS: *m/z* = 462.2 $[M+Na]^+$, 901.3 $[2M+Na]^+$, 438.2 $[M-H]^-$.

ESI-HRMS: *m/z* calculated for $C_{23}H_{29}N_3O_4SiNa$ $[M+Na]^+$: 462.1820, found: 462.1819.

5.3.4.4 Cbz-D-β³-hHpg(TBDMS)-OH (54)

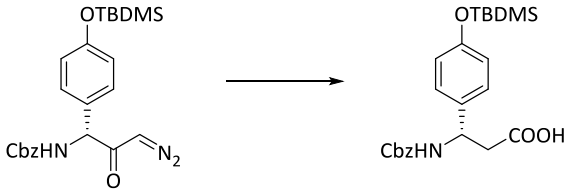

$C_{23}H_{29}N_3O_4Si$ [439.59] **53**

$C_{23}H_{31}NO_5Si$ [429.59] **54**

Diazo ketone **53** (2.57 g, 5.90 mmol, 1.00 eq) was dissolved in THF/H_2O (9:1, 24.0 mL), cooled to 0 °C and then treated with AgOCOPh (110 mg, 470 μmol, 0.08 eq) under light exclusion and sonication at rt for 2 h. Afterwards, H_2O (50.0 mL) and EtOAc (50.0 mL) were added and the aqueous phase was acidified with 2 M aq HCl solution to a pH of 2. Then, the aqueous phase was extracted with EtOAc (3 x 50.0 mL). The combined organic phases were washed with saturated aq NaCl solution (3 x 50.0 mL) and dried over $MgSO_4$. The solvent was removed under reduced pressure to give the Cbz-protected β-amino acid **54** (2.48 g, 5.80 mmol, 98%) as a yellowish oil.

^{1}H-NMR (300 MHz, DMSO-d_6): δ (ppm) = 12.17 (s_{br}, 1 H, COO*H*), 7.78 (d, $^3J_{HH}$ = 8.7 Hz, 1 H, N*H*), 7.43–7.27 (m, 5 H, aromatic C*H*), 7.21 (d, $^3J_{HH}$ = 8.5 Hz, 2 H, aromatic C*H*), 6.78 (d, $^3J_{HH}$ = 8.5 Hz, 2 H, aromatic C*H*), 5.03–4.87 (m, 3 H, β-C*H*, CH_2), 2.75–2.55 (m, 2 H, α-CH_2), 0.95 (s, 9 H, 3 x CH_3), 0.18 (s, 6 H, 2 x CH_3).

^{13}C-NMR (75 MHz, DMSO-d_6): δ (ppm) = 171.61 (*C*OOH), 155.20 (Cbz *C*ONH), 153.98 (aromatic *C*-OTBDMS), 137.02, 135.57, 128.22, 127.65, 127.59, 127.55, 119.36 (aromatic *C*), 65.21 (*C*H_2), 59.66 (α-*C*H_2), 51.03 (β-*C*H), 25.49 (C(*C*H_3)$_3$), 17.83 (*C*(CH$_3$)$_3$), -4.61 (*C*H_3).

ESI-MS: *m/z* = 430.2 $[M+H]^+$, 452.2 $[M+Na]^+$, 881.4 $[2M+Na]^+$, 428.2 $[M-H]^-$.

ESI-HRMS: *m/z* calculated for $C_{23}H_{31}NO_5SiNa$ $[M+Na]^+$: 452.1864, found: 452.1855.

5.3.4.5 Cbz-D-β³-hHpg-OBn (59)

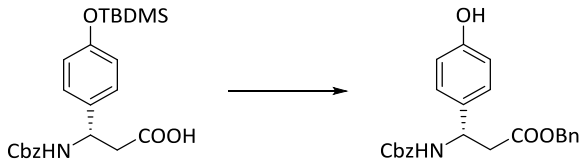

$C_{23}H_{31}NO_5Si$
[429.59]
54

$C_{24}H_{23}NO_5$
[405.45]
59

To amino acid **54** (500 mg, 1.16 mmol, 1.00 eq) dissolved in DCM (3.00 mL), BnOH (1.50 mL) and conc. HCl (37%, 14.5 mL) were added. The final reaction mixture was stirred at rt for 4 h. Then, H_2O (50.0 mL) and EtOAc (50.0 mL) were added and the aqueous phase was extracted with EtOAc (3 x 50.0 mL). The combined organic phases were washed with saturated aq NaCl solution (3 x 20.0 mL), dried over $MgSO_4$ and the solvent was removed under reduced pressure. After purification by flash-column chromatography (pentane/EtOAc, 5:1 → 1:1) the desired product **59** (240 mg, 580 μmol, 50%) was obtained as a colourless solid.

^{1}H-NMR (300 MHz, DMSO-d_6): δ(ppm) = 9.29 (s, 1 H, aromatic C-O*H*), 7.80 (d, $^3J_{HH}$ = 8.8 Hz, 1 H, N*H*), 7.44–7.21 (m, 10 H, aromatic C*H*), 7.13 (d, $^3J_{HH}$ = 8.5 Hz, 2 H, aromatic C*H*), 6.70 (d, $^3J_{HH}$ = 8.5 Hz, 2 H, aromatic C*H*), 5.08–4.89 (m, 5 H, β-C*H*, 2 x CH_2), 2.97–2.62 (m, 2 H, α-CH_2).

^{13}C-NMR (75 MHz, DMSO-d_6): δ(ppm) = 170.03 (*C*OOBn), 156.45 (aromatic *C*-OH), 155.19 (Cbz *C*ONH), 137.00, 135.99, 132.52, 128.26, 128.23, 127.80, 127.69, 127.63, 127.62, 127.60, 127.46, 114.97 (aromatic *C*H), 65.40, 65.27 (*C*H_2), 51.18 (β-*C*H), 41.18 (α-*C*H_2).

ESI-MS: *m/z* = 406.2 $[M+H]^+$, 428.2 $[M+Na]^+$, 833.3 $[2M+Na]^+$.

ESI-HRMS: *m/z* calculated for $C_{24}H_{23}NO_5Na$ $[M+Na]^+$: 428.1468, found: 428.1450.

5.3.4.6 Cbz-D-β³-hHpg-OBn (59)

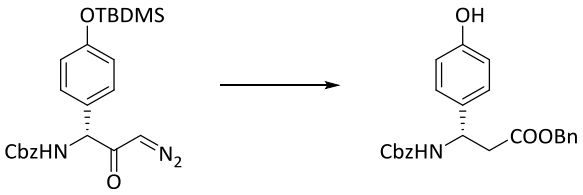

$C_{23}H_{29}N_3O_4Si$
[439.59]
53

$C_{24}H_{23}NO_5$
[405.45]
59

The benzyl protection was performed according to the procedure described by MATTHIAS KRULL.[141] Therefore, diazo ketone **53** (5.55 g, 12.6 mmol, 1.00 eq) was dissolved in dry THF/BnOH (9:1, 24.0 mL), cooled to 0 °C and then treated with AgOCOPh (230 mg, 1.01 mmol, 0.08 eq) under light exclusion and sonication at rt for 2 h. Afterwards, H_2O (100 mL) and EtOAc (100 mL) were added. The aqueous phase was acidified with 2 M aq HCl solution to a pH of 2. Then, the aqueous phase was extracted with EtOAc (3 x 75.0 mL) and the combined organic phases were washed with saturated aq NaCl solution (3 x 50.0 mL), dried over $MgSO_4$ and the solvent was removed under reduced pressure to give the benzyl-protected β-amino acid. The crude TBDMS-protected product containing residual BnOH was dissolved in MeOH (142 mL), conc. HCl (37%, 15.8 mL) was added and the final reaction mixture was stirred at rt for 1 h. Then, H_2O (100 mL) and EtOAc (100 mL) were added and the aqueous phase was extracted with EtOAc (3 x 100 mL). The combined organic phases were washed with saturated aq NaCl solution (3 x 50.0 mL), dried over $MgSO_4$ and the solvent was removed under reduced pressure. After purification by flash-column chromatography (pentane/EtOAc, 3:1 → 1:1) the desired product **59** (3.57 g, 8.82 mmol, 70%) was isolated as a colourless solid.

^{1}H-NMR (300 MHz, DMSO-d_6): δ(ppm) = 9.29 (s, 1 H, aromatic C-O*H*), 7.80 (d, $^3J_{HH}$ = 8.9 Hz, 1 H, N*H*), 7.42–7.20 (m, 10 H, aromatic C*H*), 7.13 (d, $^3J_{HH}$ = 8.5 Hz, 2 H,

aromatic C*H*), 6.70 (d, $^{3}J_{HH}$ = 8.5 Hz, 2 H, aromatic C*H*), 5.14–4.83 (m, 5 H, β-C*H*, 2 x CH_2), 2.94–2.61 (m, 2 H, α-CH_2).

^{13}C-NMR (75 MHz, DMSO-d_6): δ(ppm) = 169.98 (*C*OOBn), 156.39 (aromatic *C*-OH), 155.14 (Cbz *C*ONH), 136.77, 135.95, 132.47, 128.22, 128.19, 127.76, 127.65, 127.59, 127.56, 127.41, 127.34, 114.92 (aromatic *C*), 65.35, 65.22 (*C*H_2), 51.13 (β-*C*H), 41.13 (α-*C*H_2).

ESI-MS: *m/z* = 406.2 $[M+H]^+$, 428.2 $[M+Na]^+$, 833.3 $[2M+Na]^+$, 404.2 $[M-H]^-$.

ESI-HRMS: *m/z* calculated for $C_{24}H_{23}NO_5Na$ $[M+Na]^+$: 428.1468, found: 428.1459.

5.3.4.7 Cbz-D-β³-hHpg(Tf)-OBn (61)

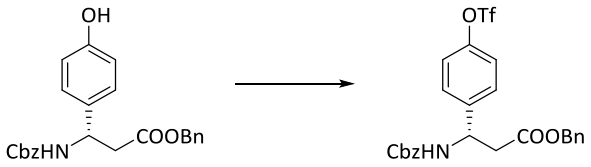

$C_{24}H_{23}NO_5$
[405.45]
59

$C_{25}H_{22}F_3NO_7S$
[537.51]
61

To a 0 °C cooled solution of Cbz-D-β³-hHpg-OBn (**59**) (4.79 g, 11.8 mmol, 1.00 eq) and pyridine (2.75 mL, 2.69 g, 35.4 mmol, 3.0 eq) in dry DCM (36.0 mL) Tf_2O (5.00 g, 17.7 mmol, 1.50 eq) was added slowly and stirred at 0 °C for 15 min. The mixture was warmed up to rt and stirred at rt for 20 min. The reaction mixture was quenched with saturated aq $NaHCO_3$ solution and the resulting aqueous phase was extracted with DCM (3 x 50.0 mL). The combined organic phases were washed with saturated aq NaCl solution (3 x 50.0 mL), dried over $MgSO_4$ and the solvent was removed under reduced pressure. The pyridine was removed as an azeotropic mixture with toluene to give the product **61** (6.26 g, 11.6 mmol, 99%) as brown solid.

^{1}H-NMR (300 MHz, DMSO-d_6): δ (ppm) = 8.03 (d, $^3J_{HH}$ = 8.5 Hz, 1 H, N*H*), 7.53 (d, $^3J_{HH}$ = 8.8 Hz, 2 H, aromatic C*H*), 7.43 (d, $^3J_{HH}$ = 8.8 Hz, 2 H, aromatic C*H*), 7.39–7.17 (m, 10 H, aromatic C*H*), 5.15–4.94 (m, 5 H, β-C*H*, CH_2), 2.98–2.74 (m, 2 H, α-CH_2).

^{13}C-NMR (125 MHz, DMSO-d_6): δ (ppm) = 169.71 (*C*OOBn), 155.30 (Cbz *C*ONH), 148.11, 143.23, 136.82, 135.88, 128.69, 128.34, 128.25, 128.23, 127.87, 127.74, 127.65, 121.28 (aromatic *C*), 118.20 (q, $^1J_{CF}$ = 318.8 Hz, *C*F_3), 65.59, 65.48 (*C*H_2), 51.35 (β-*C*), 40.50 (α-*C*H_2).

^{19}F-NMR (282 MHz, DMSO-d_6): δ (ppm) = -72.88 (s, 3 F, CF_3).

ESI-MS: *m/z* = 560.1 $[M+Na]^+$, 1097.3 $[2M+Na]^+$, 536.1 $[M-H]^-$.

ESI-HRMS: *m/z* calculated for $C_{25}H_{22}F_3NO_7SNa$ $[M+Na]^+$: 560.0961, found: 560.0961.

5.3.4.8 Cbz-4-pinacolboryl-D-β³-hPhg-OBn (62)

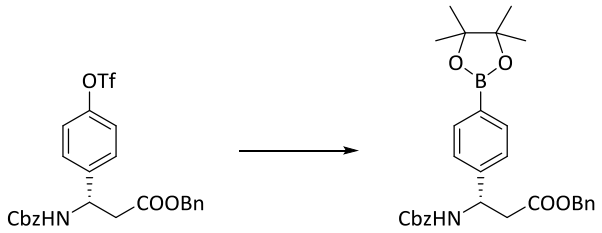

$C_{25}H_{22}F_3NO_7S$
[537.51]
61

$C_{30}H_{34}BNO_6$
[515.41]
62

Under argon atmosphere, compound **61** (1.68 g, 3.12 mmol, 1.00 eq) was dissolved in degassed dioxane (20.0 mL) and subsequently B_2pin_2 (948 mg, 3.74 mmol, 1.20 eq), KOAc (925 mg, 9.42 mmol, 3.02 eq), $PdCl_2$(dppf) (228 mg, 312 μmol, 0.10 eq) and dppf (173 mg, 132 μmol, 0.10 eq) were added. The reaction mixture was stirred at 80°C for 7 h. Then, EtOAc (300 mL) was added to the suspension and the organic phase was washed with saturated aq NaCl solution (3 x 100 mL) and dried over $MgSO_4$. Afterwards, the solvent was removed under reduced pressure. Purification by flash-column chromatography (pentane/EtOAc, 5:1 → 2:1) gave the pure product **62** (1.55 g, 3.01 mmol, 96%) as a light yellow solid.

^{1}H-NMR (300 MHz, DMSO-d_6): δ(ppm) = 7.96 (d, $^3J_{HH}$ = 8.6 Hz, 1 H, N*H*), 7.62 (d, $^3J_{HH}$ = 8.0 Hz, 2 H, aromatic C*H*), 7.42–7.15 (m, 12 H, aromatic C*H*), 5.10–4.93 (m, 5 H, CH_2, β-C*H*), 2.93–2.73 (m, 2 H, α-CH_2), 1.29 (s, 12 H, 4 x CH_3).
^{13}C-NMR (126 MHz, DMSO-d_6): δ(ppm) = 169.74 (*C*OOBn), 155.19 (Cbz *C*ONH), 145.51, 136.85, 135.86, 134.42, 128.18, 127.75, 127.65, 127.59, 125.82 (aromatic *C*), 83.49 (*C*$(CH_3)_2$), 65.43, 65.30 (*C*H_2), 51.69 (β-*C*), 40.68 (*C*H_2), 24.54 (C(*C*$H_3)_2$).
ESI-MS: *m/z* = 516.3 $[M+H]^+$, 538.3 $[M+Na]^+$, 1053.5 $[2M+Na]^+$.
ESI-HRMS: *m/z* calculated for $C_{30}H_{34}BNO_6Na$ $[M+Na]^+$: 538.2377, found: 538.2369.

5.3.4.9 Cbz-4-dihydroxyborane-D-β³-hPhg-OBn (63)

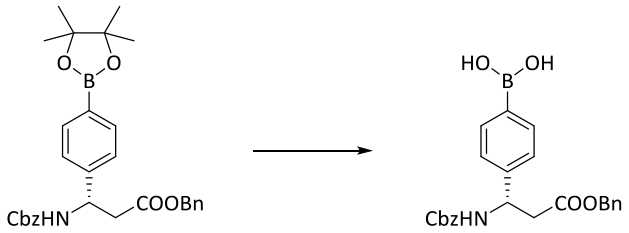

$C_{30}H_{34}BNO_6$
[515.41]
62

$C_{24}H_{24}BNO_6$
[433.27]
63

Compound **62** (3.74 g, 7.26 mmol, 1.00 eq) was dissolved in acetone (330 mL) and H_2O (291 mL). Then, NH_4OAc (1.68 g, 21.8 mmol, 3.00 eq) and $NaIO_4$ (4.81 g, 22.5 mmol, 3.10 eq) were added and the reaction mixture was stirred at rt for 2 d. Afterwards, the organic solvent was removed under reduced pressure and the residual aqueous phase was extracted with Et_2O (3 x 100 mL). The combined organic phases were washed with saturated aq NaCl solution (100 ml) and dried over $MgSO_4$. The organic solvent was removed *in vacuo* to provide the final product **63** (2.83 g, 6.54 mmol, 90%) as a white solid.

^{1}H-NMR (300 MHz, DMSO-d_6): δ (ppm) = 8.06–7.88 (m, 3 H, N*H*, aromatic C*H*), 7.76 (d, $^3J_{HH}$ = 8.0 Hz, 2 H, aromatic C*H*), 7.41–7.24 (m, 10 H, aromatic C*H*), 5.11–4.89 (m, 5 H, 2 x CH_2, β-C*H*), 2.93–2.73 (m, 2 H, α-CH_2).

^{13}C-NMR (126 MHz, DMSO-d_6): δ (ppm) = 169.93 (*C*OOBn), 155.29 (Cbz *C*ONH), 144.00, 136.95, 135.93, 134.14, 128.26, 128.23, 127.83, 127.71, 127.66, 125.35 (aromatic *C*), 65.49, 65.34 (*C*H_2), 51.71 (β-*C*), 40.68 (*C*H_2).

ESI-MS: *m/z* = 448.2 $[M+H]^+$, 470.2 $[M+Na]^+$, 917.4 $[2M+Na]^+$.

ESI-HRMS: *m/z* calculated for $C_{24}H_{24}BNO_6Na$ $[M+Na]^+$: 470.1750, found: 470.1740.

5.3.4.10 Cbz-4-(3,3,5,5-tetramethyl-2,6-dioxopiperazine-1-yl)-D-β³-hPhg-OBn (64)

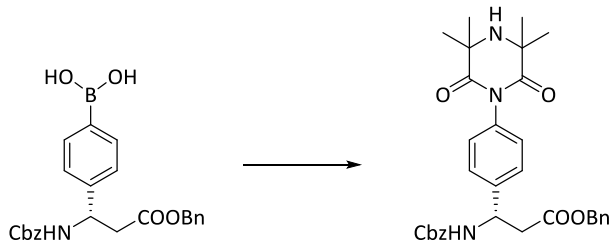

$C_{24}H_{24}BNO_6$
[433.27]
63

$C_{32}H_{35}N_3O_6$
[557.65]
64

A suspension of **63** (2.80 g, 6.47 mmol, 1.00 eq), piperazine-2,6-dione **33** (1.10 g, 6.47 mmol, 1.00 eq), $Cu(OAc)_2$ (1.17 g, 6.47 mmol, 1.00 eq), Et_3N (1.26 mL, 920 mg, 9.06 mmol, 1.40 eq) and powdered 4 Å molecular sieve (4.00 g) in DMSO (135 mL) was stirred at rt under an oxygen atmosphere for 14 d. Then, the mixture was filtrated over Celite®. The filtrate was mixed with EtOAc (100 mL), H_2O (100 mL) and 2 M aq HCl (100 mL) and the phases were separated. The aqueous phase was extracted with EtOAc (3 x 100 mL). The combined organic phases were washed with saturated aq NaCl solution (3 x 100 mL), dried over $MgSO_4$ and the solvent was removed under reduced pressure. Purification by flash-column chromatography (pentane/EtOAc, 1:1 → 1:3) gave the final product **64** (2.58 g, 4.62 mmol, 71%) as a white solid.

^{1}H-NMR (300 MHz, DMSO-d_6): δ(ppm) = 7.98 (d, $^3J_{HH}$ = 8.7 Hz, 1 H, N*H*), 7.41 (d, $^3J_{HH}$ = 8.3 Hz, 2 H, aromatic C*H*), 7.37–7.28 (m, 10 H, aromatic C*H*), 7.05 (d, $^3J_{HH}$ = 8.3 Hz, 2 H, aromatic C*H*), 5.14–4.94 (m, 5 H, 2 x CH_2, β-C*H*), 2.91–2.82 (m, 2 H, α-CH_2), 1.39 (s, 12 H, 2 x CH_3).

^{13}C-NMR (126 MHz, DMSO-d_6): δ(ppm) = 176.50 (*C*ONR_2), 169.85 (*C*OOBn), 155.26 (Cbz *C*ONH), 141.98, 136.82, 135.87, 134.93, 128.46, 128.25, 128.20, 127.81, 127.72, 127.67,

126.70 (aromatic *C*), 65.54, 65.39 (*C*H_2), 59.61 (*C*$(CH_3)_2$), 51.17 (β-*C*), 40.67 (*C*H_2), 27.95 (C(*C*$H_3)_2$).

ESI-MS: *m/z* = 558.3 $[M+H]^+$, 580.3 $[M+Na]^+$, 1137.5 $[2M+Na]^+$.

ESI-HRMS: *m/z* calculated for $C_{32}H_{35}N_3O_6Na$ $[M+Na]^+$: 580.2418, found: 580.2411.

5.3.4.11 Fmoc-4-(3,3,5,5-tetramethyl-2,6-dioxopiperazine-1-yl)-D-β³-hPhg-OH (66)

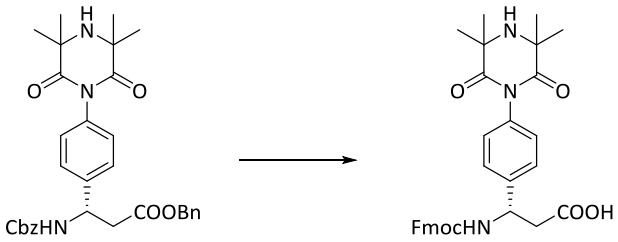

$C_{32}H_{35}N_3O_6$
[557.65]
64

$C_{32}H_{33}N_3O_6$
[555.63]
66

Amino acid **64** (500 mg, 897 μmol, 1.00 eq) was dissolved in MeOH (21.2 mL) and DCM (3.00 mL). Then, $Pd(OH)_2/C$ (50% H_2O, 101 mg, 717 μmol, 0.80 eq) was added and H_2 was passed through the suspension at rt for 1 h, and subsequently it was stirred at rt under a H_2 atmosphere for 21 h. Afterwards, the suspension was first filtered through a pleated filter and then the filtrate was passed through a micron syringe filter. The solvent was removed under reduced pressure to give the crude unprotected amino acid. To the crude intermediate $NaHCO_3$ (152 mg, 1.79 mmol, 2.00 eq) and DMF (5.23 mL) were added. Then, Fmoc-OSu (303 mg, 897 μmol, 1.00 eq) was added and the reaction mixture was stirred at rt for 20 h. Afterwards, H_2O was added to the reaction. The aqueous phase was acidified to pH 2 with 2 M aq HCl and extracted with EtOAc (3 x 50.0 mL). The combined organic phases were washed with saturated aq NaCl solution (50.0 mL), dried over $MgSO_4$ and the solvent was removed under reduced pressure. Purification by flash-column chromatography (DCM/MeOH/AcOH, 100:0:0.1 → 94:6:0.1) gave the pure product **66** (419 mg, 750 μmol, 84%) as a white solid.

^{1}H-NMR (300 MHz, DMSO-d_6): δ(ppm) = 8.00 (d, $^3J_{HH}$ = 8.7 Hz, 1 H, N*H*), 7.42 (d, $^3J_{HH}$ = 8.4 Hz, 2 H, aromatic C*H*), 7.39–7.29 (m, 8 H, aromatic C*H*), 7.06 (d, $^3J_{HH}$ = 8.4 Hz, 2 H, aromatic C*H*), 5.08–4.96 (m, 1 H, C*H*), 4.32–4.17 (m, 3 H, CH_2, β-C*H*), 2.77–2.65 (m,

2 H, α-CH_2), 1.41 (s, 12 H, 2 x CH_3).

^{13}C-NMR (126 MHz, DMSO-d_6): δ(ppm) = 176.52 (*C*ONR$_2$), 171.54 (*C*OOH), 155.27 (Fmoc *C*ONH), 143.77, 143.73, 142.50, 140.61, 134.78, 128.38, 127.49, 126.98, 126.70, 125.07, 119.97, 119.20 (aromatic *C*), 65.38 (*C*H$_2$), 55.31 (*C*(CH$_3$)$_2$), 51.19 (β-*C*), 46.65 (*C*H), 40.83 (*C*H$_2$), 27.96 (C(*C*H$_3$)$_2$).

ESI-MS: *m/z* = 556.3 [M+H]$^+$, 578.3 [M+Na]$^+$, 1111.5 [2M+H]$^+$.

ESI-HRMS: *m/z* calculated for $C_{32}H_{33}N_3O_6Na$ [M+Na]$^+$: 578.2262, found: 578.2242.

5.3.4.12 Fmoc-4-(3,3,5,5-Tetramethyl-2,6-dioxo-4-oxylpiperazine-1-yl)-D-β³-hPhg-OH (67)

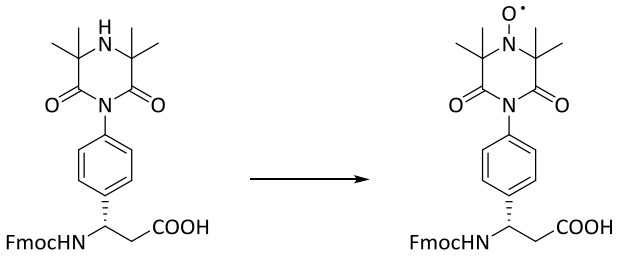

$C_{32}H_{33}N_3O_6$
[555.63]
66

$C_{32}H_{32}N_3O_7$
[570.62]
67

Compound **66** (413 mg, 743 µmol, 1.00 eq) was dissolved in DCM (99.0 mL) and the solution was cooled to 0 °C. Then, *m*-CPBA (70%, 366 mg, 2.12 mmol, 2.00 eq) was added and the resulting reaction mixture was stirred at 0 °C for 15 min followed by stirring at rt for 5 h. The solvent was removed under reduced pressure and the crude product was purified by flash-column chromatography (DCM/MeOH/AcOH, 100:0:0.1 → 98:2:0.1) to give product **67** (288 mg, 505 µmol, 68%) as an orange solid.

ESI-MS: *m/z* = 571.2 $[M+H]^+$, 588.3 $[M+NH_4]^+$, 593.2 $[M+Na]^+$, 1163.4 $[2M+Na]^+$.
ESI-HRMS: *m/z* calculated for $C_{32}H_{32}N_3O_7Na$ $[M+Na]^+$: 593.2132, found: 593.2130.

5.3.5 Synthesis of Racemic Cbz-β³-hHpg(Tf)-OBn

The synthetic routes of the racemic amino acids were performed as described in section 5.3.4. A mixture of D-Hpg-OH (**50**) and L-Hpg-OH (**25**) (1:1, 4.00 g, 23.8 mmol) was used as starting material.

5.3.5.1 Cbz-D/L-β³-hHpg(TBDMS)-OBn (70)

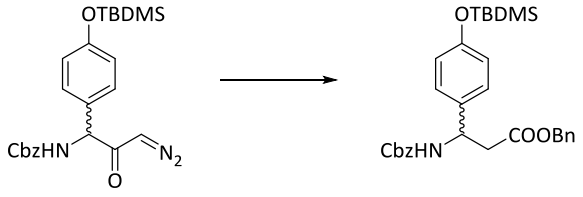

$C_{23}H_{29}N_3O_4Si$ [439.59] | $C_{30}H_{37}NO_5Si$ [519.71]

70

The synthesis of **70** was performed by using the procedure described in subsection 5.3.4.6. D/L-Diazo ketone (1.83 g, 4.16 mmol, 1.00 eq) was used as starting material. Small amounts of the crude β³-amino acid **70** were purified by HPLC and lyophilised. Then, the two enantiomers of the pure amino acid **70** dissolved in hexane/isopropanol (1:1, 500 µL) were separated *via* HPLC using a chiral column.

HPLC: (analytical, gradient 70 → 100% B in 30 min): t_R = 28.00 min.

ESI-MS: *m/z* = 520.3 $[M+H]^+$, 1039.5 $[2M+H]^+$.

ESI-HRMS: *m/z* calculated for $C_{30}H_{38}NO_5$ $[M+H]^+$: 520.2514, found: 520.2490.

HPLC: (chiral, Chialpak® IA, flow 0.6 mL/min, isocratic (hexane/isopropanol, 98:2 in 150 min): t_{R1} = 71.4 min, t_{R2} = 91.7 min.

5.3.5.2 Cbz-D/L-β³-hHpg(Tf)-OH (72)

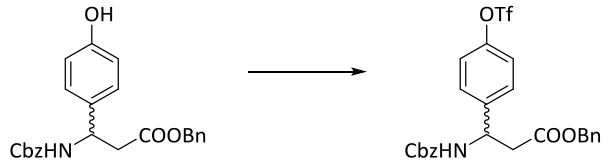

$C_{24}H_{23}NO_5$
[405.45]
71

$C_{25}H_{22}F_3NO_7S$
[537.51]
72

The synthesis of compound **72** was performed according to the procedure described in 5.3.4.7. The phenol derivative (1.83 g, 4.16 mmol, 1.00 eq) was used as starting material. The crude product **72** (1 mg) were directly dissolved in hexane/isopropanol (1:1, 500 μL) and the enantiomers were separated *via* HPLC using a chiral column.

Analytical data are in accordance with the data mentioned in subsection 5.3.4.7.

HPLC: (chiral, Chialpak® IA, flow 0.6 mL/min, isocratic (hexane/isopropanol, 90:10 in 90 min): t_{R1} = 34.5 min, t_{R2} = 58.0 min.

5.3.6 Synthesis of β-amino acids

5.3.6.1 Fmoc-D-β³-hLys(Boc)-OH (74)

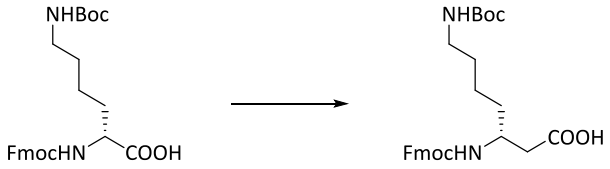

$C_{26}H_{32}N_2O_6$
[468.55]

$C_{27}H_{34}N_2O_6$
[482.58]
74

The synthesis of **74** was performed according to 5.2.1. Fmoc-D-Lys(Boc)-OH (5.00 g, 10.7 mmol, 1.00 eq) was used as starting material. The crude β³-amino acid was dissolved in DCM (10.0 mL) and was added drop-wise to cold pentane (-22 °C) (1.00 L). The white solid was filtered off and washed with cold pentane. Drying in *vacuo* gave the desired product **74** (4.22 g, 8.74 mmol, 82%) as a white solid.

^{1}H-NMR (300 MHz, DMSO-d_6): δ (ppm) = 12.10 (s_{br}, 1 H, COO*H*), 7.88 (d, $^3J_{HH}$ = 7.5 Hz, 2 H, Fmoc CH_{Ar}), 7.69 (d, $^3J_{HH}$ = 7.2 Hz, 2 H, Fmoc CH_{Ar}), 7.48–7.28 (m, 4 H, Fmoc CH_{Ar}), 7.14 (d, $^3J_{HH}$ = 8.6 Hz, 1 H, Fmoc N*H*), 6.75–6.61 (m, 1 H, Boc C*H*), 4.35–4.15 (m, 3 H, Fmoc C*H*, Fmoc CH_2), 3.85–3.67 (m, 1 H, β-C*H*), 2.88 (q, $^3J_{HH}$ = 6.6, 2 H, ζ-C*H*), 2.41–2.24 (m, 2 H, α-CH_2), 1.49–1.12 (m, 15 H, γ-CH_2, δ-CH_2, ε-CH_2, Boc CH_3).

^{13}C-NMR (126 MHz, DMSO-d_6): δ (ppm) = 172.13 (*C*OOH), 155.30, 155.26 (Boc *C*ONH, Fmoc *C*ONH), 143.73, 143.60, 140.49, 127.39, 127.34, 126.80, 126.78, 124.96, 124.93, 119.85 (aromatic *C*), 77.15 (*C*$(CH_3)_3$), 65.02 (Fmoc *C*H_2), 47.82 (β-*C*H), 46.75 (Fmoc *C*H), 33.82 (ε-*C*H_2), 29.23 (γ-*C*H_2), 28.20 (*C*$(CH_3)_3$), 22.69 (ζ-*C*H_2).

ESI-MS: *m/z* = 505.3 $[M+Na]^+$, 987.5 $[2M+Na]^+$, 481.3 $[M-H]^-$.

ESI-HRMS: *m/z* calculated for $C_{27}H_{34}N_2O_6Na$ $[M+Na]^+$: 505.2309, found: 505.2311.

5.3.6.2 Fmoc-D-β³-hTrp(Boc)-OH (75)

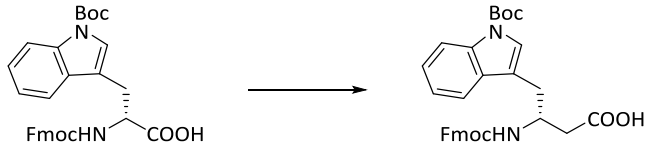

$C_{31}H_{30}N_2O_6$
[526.59]

$C_{32}H_{32}N_2O_6$
[540.62]
75

The synthesis of **75** was carried out as described in 5.2.1 and Fmoc-D-Trp(Boc)-OH (5.00 g, 9.5 mmol, 1.00 eq) as starting material. The crude Fmoc-D-β³-hTrp-OH (**15**) was dissolved in DCM (10.0 mL) and was added drop-wise to cold pentane (-22 °C) (1.00 L). The solid was filtered off and washed with cold pentane. Drying in *vacuo* led to the product **75** (4.07 g, 7.53 mmol, 79%) as a white solid.

¹H-NMR (300 MHz, DMSO-d_6): δ (ppm) = 12.30 (s_{br}, 1 H, COO*H*), 8.03 (d, $^3J_{HH}$ = 8.2 Hz, 1 H, aromatic C*H*), 7.87 (d, $^3J_{HH}$ = 7.6 Hz, 2 H, aromatic C*H*), 7.70 (d, $^3J_{HH}$ = 7.8 Hz, 2 H, aromatic C*H*), 7.65–7.58 (m, 2 H, aromatic C*H*), 7.51 (s, 1 H, aromatic C*H*), 7.46–7.15 (m, 7 H, N*H*, aromatic C*H*), 4.30–4.00 (m, 4 H, Fmoc C*H*, Fmoc CH_2, β-C*H*), 2.92–2.81 (m, 2 H, α-CH_2), 2.53–2.44 (γ-CH_2, overlapped with the DMSO signal), 1.55 (s, 9 H, CH_3).
¹³C-NMR (126 MHz, DMSO-d_6): δ (ppm) = 172.13 (*C*OOH), 155.24 (Fmoc *C*ONH), 148.78 (Boc *C*ONH), 143.57, 140.44, 134.57, 132.54, 130.54, 129.01, 128.29, 127.33, 126.75, 124.93, 124.89, 124.04, 123.45, 122.25, 119.83, 119.05, 117.17, 114.50 (aromatic *C*), 83.26 (*C*$(CH_3)_3$), 65.24 (Fmoc *C*H_2), 47.95 (β-*C*H), 46.66 (Fmoc *C*H), 40.11–39.02 (α-*C*H_2 overlapped with DMSO signal), 29.54 (γ-*C*H_2) 27.59 (C(*C*$H_3)_3$).
ESI-MS: *m/z* = 541.2 $[M+H]^+$, 563.2 $[M+Na]^+$, 1103.4 $[2M+Na]^+$, 539.3 $[M-H]^-$.
ESI-HRMS: *m/z* calculated for $C_{32}H_{32}N_2O_6Na$ $[M+Na]^+$: 563.2153, found: 523.2141.

5.3.6.3 Fmoc-D-β³-hVal-OH (76)

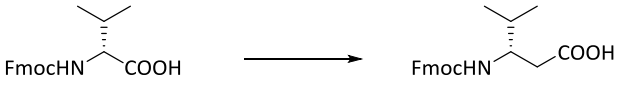

$C_{20}H_{21}NO_4$
[339.39]

$C_{21}H_{23}NO_4$
[353.42]
76

Synthesis of **76** was performed by using procedure 5.2.1 and Fmoc-D-Val-OH (5.00 g, 14.7 mmol, 1.00 eq) as starting material. The crude amino acid was purified *via* flash-column chromatography (DCM/MeOH/AcOH, 40:1:0.1) to give the pure product **76** (3.55 g, 10.0 mmol, 68%) as a white solid.

^{1}H-NMR (300 MHz, DMSO-d_6): δ (ppm) = 12.07 (s_{br}, 1 H, COO*H*), 7.87 (d, $^3J_{HH}$ = 7.4 Hz, 2 H, aromatic C*H*), 7.77–7.64 (m, 2 H, aromatic C*H*), 7.41 (t, $^3J_{HH}$ = 7.4, 2 H, aromatic C*H*), 7.36–7.27 (m, 2 H, aromatic C*H*), 4.38–4.11 (m, 3 H, Fmoc C*H*, Fmoc CH_2), 3.82–3.67 (m, 1 H, β-C*H*), 2.46–2.23 (m, 2 H, α-CH_2), 1.80–1.65 (m, 1 H, C*H*), 0.83 (d, $^3J_{HH}$ = 6.7 Hz, CH_3).
^{13}C-NMR (126 MHz, DMSO-d_6): δ (ppm) = 172.75 (*C*OOH), 155.28 (Fmoc *C*ONH), 143.95, 143.77, 140.66, 140.65 (Fmoc C_{Ar}), 127.52, 126.99, 126.95, 125.19, 125.16, 120.01, 120.00 (Fmoc *C*H_{Ar}), 65.16 (Fmoc *C*H_2), 53.00 (β-*C*H), 46.78 (Fmoc *C*H), 36.69 (α-*C*H_2), 31.70 (*C*H), 18.81, 17.96 (*C*H_3).
ESI-MS: *m/z* = 354.2 $[M+H]^+$, 376.1 $[M+Na]^+$, 729.3 $[2M+Na]^+$, 352.2 $[M-H]^-$, 705.4 $[2M-H]^-$.
ESI-HRMS: *m/z* calculated for $C_{21}H_{23}NO_4Na$ $[M+Na]^+$: 376.1519, found: 376.1518.

5.3.7 β-Peptide Synthesis

5.3.7.1 Synthesis of P5

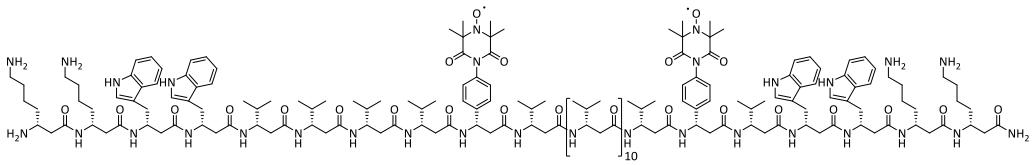

$C_{212}H_{334}N_{40}O_{33}$
[3971.25]
P5

Peptide synthesis of **P5** was carried out using a NovaPEG Rink Amide resin LL (0.19 mmol/g, 50.0 μmol, 263 mg) and all amino acid coupling steps were performed in a solvent volume of 600 μL. The resin was loaded with Fmoc-β^3-D-hLys(Boc)-OH as described in section 5.2.2. The chain elongation was performed as mentioned in section 5.2.6 and the amino acids Fmoc-β^3-D-hLys(Boc)-OH (**74**), Fmoc-β^3-D-hTrp(Boc)-OH (**75**) and Fmoc-β^3-D-hVal-OH (**76**). The first hTOPP label **67** was coupled according to section 5.2.8. After the 7th amino acid the power was reduced to 15 W. The second hTOPP label **67** was attached using conditions in section 5.2.8. The other amino acids were coupled as mentioned in section 5.2.6. The resin was cleaved using procedure shown in section 5.2.9 and the re-oxidation of the radical (MeCN/MeOH, 1:1) was carried out using the procedure described in section 5.2.10.

HPLC: (60 °C, gradient 68 → 80% C in 40 min): t_R = 29.43 min.

ESI-MS: *m/z* = 662.8 $[M+6H]^{6+}$, 795.1 $[M+5H]^{5+}$, 993.7 $[M+4H]^{4+}$, 1324.5 $[M+3H]^{3+}$, 1986.3 $[M+2H]^{2+}$.

ESI-HRMS: *m/z* calculated for $C_{212}H_{339}N_{40}O_{33}$ $[M+5H]^{5+}$: 795.1222, found: 795.1227.

5.3.7.2 Synthesis of P6

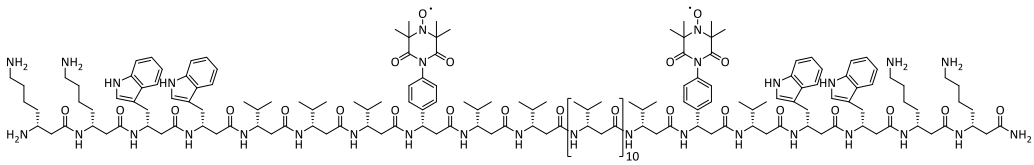

$C_{212}H_{334}N_{40}O_{33}$
[3971.25]
P6

Peptide synthesis of **P6** (17.0 μmol) was performed as described in subsection 5.3.7.1. All amino acid coupling steps were performed in a solvent volume of 300 μL. After the 7th amino acid the power was reduced to 8 W. The re-oxidation of the radical (MeCN/MeOH, 1:1) was carried out using procedure described in 5.2.10.

HPLC: (60 °C, gradient 69 → 79% C in 40 min): t_R = 33.93 min.

ESI-MS: *m/z* = 662.8 $[M+6H]^{6+}$, 795.1 $[M+5H]^{5+}$, 993.7 $[M+4H]^{4+}$, 1324.5 $[M+3H]^{3+}$, 1986.3 $[M+2H]^{2+}$.

ESI-HRMS: *m/z* calculated for $C_{212}H_{339}N_{40}O_{33}$ $[M+5H]^{5+}$: 795.1222, found: 795.1225.

5.3.7.3 Synthesis of P7

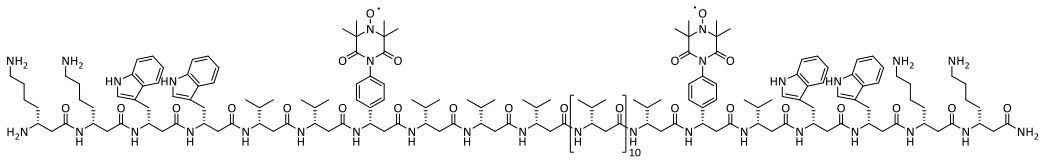

$C_{212}H_{334}N_{40}O_{33}$
[3971.25]
P7

Peptide synthesis of **P7** (17.0 μmol) was carried out as described in subsection 5.3.7.1. All amino acid coupling steps were performed in a solvent volume of 300 μL. After the 7th amino acid the power was reduced to 8 W. The re-oxidation of the radical (MeCN/MeOH, 1:1) was carried out using procedure described in 5.2.10.

HPLC: (60 °C, gradient 68 → 80% C in 40 min): t_R = 30.80 min.

ESI-MS: *m/z* = 662.8 $[M+6H]^{6+}$, 795.1 $[M+5H]^{5+}$, 993.7 $[M+4H]^{4+}$, 1324.5 $[M+3H]^{3+}$, 1986.3 $[M+2H]^{2+}$.

ESI-HRMS: *m/z* calculated for $C_{212}H_{339}N_{40}O_{33}$ $[M+5H]^{5+}$: 795.1222, found: 795.1238.

5.3.7.4 Synthesis of P8

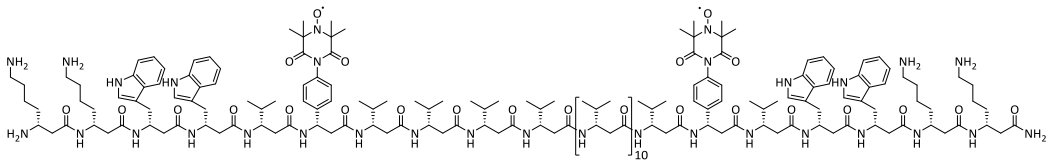

$C_{212}H_{334}N_{40}O_{33}$
[3971.25]
P8

Peptide synthesis of **P8** (17.0 μmol) was performed as described in subsection 5.3.7.1. All amino acid coupling steps were performed in a solvent volume of 300 μL. After the 7th amino acid the power was reduced to 8 W. The re-oxidation of the radical (MeCN/MeOH, 1:3) was carried out using procedure described in 5.2.10.

HPLC: (60 °C, gradient 68 → 80% C in 40 min): t_R = 29.01 min.

ESI-MS: *m/z* = 662.8 $[M+6H]^{6+}$, 795.1 $[M+5H]^{5+}$, 993.7 $[M+4H]^{4+}$, 1324.5 $[M+3H]^{3+}$, 1986.3 $[M+2H]^{2+}$.

ESI-HRMS: *m/z* calculated for $C_{212}H_{339}N_{40}O_{33}$ $[M+5H]^{5+}$: 795.1222, found: 795.1227.

6 Appendix

A.1 Synthesis and Structural Investigation of Labelled Transmembrane α-Peptides

A.1.1 Synthesis of the TOPP-Labelled WALP24 Peptide

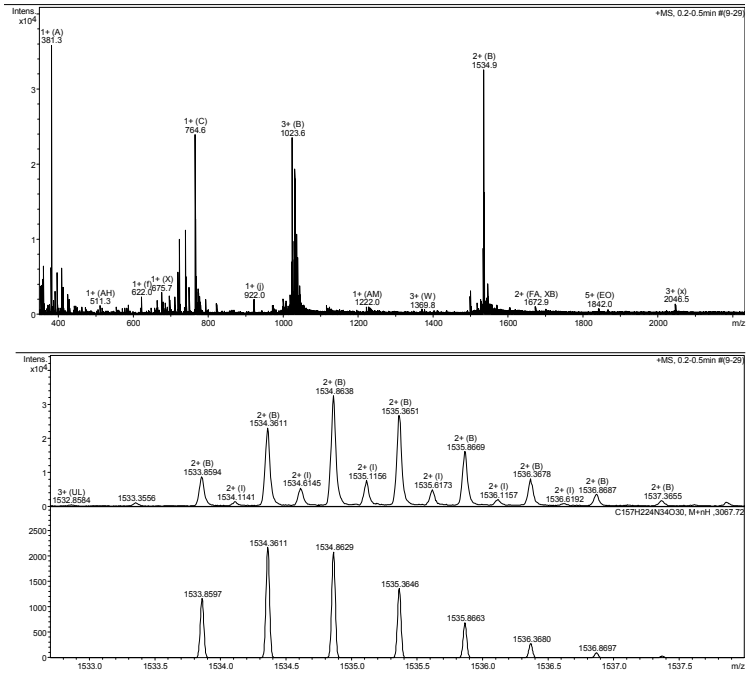

Figure A 1: ESI mass spectra of **P1**. Top: ESI mass spectrum. Bottom: ESI-HRMS spectrum of the $[M+2H]^{2+}$-species.

A.1.2 Synthesis of the MTSSL-Labelled WALP24 Peptide

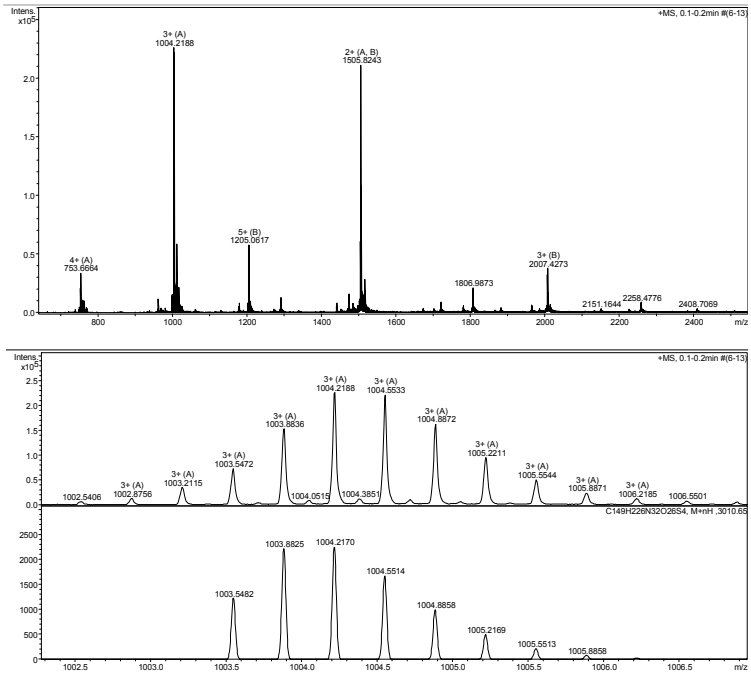

Figure A 2: ESI mass spectra of **P3**. Top: ESI mass spectrum. Bottom: ESI-HRMS spectrum of the $[M+3H]^{3+}$-species.

A.1.3 Enhancement of the TOPP Rigidity

Other preliminary approaches and attempts: One conceivable retro-synthetic route is illustrated in **Scheme A 1**.

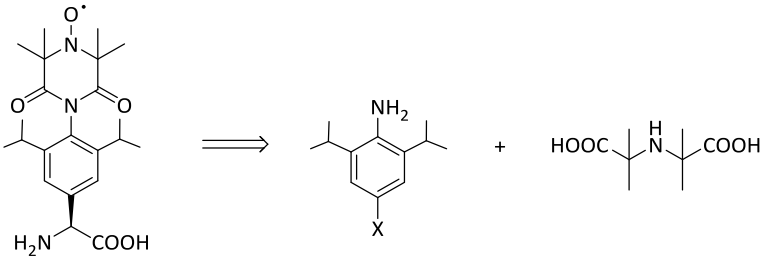

A-1 **A-2** **A-3**

Scheme A 1: Retrosynthesis for compound **38**. Compound **38** might be generated using aniline derivative **A-2** and *N*-(1-carboxy-1-methylethyl)-2-methylalanine (**A-3**). X should illustrate the functionalisation which is needed to introduce the amino acid backbone

In this synthesis the piperzine-2,6-dione moiety will be generated through the reaction of the aniline **A-2** with a *N*-(1-carboxy-1-methylethyl)-2-methylalanine (**A-3**) (activated as anhydride or acyl chloride). The amino acid back functionalisation should be performed *via* enantioselective Pd catalysis as described in literature[102,174].

First, the commercially available 2,6-diisopropyl aniline (**A-4**) was transformed into to 4-bromo-2,6-diisopropyl aniline (**A-5**) using NBS (**Scheme A 2**) to generate a suitable leaving group for the Pd-catalysed amino acid functionalisation.

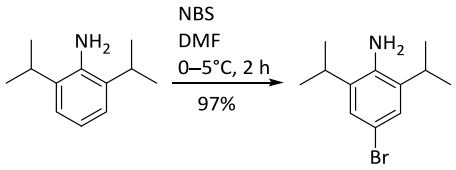

A-4 **A-5**

Scheme A 2: Bromination of aniline **A-4** which led to product **A-5**.

To obtain the dicarboxylic acid **A-3** several synthetic routes were tested. For a nucleophilic substitution 2-aminoisobutyric ethylester hydrochlorid (**A-7**) and 2-tosyl-

isobutyric ethylester (**A-9**) were synthesised (**Scheme A 3**).

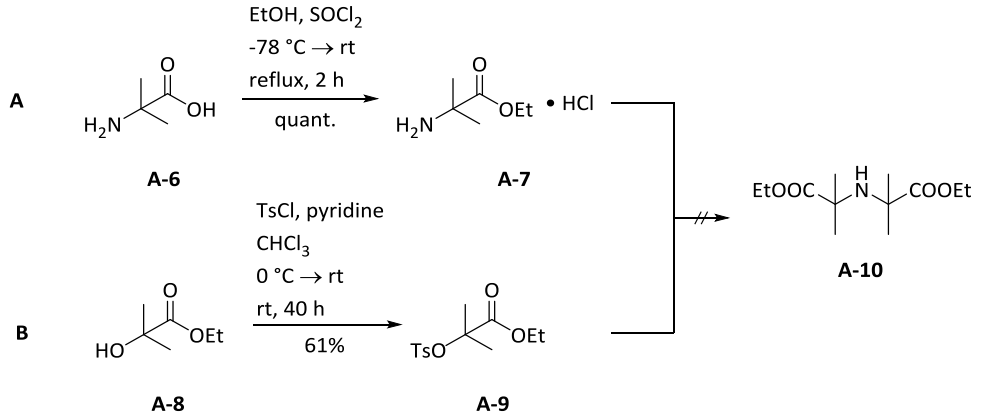

Scheme A 3: The synthesis of the nucleophile **A-7** and the electrophile **A-9** for the nucleophilic substitution. Amine **A-7** was generated using $SOCl_2$ and EtOH. The electrophile **A-9** was obtained using alcohol **A-8** and *p*-toluenesulfonyl chlorid (TsCl). Tested reaction conditions for a nucleophilic substation (see **Table A 1**) did not lead to the desired product **A-10**.

Both compounds were added together under various conditions (**Table A 1**), yet none of these led to the desired product **A-10**.

Table A 1: Tested conditions for the nucleophilic substitution.

conditions
K_2CO_3, DMF, 3 h MW (17 bar, 90 °C, 50 W)
K_2CO_3, EtOH, 8 h reflux
K_2CO_3, EtOH, 4 h MW (100 °C, 50 W), 48 h reflux
K_2CO_3, H_2O/EtOH (4:1), 4 h MW (100 °C, 50 W)
K_2CO_3, DMF, 4 h MW (120 °C, 50 W)

The steric demand of the methyl groups and the partial charge of C_α (compound **A-9**) are not suitable for this reaction typ. Thus, another synthetic route was examined which included the synthesis of 3,3,5,5-tetramethylmorpholine-2-one (**A-12**) using 2-amino-2-methylpropan-1-ol (**A-11**), acetone and $CHCl_3$ as starting materials**,** and should

proceed *via* a procedure described by McNALLY *et al*.[175]. Then, basic hydrolysis and oxidation of **A-12** using $KMnO_4$ did not lead to the desired product **A-3** (**Scheme A 4**).

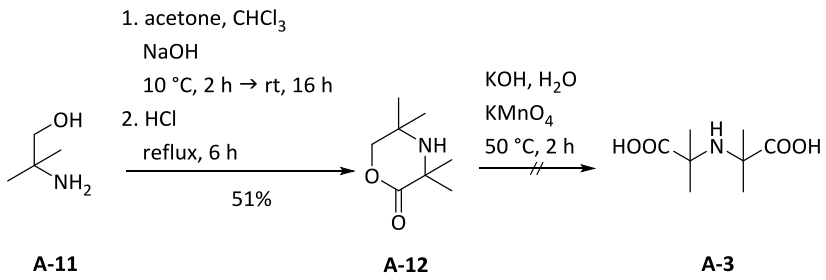

A-11 **A-12** **A-3**

Scheme A 4: The synthesis of dicarboxylic acid **A-3** *via* lactone formation followed by basic hydrolysis and oxidation. The lactone **A-12** was synthesised according to a literature protocol described by McNALLY *et al*.[175] The basic hydrolytic oxidation did not lead to the dicarboxylic acid **A-3**.

The mass spectrum gave no hint for the product **A-3**. However, the hydrolysis of the nitrile **32** led to the desired product **A-3** (**Scheme A 5**).[76]

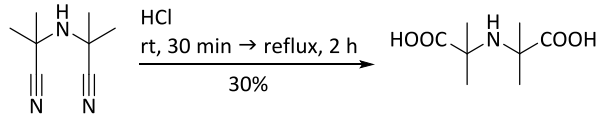

32 **A-3**

Scheme A 5: Acidic hydrolyse of nitrile **32**. The treatment with acid led to the dicarboxylic acid **A-3**.

Unfortunately, it was not possible to activate (transformation into an anhydride or an acyl chloride) the dicarboxylic acid **A-3** for further reactions, since it was only slightly soluble (used solvents DMSO, DMF, THF, NMP and dioxane). Thus, in future attempts the insertion of groups, which increase the solubility, might be reasonable.

A.2 Synthesis and Structural Investigation of Labelled Transmembrane β-Peptides

A.2.1 Development and Synthesis of the β^3-hTOPP Label

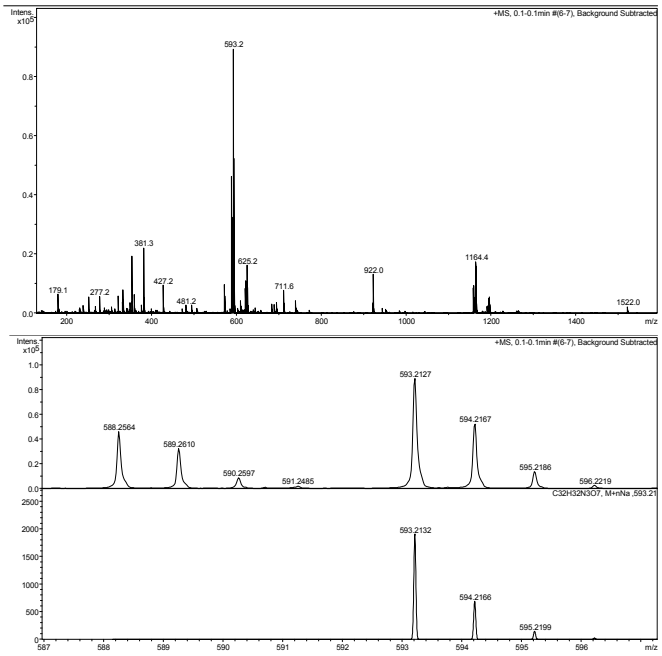

Figure A 3: ESI mass spectra of the β^3-hTOPP label **25.** Top: ESI mass spectrum. Bottom: ESI-HRMS spectrum of the $[M+2H]^{2+}$-species.

A.2.1.1 Investigation of the Enantioselectivity of Selected Reaction Steps

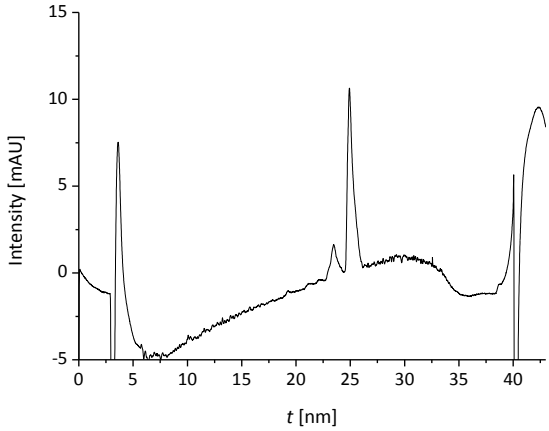

Figure A 4: HPLC chromatogram of compound **67** regarding its *ee* by HPLC. Absorption was recorded at 254 nm. HPLC was performed using a Chiralpak® OD column and a gradient 10 → 100% C (A: H_2O + 0.1% TFA and C: MeCN + 0.1% TFA) in 30 min, flow 1.0 mL/min).

A.2.2 Development and Synthesis of the TOPP-Labelled β^3-Peptides

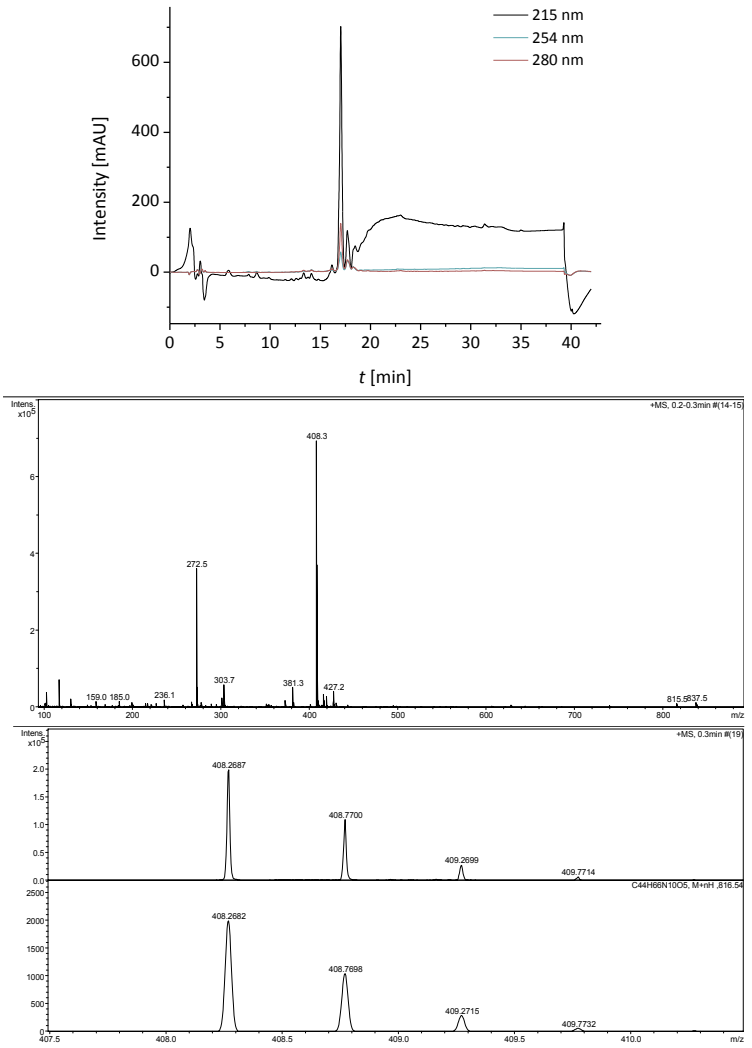

Figure A 5: HPLC chromatogram and ESI mass spectra of **P5B**. Top: HPLC chromatogram. Absorption was recorded at 215, 254 and 280 nm, 10 → 100% B (A: H_2O + 0.1% TFA and B: MeOH + 0.1% TFA) in 30 min, flow 1.0 mL/min. Centre: ESI mass spectrum. Bottom: ESI-HRMS spectrum of the $[M+2H]^{2+}$-species.

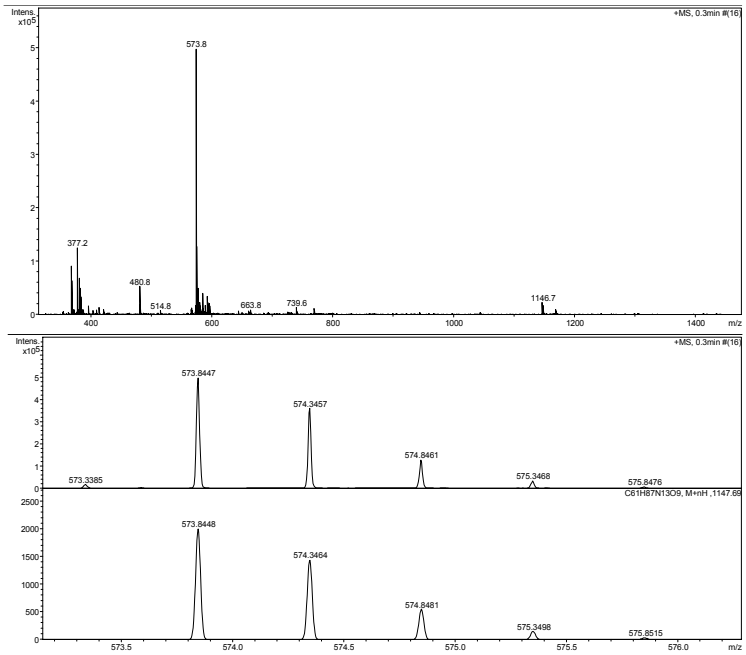

Figure A 6: ESI mass spectra of **P5C**. Top: ESI mass spectrum. Bottom: ESI-HRMS spectrum of the $[M+2H]^{2+}$-species.

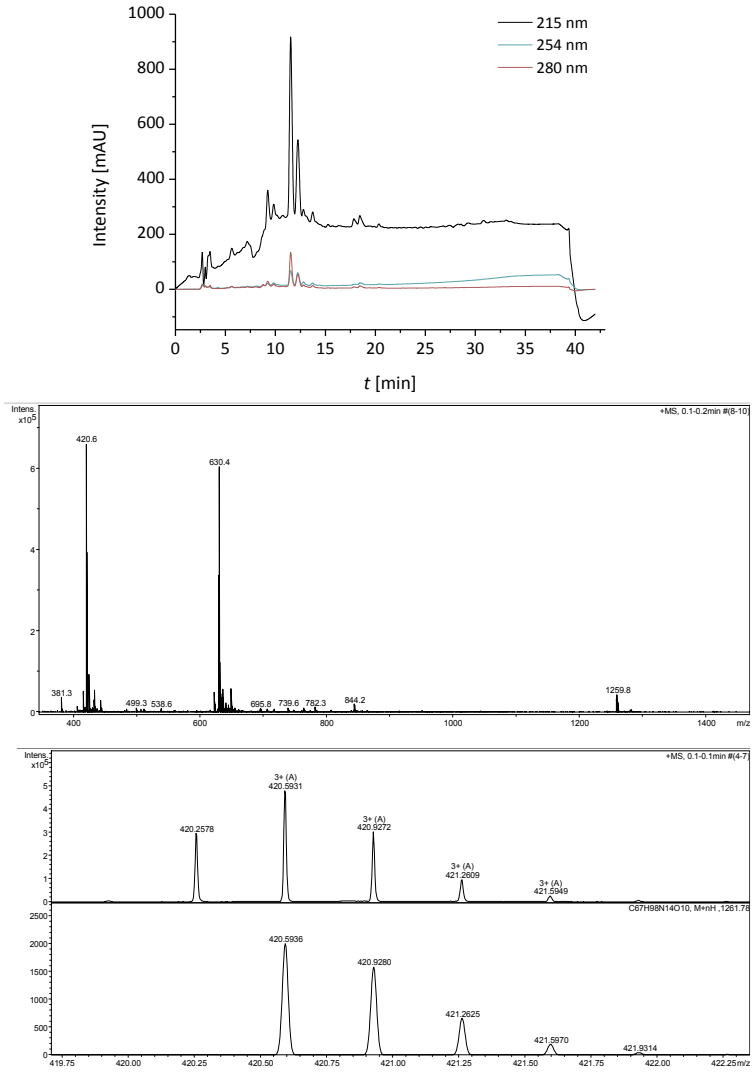

Figure A 7: HPLC chromatogram and ESI mass spectra of **P5D**. Top: HPLC chromatogram. Absorption was recorded at 215, 254 and 280 nm, 10 → 100% B (A: H_2O + 0.1% TFA and B: MeOH + 0.1% TFA) in 30 min, flow 1.0 mL/min. Centre: ESI mass spectrum. Bottom: ESI-HRMS spectrum of the $[M+3H]^{3+}$-species.

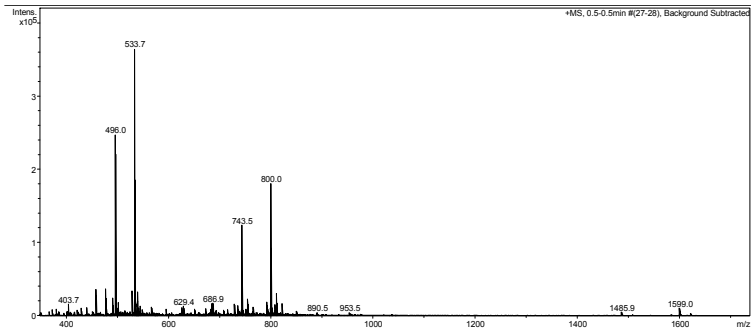

Figure A 8: ESI mass spectrum of **P5E – 1 hVal**.

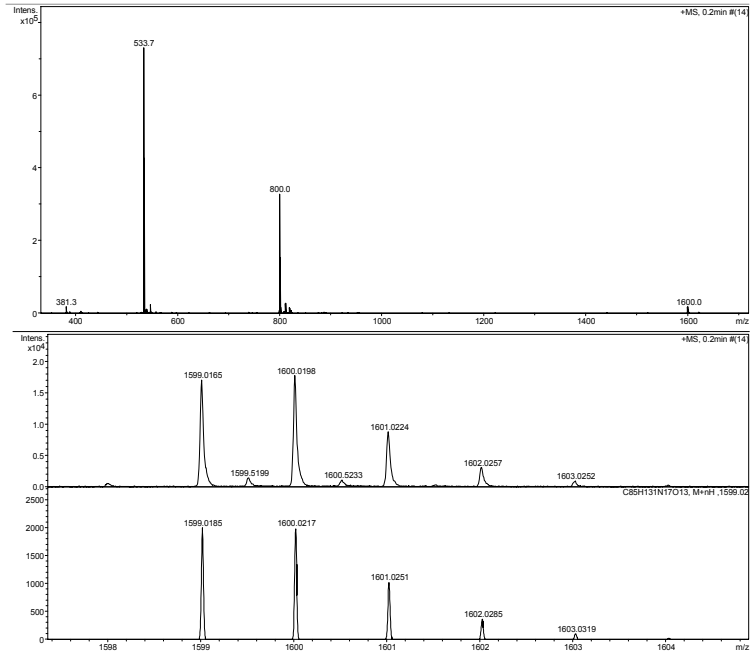

Figure A 9: ESI mass spectrum of **P5E**. Top: ESI mass spectrum. Bottom: ESI-HRMS spectrum of the $[M+H]^+$-species.

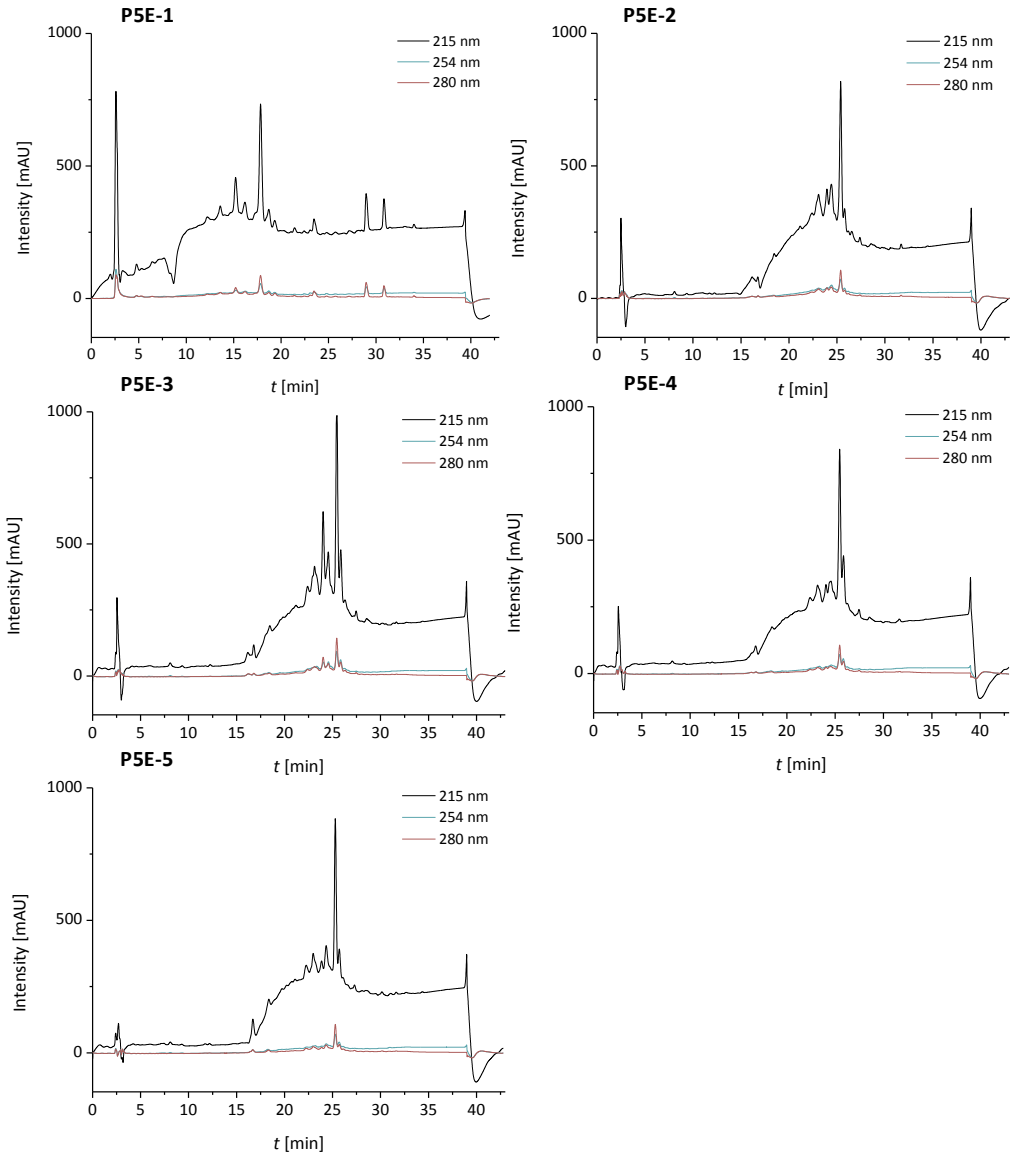

Figure A 10: HPLC chromatograms of different coupling conditions for synthesising **P5E**. Absorption was recorded at 215, 254 and 280 nm, 10 → 100% B (A: H_2O + 0.1% TFA and B: MeOH + 0.1% TFA) in 30 min, flow 1.0 mL/min.

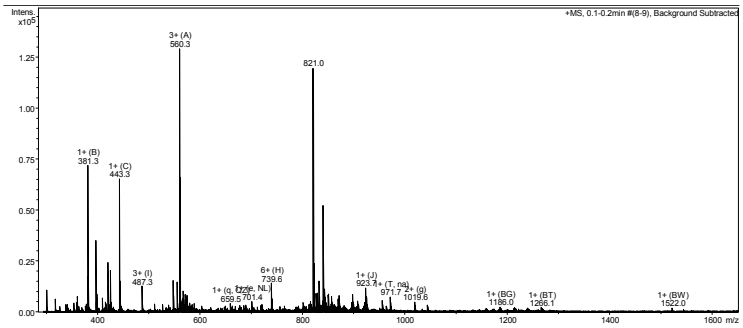

Figure A 11: ESI mass spectrum of **P5E-cap**.

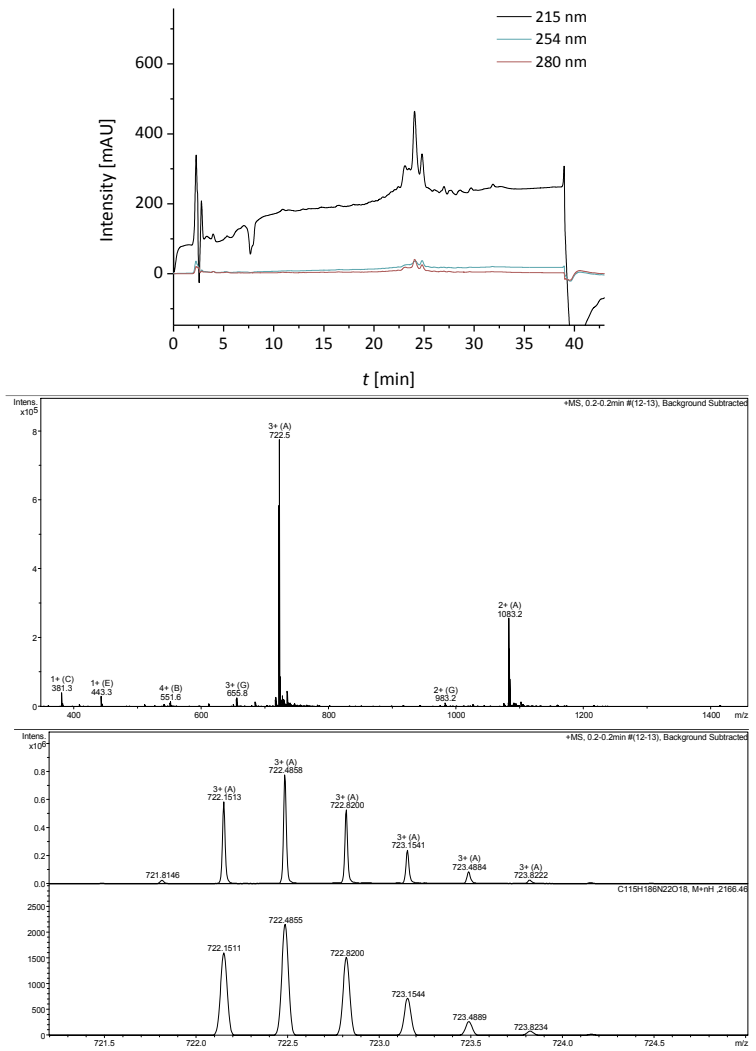

Figure A 12: HPLC chromatogram and ESI mass spectra of **P5F.** Top: HPLC chromatogram. Absorption was recorded at 215, 254 and 280 nm, 50 → 100% B (A: H_2O + 0.1% TFA and B: MeOH + 0.1% TFA) in 30 min, flow 1.0 mL/min. Centre: ESI mass spectrum. Bottom: ESI-HRMS spectrum of the $[M+3H]^{3+}$-species.

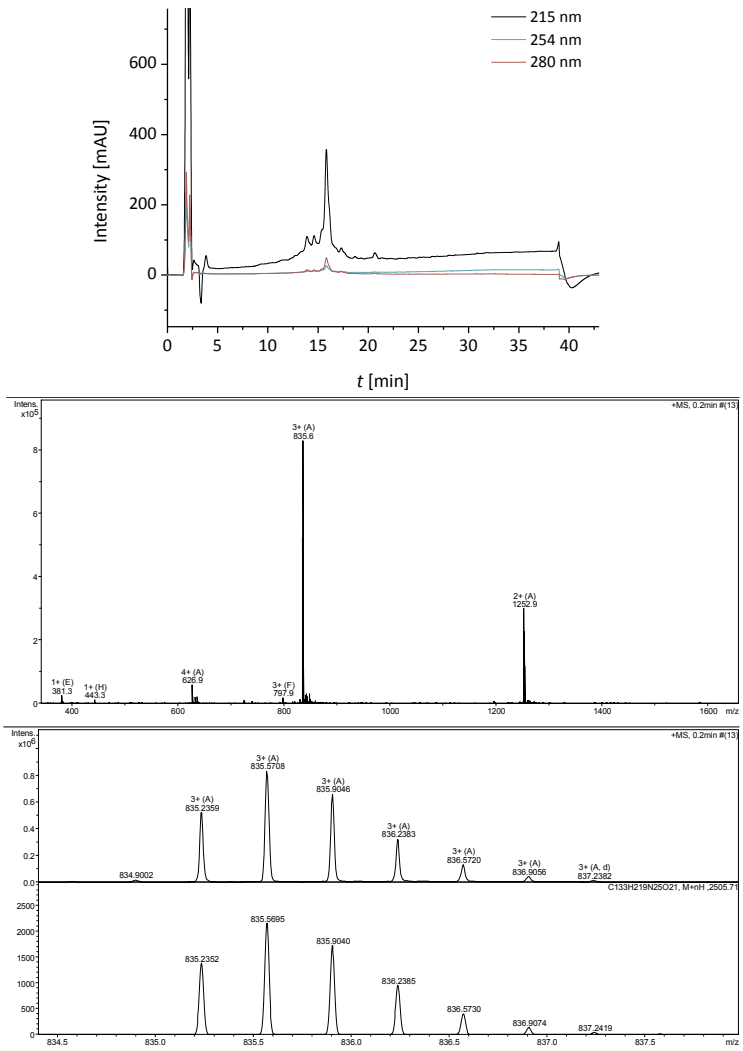

Figure A 13: HPLC chromatogram and ESI mass spectra of **P5G**. Top: HPLC chromatogram. Absorption was recorded at 215, 254 and 280 nm, 75 → 100% B (A: H_2O + 0.1% TFA and B: MeOH + 0.1% TFA) in 30 min at 60 °C, flow 1.0 mL/min. Centre: ESI mass spectrum. Bottom: ESI-HRMS spectrum of the $[M+3H]^{3+}$-species.

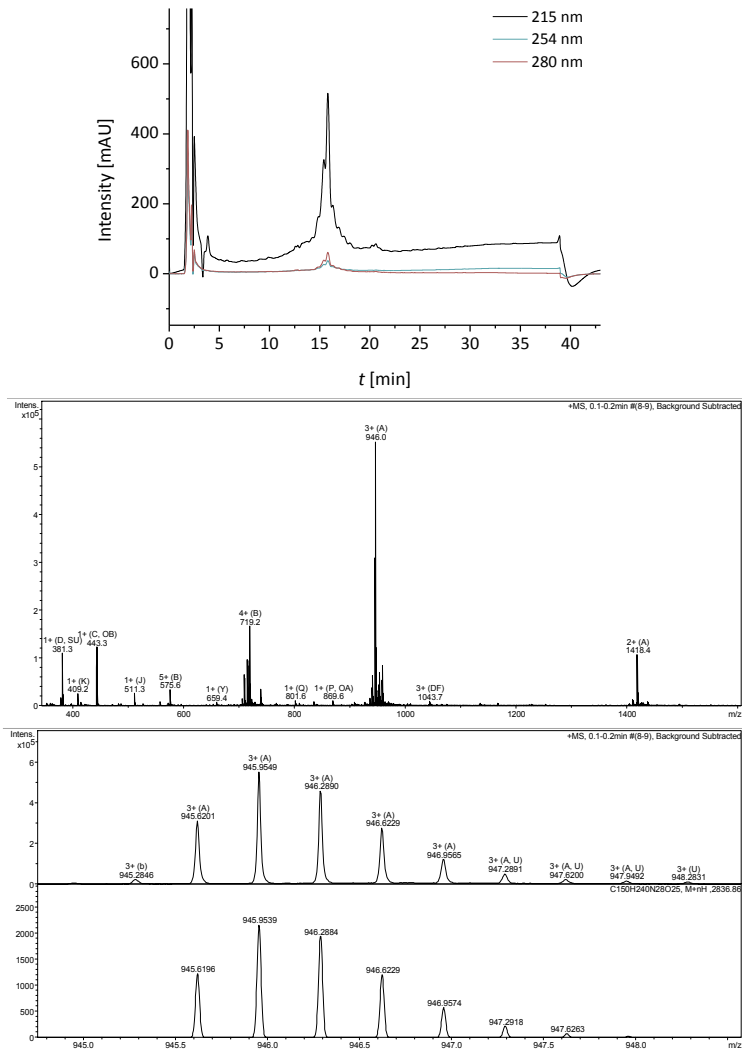

Figure A 14: HPLC chromatogram and ESI mass spectra of **P5H**. Top: HPLC chromatogram. Absorption was recorded at 215, 254 and 280 nm, 70 → 95% B (A: H_2O + 0.1% TFA and B: MeOH + 0.1% TFA) in 30 min at 60 °C, flow 1.0 mL/min. Centre: ESI mass spectrum. Bottom: ESI-HRMS spectrum of the $[M+3H]^{3+}$-species.

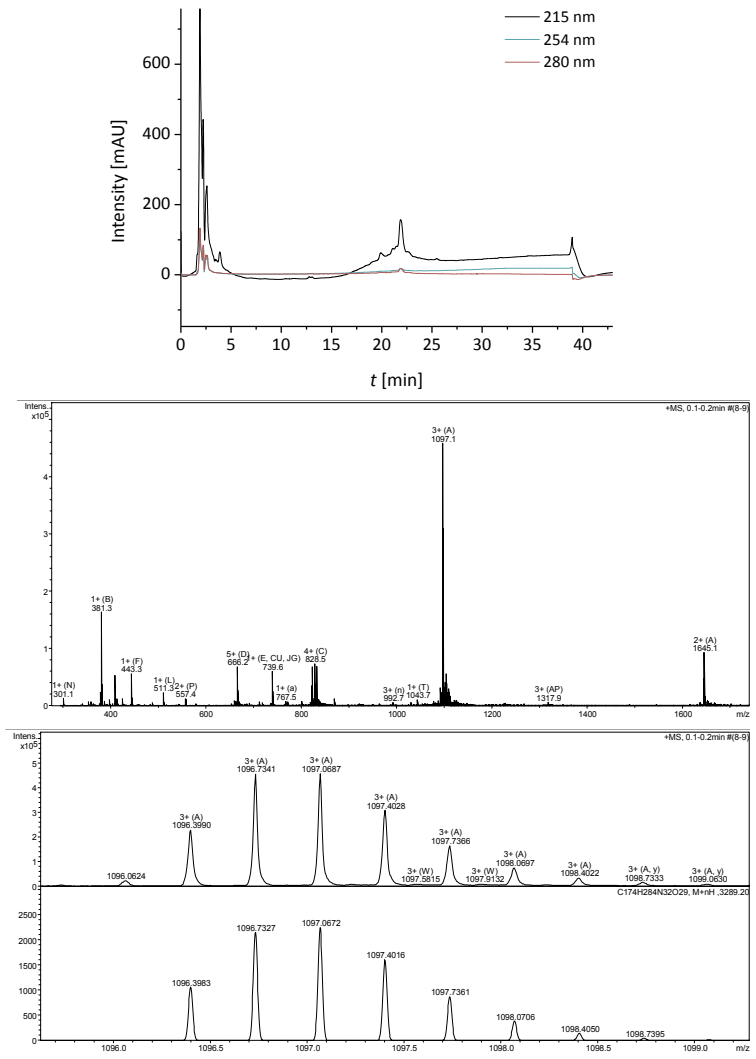

Figure A 15: HPLC chromatogram and ESI mass spectra of **P5I**. Top: HPLC chromatogram. Absorption was recorded at 215, 254 and 280 nm, 75 → 100% B (A: H_2O + 0.1% TFA and B: MeOH + 0.1% TFA) in 30 min at 60 °C, flow 1.0 mL/min. Centre: ESI mass spectrum. Bottom: ESI-HRMS spectrum of the $[M+3H]^{3+}$-species.

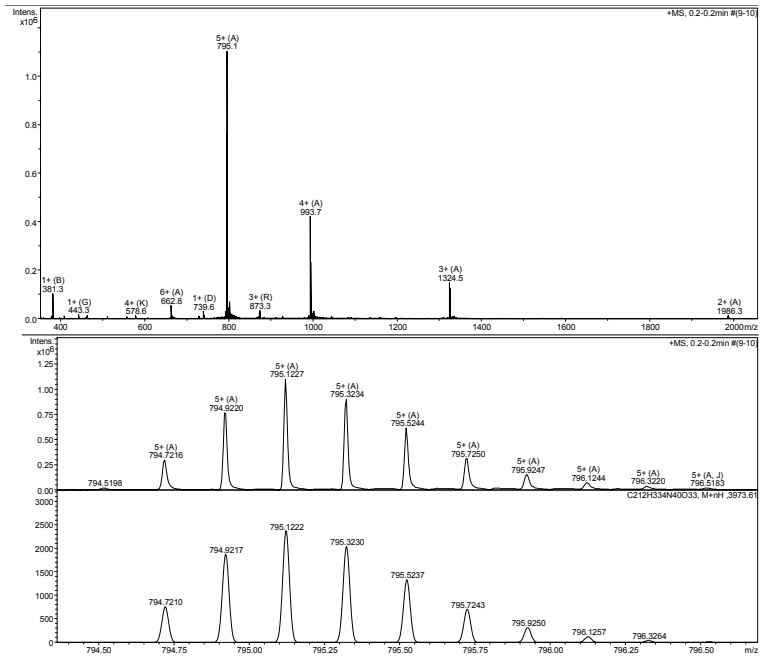

Figure A 16: ESI mass spectrum of **P5**. Top: ESI mass spectrum. Bottom: ESI-HRMS spectrum of the $[M+5H]^{5+}$-species.

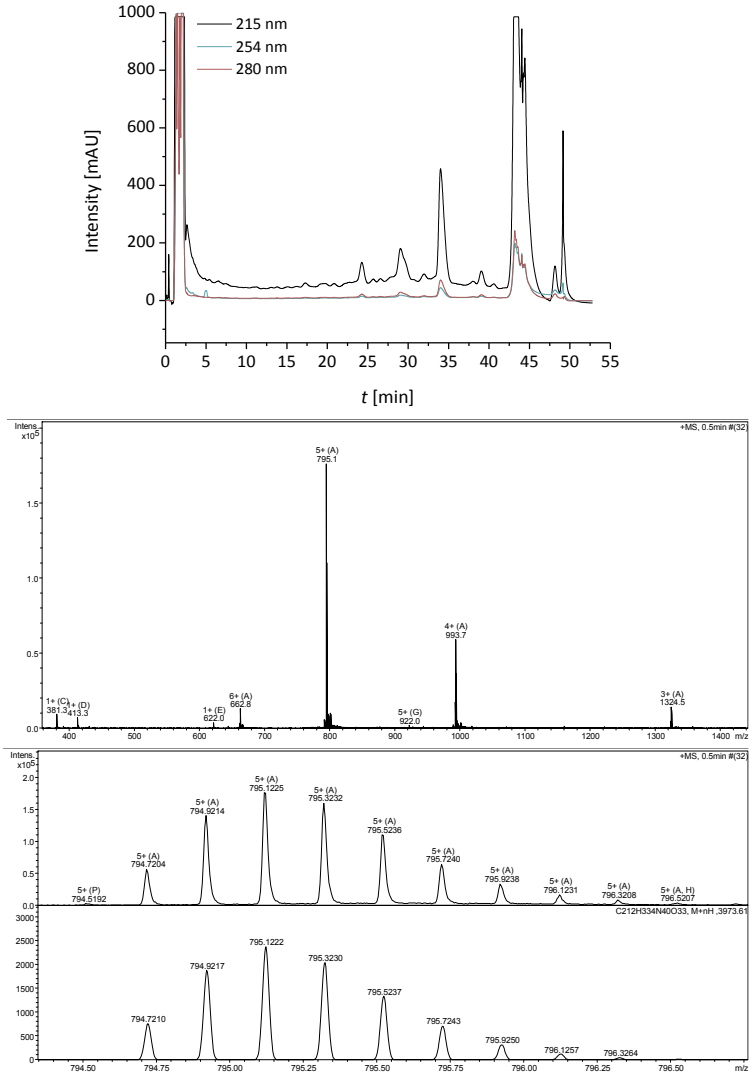

Figure A 17: HPLC chromatogram and ESI mass spectra of **P6**. Top: HPLC chromatogram. Absorption was recorded at 215, 254 and 280 nm, 69 → 79% C (A: H_2O + 0.1% TFA and C: MeCN + 0.1% TFA) in 40 min at 60 °C, flow 1.0 mL/min. Centre: ESI mass spectrum. Bottom: ESI-HRMS spectrum of the $[M+5H]^{5+}$-species.

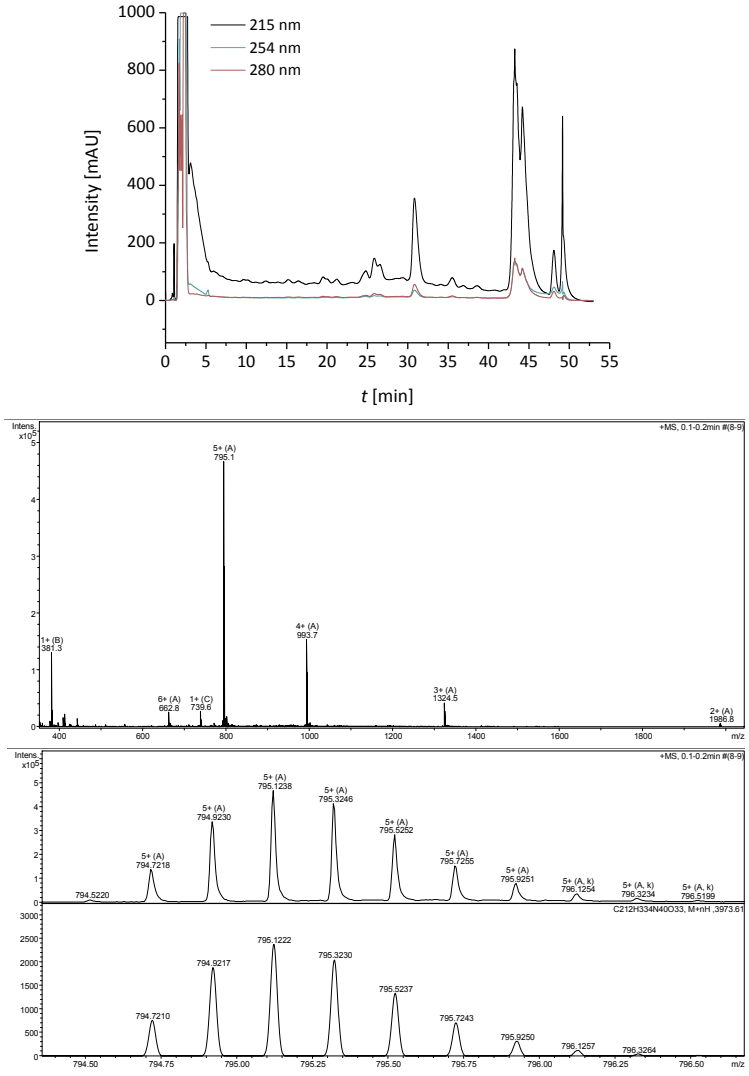

Figure A 18: HPLC chromatogram and ESI mass spectra of **P7**. Top: HPLC chromatogram. Absorption was recorded at 215, 254 and 280 nm, 68 → 80% C (A: H_2O + 0.1% TFA and C: MeCN + 0.1% TFA) in 40 min at 60 °C, flow 1.0 mL/min. Centre: ESI mass spectrum. Bottom: ESI-HRMS spectrum of the $[M+5H]^{5+}$-species.

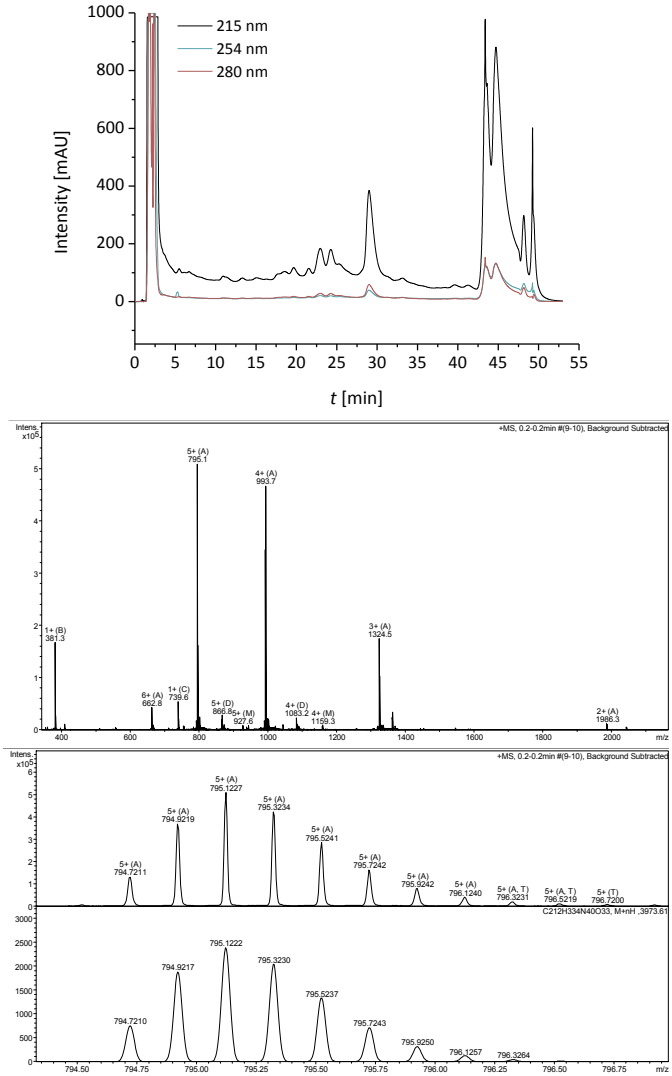

Figure A 19: HPLC chromatogram and ESI mass spectra of **P8**. Top: HPLC chromatogram. Absorption was recorded at 215, 254 and 280 nm, 68 → 80% C (A: H_2O + 0.1% TFA and C: MeCN + 0.1% TFA) in 40 min at 60 °C, flow 1.0 mL/min. Centre: ESI mass spectrum. Bottom: ESI-HRMS spectrum of the $[M+5H]^{5+}$-species.

A.2.3 Secondary Structure Determination by CD Spectroscopy

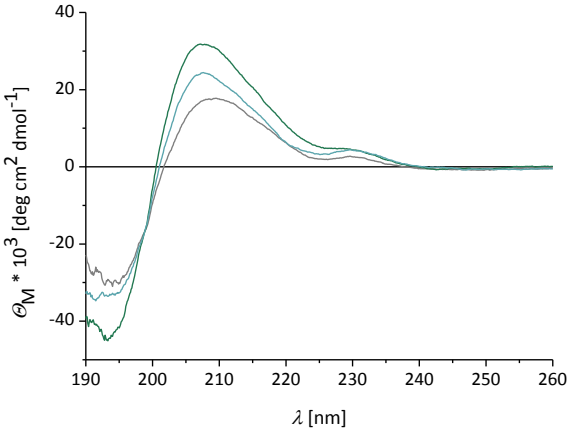

Figure A 20: CD spectra of the β-peptide **P5** in lipid bilayer. DOPC SUVs (P/L = 1/20, *c*(β-peptides) = 20 μM, phosphate buffer (50 mM, pH 7.5)). The CD measurements were performed at 20 °C.

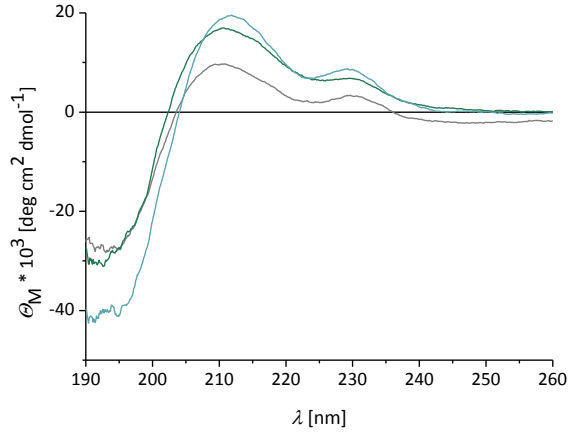

Figure A 21: CD spectra of the β-peptide **P6** in lipid bilayer. DOPC SUVs (P/L = 1/20, *c*(β-peptides) = 20 μM, phosphate buffer (50 mM, pH 7.5)). The CD measurements were performed at 20 °C.

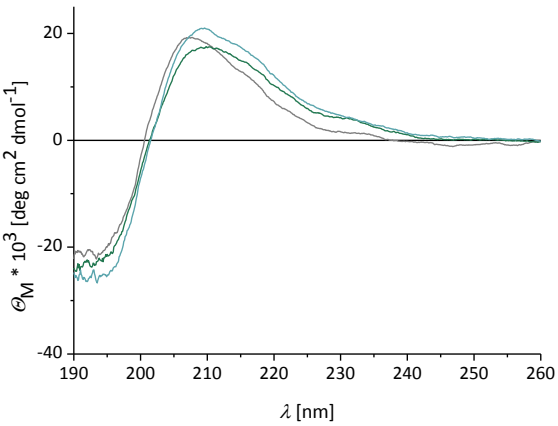

Figure A 22: CD spectra of the β-peptide **P7** in lipid bilayer. DOPC SUVs (P/L = 1/20, *c*(β-peptides) = 20 μM, phosphate buffer (50 mM, pH 7.5)). The CD measurements were performed at 20 °C.

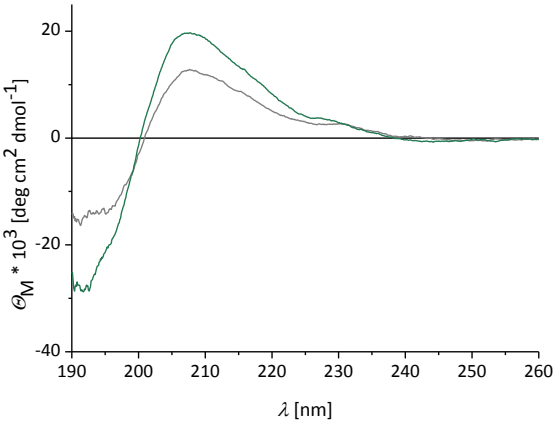

Figure A 23: CD spectra of the β-peptide **P7** in lipid bilayer. DOPC SUVs (P/L = 1/20, *c*(β-peptides) = 20 μM, phosphate buffer (50 mM, pH 7.5)). The CD measurements were performed at 20 °C.

A.2.4 Inter-Spin Distances from Modelled β^3-Peptides

Table A 2: Calculated distances *r* [nm] from the theoretical model of β-peptide **P5**.

	3_{14} lit.	**3_{14} crystal**	**3_{14} ideal**
***r* (O–O)**	2.0525	2.3656	2.2133
***r* (O–N)**	2.0461	2.3336	2.1609
***r* (N–O)**	2.0753	2.3227	2.1912
***r* (N–N)**	2.0597	2.2861	2.1337

Table A 3: Calculated distances *r* [nm] from the theoretical model of β-peptide **P6**.

	3_{14} lit.	**3_{14} crystal**	**3_{14} ideal**
***r* (O–O)**	2.9592	3.1896	3.0241
***r* (O–N)**	2.8830	3.0809	2.9099
***r* (N–O)**	2.8843	3.1000	2.9277
***r* (N–N)**	2.8084	2.9943	2.8161

Table A 4: Calculated distances *r* [nm] from the theoretical model of β-peptide **P7**.

	3_{14} lit.	**3_{14} crystal**	**3_{14} ideal**
***r* (O–O)**	3.0211	2.3708	2.1480
***r* (O–N)**	2.9533	2.3659	2.1420
***r* (N–O)**	2.9345	2.3583	2.1241
***r* (N–N)**	2.8688	2.3488	2.1129

Table A 5: Calculated distances *r* [nm] from the theoretical model of β-peptide **P8**.

	3_{14} lit.	**3_{14} crystal**	**3_{14} ideal**
***r* (O–O)**	2.5312	2.7378	2.4616
***r* (O–N)**	2.5383	2.7051	2.4261
***r* (N–O)**	2.5234	2.7245	2.4456
***r* (N–N)**	2.5234	2.6884	2.4066

7 Literature

[1] K. R. Acharya, M. D. Lloyd, *Trends Pharmacol. Sci.* **2005**, *26*, 10.

[2] J. L. Parker, S. Newstead, *Adv. Exp. Med. Biol.* **2016**, *922*, 61.

[3] D.-W. Sim, Z. Lu, H.-S. Won, S.-N. Lee, M.-D. Seo, B.-J. Lee, J.-H. Kim, *Molecules* **2017**, *22*, 1347.

[4] D. P. Frueh, A. C. Goodrich, S. H. Mishra, S. R. Nichols, *Curr. Opin. Struct. Biol.* **2013**, *23*, 734.

[5] C. Altenbach, S. L. Flitsch, H. G. Khorana, W. L. Hubbell, *Biochemistry* **1989**, *28*, 7806.

[6] a) C. R. Timmel, J. R. Harmer (Eds.) *Structure and Bonding*, *Vol. 152*, Springer Berlin Heidelberg, Berlin, Heidelberg, s.l., **2013**; b) E. Narr, A. Godt, G. Jeschke, *Angew. Chem. Int. Ed.* **2002**, *41*, 3907; c) J. S. Becker, S. Saxena, *Chem. Phys. Lett.* **2005**, *414*, 248.

[7] D. Goldfarb, *Phys. Chem. Chem. Phys.* **2014**, *16*, 9685.

[8] H. Y. V. Ching, F. C. Mascali, H. C. Bertrand, E. M. Bruch, P. Demay-Drouhard, R. M. Rasia, C. Policar, L. C. Tabares, S. Un, *J. Phys. Chem. Lett.* **2016**, *7*, 1072.

[9] B. E. Bode, J. Plackmeyer, M. Bolte, T. F. Prisner, O. Schiemann, *J. Organomet. Chem.* **2009**, *694*, 1172.

[10] a) Z. Yang, Y. Liu, P. Borbat, J. L. Zweier, J. H. Freed, W. L. Hubbell, *J. Am. Chem. Soc.* **2012**, *134*, 9950; b) G. W. Reginsson, N. C. Kunjir, S. T. Sigurdsson, O. Schiemann, *Chem. Eur. J.* **2012**, *18*, 13580.

[11] M. M. Haugland, E. A. Anderson, J. E. Lovett in *A specialist periodical report* (Eds.: V. Chechik, D. Murphy, E. A. Anderson), Royal Society of Chemistry, Cambridge, **2017**, pp. 1–34.

[12] M. M. Haugland, J. E. Lovett, E. A. Anderson, *Chem. Soc. Rev.* **2018**.

[13] H. Karoui, F. Le Moigne, O. Ouari, P. Tordo in *Stable Radicals*, John Wiley & Sons, Ltd, **2010**, pp. 173–229.

[14] a) B. P. Soule, F. Hyodo, K.-I. Matsumoto, N. L. Simone, J. A. Cook, M. C. Krishna, J. B. Mitchell, *Free Radic. Biol. Med.* **2007**, *42*, 1632; b) M. M. Haugland, J. E. Lovett,

E. A. Anderson, *Chem. Soc. Rev.* **2018**.

[15] a) I. Krstić, R. Hänsel, O. Romainczyk, J. W. Engels, V. Dötsch, T. F. Prisner, *Angew. Chem. Int. Ed.* **2011**, *50*, 5070; b) W. R. Couet, R. C. Brasch, C. Sosnovsky, J. Lukszo, I. Prakash, C. T. Gnewech, T. N. Tozer, *Tetrahedron* **1985**, *41*, 1165; c) M. Azarkh, O. Okle, P. Eyring, D. R. Dietrich, M. Drescher, *J. Magn. Reson.* **2011**, *212*, 450.

[16] I. A. Kirilyuk, A. A. Bobko, S. V. Semenov, D. A. Komarov, I. G. Irtegova, I. A. Grigor'ev, E. Bagryanskaya, *J. Org. Chem.* **2015**, *80*, 9118.

[17] a) J. T. Paletta, M. Pink, B. Foley, S. Rajca, A. Rajca, *Org. Lett.* **2012**, *14*, 5322; b) Y. Wang, J. T. Paletta, K. Berg, E. Reinhart, S. Rajca, A. Rajca, *Org. Lett.* **2014**, *16*, 5298.

[18] a) A. Rajca, V. Kathirvelu, S. K. Roy, M. Pink, S. Rajca, S. Sarkar, S. S. Eaton, G. R. Eaton, *Chem. Eur. J.* **2010**, *16*, 5778; b) V. Kathirvelu, C. Smith, C. Parks, M. A. Mannan, Y. Miura, K. Takeshita, S. S. Eaton, G. R. Eaton, *Chem. Commun.* **2009**, 454.

[19] A. A. Kuzhelev, R. K. Strizhakov, O. A. Krumkacheva, Y. F. Polienko, D. A. Morozov, G. Y. Shevelev, D. V. Pyshnyi, I. A. Kirilyuk, M. V. Fedin, E. G. Bagryanskaya, *J. Magn. Reson.* **2016**, *266*, 1.

[20] V. Meyer, M. A. Swanson, L. J. Clouston, P. J. Boratyński, R. A. Stein, H. S. Mchaourab, A. Rajca, S. S. Eaton, G. R. Eaton, *Biophys. J.* **2015**, *108*, 1213.

[21] J. P. Klare, H.-J. Steinhoff, *Photosyn. Res.* **2009**, *102*, 377.

[22] a) K. Sale, L. Song, Y.-S. Liu, E. Perozo, P. Fajer, *J. Am. Chem. Soc.* **2005**, *127*, 9334; b) D. Klose, J. P. Klare, D. Grohmann, C. W. M. Kay, F. Werner, H.-J. Steinhoff, *PloS one* **2012**, *7*, e39492.

[23] Y. Polyhach, G. Jeschke, *Spectroscopy* **2010**, *24*, 651.

[24] E. Matalon, T. Huber, G. Hagelueken, B. Graham, V. Frydman, A. Feintuch, G. Otting, D. Goldfarb, *Angew. Chem. Int. Ed.* **2013**, *52*, 11831.

[25] N. L. Fawzi, M. R. Fleissner, N. J. Anthis, T. Kálai, K. Hideg, W. L. Hubbell, G. M. Clore, *J. Biomol. NMR* **2011**, *51*, 105.

[26] T. Kálai, M. Balog, J. Jekö, K. Hideg, *Synthesis* **1999**, *1999*, 973.

[27] I. D. Sahu, R. M. McCarrick, K. R. Troxel, R. Zhang, H. J. Smith, M. M. Dunagan, M. S.

Swartz, P. V. Rajan, B. M. Kroncke, C. R. Sanders et al., *Biochemistry* **2013**, *52*, 6627.

[28] J. P. Klare, *Biol. Chem.* **2013**, *394*, 1281.

[29] K. Hideg, T. Kálai, C. P. Sár, *J. Heterocycl. Chem.* **2005**, *42*, 437.

[30] L. J. Berliner, H. M. McConnell, *Proc. Natl. Acad. Sci.* **1966**, *55*, 708.

[31] M. Adackaparayil, J. H. Smith, *J. Org. Chem.* **1977**, *42*, 1655.

[32] O. H. Hankovszky, K. Hideg, E. V. Goldammer, E. Matuszak, H. Kolkenbrock, H. Tschesche, H. R. Wenzel, *Biochim. Biophys. Acta, Protein Struct. Mol. Enzymol.* **1987**, *916*, 152.

[33] T. Kálai, W. L. Hubbell, K. Hideg, *Synthesis* **2009**, *2009*, 1336.

[34] C. Baldauf, K. Schulze, P. Lueders, E. Bordignon, R. Tampé, *Chem. Eur. J.* **2013**, *19*, 13714.

[35] a) C. J. Noren, S. J. Anthony-Cahill, M. C. Griffith, P. G. Schultz, *Science* **1989**, *244*, 182; b) C. C. Liu, P. G. Schultz, *Annu. Rev. Biochem.* **2010**, *79*, 413.

[36] M. J. Schmidt, J. Borbas, M. Drescher, D. Summerer, *J. Am. Chem. Soc.* **2014**, *136*, 1238.

[37] M. R. Fleissner, E. M. Brustad, T. Kálai, C. Altenbach, D. Cascio, F. B. Peters, K. Hideg, S. Peuker, P. G. Schultz, W. L. Hubbell, *Proc. Natl. Acad. Sci.* **2009**, *106*, 21637.

[38] T. Kálai, M. R. Fleissner, J. Jekő, W. L. Hubbell, K. Hideg, *Tetrahedron Lett.* **2011**, *52*, 2747.

[39] W. L. Hubbell, C. J. López, C. Altenbach, Z. Yang, *Curr. Opin. Struct. Biol.* **2013**, *23*, 725.

[40] S. Schreier, J. C. Bozelli, N. Marín, R. F. F. Vieira, C. R. Nakaie, *Biophys. Rev.* **2012**, *4*, 45.

[41] E. F. Vicente, L. G. M. Basso, G. F. Cespedes, E. N. Lorenzón, M. S. Castro, M. J. S. Mendes-Giannini, A. J. Costa-Filho, E. M. Cilli, *PloS one* **2013**, *8*, e60818.

[42] A. Bettio, V. Gutewort, A. Pöppl, M. C. Dinger, O. Zschörnig, A. Klaus, C. Toniolo, A. G. Beck-Sickinger, *J. Pept. Sci.* **2002**, *8*, 671.

[43] a) M. H. Shabestari, M. van Son, A. Moretto, M. Crisma, C. Toniolo, M. Huber,

Biopolymers **2014**, *102*, 244; b) J. C. McNulty, J. L. Silapie, M. Carnevali, C. T. Farrar, R. G. Griffin, F. Formaggio, M. Crisma, C. Toniolo, G. L. Millhauser, *Biopolymers* **2000**, *55*, 479.

[44] D. Marsh, *J. Magn. Reson.* **2006**, *180*, 305.

[45] a) C. Toniolo, E. Valente, F. Formaggio, M. Crisma, G. Pilloni, C. Corvaja, A. Toffoletti, G. V. Martinez, M. P. Hanson, G. L. Millhauser, *J. Pept. Sci.* **1995**, *1*, 45; b) J. J. Inbaraj, T. B. Cardon, M. Laryukhin, S. M. Grosser, G. A. Lorigan, *J. Am. Chem. Soc.* **2006**, *128*, 9549.

[46] K. Wright, M. Sarciaux, A. de Castries, M. Wakselman, J.-P. Mazaleyrat, A. Toffoletti, C. Corvaja, M. Crisma, C. Peggion, F. Formaggio et al., *Eur. J. Org. Chem.* **2007**, *2007*, 3133.

[47] a) M. Tominaga, S. R. Barbosa, E. F. Poletti, J. Zukerman-Schpector, R. Marchetto, S. Schreier, A. C. Paiva, C. R. Nakaie, *Chem. Pharm. Bull.* **2001**, *49*, 1027; b) K. Wright, M. Wakselman, J.-P. Mazaleyrat, L. Franco, A. Toffoletti, F. Formaggio, C. Toniolo, *Chem. Eur. J.* **2010**, *16*, 11160.

[48] S. Stoller, G. Sicoli, T. Y. Baranova, M. Bennati, U. Diederichsen, *Angew. Chem. Int. Ed.* **2011**, *50*, 9743.

[49] I. Tkach, S. Pornsuwan, C. Höbartner, F. Wachowius, S. T. Sigurdsson, T. Y. Baranova, U. Diederichsen, G. Sicoli, M. Bennati, *Phys. Chem. Chem. Phys.* **2013**, *15*, 3433.

[50] M. Gordon-Grossman, Y. Gofman, H. Zimmermann, V. Frydman, Y. Shai, N. Ben-Tal, D. Goldfarb, *J. Phys. Chem. B* **2009**, *113*, 12687.

[51] F. Scarpelli, M. Drescher, T. Rutters-Meijneke, A. Holt, D. T. S. Rijkers, J. A. Killian, M. Huber, *J. Phys. Chem. B* **2009**, *113*, 12257.

[52] G. W. Reginsson, O. Schiemann, *Biochem. J.* **2011**, *434*, 353.

[53] K. Halbmair, J. Wegner, U. Diederichsen, M. Bennati, *Biophys. J.* **2016**, *111*, 2345.

[54] A. Holt, J. A. Killian, *Eur. Biophys. J.* **2010**, *39*, 609.

[55] M. R. R. de Planque, J. A. Killian, *Mol. Membr. Biol.* **2003**, *20*, 271.

[56] J. A. Killian, T. K. M. Nyholm, *Curr. Opin. Struct. Biol.* **2006**, *16*, 473.

[57] J. A. Killian, I. Salemink, M. R. de Planque, G. Lindblom, R. E. Koeppe, D. V. Greathouse, *Biochemistry* **1996**, *35*, 1037.

[58] W. C. Wimley, S. H. White, *Biochemistry* **2002**, *32*, 6307.

[59] M. R. R. de Planque, B. B. Bonev, J. A. A. Demmers, D. V. Greathouse, R. E. Koeppe, F. Separovic, A. Watts, J. A. Killian, *Biochemistry* **2003**, *42*, 5341.

[60] a) D. A. Doyle, J. M. Cabral, R. A. Pfuetzner, A. Kuo, J. M. Gulbis, S. L. Cohen, B. T. Chait, R. MacKinnon, *Science* **1998**, *280*, 69; b) I. M. Williamson, S. J. Alvis, J. M. East, A. G. Lee, *Cell. Mol. Life Sci.* **2003**, *60*, 1581; c) K. Seshadri, R. Garemyr, E. Wallin, G. V. Heijne, A. Elofsson, *Protein Sci.* **1998**, *7*.

[61] N. Kučerka, M.-P. Nieh, J. Katsaras, *Biochim. Biophys. Acta.* **2011**, *1808*, 2761.

[62] a) D. P. Siegel, V. Cherezov, D. V. Greathouse, R. E. Koeppe, J. A. Killian, M. Caffrey, *Biophys. J.* **2006**, *90*, 200; b) T. M. Weiss, P. C.A. van der Wel, J. A. Killian, R. E. Koeppe, H. W. Huang, *Biophys. J.* **2003**, *84*, 379.

[63] E. Sparr, W. L. Ash, P. V. Nazarov, D. T. S. Rijkers, M. A. Hemminga, D. P. Tieleman, J. A. Killian, *J. Biol. Chem.* **2005**, *280*, 39324.

[64] A. Holt, L. Rougier, V. Réat, F. Jolibois, O. Saurel, J. Czaplicki, J. A. Killian, A. Milon, *Biophys. J.* **2010**, *98*, 1864.

[65] M. R. R. de Planque, E. Goormaghtigh, D. V. Greathouse, R. E. Koeppe, J. A. W. Kruijtzer, R. M. J. Liskamp, B. de Kruijff, J. A. Killian, *Biochemistry* **2001**, *40*, 5000.

[66] M. R. R. de Planque, J. A. W. Kruijtzer, R. M. J. Liskamp, D. Marsh, D. V. Greathouse, R. E. Koeppe, B. de Kruijff, J. A. Killian, *J. Biol. Chem.* **1999**, *274*, 20839.

[67] F. A. Nezil, M. Bloom, *Biophys. J.* **1992**, *61*, 1176.

[68] N. Kucerka, S. Tristram-Nagle, J. F. Nagle, *J. Membr. Biol.* **2005**, *208*, 193.

[69] B. A. Lewis, D. M. Engelman, *J. Mol. Biol.* **1983**, *166*, 211.

[70] E. Strandberg, S. Ozdirekcan, D. T. S. Rijkers, P. C. A. van der Wel, R. E. Koeppe, R. M. J. Liskamp, J. A. Killian, *Biophys. J.* **2004**, *86*, 3709.

[71] P. Y.S. Lam, C. G. Clark, S. Saubern, J. Adams, M. P. Winters, D. M.T. Chan, A. Combs, *Tetrahedron Lett.* **1998**, *39*, 2941.

[72] D. M.T. Chan, K. L. Monaco, R.-P. Wang, M. P. Winters, *Tetrahedron Lett.* **1998**, *39*, 2933.

[73] D. A. Evans, J. L. Katz, T. R. West, *Tetrahedron Lett.* **1998**, *39*, 2937.

[74] a) J. Simon, S. Salzbrunn, G. K. Surya Prakash, N. A. Petasis, G. A. Olah, *J. Org. Chem.* **2001**, *66*, 633; b) P. Fontani, B. Carboni, M. Vaultier, G. Maas, *Synthesis* **1991**, *1991*, 605; c) E. Kianmehr, M. Yahyaee, K. Tabatabai, *Tetrahedron Lett.* **2007**, *48*, 2713.

[75] J. Qiao, P. Lam, *Synthesis* **2011**, *2011*, 829.

[76] S. Stoller, *Synthese und Anwendung eines neuen Spinlabels und Untersuchung der Assoziation von Nukleobasen-funktionalisierten Transmembranpeptiden in Lipiddoppelschichten*, Cuvillier Verlag, Göttingen, **2011**.

[77] R. B. Merrifield, *J. Am. Chem. Soc.* **1963**, *85*, 2149.

[78] a) C. D. Chang, J. Meienhofer, *Int. J. Pept. Protein Res.* **1978**, *11*, 246; b) E. Atherton, H. Fox, D. Harkiss, C. J. Logan, R. C. Sheppard, B. J. Williams, *J. Chem. Soc., Chem. Commun.* **1978**, 537.

[79] S. B. Kent, *Annu. Rev. Biochem.* **1988**, *57*, 957.

[80] J. P. Tam, Y.-A. Lu, *J. Am. Chem. Soc.* **1995**, *117*, 12058.

[81] R. C. d. L. Milton, S. C. F. Milton, P. A. Adams, *J. Am. Chem. Soc.* **1990**, *112*, 6039.

[82] a) W. R. Sampson, H. Patsiouras, N. J. Ede, *J. Pept. Sci.* **1999**, *5*, 403; b) P. K. Ajikumar, K. S. Devaky, *J. Pept. Sci.* **2001**, *7*, 641.

[83] M. Amblard, J.-A. Fehrentz, J. Martinez, G. Subra, *Mol. Biotechnol.* **2006**, *33*, 239.

[84] G. B. Fields, C. g. Fields, *J. Am. Chem. Soc.* **1991**, *113*, 4202.

[85] a) R. Knorr, A. Trzeciak, W. Bannwarth, D. Gillessen, *Tetrahedron Lett.* **1989**, *30*, 1927; b) S.-Y. Han, Y.-A. Kim, *Tetrahedron* **2004**, *60*, 2447.

[86] Y.-H. Ye, H. Li, X. Jiang, *Biopolymers* **2005**, *80*, 172.

[87] D. A. Pearson, M. Blanchette, M. L. Baker, C. A. Guindon, *Tetrahedron Lett.* **1989**, *30*, 2739.

[88] A. J. Miles, B. A. Wallace, *Chem. Soc. Rev.* **2016**, *45*, 4859.

[89] a) G. Holzwarth, P. Doty, *J. Am. Chem. Soc.* **1965**, *87*, 218; b) Y. Wei, A. A.

Thyparambil, R. A. Latour, *Biochim. Biophys. Acta.* **2014**, *1844*, 2331.

[90] Y. Chen, B. A. Wallace, *Biophys. Chem.* **1997**, *65*, 65.

[91] B. A. Wallace, *Q. Rev. Biophys.* **2009**, *42*, 317.

[92] a) W. F. DeGrado, J. D. Lear, *J. Am. Chem. Soc.* **1985**, *107*, 7684; b) D. Salom, B. R. Hill, J. D. Lear, W. F. DeGrado, *Biochemistry* **2000**, *39*, 14160; c) C. J. Pike, A. J. Walencewicz-Wasserman, J. Kosmoski, D. H. Cribbs, C. G. Glabe, C. W. Cotman, *J. Neurochem.* **1995**, *64*, 253; d) W. F. DeGrado, H. Gratkowski, J. D. Lear, *Protein Sci.* **2003**, *12*, 647; e) W. C. Pomerantz, T. L. R. Grygiel, J. R. Lai, S. H. Gellman, *Org. Lett.* **2008**, *10*, 1799.

[93] D. A. Brown, E. London, *J. Biol. Chem.* **2000**, *275*, 17221.

[94] a) A. D. Milov, K. M. Salikhov, M. D. Shirov, *Sov. Phys. Solid State* **1981**, *23*, 565; b) R. E. Martin, M. Pannier, F. Diederich, V. Gramlich, M. Hubrich, H. W. Spiess, *Angew. Chem. Int. Ed.* **1998**, *37*, 2833; c) M. Pannier, S. Veit, A. Godt, G. Jeschke, H. W. Spiess, *J. Magn. Reson.* **2000**, *142*, 331.

[95] A. Bowman, C. M. Hammond, A. Stirling, R. Ward, W. Shang, H. El-Mkami, D. A. Robinson, D. I. Svergun, D. G. Norman, T. Owen-Hughes, *Nucleic Acids Res.* **2014**, *42*, 6038.

[96] Y. Polyhach, E. Bordignon, G. Jeschke, *Phys. Chem. Chem. Phys.* **2011**, *13*, 2356.

[97] S. Mall, R. Broadbridge, R. P. Sharma, J. M. East, A. G. Lee, *Biochemistry* **2001**, *40*, 12379.

[98] E. Sparr, D. N. Ganchev, M. M. E. Snel, A. N. J. A. Ridder, L. M. J. Kroon-Batenburg, V. Chupin, D. T. S. Rijkers, J. A. Killian, B. de Kruijff, *Biochemistry* **2005**, *44*, 2.

[99] Y. G. Yu, T. E. Thorgeirsson, Y. K. Shin, *Biochemistry* **1994**, *33*, 14221.

[100] B. Dzikovski, D. Tipikin, J. Freed, *J. Phys. Chem. B* **2012**, *116*, 6694.

[101] M. R. de Planque, D. V. Greathouse, R. E. Koeppe, H. Schäfer, D. Marsh, J. A. Killian, *Biochemistry* **1998**, *37*, 9333.

[102] T. Beisel, A. M. Diehl, G. Manolikakes, *Org. Lett.* **2016**, *18*, 4116.

[103] W. E. Smith, *J. Org. Chem.* **1972**, *37*, 3972.

[104] I. Seven, T. Weinrich, M. Gränz, C. Grünewald, S. Brüß, I. Krstić, T. F. Prisner, A. Heckel, M. W. Göbel, *Eur. J. Org. Chem.* **2014**, *2014*, 4037.

[105] R. P. Cheng, S. H. Gellman, W. F. DeGrado, *Chem. Rev.* **2001**, *101*, 3219.

[106] D. Seebach, A. K. Beck, D. J. Bierbaum, *Chem. Biodivers.* **2004**, *1*, 1111.

[107] D. Seebach, D. F. Hook, A. Glättli, *Biopolymers* **2006**, *84*, 23.

[108] J. Frackenpohl, P. I. Arvidsson, J. V. Schreiber, D. Seebach, *ChemBioChem* **2001**, *2*, 445.

[109] H. Wiegand, B. Wirz, A. Schweitzer, G. P. Camenisch, M. I. Rodriguez Perez, G. Gross, R. Woessner, R. Voges, P. I. Arvidsson, J. Frackenpohl et al., *Biopharm. Drug Dispos.* **2002**, *23*, 251.

[110] a) E. A. Porter, X. Wang, H. S. Lee, B. Weisblum, S. H. Gellman, *Nature* **2000**, *404*, 565; b) Y. Hamuro, J. P. Schneider, W. F. DeGrado, *J. Am. Chem. Soc.* **1999**, *121*, 12200; c) L. Bildirici, P. Smith, C. Tzavelas, E. Horefti, D. Rickwood, *Nature* **2000**, *405*, 298.

[111] C. Mora-Navarro, J. Méndez-Vega, J. Caraballo-León, M.-R. Lee, S. Palecek, M. Torres-Lugo, P. Ortiz-Bermúdez, *PloS one* **2016**, *11*, e0149271.

[112] P. I. Arvidsson, M. Rueping, D. Seebach, *Chem. Commun.* **2001**, 649.

[113] D. Seebach, P. E. Ciceri, M. Overhand, B. Jaun, D. Rigo, L. Oberer, U. Hommel, R. Amstutz, H. Widmer, *Helv. Chim. Acta* **1996**, *79*, 2043.

[114] M. Brenner, D. Seebach, *Helv. Chim. Acta* **2001**, *84*, 2155.

[115]D. H. Appella, L. A. Christianson, I. L. Karle, D. R. Powell, S. H. Gellman, *J. Am. Chem. Soc.* **1996**, *118*, 13071.

[116] D. S. Daniels, E. J. Petersson, J. X. Qiu, A. Schepartz, *J. Am. Chem. Soc.* **2007**, *129*, 1532.

[117] a) T. Hintermann, D. Seebach, *Synlett* **1997**, *1997*, 437; b) D. Seebach, K. Gademann, J. V. Schreiber, J. L. Matthews, T. Hintermann, B. Jaun, L. Oberer, U. Hommel, H. Widmer, *Helv. Chim. Acta* **1997**, *80*, 2033.

[118]a) R. Caputo, E. Cassano, L. Longobardo, G. Palumbo, *Tetrahedron* **1995**, *51*, 12337;

b) P. Sutton, *Tetrahedron* **2000**, *56*, 7947; c) E. Arvanitis, H. Ernst, A. A. LudwigéD'Souza, A. J. Robinson, P. B. Wyatt, *J. Chem. Soc., Perkin Trans. 1* **1998**, 521; d) D. A. Evans, L. D. Wu, J. J. M. Wiener, J. S. Johnson, D. H. B. Ripin, J. S. Tedrow, *J. Org. Chem.* **1999**, *64*, 6411; e) S. G. Davies, N. M. Garrido, D. Kruchinin, O. Ichihara, L. J. Kotchie, P. D. Price, A. J. P. Mortimer, A. J. Russell, A. D. Smith, *Tetrahedron: Asymmetry* **2006**, *17*, 1793; f) D. Seebach, L. Schaeffer, F. Gessier, P. Bindschädler, C. Jäger, D. Josien, S. Kopp, G. Lelais, Y. R. Mahajan, P. Micuch et al., *Helv. Chim. Acta* **2003**, *86*, 1852.

[119] D. Seebach, S. Abele, K. Gademann, G. Guichard, T. Hintermann, B. Jaun, J. L. Matthews, J. V. Schreiber, L. Oberer, U. Hommel et al., *Helv. Chim. Acta* **1998**, *81*, 932.

[120] J. Podlech, D. Seebach, *Liebigs Ann.* **1995**, *1995*, 1217.

[121] D. Seebach, M. Overhand, F. N. M. Kühnle, B. Martinoni, L. Oberer, U. Hommel, H. Widmer, *Helv. Chim. Acta* **1996**, *79*, 913.

[122] G. Guichard, S. Abele, D. Seebach, *Helv. Chim. Acta* **1998**, *81*, 187.

[123] F. Arndt, B. Eistert, *Ber. dtsch. Chem. Ges. A/B* **1935**, *68*, 200.

[124] B. Eistert, *Ber. dtsch. Chem. Ges. A/B* **1935**, *68*, 208.

[125] W. Kirmse, *Eur. J. Org. Chem.* **2002**, *2002*, 2193.

[126] D. Seebach, S. Abele, K. Gademann, B. Jaun, *Angew. Chem. Int. Ed.* **1999**, *38*, 1595.

[127] S. Abele, K. Vögtli, D. Seebach, *Helv. Chim. Acta* **1999**, *82*, 1539.

[128] K. Gademann, T. Kimmerlin, D. Hoyer, D. Seebach, *J. Med. Chem.* **2001**, *44*, 2460.

[129] a) W. F. DeGrado, J. P. Schneider, Y. Hamuro, *J. Pept. Res.* **1999**, *54*, 206; b) J. M. Langenhan, S. H. Gellman, *Org. Lett.* **2004**, *6*, 937.

[130] D. Seebach, J. L. Matthews, *Chem. Commun.* **1997**, 2015.

[131] R. P. Cheng, W. F. DeGrado, *J. Am. Chem. Soc.* **2001**, *123*, 5162.

[132] I.-I. C. o. B. Nomencl, *Biochemistry* **2002**, *9*, 3471.

[133] A. Banerjee, P. Balaram, *Curr. Sci* **1997**, *73*, 1067.

[134] J. A. Kritzer, O. M. Stephens, D. A. Guarracino, S. K. Reznik, A. Schepartz, *Bioorg.*

Med. Chem. **2005**, *13*, 11.

[135] D. Seebach, R. I. Mathad, T. Kimmerlin, Y. R. Mahajan, P. Bindschädler, M. Rueping, B. Jaun, C. Hilty, T. Etezady-Esfarjani, *Helv. Chim. Acta* **2005**, *88*, 1969.

[136] U. Rost, Y. Xu, T. Salditt, U. Diederichsen, *Chemphyschem* **2016**, *17*, 2525.

[137] U. Rost, C. Steinem, U. Diederichsen, *Chem. Sci.* **2016**, *7*, 5900.

[138] J. A. Kritzer, J. Tirado-Rives, S. A. Hart, J. D. Lear, W. L. Jorgensen, A. Schepartz, *J. Am. Chem. Soc.* **2005**, *127*, 167.

[139] J. Wegner, *Master Thesis*, Georg-August Universität, Göttingen, **2013**.

[140] E. J. Corey, A. Venkateswarlu, *J. Am. Chem. Soc.* **1972**, *94*, 6190.

[141] M. Krull, *Master Thesis*, Georg-August Universität, Göttingen, **2015**.

[142] a) M. Pais, R. Sarfati, F. X. Jarreau, *Bull. Soc. Chim. Fr.* **1973**, 331; b) A. Müller, *Synthesis* **1998**, *1998*, 837.

[143] P. I. Arvidsson, J. Frackenpohl, D. Seebach, *Helv. Chim. Acta* **2003**, *86*, 1522.

[144] M. Amar, S. Bar, M. A. Iron, H. Toledo, B. Tumanskii, L. J. W. Shimon, M. Botoshansky, N. Fridman, A. M. Szpilman, *Nat. Commun.* **2015**, *6*, 6070.

[145] J. K. Murray, S. H. Gellman, *Org. Lett.* **2005**, *7*, 1517.

[146] G. Lelais, D. Seebach, B. Jaun, R. I. Mathad, O. Flögel, F. Rossi, M. Campo, A. Wortmann, *Helv. Chim. Acta* **2006**, *89*, 361.

[147] D. M. Pahlke, U. Diederichsen, *J. Pept. Sci.* **2016**, *22*, 636.

[148] B. Merrifield, *Brit. Poly.J.* **1984**, *16*, 173.

[149] F. García-Martín, M. Quintanar-Audelo, Y. García-Ramos, L. J. Cruz, C. Gravel, R. Furic, S. Côté, J. Tulla-Puche, F. Albericio, *J. Comb. Chem.* **2006**, *8*, 213.

[150] V. K. Sarin, S. B. H. Kent, R. B. Merrifield, *J. Am. Chem. Soc.* **1980**, *102*, 5463.

[151] a) C. K. Taylor, P. W. Abel, M. Hulce, D. D. Smith, *J. Pept. Res.* **2005**, *65*, 84; b) C. Hyde, T. Johnson, R. C. Sheppard, *J. Chem. Soc., Chem. Commun.* **1992**, 1573; c) M. Forest, A. Fournier, *Int. J. Pept. Protein Res.* **1990**, *35*, 89.

[152] a) L. A. Carpino, *J. Am. Chem. Soc.* **1993**, *115*, 4397; b) J. Klose, A. El-Faham, P. Henklein, L. A. Carpino, M. Bienert, *Tetrahedron Lett.* **1999**, *40*, 2045; c) T. I. Al-

Warhi, H. M.A. Al-Hazimi, A. El-Faham, *J. Saudi Chem. Soc.* **2012**, *16*, 97.

[153] a) R. Epton (Ed.) *Innovation and perspectives in solid phase synthesis - 1990. Peptides, polypeptides and oligonucleotides ; macro-organic reagents and catalysts ; collected papers First International Symposium, August 29 - September 2, 1989, Oxford, England*, SPCC (UK) Ltd, Birmingham, **1990**; b) A. Thaler, D. Seebach, F. Cardinaux, *Helv. Chim. Acta* **1991**, *74*, 617; c) A. Thaler, D. Seebach, F. Cardinaux, *Helv. Chim. Acta* **1991**, *74*, 628.

[154] a) M. Rueping, B. Jaun, D. Seebach, *Chem. Commun.* **2000**, 2267; b) M. Rueping, Y. R. Mahajan, B. Jaun, D. Seebach, *Chemistry* **2004**, *10*, 1607; c) D. Seebach, A. Jacobi, M. Rueping, K. Gademann, M. Ernst, B. Jaun, *Helv. Chim. Acta* **2000**, *83*, 2115.

[155] D. Seebach, J. V. Schreiber, S. Abele, X. Daura, W. F. van Gunsteren, *Helv. Chim. Acta* **2000**, *83*, 34.

[156] a) R. W. Woody, *Biopolymers* **1978**, *17*, 1451; b) A. Chakrabartty, T. Kortemme, S. Padmanabhan, R. L. Baldwin, *Biochemistry* **2002**, *32*, 5560; c) H. E. Auer, *J. Am. Chem. Soc.* **1973**, *95*, 3003.

[157] J. W. Nelson, N. R. Kallenbach, *Proteins* **1986**, *1*, 211.

[158] M. Buck, *Q. Rev. Biophys.* **1998**, *31*, 297.

[159] R. Woody, *Eur. Biophys. J.* **1994**, *23*, 253.

[160] K. A. Bode, J. Applequist, *Macromolecules* **1997**, *30*, 2144.

[161] S. J. Shandler, M. V. Shapovalov, R. L. Dunbrack, W. F. DeGrado, *J. Am. Chem. Soc.* **2010**, *132*, 7312.

[162] T. A. Halgren, *J. Comput. Chem.* **1996**, *17*, 490.

[163]M. D. Hanwell, D. E. Curtis, D. C. Lonie, T. Vandermeersch, E. Zurek, G. R. Hutchison, *J. Cheminform.* **2012**, *4*, 17.

[164] J. A. Cieslak, P. J. Focia, A. Gross, *Biochemistry* **2010**, *49*, 1486.

[165] J. E. Bailey, G. H. Beaven, D. A. Chignell, W. B. Gratzer, *Eur. J. Biochem.* **1968**, *7*, 5.

[166] M. Gude, *Lett. Pept. Sci.* **2002**, *9*, 203.

[167] Luzzi John J., C. E. Ramey, US3920659 A, **1975**.

[168] S. Zhu, C. Wang, L. Chen, R. Liang, Y. Yu, H. Jiang, *Org. Lett.* **2011**, *13*, 1146.

[169] T. Shiraishi, K. Kameyama, N. Imai, T. Domoto, I. Katsumi, K. Watanabe, *Chem. Pharm. Bull.* **1988**, *36*, 974.

[170] P. P. Geurink, B. I. Florea, N. Li, M. D. Witte, J. Verasdonck, C.-L. Kuo, G. A. van der Marel, H. S. Overkleeft, *Angew. Chem. Int. Ed.* **2010**, *49*, 6802.

[171] J. Cianci, J. B. Baell, A. J. Harvey, *Tetrahedron Lett.* **2007**, *48*, 5973.

[172] J. T. Lai, *Synthesis* **1984**, *1984*, 122.

[173] E. Barron, J. Brooks, Z. Elshenawy, J. Fiordelisio, G. Kottas, S. Layek, D. Z. Li, B. Ma, C. XIA, W. Yeager, US2012/026396, **2012**.

[174] T. Ooi, M. Kameda, K. Maruoka, *J. Am. Chem. Soc.* **1999**, *121*, 6519.

[175] A. McNally, B. Haffemayer, B. S. L. Collins, M. J. Gaunt, *Nature* **2014**, *510*, 129.

Danksagung

Mein besonderer Dank gilt meinem Doktorvater Prof. Dr. Ulf Diederichsen für die interessante Themenstellung, seine gute Betreuung, seine freundliche, unterstützende Art, sein immer offenes Ohr, seine ständige Diskussionsbereitschaft und sein Vertrauen in meine Arbeit.

Bei Prof. Dr. Marina Bennati bedanke ich mich für die intensive Kooperation, ihre Diskussionsbereitschaft, ihre freundliche Art und die Übernahme des Korreferats.

Darüber hinaus danke ich den weiteren Mitgliedern meiner Prüfungskommission Prof. Dr. Manuel Alcarazo, Prof. Dr. Konrad Koszinowski, Dr. Michael John und Dr. Franziska Thomas für ihr Interesse an meiner Arbeit und die Zeit, die sie sich für die Begutachtung genommen haben.

Ein besonderer Dank geht auch an Dr. Karin Halbmair für ihre intensive Kooperationsbereitschaft, Unterstützung rund um PELDOR und ihre ständige Diskussionsbereitschaft.

Dr. Holm Frauendorf, Dr. Michael John und allen Mitarbeitern der Massenabteilung sowie den Mitarbeitern der NMR-Abteilung danke ich für die Anfertigung der Massenspektren bzw. der Kernresonanzspektren und für ihre ständige Hilfsbereitschaft.

Des Weiteren möchte ich Brigitte Worbs dafür danken, dass sie mich in den letzten Wochen so tatkräftig bei den Synthesen unterstützt hat.

Auch möchte ich mich bei Gabriele Valora und Annemarie Kehl bedanken für die Bereitschaft PEDLOR Experimente im Lipid Bilayer durchzuführen.

Weiter möchte ich mich bei Angela Heinemann und Aoife Neville für die organisatorische Unterstützung bedanken.

Meinen Laborkollegen Dr. Julia Graf, Dr. Selda Kabatas, Dr. Zeynep Kanlidere, Dr. Ulrike Rost, Denis Pahlke, Markus Wiegand, Dr. Dina Zanbot und speziell Dr. Julia Schneider danke ich für die freundliche, entspannte Atmosphäre und die vielen humorvollen Stunden.

Auch möchte ich mich bei Dr. Marta Cal, Dr. Florian Czerny, Dr. Selda Kabatas, Mathis Rink, Dr. Ulrike Rost und Dr. Franziska Thomas dafür bedanken, dass sie mir mit einer Vielzahl von Diskussionen und guten Ratschlägen geholfen haben.

Weiter möchte ich mich bei Lars Hoffmann, Matthias Krull und meinen Abteilungspraktikanten bedanken, die mir bei der Spin Label-Synthese geholfen haben.

Dem gesamten AK Diederichsen und AK Thomas danke ich für die stete Hilfsbereitschaft, die entspannte Arbeitsatmosphäre und die vielen lustigen Stunden bei Wein und Käse.

Dr. Marta Cal, Mike Groth, Dr. Selda Kabatas, Benedikt Kugler, Patrick Menzel, Aoife Neville, Dr. Thomas Niklas, Iryna Portnova, Mathis Rink, und Dr. Igor Tkach danke ich für das Korrekturlesen meiner Arbeit und ihre hilfreichen Korrekturvorschläge.

Danke an meine Freunde, die mich in den schweren und leichten Stunden meines Lebens begleitet haben.

Schließlich danke ich P. M. M. B. M. C. und T. dafür, dass sie mich in jeder Lebenslage unterstützen und immer für mich da sind.